Effector mechanisms of non-canonical inflammasome activation

Inauguraldissertation

zur
Erlangung der Würde eines Doktors der Philosophie
vorgelegt der
Philosophisch-Naturwissenschaftlichen Fakultät at der Universität Basel
von

Sebastian Rühl

aus Deutschland

Basel 2018

Genehmigt von der Philosophisch-Naturwissenschaftlichen Fakultät auf Antrag von Prof. Dr. Sebastian Hiller, Prof. Dr. Petr Broz und Prof. Dr. Jean Pieters

Basel, den 27.03.2018

Prof. Dr. Martin Spiess

Dekan der Philosophisch-

Naturwissenschaftlichen Fakultät

1 Abstract

Our body constantly faces all kinds immunological challenges, ranging from sterile wounds to non-pathogenic and sometimes pathogenic microorganisms. The innate immune system represents the first line of defense against these challenges. It is capable of detecting invading microorganisms and tissue damage by conserved, germline-encoded pattern recognition receptors (PRRs) and launches a first counterstrike through mechanisms including phagocytosis, reactive oxygen species (ROS) or anti-microbial peptides. Concomitant production and secretion of cytokines alerts the adaptive immune system and initializes are very potent, highly specific and sustained immune response governed by the activation and expansion of T- and B-cells.

Inflammasomes are one important class of cytosolic PRRs as they recognize a large variety of pathogens. Engagement of inflammasome pathways leads to death of the infected host cell by pyroptosis and secretion of pro-inflammatory cytokines like IL-1β and IL-18. The recently discovered non-canonical inflammasome pathway is triggered by intracellular bacterial lipopolysaccharide (LPS), which binds to caspase-11 to activate it. Active caspase-11 triggers pyroptosis and activates a canonical Nlrp3 inflammasome to promote caspase-1 activation and IL-1 secretion.

The molecular details of pyroptosis execution and the signaling events downstream of caspase-11 have not been thoroughly characterized, which is why this was the main interest underlying my PhD work. I investigated the connection between caspase-11 activation and cytokine release triggered by the canonical NLRP3 inflammasome. I could show that caspase-11 stimulates NLRP3 activation by promoting potassium efflux, a well characterized trigger for the NLRP3 inflammasome, in a cell autonomous manner. Subsequently I got interested in the molecular mechanisms underlying pyroptosis induction by Gasdermin-D. We could characterize pore formation by the Gasdermin-D N-terminal fragment as the final step of pyroptosis. Finally, I investigated if cells are capable of preventing or delaying pyroptosis downstream of caspase-11/gasdermin-D. I found that removal of Gasdermin-D pores by ESCRT-III mediated membrane repair represents one mechanism by which cells prevent Gasdermin-D dependent cell death. Overall my results revealed connections between innate immunity signaling pathways, uncovered a novel form of cellular pore forming toxins and demonstrated an unexpected regulation of pyroptosis by cellular survival pathways.

2 Table of contents

3 Introduction

3.1 Cells of the innate immune system

Cells of the innate immune system are responsible to detect the presence of foreign, pathogenic microorganisms like viruses and bacteria. They express germline encoded, conserved pattern recognition receptors to orchestrate the initial (<96 hours) inflammatory response to pathogenic or sterile insults. The cells of the innate immune system reside naturally with many tissues like the gut, liver or skin where they react to invading microorganisms or tissue damage.

Macrophages develop from precursor cells residing in the bone-marrow. They represent an important first line of defense as they are capable of engulfing and degrading foreign matter and dead host cells without the help of the adaptive immune system. They express a variety of PRRs allowing them to sense pathogen or host derived molecules. Their primary functions are to produce cytokines to recruit other immune cells (Cader & Kaser, 2013; Zigmond & Jung, 2013)and present antigens of engulfed microorganisms to cells of the adaptive immune system.

Dendritic cells (DCs) are the main antigen-presenting-cells (APCs) of the immune system as they are extremely proficient in digesting and presenting microorganisms and proteins. As macrophages, they originate from a common granulocyte macrophage precursor (GMP) from the bone marrow and they are found in various tissues like the skin, the gut or the spleen. Plasmacytoid DCs are circulating in the periphery and are crucial components of the anti-viral response, as they produce large amounts of type-I interferons upon stimulation. DCs get easily stimulated by a variety of signals, as they express different receptors, which leads to secretion of various inflammatory cytokines(Dzopalic *et al*, 2012; Farache *et al*, 2013) . Despite their importance for the induction of the adaptive immune response, DCs also function to terminate the immune response, by rendering T-cells inactive or by promoting the development of regulatory T-cells(Farache *et al*, 2013).

Neutrophils have long been neglected as an important part of the innate immune response. They have been considered short lived ‘cannon fodder’ to initiate the acute phase of inflammation and control extracellular pathogens (Borregaard, 2010; Mantovani *et al*, 2011; Amulic *et al*, 2012). They possess a high phagocytic activity, store anti-microbial components in their secretory granules and are important producers of cytokines upon tissue

damage or microbial invasion(Chen *et al*, 2014; Jaillon *et al*). They are capable of fighting several bacteria and viruses by the formation of neutrophil extracellular traps (NETs) (Brinkmann & Zychlinsky, 2007) and are important for communication to other cells of the innate immune system like NK cells(Jaeger *et al*, 2012; Costantini *et al*, 2011; 2010).
Other cells of the innate immune system are **innate lymphoid cells (ILCs)**, which are made up of ILC1, ILC2 and ILC3 and **mast cells**. Both cell types are important producers of cytokines in order to communicate to other innate immune cells or the adaptive immune system. Their exact properties and functions are reviewed elsewhere(Hwang & McKenzie, 2013; John & Abraham, 2013).

3.2 Pattern recognition receptors

The innate immune system uses germline encoded, conserved receptors to recognize pathogen associated molecular patterns (PAMPs) or endogenous, danger-associated molecular patterns (DAMPs). The ligands for these pattern recognition receptors (PRRs) are usually conserved molecules, essential to the survival of pathogenic microorganisms and are therefore invariable in their molecular composition (Kumar *et al*, 2011). Most of the receptors can be classified into five families, based on their protein homology domain. These families are the Toll-like receptors (TLRs), C-type lectin receptors (CLRs), nucleotide-binding domain, leucine-rich repeat (LRR)-containing (or NOD-like) receptors (NLRs), RIG-I- like receptors (RLRs), and the AIM2-like receptors (ALRs) (**Table 1**)(Kumar *et al*, 2011).

Family	Members	Shared domains	Localization
TLR	1-10 in humans, 1-9 and 11-13 in mice	LRR, TIR	Cell surface, endosomal compartments
CLR	Dectins	C-type lectin	Cell surface
NLR	NLRC1&2 (=NOD1&2). NLRC3-5, NLRP1-9, and 11-14, NAIP1, -2, -5, -6	Nucleotide binding, LRR	Cytoplasm, plasma and endosomal membrane associated
RLR	RIG-I, MDA5, LGP2	DExD/H, helicase	Cytoplasm
ALR	AIM2, IFI16	Pyrin, HIN-200	Cytoplasm and nucleus (IFI16)

Table 1 Overview of PRRs of the innate immune system

TLRs and CLRs are membrane bound receptors and sample the endosomal and the extracellular space for the presence of microbial ligands. NLRs, RLRs and ALRs are cytosolic proteins, which are activated by intracellular pathogens or components thereof. One major consequence of PRR activation is the production of pro-inflammatory cytokines and interferons. Beyond these transcriptional responses, PRR also induce non-transcriptional consequences like phagocytosis, autophagy, cell death and cytokine processing(Drummond & Brown, 2011; Deretic *et al*, 2013; Broz & Dixit, 2016). The coordination of all these pathways initiates an innate immune response, which is essential for microbial control and induction of an appropriate adaptive immune response(Palm & Medzhitov, 2009).

A common theme that has emerged in the PRR field is the use of adaptor proteins. These proteins are capable of integrating signals, often from multiple types of receptors and couple these receptors to enzymatic effector proteins. Some of the adaptor proteins and their receptors are summarized in **Table 2**. The role of these adaptors often seems to go beyond a simple coupling-protein function connecting the sensor protein/s to the effector protein/s. Indeed, most of these adaptors for oligomers or filamentous assemblies (ASC speck, Myddosome) which are thought to be necessary for signal amplification (Dick *et al*, 2016; Lin *et al*, 2010; Qiao *et al*, 2013)

Adaptor or Adaptor set	**Receptor interaction**	**Examples for receptors using adaptor**	**Signaling interaction**	**Localization**
TIRAP/MyD88	TIR domain	TLR2,4,5	Death domain	Cell surface, endosomal compartments
TRAM/TRIF	TIR domain	TLR3,4	TRAF binding, RHIM domain	Cell surface, endosomal compartments
MAVS	CARD domain	RIG-I	Proline-rich region, TRAF binding	Mitochondrial, peroxisomal and mitochondria associated membranes
ASC	Pyrin domain	NLRs, AIM2	CARD domain	Cytosol

Table 2 Adaptor proteins of PRRs

Charles Janeway predicted two key features of innate immunity: 1) The ability to distinguish self from non-self and 2) the ability to activate the innate immune system(Janeway, 1989). Since his predictions, researcher could show that a variety of microbial molecules are recognized by PRRs and how these pathways lead to the mounting of an effective immune response(Akira & Takeda, 2004; Geijtenbeek & Gringhuis, 2009; Chen *et al*, 2009; Loo & Gale, 2011; Hornung & Latz, 2010).

3.3 PRR signaling from the plasma membrane

3.3.1 Toll like receptors

TLR4 is the best studied member of this family and possesses some unique features that distinguishes it from the other members of the TLR family. TLR4 recognizes a variety of bacterial and endogenous ligands but is best known for its high sensitivity for Lipopolysaccharide (LPS) from gram-negative bacteria(Poltorak *et al*, 1998). Activation of TLR4 by LPS requires a multi-receptor complex composed of LPS-binding protein (LBP), CD14 and MD2, which are required to bind LPS and transfer it to TLR4 to induce its dimerization(Schumann *et al*, 1990; Eckert *et al*, 2013; da Silva Correia *et al*, 2001; Gioannini & Weiss, 2007). The sequential transfer of LPS from one molecule to another is thought to enable high sensitivity of TLR4 for LPS. It has been estimated that enough LPS monomers can be extracted from one bacterium to activate TLR4 signaling on 1000 macrophages (Gioannini & Weiss, 2007). Upon activation, TLR4 recruits TIRAP (TIR Domain-Containing Adaptor Protein) and MyD88, which culminates in the activation of NF-kB and AP-1 leading to expression of pro-inflammatory cytokines like IL-1ß or TNFα (**Figure 3.1**). TLR4 is also internalized to endosomes, where it recruits different adaptor proteins and engages additional signaling pathways (discussed below).

Other TLRs present on the plasma membrane are TLR1, -2, -5 and -6. All these receptors engage MyD88 (Myeloid differentiation primary response 88) dependent NF-κB (nuclear factor 'kappa-light-chain-enhancer' of activated B-cells) activation. TLR2 mainly acts as heterodimer with other TLRs(Ozinsky *et al*, 2000). TLR2 forms heterodimers with either TLR-1 or TLR6, and is activated by a variety of lipopeptides and viruses(Buwitt-Beckmann *et al*, 2006; Boehme *et al*, 2006; Szomolanyi-Tsuda *et al*, 2006; Kurt-Jones *et al*, 2004; Chang *et al*, 2007; Erridge, 2010). Similar to TLR4, these heterocomplexes signal from lipid rafts(Triantafilou *et al*, 2004) and use co-receptors, for example CD36 (Hoebe *et al*, 2005). In a cell type specific manner (Plasmacytoid DCs), TLR2 can lead to interferon (IFN) production upon endocytosis(Barbalat *et al*, 2009; Dietrich *et al*, 2010).

TLR5 is expressed on neutrophils, monocytes, DCs and epithelial cells(Shibata *et al*; Gewirtz *et al*, 2001) and is the receptor for bacterial flagellin(Hayashi *et al*, 2001; Smith *et al*, 2003). TLR5 also activates MyD88 dependent signaling(Hayashi *et al*, 2001), however it is not clear if TIRAP is required in all cell types(Choi *et al*, 2012).

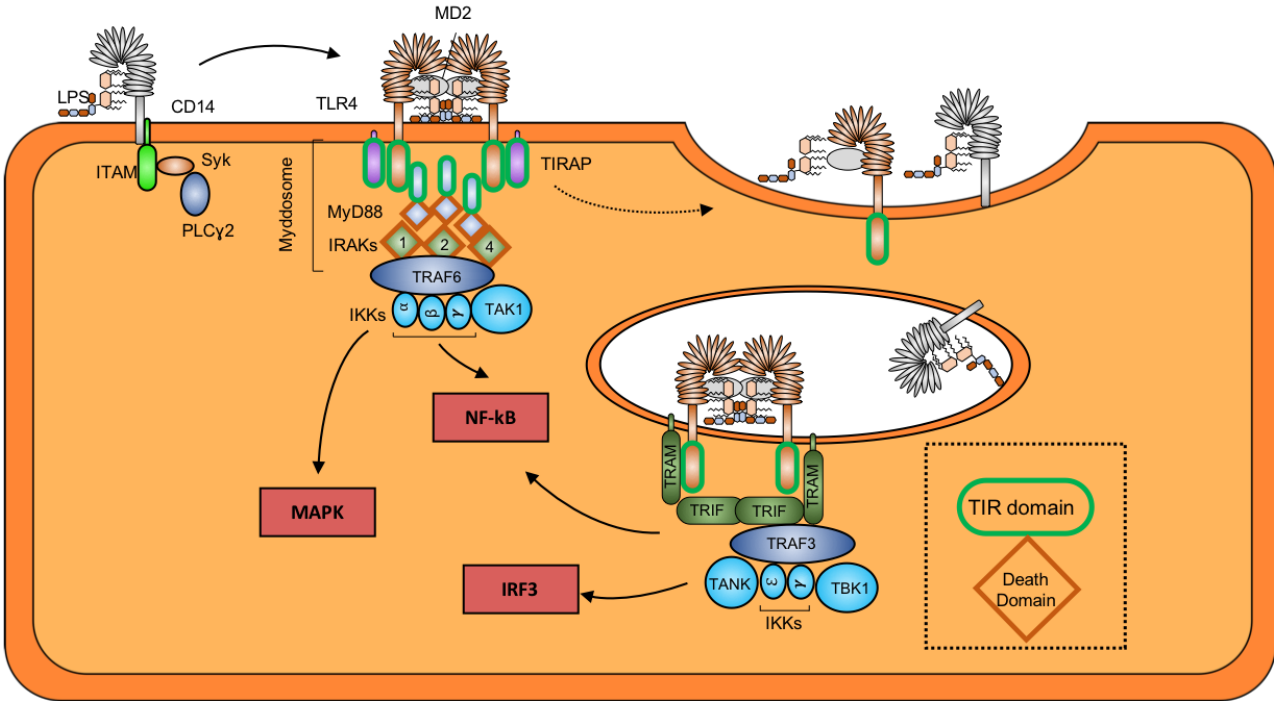

Figure 3.1 TLR4 signaling

TLR4 signals from the plasma membrane and endosomes. TLR4 requires translocation to lipid rafts enriched with TIRAP for signaling from the plasma membrane. This facilitates interactions with MyD88 upon ligand binding for the formation of the myddosome containing MyD88, TIRAP, and IRAKs. The IRAKs recruit the E3 ubiquitin ligase TRAF6, which interacts with a complex formed by TAB1, TAB2, TAB3, and TAK1. This complex regulates NF-κB activation via IKKs. TAK1 release into the cytoplasm also directs MAPK activation. CD14 controls the movement of TLR4 from the plasma membrane into endosomes through the activation of ITAM, Syk, and PLCγ2. From endosomes, TLR4 interacts with the sorting adaptor TRAM and the signaling adaptor TRIF to sustain NF-κB activation and to induce IRF3-mediated type I IFN production. IRF3 activation controls type I IFN production and requires TRAF3 recruitment to TRIF. TRAF3 then interacts with TANK (or TANK-related proteins) to recruit IKKγ, IKKε, and TBK1, which activate IRF3. (Solid lines indicate signal transduction; dotted lines indicate trafficking events.) (Abbreviations: IKK, IκB kinase; IRAK, interleukin-1 receptor-associated kinase; IRF, IFN regulatory factor; ITAM, immunoreceptor tyrosine-based activation motif; MAPK, mitogen-activated protein kinase; NF-κB, nuclear factor-κB; PLCγ2, phospholipase Cγ2; TAK, TGF-β-activated kinase; TANK, TRAF family member–associated NF-κB activator; TBK, TANK-binding kinase; TIRAP, TIR-containing adaptor protein; TRADD, TNF receptor type 1–associated death domain; TRAF, TNF receptor–associated factor.) Adapted from (Brubaker *et al*, 2015).

3.3.2 Dectins

CLRs are a heterogeneous group of hundreds of receptors, which share a characteristic C-type lectin-like domain (CTLD). The CTLD was identified as a double-loop domain capable of binding calcium and carbohydrates but up to today, CLRs have been shown to bind a variety of different ligands. Dectin-1 and -2 are the best studied members of this class of receptors, which is further divided into 17 sub-families(Brubaker *et al*, 2015). Most dectins act as opsonins, however for example Dectin-1 is capable of activating NF-kB upon recognition of fungal beta-1,3-glucans, which promotes phagocytosis and downstream signaling. Dectin-1 activates Syk kinases(Fuller *et al*, 2007), which are responsible for NF-kB activation and in turn are also capable of activating PLC(phospholipase-c) γ2, which promotes additional NFAT (nuclear factor of activated T-cells) activation (Tassi *et al*, 2009). Dectin-1 has been shown to be essential for anti-fungal-defense in both mice and humans(Brown *et al*, 2003; Ferwerda *et al*, 2009).

3.4 Signaling from endosomes

3.4.1 TLR signaling from endosomes

As mentioned above, TLR4 undergoes endocytosis but interestingly, signaling is not terminated at this point, like for many other receptors e.g. GPCRs (G-protein coupled receptors). TLR4 continues to signal from endosomes inducing a late wave of NF-κB activation and, importantly, type I IFN production. Both pathways are dependent on the adaptors TRAM (TIR Domain-Containing Adaptor Protein) and TRIF(TIR-domain-containing adaptor inducing interferon-β)(Yamamoto *et al*, 2003a; 2003b). TRAM moves independently of CD14 from the plasma membrane to endosomes and it is thought that TRAM displaces TIRAP from TLR4, leading to engagement of the TRIF dependent signaling pathways(Kagan *et al*, 2008; Enokizono *et al*, 2013; Piao *et al*, 2013). TRIF is capable of recruiting TRAF3 to induce TBK1 and subsequent IRF3 activation, leading to type I IFN production (**Figure 3.1**)(Häcker *et al*, 2006; Fitzgerald *et al*, 2003; Hemmi *et al*, 2004; McWhirter *et al*, 2004). How TRIF controls late NF-κB activation is not entirely clear, though it seems to be dependent on RIPK1, TRADD and caspase-8(Weng *et al*, 2014; Brubaker *et al*, 2015).

Other TLRs that signal from endosomes recognize different varieties of nucleic acids and induce type I IFNs, partially in a cell type specific manner. TLR3 recognizes dsRNA molecules and induces type I IFN production through, TRIF, but independently of TRAM, as the TIR domain of TLR3 is capable of directly binding TRIF(Brown *et al*, 2006; Ulrichts & Tavernier, 2008). In pDCs, TLR7/9 are capable of inducing type I IFN production through a MyD88/IRF7 dependent signaling axis, however which other factors are required for this process is not entirely clear(Honda *et al*, 2005).

3.4.2 NOD1/2 signaling from endosomes

With their N-terminal CARD (Caspase activation and recruitment domain), their central NACHT and their C-terminal LRR (Leucine rich repeat) domain, NOD1/2 are prototypical members of the NLR (Nod like receptor) family(Saleh, 2011). They recognize components of the bacterial outer membranes or cell wall like γD-glutamyl-meso-diaminopimelic acid (iE-DAP) or muramyl dipeptide (MDP)(Girardin *et al*, 2003a; 2003b; Chamaillard *et al*, 2003). Upon activation, they associate with RIPK2 to induce MAPK and NF-kB activation(Park *et al*, 2007). Although synthesized in the cytosol, NOD1 and NOD2 have been observed to localize to endosomes(Barnich *et al*, 2005; Irving *et al*, 2014; Nakamura *et al*, 2014; Travassos *et al*, 2010). Interestingly a Crohn´s disease associated NOD2 mutant, which is not activated by MDP, also shows aberrant subcellular localization(Barnich *et al*, 2005). Independent of NF-kB activation, NODs can induce autophagy to eliminate bacterial pathogens(Travassos *et al*, 2010). This function is also impaired in cells expressing the Crohn´s disease –associated NOD2 variant.

3.5 PRR signaling in the cytosol

3.5.1 Rig-I like receptors

Three DExH/D box helicases, retinoic acid-inducible gene-I (RIG-I), melanoma differentiation gene 5 (MDA5) and laboratory of genetics and physiology 2 (LGP2), make up the RLR family. All of these proteins detect the presence of RNA in the cytosol(Yoneyama *et al*, 2005; 2004) and although they are generally depicted as cytosolic proteins, they might localize to specific locations, where viral entry or replication takes place. To distinguish self from viral RNA, RLRs detect motifs and features, specific to viral genomes or replication

intermediates like 5' triphosphate RNA, long dsRNA and specific sequences such as the poly-U region of the hepatitis C virus RNA(Hornung *et al*, 2006; Pichlmair *et al*, 2009; 2006; Kato *et al*, 2008; Saito *et al*, 2008; Uzri & Gehrke, 2009). Upon activation by cytosolic RNA, MDA5 and RIG-I bind to MAVS (mitochondrial anti-viral signaling protein) via CARD-CARD interaction for further downstream signaling(Seth *et al*, 2005; Kawai *et al*, 2005; Meylan *et al*, 2005; Xu *et al*, 2005). Similar to TLRs, RIG-I undergoes ligand induced translocation to the limiting membranes of mitochondria, peroxisomes and the mitochondrial outer membrane (MAM), where MAVS are localized(Seth *et al*, 2005; Dixit *et al*, 2010; Horner *et al*, 2011). Upon activation, MAVS undergo CARD mediated self-polymerization, which leads to recruitment of the ubiquitin ligases TRAF-2,-5 and-6, which are required for activation of TBK1 (Tank binding kinase 1) and the IKK (inhibitor of κB kinase) complex(Liu *et al*, 2013). These kinases promote the activation of NF-kB, IRF3 and IRF7, which ultimately leads to production of IFNs, pro-inflammatory cytokines and interferon stimulated gens (ISGs) (**Figure 3.2a**). Interestingly, the ability of MAVS to initiate IFN signaling is strictly dependent on its C-terminal transmembrane domain, which shows that interaction with RLRs is not sufficient to trigger downstream signaling, but that MAVS activation is regulated by receptor recruitment and proper membrane localization(Seth *et al*, 2005; Dixit *et al*, 2010).

3.5.2 Cytosolic DNA sensing: The cGAS/STING signaling axis

The stimulator of IFN genes (STING) hast been known to be involved in cytosolic DNA sensing and promotion of downstream signaling(Ishikawa & Barber, 2008; Zhong *et al*, 2008; Sun *et al*, 2009). STING has been proposed to act both, as an adaptor and receptor in different scenarios. During viral infections it has been proposed to act as an adaptor for potential DNA sensors like IFI16 and DDX41, although the exact mechanisms were unclear(Unterholzner *et al*, 2010; Zhang *et al*, 2011). Induction of IFN responses upon infection with cytosolic bacteria by STING could be well explained, as STING is activated by cyclic di-nucleotides (CDNs), which are second-messengers frequently produced in and even secreted from bacteria(Burdette *et al*, 2011; Yin *et al*, 2012; Ouyang *et al*, 2012; Huang *et al*, 2012; Shang *et al*, 2012; Shu *et al*, 2012). Although CDNs synthesis has been thought be a unique feature of bacteria, the mammalian CDNs synthase cGAS (cyclic di-GMP-AMP synthase) has been identified(Wu *et al*, 2013; Sun *et al*, 2013). Upon binding of cytosolic

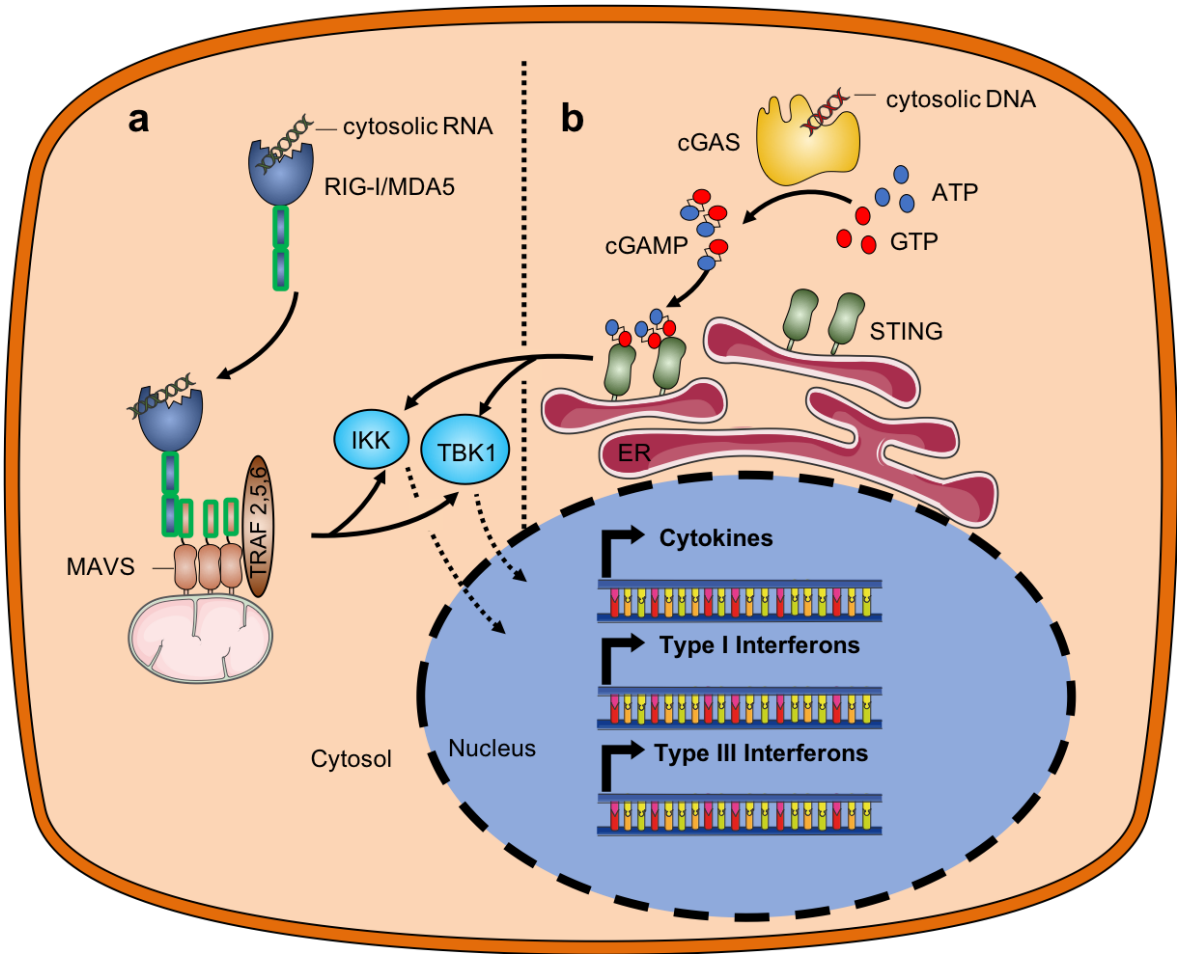

Figure 3.2 Nucleic acid sensing in the cytosol
The RLRs detect pathogen-derived RNA within the cytosol to induce the production of IFN and pro-inflammatory cytokines. The TBK1, IKK, and MAVS pathways lead to activation of the transcription factors for the induction of IFN and other cytokine genes. MAVS activity is regulated by polymerization and signaling from mitochondria results in production of type I and III IFN, whereas peroxisomal signaling induces the production only of type III IFN. (b) cGAS detects pathogen-derived DNA from within the cytosol and nucleus to induce the production of IFN. In the presence of DNA, the enzyme cGAS converts ATP and GTP to the cyclic dinucleotide cGAMP. Production of cGAMP induces the activation of STING. TBK1 is recruited to this site of signaling to induce the production of type I IFN. (Solid lines indicate signal transduction; dotted lines indicate trafficking events.) (Abbreviations cGAMP, cyclic di-GMP/AMP; cGAS, cyclic GMP-AMP synthase; IKK, IκB kinase; MAVS, mitochondrial antiviral signaling protein; MDA, melanoma differentiation gene; RIG-I, retinoic acid–inducible gene I; STING, stimulator of IFN gene; TBK, TANK-binding kinase; TRAF, TNF receptor–associated factor). Adapted from *Brubaker et al., 2015*.

DNA stretches, cGAS synthesizes cyclic-di-GMP-AMP (cGAMP) from ATP and GTP, which acts as a second messenger, binds and activates STING. STING is a localized at the ER during steady state and undergoes trafficking to poorly defined vesicles or puncta at the

GOLGI apparatus(Ishikawa & Barber, 2008; Saitoh *et al*, 2009). This relocation is dependent on ATG9a and VPS34, leads to activation of TBK1 and IRF3 and subsequent IFN production(Saitoh *et al*, 2009; Konno *et al*, 2013)(**Figure 3.2b**). The cGAS/STING signaling axis seems to be the sensor in most scenarios, ranging from recognition of nuclear self-DNA, infection with DNA viruses, cytosolic bacteria or engulfment of dead cells (reviewed in (Chen *et al*, 2016a)).

3.5.3 Canonical inflammasomes

In 2002, Tschopp and co-workers described a high molecular weight complex that is formed in the cytosol of stimulated immune cells and that mediates the activation of inflammatory caspases, hence termed an inflammasome (Martinon *et al*, 2002). Since then, the field has expanded rapidly and our understanding of activation and regulation of inflammasome signaling has increased tremendously. Canonical inflammasomes consist of a PRR, which recognizes microbial molecules(Moltke *et al*, 2013) or other signals altering the homeostasis of the cytosol(Liston & Masters, 2017). Upon activation, the receptors oligomerize and recruit the adaptor protein ASC (Apoptosis-associated speck-like protein containing a CARD, also called PYCARD, because it has a Pyrin domain (PYD) and a Caspase recruitment domain (CARD)), which forms a large oligomeric structure, referred to as the 'ASC Speck' (Broz *et al*, 2010; Guey *et al*, 2014). ASC is required to bridge the receptor to pro-caspase-1 and the formation of the ASC speck is an efficient mechanism for signal amplification to enhance caspase-1 activation(Dick *et al*, 2016). Recruitment of pro-caspase-1 leads to proximity induced autoproteolytic cleavage and activation of the caspase. Caspase-1, cysteine-specific aspartate directed protease, then induces two main signaling pathways: 1) the proteolytic maturation and release of pro-inflammatory cytokines like IL-1β and IL-18 and 2) the cleavage and activation of gasdermin-D(Kayagaki *et al*, 2015; Shi *et al*, 2015a), which is capable for permeabilizing cellular membranes through the formation of pores(Liu *et al*, 2016; Sborgi *et al*, 2016; Aglietti *et al*, 2016; Chen *et al*, 2016b; Ding *et al*, 2016) leading to a pro-inflammatory, lytic form of cell death called pyroptosis(Fink & Cookson, 2005).

To date, five different receptors which form inflammasomes have been identified. The nucleotide binding oligomerization domain (NOD), leucine-rich repeat (LRR)-containing protein (NLR) family members NLRP1, NLRP3 and NLRC4, the PYHIN protein AIM2 and the protein pyrin (reviewed in(Broz & Dixit, 2016)). The molecular activation mechanisms

of these inflammasomes are fairly well understood and the mechanisms underlying NLRP3, NLRC4 and AIM2 activation, which are relevant to my work, are discussed below.

3.5.3.1 NLRP3

The NLRP3 inflammasome (also known as cryopyrin), responds to a variety of different stimuli, among them crystalline substances like monosodium urate (MSU), bacterial pore forming toxins (nigericin, gramicidin), extracellular ATP and a variety of viral and bacterial pathogens(Latz *et al*, 2013). Given the diversity of these stimuli, it is likely that all these stimuli converge on one common cellular event, to trigger NLRP3 activation. To date, several possible triggers, including mitochondrial reactive oxygen species (mtROS) (Groß *et al*, 2016), mitochondrial DNA release(Shimada *et al*, 2012), lysosomal rupture(Hornung *et al*, 2008) and others have been implicated. It has been convincingly shown by several groups, that potassium efflux from the cytosol is one common event for a large variety of stimuli(Rühl & Broz, 2015; Muñoz-Planillo *et al*, 2013; Gross *et al*, 2012). The hypothesis, that potassium efflux is one important step during NLRP3 activation is underpinned by the fact, that low potassium medium is capable of activating NLRP3 independently of sodium and calcium influx(Muñoz-Planillo *et al*, 2013) and this activation is not blocked by mitochondrial ROS scavengers (S.R. and P.B. unpublished observations). Recently an additional regulator of the NLRP3 inflammasome, the NIMA related kinase 7 (NEK7), was identified(He *et al*, 2016; Schmid-Burgk *et al*, 2015a; Shi *et al*, 2016). NEK7 directly interacts with NLRP3, in manner dependent on potassium efflux to induce its oligomerization. Interestingly the catalytic domain of NEK7, but not the catalytic activity is required for NLRP3 activation (**Figure 3.3c**(He *et al*, 2016).

While other inflammasomes are mainly involved in host defense against pathogens, several NLRP3 gain-of-function mutations(Meng *et al*, 2009; Brydges *et al*, 2009) have been identified, which lead to auto-inflammatory diseases referred to as Cryopyrin-Associated Periodic Syndromes (CAPS). The disease pathology is mainly caused by massive, periodic IL-1 production, as treatment with an IL-1R antagonist provides significant improvement in mice carrying these mutations(Meng *et al*, 2009).

3.5.3.2 NAIP-NLRC4

NLRC4 was initially identified due to its homology to apoptotic protease activating factor 1 (APAF1). It was shown, that bacterial flagellin(Mariathasan *et al*, 2004; Miao *et al*, 2006;

Franchi *et al*, 2006) and components of the bacterial Type-3 secretion system (T3SS)(Zhao *et al*, 2011; Miao *et al*, 2010) activate the NLRC4 inflammasome. Interestingly, NLRC4 is not the receptor for these ligands but it uses the NLR family, apoptosis inhibitory proteins (NAIPs) as receptors. In murine cells, binding of their cognate ligands by NAIP proteins - the T3SS rod is bound by NAIP2, the T3SS needle by NAIP1 and flagellin by NAIP5 and NAIP6 - allows a conformational change and binding to NLRC4(Zhao *et al*, 2011; Kofoed & Vance, 2011). It was always thought that ligand binding happens via the LRR of NLRC4, but instead NAIPs bind NLRC4 via the NOD domain(**Figure 3.3b**)(Tenthorey *et al*, 2014). Human cells only have one NAIP gene, but it was shown recently, that an extended isoform *NAIP** is expressed in primary human monocyte-derived macrophages, which confers responsiveness to Salmonella flagellin(Kortmann *et al*, 2015).

3.5.3.3 AIM2

The observation that microbial and host derived cytosolic DNA induces caspase-1 activation, dependent on ASC, but independent of NLRP3, TLRs or interferons, prompted the hypothesis that there must be a dedicated cytosolic DNA receptor leading to inflammasome formation(Muruve *et al*, 2008). Several groups showed that the absent in melanoma 2 (AIM2), a member of the PYHIN (Pyrin and HIN domain-containing) family is the responsible sensor(Hornung *et al*, 2009; Fernandes-Alnemri *et al*, 2009; Roberts *et al*, 2009). The N-terminal pyrin domain (PYD) is responsible for recruitment of ASC upon activation by DNA stretches, which bind to the C-terminal HIN-200 domain. AIM2 binds DNA via the sugar-phosphate backbone, therefore there exists no sequence specificity towards any kind of DNA (Hornung *et al*, 2009; Jin *et al*, 2012). Generation of *Aim2*$^{-/-}$ deficient mice confirmed the importance of the AIM2 inflammasome in host defense against DNA viruses and, surprisingly, against bacterial pathogens like *Francisella tularensis* subspecies *novicida* or *Listeria monocytogenes*(**Figure 3.3a**)(Sauer *et al*, 2010). AIM2 has been implicated in a variety of human diseases among then systemic lupus erythematosus(Dihlmann *et al*, 2014a; Dombrowski *et al*, 2011; Dihlmann *et al*, 2014b), Psoriasis(Dombrowski *et al*, 2011) and the development of colorectal cancer(Ponomareva *et al*, 2013; Wilson *et al*, 2015; Man *et al*, 2015). Interestingly, a recent study showed that pharmacological disruption of the nuclear envelope leads to AIM2 dependent inflammasome activation, providing strong evidence that in a variety of scenarios, leakage of self-DNA from the nucleus can have detrimental consequences(Di Micco *et al*, 2016).

3.5.4 Non-canonical inflammasome

Besides canonical inflammasomes, recently a non-canonical inflammasome pathway has been discovered(Kayagaki *et al*, 2011). Kayagaki *et al*. found that murine BMDMs infected with gram-negative bacteria die by pyroptosis, which is dependent on the presence and catalytic activity of caspase-11 and independent of caspase-1(Kayagaki *et al*, 2011). They could show that the *Casp1*-deficient mice, which were widely used at the time, are actually *Casp1/Casp11* double deficient mice, due to a passenger mutation originating from 129S mice, which only express a truncated and non-functional version of caspase-11(Kayagaki *et al*, 2011). Importantly, caspase-11 is the central mediator of septic shock during injection of bacterial Lipopolysaccharide (LPS), a model of endotoxemia. Subsequently it was shown that bacterial LPS is the ligand for caspase-11, leading to its activation(Kayagaki *et al*, 2013; Hagar *et al*, 2013). Another study showed surprisingly that this activation happens via direct binding of LPS to the CARD domain of caspase-11 (-4/-5 in humans), therefore establishing the model, that caspase-11 is at the same time the receptor and the effector caspase of the non-canonical inflammasome pathway(Shi *et al*, 2014). Caspase-11 is not capable of cleaving IL-1β but instead induces potassium efflux to activate NLRP3 in a cell autonomous manner to promote cytokine secretion(**Figure 3.3d,** (Rühl & Broz, 2015; Baker *et al*, 2015; Schmid-Burgk *et al*, 2015b).

Recently, it was proposed that beyond recognition of LPS through its CARD domain, caspase-11 binds endogenous oxidized lipids via its catalytic domain and triggers activation of the non-canonical inflammasome pathway. Interestingly this kind of activation only triggers IL-1β maturation but not cell death in dendritic cells and induces a state of so-called 'DC hyperactivation'. The authors show that the K_d for oxPAPC, the mixture of oxidizes phospholipids that binds to the catalytic domain of caspase-11, is 100 fold lower than the K_d for LPS, which could explain, why this low level activation only triggers Nlrp3 mediated cytokine secretion, without killing dendritic cells(Zanoni *et al*, 2016). A follow up study identified internalization by CD14 mediated endocytosis as a critical step for immune cell hyperactivation and two specific phospholipids (PGPC, POVPC) as stimulators of hyperactivation in BMDMs(Zanoni *et al*, 2017). It remains to be determined, if other lipid species are capable of activating caspase-11, which could establish a broader role for caspase-11 in sensing of pro-inflammatory lipid mediators.

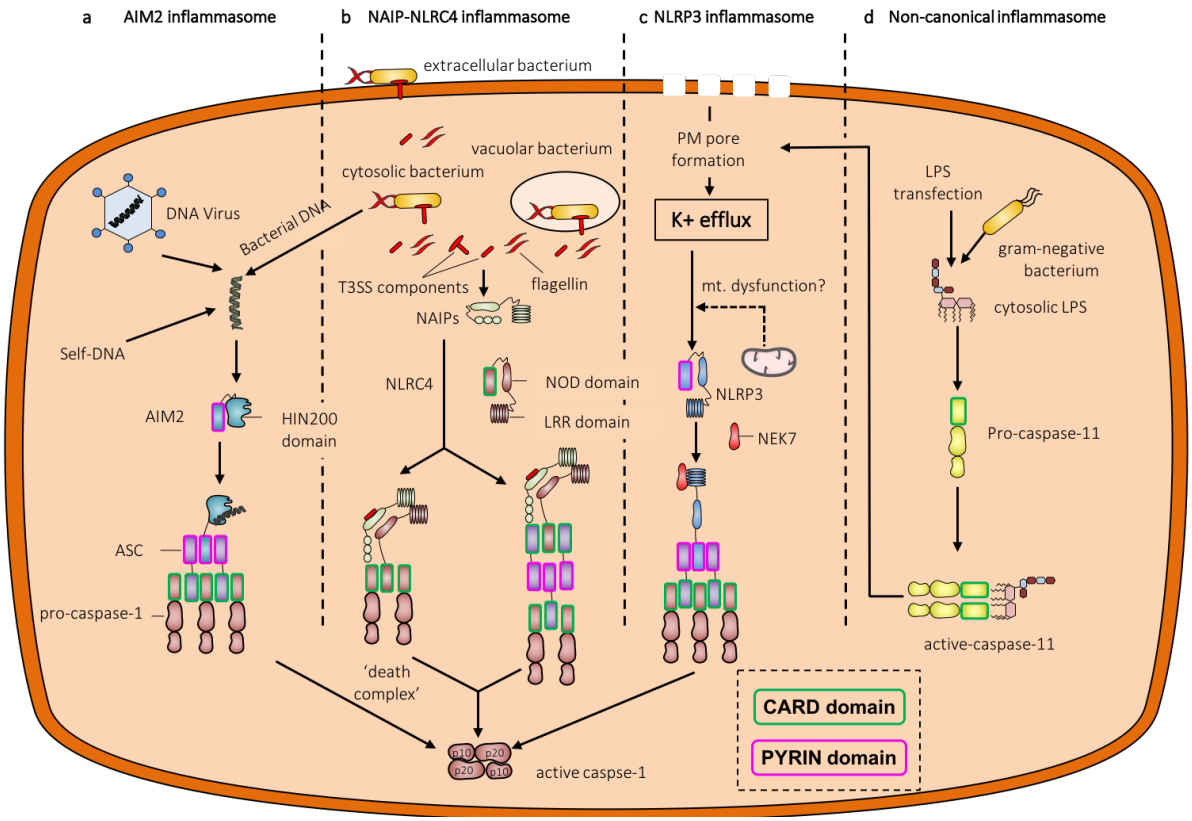

Figure 3.3 Canonical inflammasomes

a The AIM2 inflammasome detects the presence of endogenous or exogenous cytosolic DNA via its HIN200 domain. Binding of DNA leads to a conformational change and binding of ASC via the pyrin domain, which recruits pro-caspase-1. **b** The NAIP-NLRC4 inflammasome recognizes components of the T3SS and flagellin of gram-negative bacteria. Also extracellular bacteria can activate this inflammasome as the T3SS accidentally co-translocates flagellin molecules upon injection of effectors into the host cytosol or parts of the needles disintegrate after injection at the cytosolic side of the PM. NAIPs bind the bacterial proteins to activate NLRC4, which in turn exposes its CARD domain. Exposure of the CARD domains leads either to direct recruitment of pro-caspase-1('death complex') and activation, resulting in cell death with little cytokine maturation or in recruitment of ASC through CARD-CARD interaction, which in turn recruits more ASC and pro-caspase-1 which results in strong caspase-1 activation, cell death and more IL-1β maturation. **c** Formation of pores in the PM through channel opening (e.g. by extracellular ATP stimulation) or pore forming toxins (e.g. nigericin) leads to potassium efflux, which is required for most NLRP3 stimuli. For some stimuli, mitochondrial dysfunction and generation of mtROS might be required downstream of potassium efflux. Activation of NLRP3 requires recruitment of NEK7 to induce oligomerization and subsequent recruitment of ASC and pro-caspase-1. **d** Cytosolic LPS, either delivered artificially or during gram-negative bacterial infection is recognized by the CARD of caspase-1, which upon binding to LPS, oligomerizes and gets activated. To date it is not clear, if autoproteolytic cleavage is required or sufficient for caspase-11 activation. Active caspase-11 is induces potassium efflux in a cell autonomous manner to induce NLRP3 inflammasome activation.

3.6 Effector functions of inflammasome activation

3.6.1 Cytokine maturation and release

Caspase-1 was initially described as ICE (Interleukin converting enzyme)(Dandekar & Argos, 2008), as it processes IL-1β and IL-18 into their mature, bioactive forms. Expression of IL-1β and the closely related IL-1α are induced through TLR stimulation, whereas IL-18 is expressed constitutively(Gross *et al*, 2012). As discussed, IL-1β and IL-18 require processing by caspase-1 to be active, whereas IL-1α can be processed by caspase-1 but is active without processing and is released as an active cytokine also during caspase-1-independent lysis e.g. necroptosis(Wallach *et al*, 2016) or caspase-11-mediated pyroptosis(Kayagaki *et al*, 2011). Besides release of mature cytokines by lysis, several other mechanisms for 'unconventional secretion' have been implicated (discussed below), however recent studies unraveled that at least in BMDMs, pyroptosis constitutes the main release mechanism for mature cytokines after caspase-1 activation (**Figure 3.4**(Shi *et al*, 2015a).

3.6.2 Pyroptosis

Pyroptosis was first described by Fink and Cookson as a lytic, non-apoptotic caspase-1 driven cell death, characterized by cell swelling (probably due to membrane pore formation) and the subsequent lysis of the cells (Fink & Cookson, 2005). The name originates from the Greek 'pyro' (fire or fever) and 'ptosis' (to fall) indicating the pro-inflammatory nature of this cell death(Fink & Cookson, 2005). After years of research, two seminal studies in 2015 demonstrated that one substrate, gasdermin-D, of both, caspase-1 and caspase-11 is essential for induction of pyroptosis. Generation of *Gsdmd*-deficient cells and mice showed that gasdermin-D is essential for pyroptosis and activation of the non-canonical inflammasome pathway during LPS transfection and LPS induced septic shock in mice (**Figure 3.4**(Shi *et al*, 2015a; Kayagaki *et al*, 2015)). Caspase-1 driven pyroptosis depends only at early time points on gasdermin-D but prolonged caspase-1 activation results in gasdermin-D independent pyroptosis, probably due to activation of caspase-8 in response to ASC speck formation (Sagulenko *et al*, 2013) or cleavage of other cellular substrates by caspase-1 (Kayagaki *et al*, 2015; Heilig *et al*, 2017).

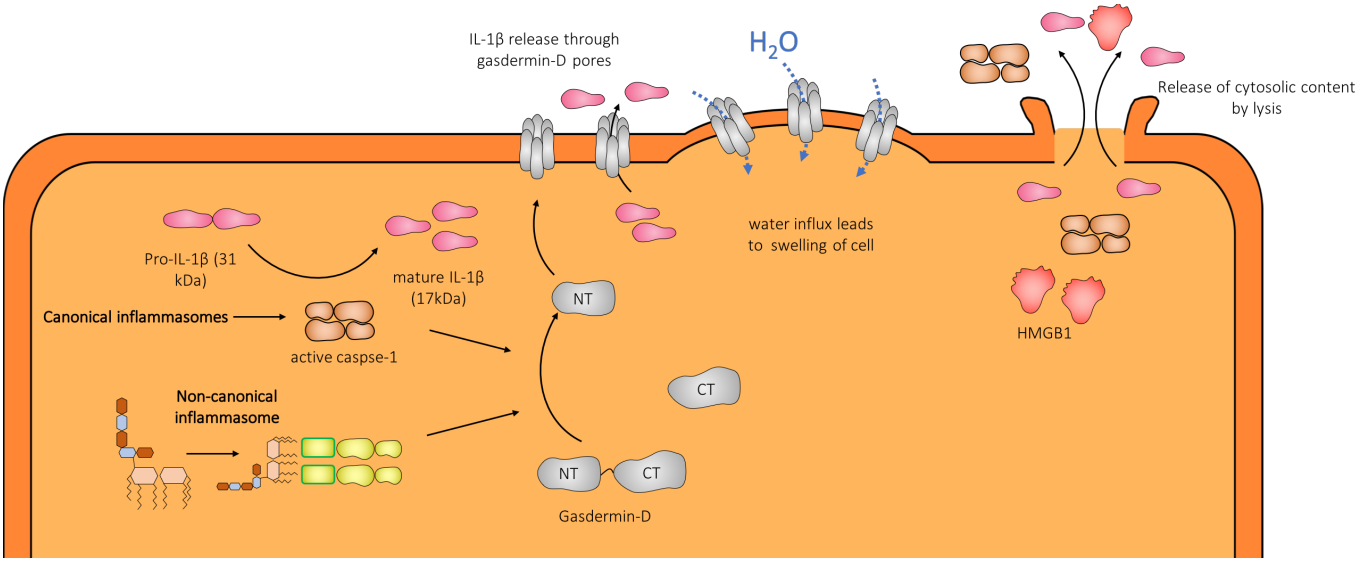

Figure 3.4 Effector functions of inflammasome activation

Active caspase-1 and caspase-11 both cleave gasdermin-D into a soluble C-terminal fragment (CT) and a cytotoxic, pore forming N-terminal fragment (NT), which translocates to cellular membranes to permeabilizes them. Caspase-1 cleaves pro-IL-1β into its mature form, which is released partially through gasdermin-D pores. Pore formation leads to water influx, swelling of cells and subsequent lysis accompanied by release of cytosolic content.

3.7 Gasdermin family of proteins

The gasdermin family of proteins is conserved in vertebrates and composed of four paralogues in humans (GSDMA, GSDMB, GSDMC and GSDMD). Mice lack GSDMB but have four Gsdmc homologues and three Gsdma homologues. Members of the gasdermin family share a distinct N-terminal and a C-terminal region connected by a linker region. This feature is shared by the Dfna5 and the Dfnb59 genes, which can be considered to be extended family members. The N-termini of all members (except Dfnb59) display similar cytotoxic properties to the gasdermin-D N-terminal fragment.

3.7.1 Gasdermin-D

Gasdermin-D is the best studied family member, as its role in pyroptosis induction downstream of inflammatory caspase activation has been investigated thoroughly. As discussed above, gasdermin-D is a substrate of both caspase-1 and caspase-11 and cleavage of gasdermin-D by these caspases at Asp276 is essential for pyroptosis induction (Kayagaki *et al*, 2015; Shi *et al*, 2015a). The N-terminal fragment is the active part of gasdermin-D, as its expression leads to pyroptotic morphology and cell death, whereas the C-terminal fragment does not kill cells upon expression. We and several other groups could show that the $GSDMD^{Nterm}$ translocates to cellular membranes upon cleavage by inflammatory caspases, where it forms pores and permeabilizes membranes (Liu *et al*, 2016; Sborgi *et al*, 2016; Aglietti *et al*, 2016; Chen *et al*, 2016b; Ding *et al*, 2016). Formation of these pores leads to breakdown of the electrochemical gradient across the PM and water influx due to osmotic pressure. The combination of these events ultimately leads to swelling, rupture and lysis of the cell.

It is thought, that the C-terminal fragment acts a solubilization factor or ‘chaperone’ for the N-terminal fragment, to prevent cytotoxicity prior to cleavage. This hypothesis is supported by the observation, that the cytotoxic activity of the gasdermin-A N-terminus can be inhibited by expressing the C-terminal fragment independently(Ding *et al*, 2016; Shi *et al*, 2015a). Therefore, pore formation by gasdermin-D represents the final step during pyroptosis induction by inflammatory caspases.

3.7.2 DFNA5/Gasdermin-E

Deafness autosomal dominant 5 (DFNA5), originates from the discovery of the gene, as mutations in the *Dfna5* gene cause heritable, nonsyndromal deafness, characterized by gradual hearing loss, typically starting at high frequency at the age of 15(Bischoff *et al*, 2004; van Laer *et al*, 1998). Bioinformatic analysis shows, that DFNA5 has putative caspase-3 cleavage site within the region, connecting the N-terminal and the C-terminal region. It was shown that DFNA5 expressing cells undergoing apoptosis, and therefore caspase-3 activation, rather dye by a necrotic cell death, characterized by cell swelling, rupture and lysis, rather than condensation and formation of apoptotic bodies. These findings implicate DFNA5 to operate as critical switch between apoptosis and secondary necrosis(Rogers *et al*, 2017). A second study could confirm these results, however the authors also went on to show, that DFNA5 (or gasdermin-E as they call it) is suppressed in many cancer cells and that enforced expression of DFNA5 enhances lytic cell death of cancer cells upon chemotherapy drug exposure. Furthermore, chemotherapy induced toxicity and inflammation was ablated in DFNA5 deficient animals(Wang *et al*, 2017). The DFNA5 N-terminal fragment, similar to the $GSDMD^{Nterm}$, permeabilizes membranes through the formation of pores after cleavage and separation from the C-terminus, explaining the mechanism how DFNA5 promotes necrotic cell death after caspase-3 activation. Further research needs to determine the physiological role of DFNA5 during apoptosis and its expression and function in specific tissues.

3.7.3 Other gasdermin family members

Multiple spontaneous mutations in gasdermin-A3 have been identified to lead to hyperkeratosis and spontaneous alopecia(Runkel *et al*, 2004; Lunny *et al*, 2005; Tanaka *et al*, 2007; Li *et al*, 2010; Zhou *et al*, 2012). The disease-causing mutations have been shown to disrupt the interaction between the cytotoxic N-terminal domain and the C-terminal part of the protein, leading to pore formation and cytotoxicity without cleavage of the linker region (10). This explains the inflammation as a depletion of skin bulge stem cells observed in mice with *Gsdma3* mutations(Zhou *et al*, 2012; Shi *et al*, 2015b). SNPs in both, human *Gsdma* and *Gsdmb*, are associated with asthma in multiple populations(Yu *et al*, 2011; Wu *et al*, 2009b; Moffatt *et al*, 2007; 2010). The N-terminal region of gasdermin-B can be cleaved by apoptotic caspases, and thus might lead to inactivation of the protein during apoptosis(Chao

et al, 2017), however if there is any biological relevance to this observation remains to be determined.

Gasdermin-C is expressed in esophagus, stomach, trachea, spleen intestines, bladder in skin {Saeki:ollkdwRF} (Wu *et al*, 2009a). It has not yet been implicated in any diseases in mice or humans.

DFNB59 is as DFNA5 associated with hearing loss(Delmaghani *et al*, 2006; Schwander *et al*, 2007). It was shown to be essential for proliferation of peroxisomes(Delmaghani *et al*, 2015), but if DFNB59 has a transport function, or also forms pores in peroxisomes needs to be determined.

3.8 Other modes of regulated cell death

3.8.1 Apoptosis (**Figure 3.5**)

Apoptotic cell death is either initiated via ligation of death receptors or by engagement of the mitochondrial pathway of apoptosis. Activation of either pathway culminates in the activation of executor caspases, namely caspase-3, -6 and -7. These executor are synthesized as inactive precursors and lack protein-protein interaction domains as their activation is achieved through inter-domain cleavage by the initiator caspases-8/-9(Salvesen & Riedl, 2008). These executioner caspases (especially -3 and -7) are capable of cleaving more than 1000 substrates(Crawford & Wells, 2011). Cleavage of these substrates activates or represses certain cellular signaling pathways leading to the characteristic changes associated with apoptosis. These include chromatin condensation (pyknosis), rounding of cells and membrane blebbing (Ricci *et al*, 2004),(Sakahira *et al*, 1998). The initiator caspases -8 and -9 are also synthesized as inactive monomers, however they possess additional protein-protein interaction domains and get activated through proximity-induced auto-proteolytic cleavage(Pop *et al*, 2007),(Oberst *et al*, 2010). Which of the initiator caspases is activated in response to a certain stimulus is determined by the different pathways of apoptosis, which can be engaged.

The mitochondrial pathway of apoptosis (intrinsic pathway) is the most common mechanism of apoptosis in vertebrates. Stimuli, which feed into this pathway include DNA damage, growth factor deprivation, ER stress and developmental cues (Bratton & Salvesen, 2010). The B-cell lymphoma-2 (Bcl-2) family of proteins is responsible for integration of these stimuli as these proteins regulate the critical step of mitochondrial outer membrane permeabilization (MOMP), which allows subsequent activation of caspase-9 by the apoptosome(Chipuk *et al*, 2010). The Bcl-2 protein family consists of three broad classes: pro-apoptotic effector proteins (Bax and Bak), anti-apoptotic Bcl2 proteins (e.g. Bcl2, Bcl-xl, Mcl1) which block apoptosis and BH3-only proteins (e.g. Bid, Bim, Bad and Noxa) which repress anti-apoptotic Bcl2 family members. Bax and Bak are in the found in the cytosol in healthy cells, however upon activation, or more precisely loss of inhibition by one of the anti-apoptotic Bcl2 family members(O'Neill *et al*, 2016), they are capable of permeablizing the mitochondrial outer membrane through the formation of large oligomeric pores (Eskes *et al*, 2000),(Dewson *et al*, 2009),(Korsmeyer *et al*, 2000).

This process referred to as MOMP, release cytochrome c as well as the secondary mitochondria derived activator of caspases (SMAC) and Omi from the mitochondrial intermembrane space. Cytochrome c release is the essential step for the intrinsic apoptotic pathway to proceed as, once in the cytosol, it binds to Apaf1 and induces its oligomerization(Zou *et al*, 1997). This allows the formation of an active apoptosome, providing an activation platform for caspase-9, which is recruited via its CARD domain and gets autoproteolytically activated(Yu *et al*, 2005),(Yuan *et al*, 2010). As discussed above, activation of caspase-9 leads to processing of executioner caspases, allowing apoptosis to proceed. The apoptotic response is potentiated by Smac and Omi which are released from the mitochondria during MOMP, as they antagonize the X-linked inhibitor of apoptosis (XIAP). In the absence of Smac and Omi XIAP inhibits the catalytic activity of the caspases -3, -7 and -9 and mediates ubiquitination of active caspases (Eckelman *et al*, 2006).

The extrinsic pathway of apoptosis in turn is initiated by death receptor signaling. Death receptors are a subset of the tumor necrosis factor receptor (TFNR) family, including TNFR1, Fas and TRAIL R1/2 (Dickens *et al*, 2012) . They recruit caspase-8 and other signaling molecules important for inflammation and cell adhesion by homotypic protein-protein interactions mediated by their death domain/s(Newton & Dixit, 2012). Upon activation of TRAIL-R or FAS by their ligands, Fas-associated protein with death domain (FADD) is recruited, which through exposure of its death effector domain (DED) brings caspase-8 molecules into close proximity triggering their protease activity. Auto-proteolytic activation of caspase-8 promotes apoptosis in some cells (type I cells) by cleaving and activating caspase-3 and -7 however in many cell types (type II cells) the executioner caspases are inhibited by XIAPs, which blocks apoptosis(Jost *et al*, 2009). In these cells cleavage of Bid by caspase-8 is required to induce MOMP and therefore release SMAC and Omi, which neutralize XIAPs and allows apoptosis to proceed (Dickens *et al*, 2012).

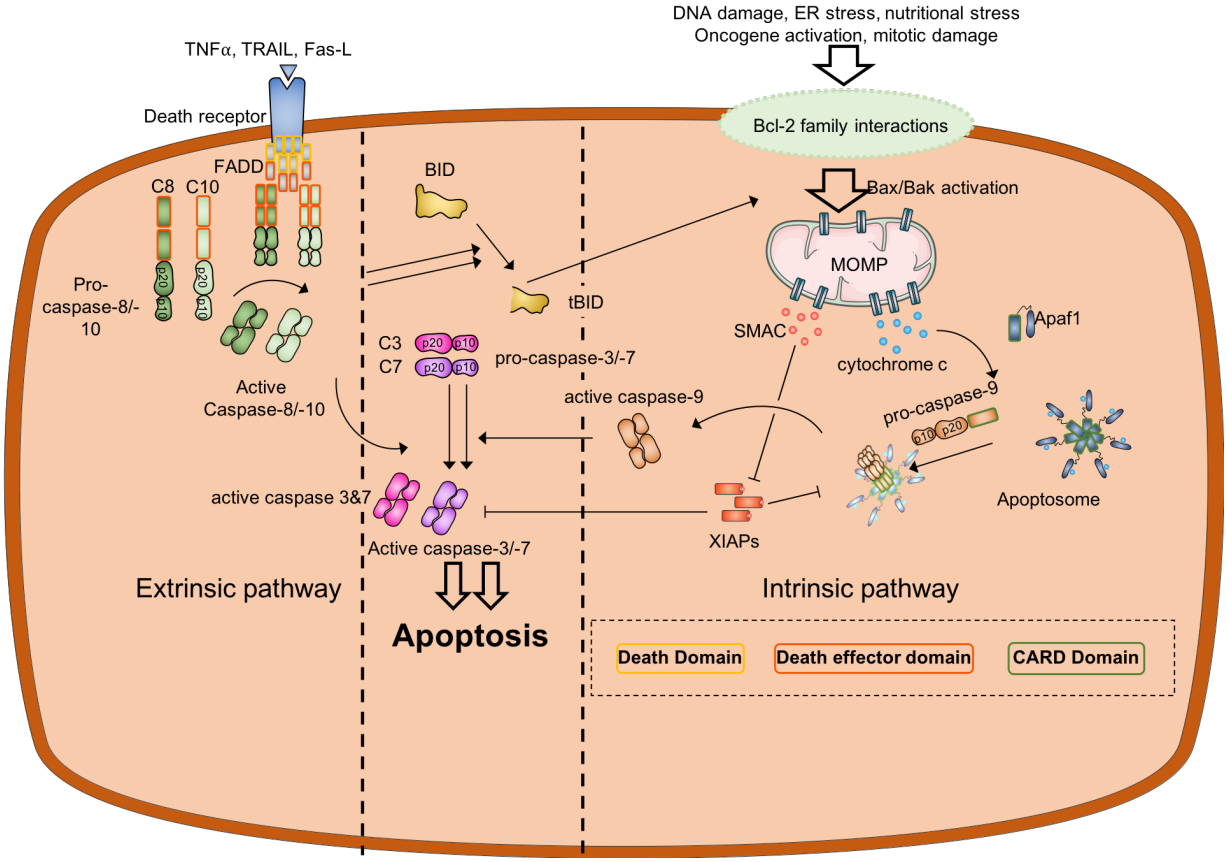

Figure 3.5 Apoptosis

The extrinsic pathway is initiated by ligation of death receptors and leads to activation of caspase-8 and -10, which in turn activate the executioner caspases 3&7. Caspase -8 and-10 can cleave BID into tBID to engage the intrinsic pathway as well. The interactions between Bcl-2 family members regulate the critical step of MOMP, which decides if a cell undergoes apoptosis or not. Once MOMP is initiated, release of SMAC and cytochrome c lead to inhibition of XIAPs and apoptosome assembly respectively. Caspase-9, which is activated within the apoptosome, cleaves caspase-3 and -7 to execute apoptosis (adapted from Kalkavan and Green, 2017)

3.8.2 Necroptosis (**Figure 3.6**)

Signaling downstream of TFNR1 is more complex and can lead to apoptosis, survival or necroptosis. TNFR1 recruits Tumor necrosis factor receptor type 1-associated DEATH domain protein (TRADD) and other factors to activate NF-kB, which rather culminates in an inflammatory response rather than cell death (Newton & Dixit, 2012). One consequence of NF-kB activation is the production of cellular FLICE (FADD-like IL-1β-converting enzyme)-inhibitory protein (c-FLIP) (Micheau et al, 2001). Though TNFR1 engagement leads to caspase-8 activation, by recruitment TRADD, FADD and Receptor interacting kinase (RIPK) 1 (also referred to as complex II) (Declercq et al, 2009),(Christofferson & Yuan, 2010), expression of cFLIP proteins through NF-kB activation however inhibits caspase-8 mediated apoptosis in most cells. Although in complex with cFLIP caspase-8 is catalytically active and apoptosis is not induced. It remains obscure why this is the case, although a hypothesis is, that this complex is prone to more rapid degradation (Geserick et al, 2009).Therefore TNFR1 engagement leads to inflammation and cell survival rather than apoptosis in most cells.

As discussed above, complex II formation in presence of cFLIP proteins does not promote apoptosis in response to TNFR1 ligation. Complex II formation leads, beside recruitment of RIPK1, to the recruitment of RIPK3, a crucial step for necroptotic cell death to proceed. Necroptosis is characterized by a loss of membrane integrity, dissipation of the electrochemical gradient across the plasma membrane and release of cytosolic content from the cell(Cho *et al*, 2009),(He *et al*, 2009),(Zhang *et al*, 2009). RIPK3 is recruited by RIPK1 through interaction of their RIP homology interaction motifs (RHIM) domains. In this configuration complex II is referred to as the RIPoptosome, and rather induces necrosis than apoptosis(Feoktistova *et al*, 2011),(Tenev *et al*, 2011). A series of post-translational modifications is required for assembly of this signalling platform. De-ubiquitination of RIPK1 promotes assembly of the RIPoptosome(Wang *et al*, 2008),(O'Donnell *et al*, 2011),(Moulin *et al*, 2012). Moreover, the kinase activity of RIPK1 is required for activation of RIPK3(Cho *et al*, 2009),(He *et al*, 2009),(Zhang *et al*, 2009). In addition, the caspase-8-cFLIP heterodimer negatively regulates necroptosis, as RIP1, RIP3 and CYLD (a RIP1 deubiquitinase, therefore a positive regulator of necroptosis) are cleavage substrates for caspase-8(Pop *et al*, 2011). Consequently, necroptosis in response to TNFR1 ligation only progresses if FLIP-caspase-8 activity is blocked. RIP dependent necroptosis can also be triggered downstream of TLR3 or TLR4 as these receptors signal through TIR-domain-containing RHIM-containing adaptor inducing IFN–beta (TRIF)(Imtiyaz *et al*,

2006),(Feoktistova *et al*, 2011). TRIF recruits RIPK1 and RIPK3 to induce RIP dependent necroptosis(Feoktistova *et al*, 2011). Also, viral infections can induce necroptosis. The RHIM containing cytosolic DNA sensor DAI recruits RIP3 through its RHIM domains if activated by viral dsDNA(Upton *et al*, 2010),(Upton *et al*, 2012),(Cho *et al*, 2009). Upon activation by one of the mechanisms described above, RIPK3 phosphorylates the mixed lineage kinase-domain like pseudokinase (MLKL)(Quarato *et al*, 2016), leading to translocation to the plasma membrane(Cai *et al*, 2014),loss of PM asymmetry, collapse of the ionic gradient across the PM and ultimately lysis of the cell(Chen *et al*, 2016b). It has been proposed that calcium influx mediated by MLKL through interaction with the non-voltage gated ion channel TRPM7 is critical for necroptosis, however depending on the cell type, it seems that although calcium influx is reduced, cell death is only modestly impacted (Cai *et al*, 2014). This discrepancy might be explained by the model, that MLKL itself is capable of forming pores in membranes (Wang *et al*, 2014). It remains to be investigated, if both mechanisms occur simultaneously or are in any way dependent on each other.

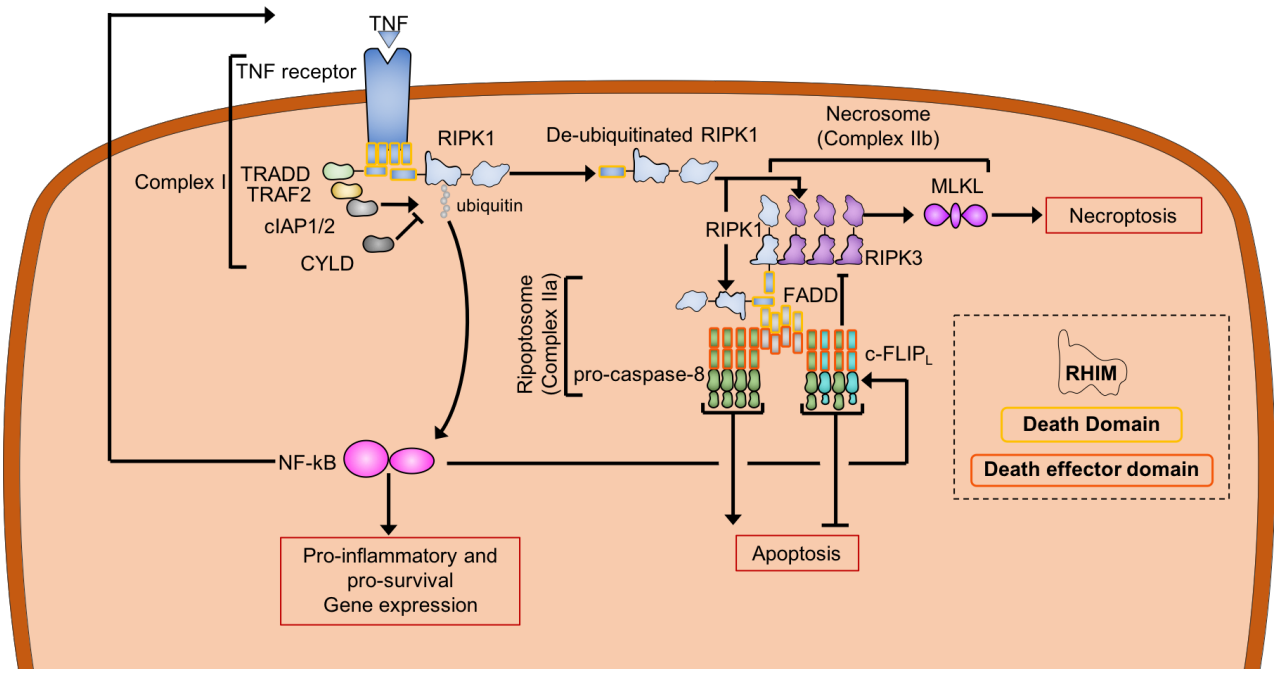

Figure 3.6 Necroptosis

Engagement of TNFR leads to complex I assembly and to RIPK1 dependent NF-kB activation and gene expression, if RIPK1 is ubiquitinated by cIAP1/2. CYLD leads to de-ubiquitination of RIPK1, enabling its interaction with RIPK3 and caspase-8 leading to formation of the Ripoptosome or the Necrosome. In the presence of c-FLIP proteins, Ripoptsome mediated apoptosis is inhibited, as capase-8 is inhibited by $cFLIPL_L$. However, the caspase-8 cFLIP complex is capable of cleaving CYLD as well as RIPK1 and RIPK3, therefore inhibiting MLKL activation and necroptosis. Therefore, necroptosis only occurs if caspase-8 is inhibited.
(adapted from *Tummers and Green*, 2017)

3.9 Plasma membrane repair mechanisms (**Figure 3.7**)

It has been known for several decades that cells can repair damage inflicted to their plasma membrane (PM) by mechanisms strictly dependent on extracellular calcium ions(Andrews *et al*, 2014). Early experiments observed large patches of membranes and vesicles(Miyake & McNeil, 1995; Bi *et al*, 1995), which were recruited to the site of injury, leading to the hypothesis that intracellular pieces of membranes fuse at the site of injury to repair the PM(McNeil *et al*, 2000). Yet, how these fusion events occur biophysically and how this leads to restoration of PM integrity couldn´t be explained. More recently two non-mutually exclusive mechanisms have been investigated to the molecular detail. These mechanisms, endocytosis of PM pores and shedding of damaged pieces of membrane, both are dependent on calcium influx and are even capable of explaining the repair and removal of stable transmembrane pores.

3.9.1 ASM mediated endocytosis of PM pores

The observation that wounding of the PM leads to massive exocytosis (Miyake & McNeil, 1995; Bi *et al*, 1995), was initially surprising but could be confirmed in multiple cell types in response to different kinds of membrane damage(Forestier *et al*, 2011; Roy *et al*, 2004). It was initially thought that the membrane patches appearing at the site of injury would serve either to ‘clog’ the hole in the PM (McNeil *et al*, 2000)or they would serve to reduce the membrane tension around the site of injury(Togo *et al*, 2000), which was supported by the findings, that lysosomal markers could be observed in punctate patterns at the PM upon injury(Reddy *et al*, 2001). The realization that stable transmembrane pores, like the bacterial toxin Streptolysin O (SLO) were removed in a calcium dependent manner prompted a closer examination of the mechanistic details(Walev *et al*, 2001; Morgan & Campbell, 1985). The fact that lysosomal hydrolases are secreted in a calcium dependent manner(Tam *et al*, 2010) upon PM injury and the observation that PM injury triggers massive endocytosis of vesicles, which look remarkably like endosomes of cells treated with bacterial sphingomyelinase(Idone *et al*, 2008; Zha *et al*, 1998) provided a first mechanistic explanation for removal of PM pores. Sphingomyelin is abundantly found in the PM(Simons & Raposo, 2009) and sphingomyelinases are capable of generating ceramide from sphingomyelin. Ceramide was shown to promote membrane invagination(Holopainen *et al*, 2000) and was implicated in the formation of intraluminal vesicles on multi-vesicular bodies (MVBs), where

cytosolic neutral sphingomyelinase is responsible for ceramide generation(Trajkovic *et al*, 2008). The lysosomal enzyme acidic sphingomyelinase (ASM) is secreted to the cell surface when they are exposed to membrane-damaging stress(Gulbins, 2003; Tam *et al*, 2010). There it acts on the outer leaflet of the PM, generating ceramide-rich micro domains(Schissel *et al*, 1998; van BLITTERSWIJK *et al*, 2003; Grassmé *et al*, 2002). These micro domains are absent during treatment with ASM inhibitors and in cells deficient for ASM during SLO treatment(Tam *et al*, 2010; Babiychuk *et al*, 2008). Importantly, under these conditions, membrane repair is inhibited and cells succumb to otherwise sub-lethal concentrations of SLO(Tam *et al*, 2010). This shows that ASM mediated ceramide generation and subsequent endocytosis of PM pores is required for membrane repair during PM pore formation. Once internalized by endocytosis, PM pores travel along the endosomal route to be degraded in MVBs or lysosomes(Corrotte *et al*, 2012).

3.9.2 ESCRT-III dependent shedding of PM pores

The ESCRT machinery is a multiprotein complex, composed of several parts (ESCRT 0, I, II, III). The name, endosomal sorting complex required for transport, originates from its discovery in yeast where the ESCRT proteins, just like in all eukaryotic cells, are responsible for sorting and trafficking of proteins along the secretory pathway(Katzmann *et al*, 2002). Most prominently, the ESCRT machinery is responsible for formation of intraluminal vesicles (ILVs) in multivesicular bodies (MVBs)(Katzmann *et al*, 2002), as it is the only machinery capable of deforming membranes away from the cytosol, leading to generation of vesicles at the distal part of a membrane. Over the years, other functions of the ESCRT machinery, including cytokinesis(Carlton & Martin-Serrano, 2007; Morita *et al*, 2007), a role for the budding of several enveloped viruses (Morita & Sundquist, 2004) and a function for restoration of nuclear envelope restoration have been implicated(Raab *et al*, 2016; Denais *et al*, 2016). More recently, it has been shown convincingly by several groups that the ESCRT-III machinery has a function in PM repair(Jimenez *et al*, 2014; Scheffer *et al*, 2014). These studies could demonstrate that several components of the ESCRT machinery are enriched in membrane fractions of cells treated with the calcium ionophore ionomyin. Validation experiments showed that this recruitment is not only dependent on calcium influx, but is observed if the PM is damaged by different means. Laser wounding, detergent treatment, bacterial pore forming toxins and perforin treatment all induced clustering of the ESCRT-III component CHMP4 at the PM. Both groups showed that other ESCRT-III components are recruited as well during micro-laser wounding and that most components of the ESCRT 0, I, and II machineries are dispensable (except ALIX and ALG-2) for PM repair. Consequently, inhibition of ESCRT-III activity by either knock-down or expression of dominant-negative proteins inhibited membrane repair and lead to enhanced cell death during laser wounding, as damaged pieces of membrane could not be removed by ectocytosis (Jimenez *et al*, 2014; Scheffer *et al*, 2014).

A recent study demonstrated that beyond repairing laser inflicted PM damage the ESCRT-III machinery also negatively controls necroptotic cell death. As discussed above, necroptosis involves pore formation at the PM by MLKL, leading to collapse of the ionic gradient across the PM and ultimately lysis of cells. The study could show that the ESCRT-III machinery is activated during necroptosis and recruited to MLKL positive parts of the PM, where it sheds ‘bubbles’ of membrane up to 0.5 µm in size. Inhibition of the ESCRT-III machinery resulted in enhanced cell death during necroptosis and prevented ‘resuscitation’ of cells. Resuscitation

is a phenomenon, where cells which have received a necroptotic stimulus (have exposed PS at the PM and are therefore Annexin-V positive) can come back to life if the stimulus is removed. Interestingly, premature death of cells during necroptosis leads to reduced cytokine secretion and T-cell cross-priming as stimulated cells have too little time to engage NF-κB dependent signaling and cytokine production. This study for the first time implicated a role for membrane repair mechanism in the regulation of cellular death programs, showing an interesting connection between cellular survival and cell death pathways(Gong *et al*, 2017).

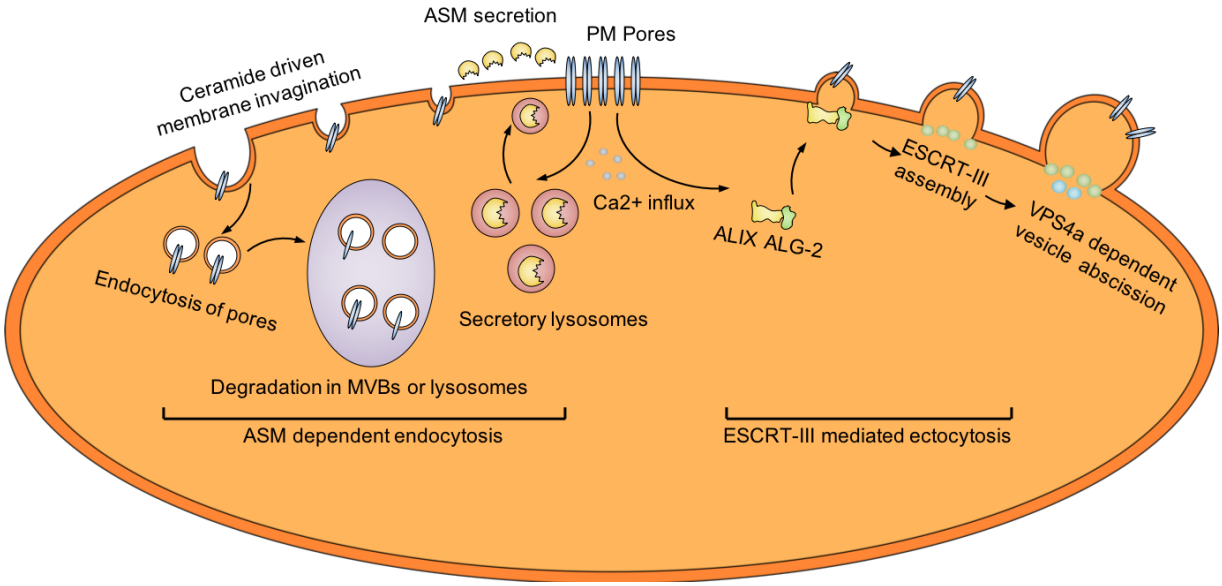

Figure 3.7 Plasma membrane repair mechanisms

Damage or pore formation at the PM (middle) leads to calcium influx, which is essential for triggering both described membrane repair mechanisms. ASM dependent endocytosis (left part) is initiated by rapid secretion of ASM to the supernatant of cells, from secretory lysosomes. ASM hydrolyses sphingomyelin to ceramide around the site of exocytosis, leading to ceramide driven invagination of the damaged area of the membrane. Pores are sequestered within endosomes and travel to MVBs to be degraded. ESCRT dependent ectocytosis (right part) is initiated by activation of ALG-2 through calcium flux, which is turn recruits ALIX (ALG-2 interacting protein X). Components of the ESCRT-III machinery are consecutively recruited, leading to shedding of PM pores within ectosomes to restore PM integrity

3.10 Aim of the thesis

During my PhD I was always intrigued by the simplicity of the non-canonical inflammasome pathway and how it works to protect the host from gram-negative pathogens. As the mechanisms downstream of caspase-11 activation were not well understood, my work focused on understanding these signaling events. I wanted to understand how caspase-11 acts to promote NLRP3 activation, executes pyroptosis through gasdermin-D and how the cell is capable of regulating pyroptosis downstream of caspase-11 activation. I also tried to identify unknown components of the non-canonical pathway by performing an unbiased forward genetic screen. Overall I aimed to improve our understanding of the signaling events elicited by activation of caspase-11 through intracellular LPS.

4 Results

4.1 Research Article I: Caspase-11 activates a canonical NLRP3 inflammasome by promoting K+ efflux

Sebastian Rühl[1] and Petr Broz[1]

1 Biozentrum Universität Basel, Klingelbergstrasse 50/70, 4056 Basel

Published: European Journal of Immunology 2015 Oct;45(10):2927-36.

doi: 10.1002/eji.201545772.

Epub 2015 Aug 6

Statement of contribution:

I performed all experiments described and wrote the manuscript together with Petr Broz

Eur. J. Immunol. 2015. 45: 2927–2936 DOI: 10.1002/eji.201545772 Innate immunity 2927

European Journal of Immunology

Caspase-11 activates a canonical NLRP3 inflammasome by promoting K^+ efflux

Sebastian Rühl and Petr Broz

Focal Area Infection Biology, Biozentrum, University of Basel, Basel, Switzerland

Recognition of microbe-associated molecular patterns or endogenous danger signals by a subset of cytosolic PRRs results in the assembly of multiprotein signaling complexes, the so-called inflammasomes. Canonical inflammasomes are assembled by NOD-like receptor (NLR) or PYHIN family members and activate caspase-1, which promotes the induction of pyroptosis and the release of mature interleukin-1β/-18. Recently, a non-canonical inflammasome pathway was discovered that results in caspase-11 activation in response to bacterial lipopolysaccharide (LPS) in the cytosol. Interestingly, caspase-11 induces pyroptosis by itself, but requires NLRP3, the inflammasome adapter ASC, and caspase-1 to promote cytokine secretion. Here, we have studied the mechanism by which caspase-11 controls IL-1β secretion. Investigating NLRP3/ASC complex formation, we find that caspase-11 functions upstream of a canonical NLRP3 inflammasome. The activation of NLRP3 by caspase-11 during LPS transfection is a cell-intrinsic process and is independent of the release of danger signals. Furthermore, we show that active caspase-11 leads to a drop of intracellular potassium levels, which is necessary to activate NLRP3. Our study, therefore, sheds new light on the mechanism of noncanonical inflammasome signaling.

Keywords: Caspase-11 · Inflammasome · Interleukin-1 beta (IL-1β) · Lipopolysaccharide · NLRP3 · Potassium efflux · Pyroptosis


See accompanying articles by Masters and colleagues and Hornung and colleagues.


See accompanying Commentary by Rivers-Auty and Brough.


Additional supporting information may be found in the online version of this article at the publisher's web-site

Introduction

Inflammasomes are multiprotein complexes assembled by cytosolic PRRs from the NOD-like receptor (NLR) and PYHIN protein family upon recognition of microbe-associated molecular patterns (MAMPs) or danger signals [1]. Ligand recognition results in receptor activation and recruitment of the adaptor ASC, which rapidly oligomerizes to form the so-called ASC speck. The ASC speck serves as an activation platform for the cysteine protease caspase-1 [2] that processes the cytokines IL-1β and IL-18 to their mature form and promotes pyroptosis, a lytic form of cell death [1]. Besides their role in host defense [1], inflammasomes attract interest since deregulation of inflammasome signaling is also linked to a number of hereditary and acquired inflammatory diseases [3].

Inflammasome receptors, such as NLRs and PYHINs, contain several functional domains that are thought to be involved in ligand recognition. Direct binding of the ligand has been demonstrated for AIM2, which binds double-stranded DNA [4], and for the NAIP proteins, which bind flagellin and type 3 secretion systems subunits [1]. However, for most other inflammasomes

Correspondence: Dr. Petr Broz
e-mail: petr.broz@unibas.ch

it remains unclear how the stimulus is recognized. This is particularly true for the NLRP3 inflammasome that is activated by a variety of structurally and chemically distinct stimuli, ranging from pathogens and pore-forming toxin to crystalline particles and UV irradiation [5]. These results suggest that some signal/s common to all of these activators must be recognized. Currently, these common denominators are thought to be K^+ efflux [6, 7], lysosomal damage and the release of Cathepsins [8, 9], mitochondrial ROS production and the release of oxidized mitochondrial DNA [10, 11]. Nevertheless, despite these advances it remains unclear if and how these events are causally linked.

Investigating the response of murine macrophages to lipopolysaccharide (LPS) and cholera toxin B, as well as other bacterial inflammasome activators, Kayagaki et al. recently discovered a noncanonical inflammasome pathway that relies on caspase-11 [12]. Subsequent studies reported that this pathway was activated by Gram-negative, but not by Gram-positive, bacteria, indicating a requirement for a conserved factor from Gram-negative bacteria [13, 14]. Consistently, it was later shown that Gram-negative bacterial LPS delivered to the cytosol by transfection or electroporation is sufficient to induce caspase-11 activation [15, 16]. While it was initially assumed that a cytosolic LPS receptor activates caspase-11, it was recently shown that caspase-11 as well as its human homologs caspase-4/5 recognize LPS directly via the CARD domain [17]. Another particularity of the noncanonical inflammasome pathway is that caspase-11 is able to induce a lytic cell death similarly to caspase-1, however, cannot by itself trigger IL-1β/-18 release [12]. To promote cytokine secretion, caspase-11 absolutely requires components of the NLRP3 inflammasome—namely NLRP3, ASC, and pro-caspase-1 [12]. However, how caspase-11 is linked to NLRP3 activation in this noncanonical inflammasome pathway remains unclear. While some results suggest that caspase-11 forms a complex together with NLRP3/ASC and pro-caspase-1 [12, 14], others indicate that caspase-11 is upstream of NLRP3 activation [13]. Here, we have addressed the link between caspase-11 and NLRP3 activation upon LPS transfection. Our results showed that caspase-11 acts indeed upstream of NLRP3 activation and controlled the assembly of NLRP3–ASC complexes (ASC specks). This process was induced on a cell-autonomous level and was independent of a released/secreted activator of NLRP3. Further investigations showed that caspase-11 activation led to a drop in intracellular K^+ concentrations and that this served as a trigger of canonical NLRP3 activation.

Results

NLRP3 activation by caspase-11 is a cell-autonomous process

Caspase-11 activation following LPS transfection induces a lytic type of cell death (measured by the release of lactate dehydrogenase (LDH)), which is mostly independent of known inflammasome components (Fig. 1A) [12, 15]. Interestingly, however, caspase-1 activation and the secretion of mature, processed IL-1β/-18 upon LPS transfection are absolutely dependent on NLRP3, ASC, and pro-caspase-1 (Fig. 1B and F) [12, 15], indicating the existence of a noncanonical pathway of NLRP3 activation that involves caspase-11. In contrast to this pathway, treatment with the canonical NLRP3 stimulus nigericin resulted in comparable levels of cell death and cytokine production in WT and *Casp11*-deficient cells, but not in *Nlrp3*-deficient cells (Fig. 1F, Supporting Information Fig. 1A and B). Based on similar findings, previous publications suggested that during LPS transfection caspase-11 is either part of a noncanonical NLRP3 complex [12, 14] or acts upstream of NLRP3 activation [13]. In order to determine if caspase-11 is required for the formation of NLRP3–ASC complexes, we assayed ASC oligomerization and ASC speck formation in PAM_3CSK_4-primed WT, *Nlrp3*$^{-/-}$, and *Casp11*$^{-/-}$ BM-derived macrophages (BMDMs) following LPS transfection. Importantly, ASC specks form even in the absence of inflammatory caspases [2] and provide a robust measure of inflammasome complex formation. While WT cells formed detectable ASC specks (>60%) at 16 h post transfection, the rate of ASC speck formation in *Nlrp3*$^{-/-}$ and *Casp11*$^{-/-}$ cells was below 5% (Fig. 1C and D). Consistent with reduced ASC speck formation, knockout of *Nlrp3* or *Casp11* abrogated ASC oligomerization as determined by the disappearance of ASC oligomers in DSS-cross-linked nonsoluble fractions of LPS-transfected cells (Fig. 1E). Again canonical inflammasome activation by nigericin induced a comparable response in WT and *Casp-11*-deficient macrophages (Fig. 1E, Supporting Information Fig. 1C and D). In conclusion, these results argue for a model in which active caspase-11 is upstream of a canonical NLRP3 inflammasome and against the existence a noncanonical NLRP3 complex.

The NLRP3 inflammasome responds to a variety of chemically and structurally diverse stimuli, among them are released danger signals such as extracellular ATP [1]. To address if caspase-11-induced host-cell lysis results in the release of cytosolic content and the activation of NLRP3 in neighboring cells, we assayed inflammasome activation in the presence of osmoprotectants. PAM_3CSK_4-primed WT, *Nlrp3*$^{-/-}$, and *Casp11*$^{-/-}$ BMDMs were transfected with LPS and 50 mM of the osmoprotectant glycine was added 1 h post LPS transfection. Extracellular glycine effectively blocked release of cytosolic content in WT and *Nlrp3*$^{-/-}$ BMDMs as assayed by the release of LDH (Fig. 1A) or the danger signal HMGB1 (Fig. 1F). Addition of glycine, however, did not result in reduced levels of NLRP3 activation, as IL-1β release remained unchanged (Fig. 1B and F), indicating that lysis and the release of cytosolic contents were not a trigger of NLRP3 activation. Consistently, glycine treatment did also not block NLRP3–ASC complex assembly as ASC speck formation and ASC oligomerization remained unchanged (Fig. 1C–E). Interestingly, glycine treatment reduced the release of caspase-1 p10 and NLRP3, probably due to reduced release of NLRP3–ASC specks from lytic cells (Fig. 1F).

Since cells containing active caspase-11 might also release or secrete danger signals independently of lysis, we used coculture experiments to determine if caspase-11-mediated NLRP3 activation is a cell-intrinsic process. We cocultured unlabeled

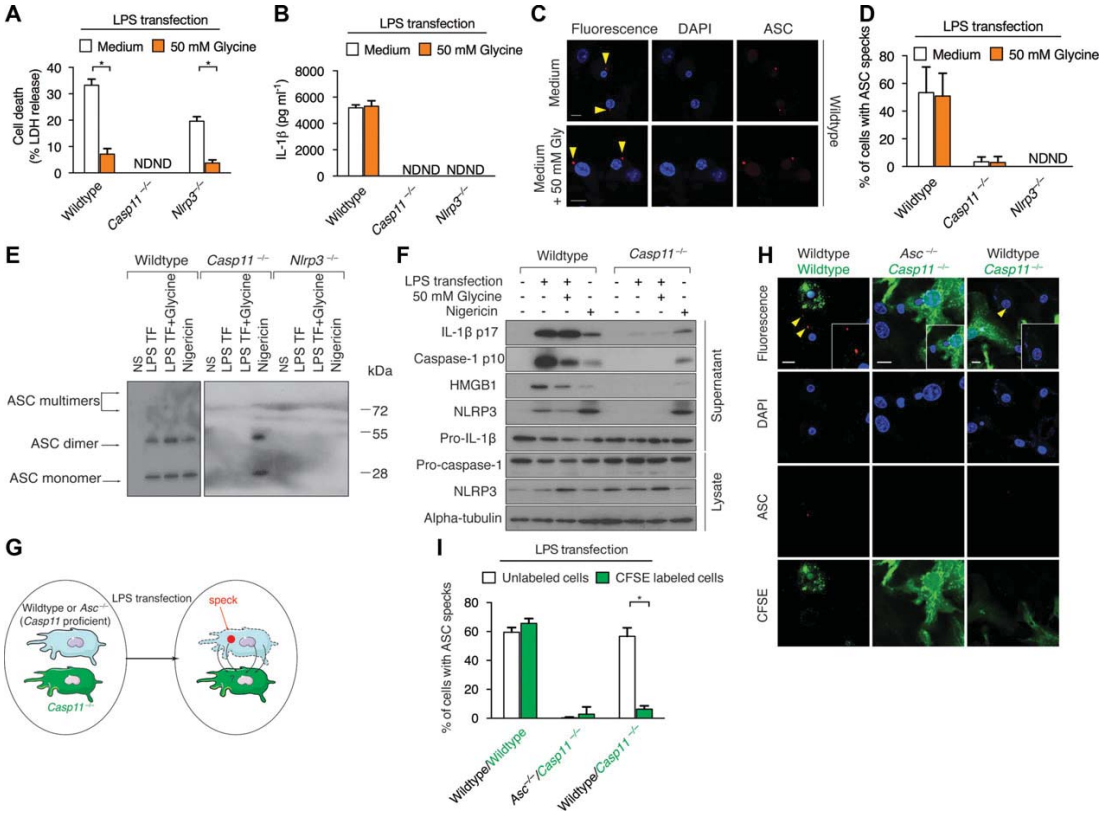

Figure 1. Caspase-11 activates a canonical NLRP3 inflammasome on a cell-autonomous level independently of the release of danger signals. (A–F) Pam_3CSK_4-primed BMDMs from WT, *Nlrp3*$^{-/-}$, and *Casp11*$^{-/-}$mice were transfected with LPS for 16 h in the presence or absence of glycine, or treated with nigericin for 1 h. (A and B) Cell death was quantified by measuring LDH release, IL-1β release was measured by ELISA. Graphs show average (±SD) of quadruplicate wells and are representative of at least three independent experiments. (C and D) Immunofluorescence analysis and quantification of ASC speck formation. (E) ASC oligomerization after DSS cross-linking was analyzed by Western blot. LPS TF, LPS transfection. (F) Western blot analysis for the release of processed caspase-1 p10, IL-1β, HMGB-1, and NLRP3 (alpha tubulin as loading control). (G) Experimental scheme for coculture experiments. (H and I) Immunofluorescence analysis and quantification of ASC speck formation in cocultured Pam_3CSK_4-primed WT/WT, *Asc*$^{-/-}$/*Casp11*$^{-/-}$, and WT/*Casp11*$^{-/-}$ BMDMs (ratio 3:1 unlabeled/labeled) transfected with LPS for 16 h. (A, B, D, and I) Data are shown as mean ± SD ($n = 4$ replicates) and are pooled from three independent experiments. (E and F) Western blots are representative of three independent experiments. (C and H) Magnification 63×, scale bars 10 μm. Images are representative of three independent experiments. $^{*}p < 0.05$; Student's *t*-test; ND, not detectable.

WT or *Asc*-deficient BMDMs with CFSE-labeled WT (control) or *Casp11*-deficient cells at different ratios (3:1 and 2:1), activated caspase-11 by LPS transfection, and quantified the rate of NLRP3–ASC speck formation as a readout for NLRP3 activation in respective cell populations (Fig. 1G). If a factor released from caspase-11-proficient cells is sufficient to trigger NLRP3 activation upon LPS transfection, we expected to see formation of ASC specks in cocultured *Casp11*-deficient cells. Analysis of ASC speck formation in the labeled and unlabeled populations showed that caspase-11-deficient BMDMs were not able to initiate ASC speck formation and consequently had not activated NLRP3, when cocultured with either WT or *Asc*$^{-/-}$ BMDMs transfected with LPS (Fig. 1H and I, Supporting Information Fig. 2). In conclusion, our results demonstrated that active caspase-11 triggers a canonical NLRP3 pathway in a cell-intrinsic manner, independent of the release of danger signals or cytokines from adjacent cells.

Involvement of mitochondria in NLRP3 activation by caspase-11

Since canonical NLRP3 activation has been linked to mitochondrial ROS production and ROS scavengers are known to reduce NLRP3 inflammasome activation [11], we next investigated if mitochondrial ROS generation was required for caspase-11-mediated NLRP3 activation. Pretreatment of BMDMs with the ROS scavenger *N*-acetyl-cysteine (NAC, Sigma-Aldrich) before LPS transfection or nigericin stimulation resulted in a significant reduction of reduction in IL-1β release (Fig. 2A). Consistently, NAC reduced cell death in nigericin-treated cells. However, NAC also reduced cell death levels in LPS-transfected cells indicating that NAC interferes with caspase-11 activation or that ROS is required for caspase-11-induced cell death (Fig. 2A). To specifically monitor the production of mitochondrial ROS, we used MitoSOX, a mitochondrial

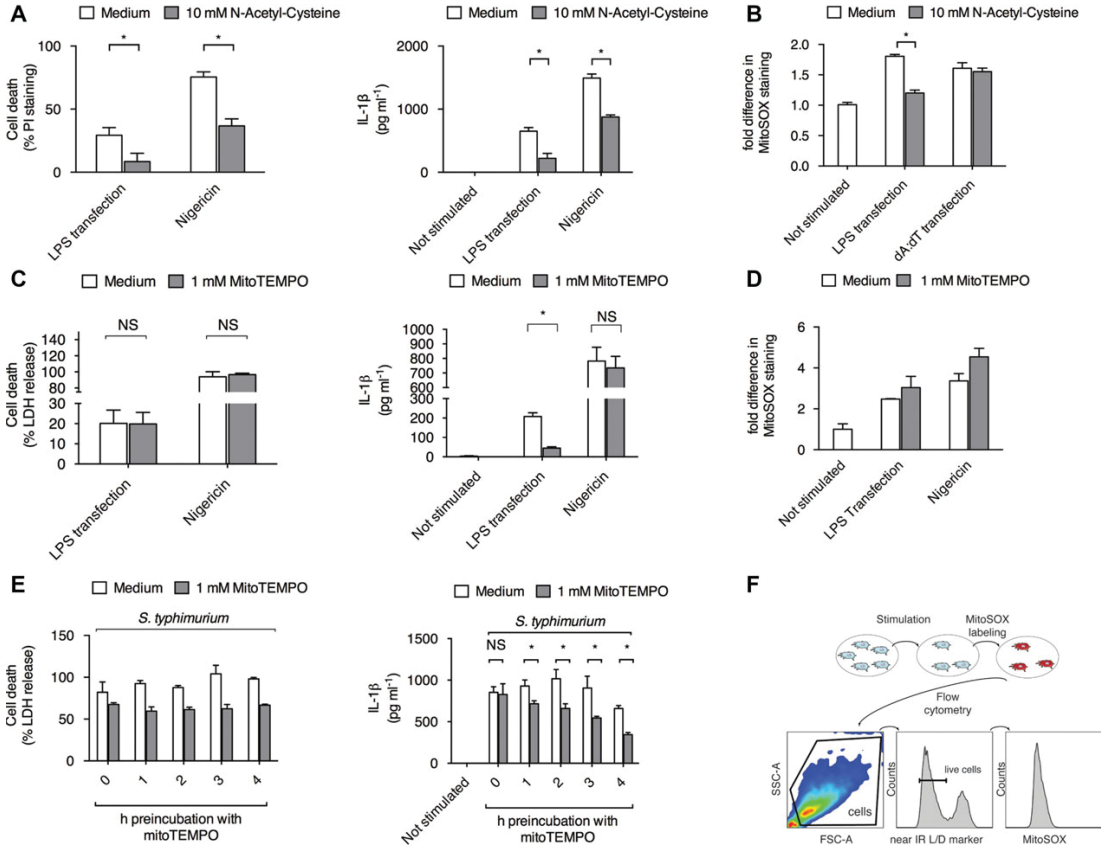

Figure 2. Involvement of mitochondria in noncanonical NLRP3 activation. (A) LDH and IL-1β release from PAM_3CSK_4-primed WT BMDMs transfected with LPS for 4 h or stimulated with nigericin for 1 h in Opti-MEM with or without 10 mM NAC. (B) Flow cytometry analysis of mitochondrial ROS levels in PAM_3CSK_4-primed WT BMDMs transfected with LPS for 4 h or transfected with deoxy-adenosine:deoxy-thymidinde (0.3 μg/2.5 × 10^4 cells) to stimulate caspase-1-induced mitochondrial ROS via the AIM2 inflammasome for 3 h in Opti-MEM with or without 10 mM NAC. Live cells were analyzed for MitoSOX staining by flow cytometry (as shown in F). Bars represent the fold change in MFI compared to nonstimulated controls. (C and D) LDH and IL-1β release and flow cytometry analysis of mitochondrial ROS levels (as described in F) in PAM_3CSK_4-primed WT BMDMs transfected with LPS for 4 h or stimulated with nigericin for 0.5 h in Opti-MEM with or without 1 mM MitoTEMPO. (E) LDH and IL-1β release from PAM_3CSK_4-primed WT BMDMs infected with log-phase *S. typhimurium* (MOI 25) for 1 h in Opti-MEM with or without 1 mM MitoTEMPO (x-axis indicates hours of MitoTEMPO incubation). (F) Staining procedure and gating scheme for MitoSOX analysis. ND, not detectable. All data show average (±SD) of triplicate wells representative of at least two independent experiments. $^*p < 0.05$, Student's *t*-test.

ROS indicator. Consistent with reduced inflammasome activation, NAC reduced caspase-11-induced mitochondrial ROS (Fig. 2B) but NAC could not reduce mitochondrial ROS that was induced during AIM2 inflammasome activation by deoxy adenosine:deoxy thymidinde transfection. These data questioned the ability of NAC to specifically reduce mitochondrial ROS (Fig. 2B) and suggested that NAC might have unspecific effects on caspase activation. In order to solve this discrepancy between NLRP3-induced IL-1β production and mitochondrial ROS levels, we decided to use the ROS scavenger MitoTEMPO (Sigma-Aldrich), which should specifically target mitochondria. IL-1β secretion upon LPS transfection was significantly reduced in the presence of MitoTEMPO; however, nigericin induced IL-1β production as well as cell death levels for both stimuli were unaffected (Fig. 2C). Furthermore, analysis of mitochondrial ROS levels showed no difference for WT macrophages stimulated in presence of MitoTEMPO or a vehicle control indicating that MitoTEMPO might unspecifically reduce NLRP3-induced IL-1β production during LPS transfection (Fig. 2D). Interestingly, when analyzing the effect of MitoTEMPO on the NLRC4 inflammasome, which is directly activated by flagellin or components of type 3 secretion systems [1], we also noticed that increasing incubation times in medium containing MitoTEMPO diminished cell death and IL-1β production, indicative of off-target effects on caspase-1 activation or IL-1β secretion (Fig. 2E). We concluded that due to off-target effects ROS scavengers cannot be used to study the involvement of mitochondria in caspase-11-driven NLRP3 activation, yet we cannot exclude a possible involvement of mitochondrial ROS or other factors of mitochondrial physiology such as the release of oxidized mitochondrial DNA or the perturbation of the mitochondrial membrane potential in caspase-11-induced NLRP3 activation.

Eur. J. Immunol. 2015. 45: 2927–2936

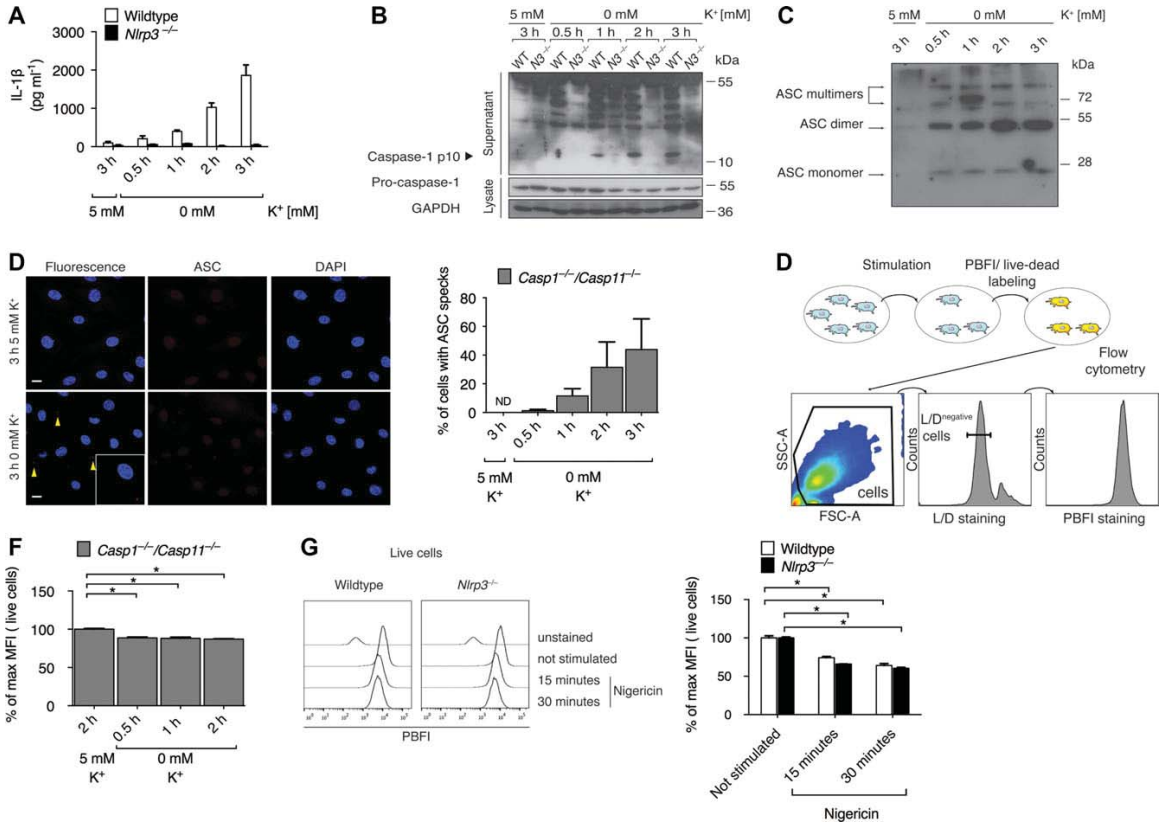

Figure 3. K^+ efflux is sufficient to stimulate NLRP3 inflammasome activation. (A–D) BMDMs from WT and *Nlrp3*$^{-/-}$ mice were primed with LPS for 3 h and incubated in Buffer A (see Materials and Methods). (A) IL-1β release was measured by ELISA. (B) Caspase-1 processing was analyzed by Western blot. Pro-caspase-1 and GAPDH are shown as loading controls. (C) ASC oligomerization (after DSS cross-linking). (B and C) Western blots are representative of three independent experiments. (D) Immunofluorescence analysis and percentage of ASC speck formation upon incubation in potassium-free medium. Magnification 63×; scale bars 10 μM (E) Schematic representation of the PBFI staining procedure and subsequent flow cytometry analysis. (F) PBFI staining intensity of L/D^{negative} *Casp1*$^{-/-}$/*Casp11*$^{-/-}$ BMDMs determined by flow cytometry following incubation in potassium-free medium. (G) PBFI staining intensity of L/D^{negative} WT and *Nlrp3*-deficient BMDMs, as determined by flow cytometry following priming with Pam_3CSK_4 and treatment with nigericin for indicated times. (A, D, F, and G) Graphs show average (±SD) and data are representative of at least two independent experiments. $^*p < 0.05$, Student's *t*-test; ND, not detectable.

K^+ efflux is sufficient to activate NLRP3

Recent work suggested that K^+ efflux is a common event during the activation of the canonical NLRP3 pathway by a number of different stimuli [7]. In agreement with these data, we found that incubation of cells in K^+-free medium was sufficient to induce caspase-1 processing and the release of mature IL-1β and from WT cells, but not from *Nlrp3*-deficient cells (Fig. 3A and B). Furthermore, incubation in K^+-free medium was also sufficient to drive assembly of the NLRP3 inflammasome as determined by quantification of ASC speck formation (Fig. 3D) and ASC oligomerization (Fig. 3C). We next validated that incubation in K^+-free medium indeed resulted in K^+-efflux from BMDMs using the cell-permeable, fluorescent indicator PBFI-AM, which binds to K^+. BMDMs were incubated in K^+-free medium, labeled with PBFI-AM and subjected to flow cytometry based analysis for PBFI intensity [18] (Fig. 3E). To reduce the possibility that active caspase-1 triggers cell death and subsequent loss of intracellular K^+, we used *Casp1*$^{-/-}$/*Casp11*$^{-/-}$ BMDMs for this analysis and added a near-infrared live–dead marker (L/D, Life Technologies) to distinguish between live and dead cells (Fig. 3E). Incubation of *Casp1*$^{-/-}$/*Casp11*$^{-/-}$ BMDMs with K^+-free medium resulted in a significant decrease of PBFI mean fluorescence intensity (MFI) in the L/D^{negative} population (Fig 3F). These results indicated that K^+-free medium was sufficient to initiate a measurable drop in intracellular K^+ concentrations, in line with published results obtained by ICP-OES (inductively coupled plasma-optical emission spectrometry) [7]. To validate our method, we next compared K^+ efflux from WT and *Nlrp3*$^{-/-}$ BMDMs treated with the canonical NLRP3 activator nigericin. Similarly to K^+-free medium, nigericin treatment resulted in a decrease of PBFI-MFI in the L/D^{negative} population in WT and *Nlrp3*-deficient cells (Fig. 3G). Similar results were obtained by using PI to separate live and dead cells (Supporting Information Fig. 3). Taken together, these results showed

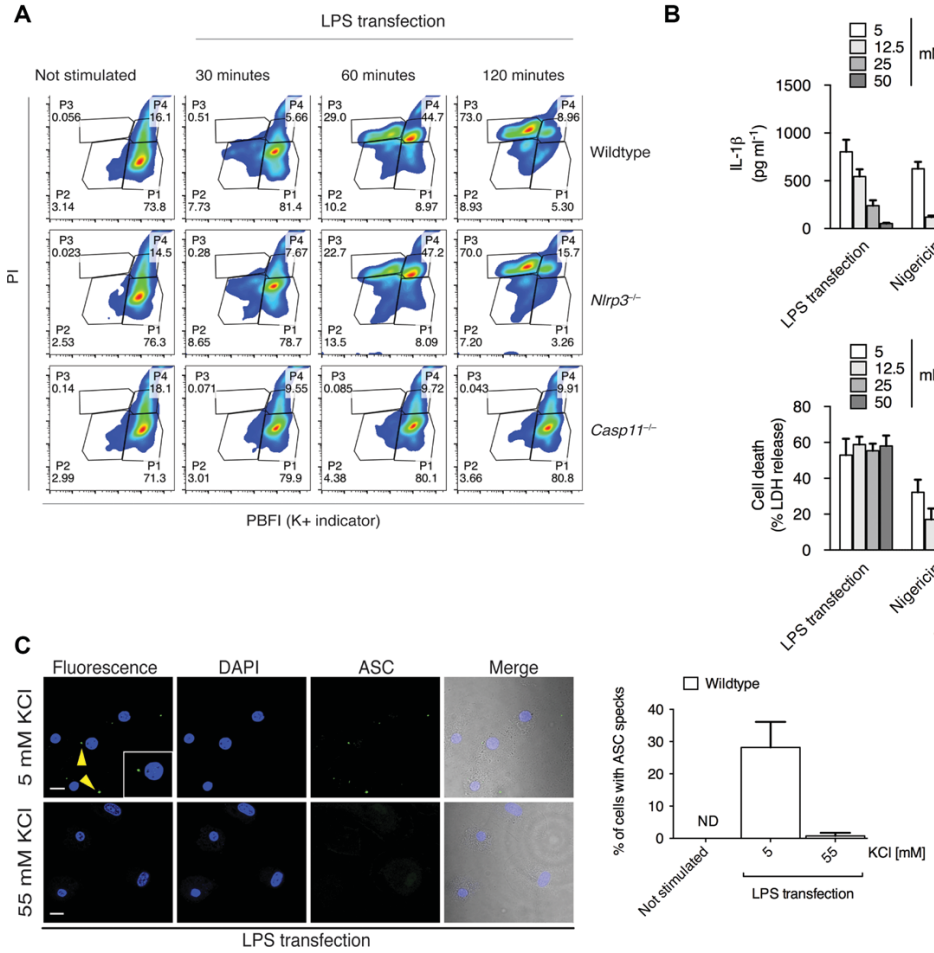

Figure 4. Caspase-11-induced K^+ efflux is essential for NLRP3 activation. (A) WT, *Nlrp3*-deficient, or *Casp11*-deficient cells were primed with PAM_3CSK_4 overnight and transfected with LPS for the indicated timepoints. PBFI staining was performed as described above and analyzed by flow cytometry. Quadrant blots show PBFI versus PI staining over time. (B and C) PAM_3CSK_4-primed WT BMDMs were transfected for 6 h with LPS, stimulated with nigericin, or infected with log-phase *S. typhimurium* for 1 h in Buffer A supplemented with the indicated KCl concentrations (see Materials and Methods). (B) Cell death was quantified by measuring LDH release, IL-1β release was measured by ELISA. (C) Pam_3CSK_4-primed WT BMDMs were left unstimulated or transfected for 6 h with LPS in Buffer A in the presence of KCl and NaCl. (Left panel) Immunofluorescence analysis and (right panel) quantification of ASC speck formation. Magnification 63×, scale bars 10 μM. (A and B) Data are show as mean ± SD of triplicate wells and are representative of three independent experiments. (C) Graphs show data pooled from three independent experiments. ND, not detectable; $^*p < 0.05$; Student's *t*-test.

that PBFI-AM fluorescence measured by flow cytometry provides a good measure of intracellular K^+ content and substantiated observations showing that K^+ efflux is sufficient to trigger NLRP3 inflammasome assembly [7].

Active caspase-11 triggers K^+ efflux, which is essential for NLRP3 activation

Since our data indicated that K^+ efflux is sufficient to drive NLRP3 assembly, we tested if caspase-11 elicits a drop of intracellular K^+ levels that would activate NLRP3 in a cell-autonomous manner. PAM_3CSK_4-primed WT, *Nlrp3*$^{-/-}$, and *Casp11*$^{-/-}$ BMDMs were transfected with LPS for different timepoints, labeled with PBFI-AM and PI as described above and their intracellular PBFI staining was quantified by flow cytometry. Analysis of the quadrant blots over time showed that in the majority of cells acquired PI staining very quickly (starting at 60 min) leading to the appearance of a $PBFI^{high}$ PI^{high} population of cells (Fig. 4A). This population then proceeded to loose PBFI staining leading to its disappearance at later timepoints (120 min) and the appearance of a $PBFI^{low}$ PI^{high} population (Fig. 4A), which represents the final state of cells following caspase-11 activation. These results suggest that caspase-11-induced membrane permeabilization occurred prior to K^+ efflux (as measured by PBFI staining), and that this population quickly proceeded to become $PBFI^{low}$ probably by complete loss

Eur. J. Immunol. 2015. 45: 2927–2936

of membrane integrity and the subsequent loss of K^+ ions or the PBFI dye itself. Yet, it remained unclear if after K^+ loss these $PBFI^{high}$ PI^{high} cells were activating NLRP3 and forming ASC specks (Fig. 4A).

To assess if this caspase-11-induced drop of intracellular K^+ levels was necessary for NLRP3 activation after intracellular delivery of LPS, we next transfected WT BMDMs with LPS in either regular medium or medium with increasing K^+ concentrations. As described previously, we isoosmotically substituted NaCl with KCl in these media [7]. Increasing extracellular K^+ concentrations did not result in reduced levels of cell death in LPS-transfected BMDMs as assayed by the release of LDH and the danger signal HMGB1 (Fig. 4B, Supporting Information Fig. 4A). In contrast, extracellular K^+ significant decreased IL-1β release and caspase-1 processing in a concentration-dependent manner (Fig. 4B, Supporting Information Fig. 4A). Consistent with reduced levels of NLRP3 activity, high extracellular K^+ levels resulted in reduced levels of ASC speck formation and ASC oligomerization in LPS-transfected WT BMDMs (Fig. 4C, Supporting Information Fig. 4B). As a control, we also analyzed the effects of increased extracellular K^+ on the canonical NLRP3 and NLRC4 inflammasomes. In contrast to the noncanonical pathway, we observed a reduction in both cell death and cytokine release in WT BMDMs treated with nigericin in presence of increasing concentrations of extracellular K^+. Furthermore, ASC oligomerization, caspase-1 processing, and HMGB1 release upon nigericin treatment were reduced as well (Fig. 4B, Supporting Information Fig. 4A and B). This is consistent with the notion that K^+ efflux is upstream of NLRP3 and thus high extracellular K^+ blocks both cell death and IL-1β release. As expected, NLRC4 inflammasome activation by *Salmonella typhimurium* infection was not affected by high extracellular KCl concentrations (Fig. 4B, Supporting Information Fig. 4A and B). In conclusion, our data demonstrate that caspase-11 activation by LPS transfection leads to a drop of intracellular K^+ levels, which is dispensable for the induction of cell death, but required for NLRP3 activation, thus highlighting two separate pathways downstream of cytosolic LPS.

Discussion

The exact cellular events involved in the activation of the NLRP3 inflammasome are still poorly understood [1]. Lysosomal damage, K^+ efflux, ROS, and mitochondrial DNA have been brought forward, but if and how these events are causally connected is unclear. The findings that caspase-11-mediated cytokine production requires the NLRP3 inflammasome has led to speculations that yet another, noncanonical NLRP3 inflammasome exists. The data presented here argue that the noncanonical inflammasome pathway does not involve a noncanonical NLRP3 inflammasome associated with or containing caspase-11, but that rather caspase-11 is upstream of NLRP3 activation. Of note, our data demonstrate that this pathway does not involve a released factor, but proceeds cell autonomously, thus excluding the possibility that NLRP3 senses caspase-11-induced pyroptosis in neighboring cells. Interestingly, we could show that the key event during caspase-11-triggered NLRP3 activation is K^+ efflux, while the involvement of mitochondrial ROS production could not be definitely determined due to off-target effects of ROS scavengers. In agreement with previous findings by Munoz-Planillo et al. [7], we show that K^+ efflux induced by K^+-free medium is sufficient to induce NLRP3 assembly and activation. It remains, however, unclear how active caspase-11 promotes a drop in intracellular K^+ levels—that is, what target proteins need to be cleaved by caspase-11 to trigger K+ efflux or if caspase-11 permeabilizes the membrane directly. Notably, our results indicate that during cytosolic LPS delivery, active caspase-11 leads to massive membrane permeabilization in a majority of cells, which can be measured by PI influx and which could at the same time lead to loss of K^+ from the cell. Yet it could not be directly assessed if these cells also activate NLRP3 before lyzing completely. Given the large number of these cells in the total population, it however seems probable that although these cells have become $PI^{positive}$, they are still proficient in activating the NLRP3 inflammasome upon membrane permeabilization and loss of K^+. Interestingly, this it would indicate that "cell death" as measured by membrane permeabilization does not exclude cellular processes such as NLRP3 activation from happening. Further work such live-cell imaging of LPS-transfected cells and additional studies aimed at identifying caspase-11 target proteins might therefore not only broaden our understanding of how caspases induce lytic cell death and what happens to cells after pyroptosis, but also identify proteins involved in regulating K^+ levels or membrane permeability.

Materials and methods

Mice

Casp1$^{-/-}$*Casp11*$^{-/-}$ (caspase-1-KO), *Asc*$^{-/-}$, *Casp11*$^{-/-}$, and *Nlrp3*$^{-/-}$ mice have been described [6, 12]. Mice were bred in the animal facility of the University of Basel. All animal experiments were approved (license 2535, Kantonales Veterinäramt Basel-Stadt) and were performed according to local guidelines (Tierschutz-Verordnung, Basel-Stadt) and the Swiss animal protection law (Tierschutz-Gesetz).

Cell culture and stimulation

BMDMs were differentiated and cultured as previously described in [2]. Cells were seeded in assay medium (DMEM, 10% FCS, 10% 3T3 conditioned MCSF medium, 10 mM HEPES, 1x NEAA) 1 day prior to stimulation at a density of 2.5×10^4 cells per well in 96-well plates. Cells were primed for 4 h with 1 μg/mL Pam_3CSK_4 in Opti-MEM. LPS/FuGeneHD complexes were prepared by mixing 100 μL Opti-MEM with 2 μg of ultrapure LPS O111:B4 (Invivogen) and 0.5 μL of FugeneHD (Promega) per well to be transfected. The transfection mixture was vortexed briefly, incubated for 15 min at room temperature and added dropwise to the cells. For osmoprotection experiments treatment, glycine was added to a final concentration of 50 mM at 1 h post transfection. Controls

were treated with an equal volume of PBS. For nigericin stimulation and *S. typhimurium* infection, cells were primed for 16 h with Pam_3CSK_4 (1 μg/mL) and stimulated with 20 μM nigericin or infected with log-phase *S. typhimurium* (MOI 25) as described previously [2] in Opti-MEM for 1 h.

Cytokine and LDH release measurement

IL-1β was measured by ELISA (eBioscience). LDH was measured using LDH Cytotoxicity Detection Kit (Clontech). To normalize for spontaneous lysis, the percentage of LDH release was calculated as follows: (LDH infected – LDH uninfected)/(LDH total lysis – LDH uninfected) × 100.

PI influx measurement

Following stimulation/infection of BMDMs, 10× PI was added to 3.9 μM final concentration and the plate was incubated for 15 min at 37°C 5% CO_2. A total of 100% lysis controls were obtained by addition of Saponin (0.04% final concentration). Plates was transferred on ice until measurement on a synergy H1 plate reader (biotek, Ex 485/Em 580, bottom read).

CFSE labeling and coculture

BMDMs were harvested and labeled with 5 μM CFSE (Abcam) in PBS for 12 min at room temperature in the dark. CFSE was quenched by addition of assay medium. Cells were pelleted, counted, and mixed with unlabeled cells at the indicated ratios before stimulation.

ASC speck immunofluorescence

BMDMs were plated at 1.5×10^5 cells per well in 24-well plates on sterile glass coverslips and treated as outlined in the figure legend. Coverslips were stained and mounted as done previously [2] using rat-anti-ASC antibodies (1:1000, Genentech) and Alexa-568 conjugated anti-rat-antibodies (1:500, goat anti-rat Alexa 568, Life Technologies, A11077). Slides were analyzed on a LSM700-Upright confocal microscope. Images were analyzed with Image-J; ASC specks and cells per field of view were counted manually. Per experiment four images (at least 100 cells per condition) from two coverslips were quantified.

ASC oligomerization

BMDMs were seeded 1.1×10^6 cells per well in 6-well plates and grown for at least 48 h. Afterward stimulation, purification, and cross-linking of ASC pyroptosomes were done as described elsewhere [7]

Western blotting

Immunoblots were done according to standard protocols. Primary antibodies were as follows: rabbit-anti-caspase-1 p10 (SCBT sc-514, 1:1000), rabbit-anti-HMGB-1 (Genetex, GTX-101277, 1:3000), goat-anti-IL-1β (R&D AF-401-NA, 1:2000), rabbit-anti-alpha-tubulin (abcam ab-4074-100, 1:1000), mouse-anti-NLRP3 (Enzo Life Sciences ALX-804-880-C100, 1:3000), anti ASC (Adipogen AG-25B-0006, 1:1000), anti-GAPDH (SCBT SC-365062, 1:500). Secondary antibodies were as follows: goat-anti-rabbit-HRP (Invitrogen G21234), rabbit-anti-mouse-HRP (Invitrogen 816720), rabbit-anti-goat (Invitrogen 811620).

MitoSOX staining

BMDMs were seeded at 0.25×10^6 cells per well in 24-well plates and allowed to adhere overnight. After stimulation, cells were washed once with warm PBS and stained with 300 μL of assay medium containing MitoSOX reagent (5 μM) for 15 minutes at 37°C, 5% CO_2. After labeling, the plate was transferred on ice, cells were washed with ice-cold PBS, and stained using the near-infrared L/D marker (1:1000) in PBS for 20 min on ice in the dark. Cells were washed twice, detached with a cells scraper, and transferred to FACS tubes in 300 μL PBS containing 2% FCS and 1 mM EDTA. L/D negative cells were analyzed for MitoSOX staining on a BD Canto II Flow Cytometer. At least 3000 live cells were acquired.

Stimulation for treatment with inhibitors

For treatment with NAC and MitoTEMPO, cells were primed overnight with Pam_3CSK_4 and preincubated with the inhibitor in twice the final concentration in 100 μL (PI/LDH/ELISA) or 200 μL (MitoSOX) of Opti-MEM for 30 min, prior to stimulation, if not indicated differently in the figure legends. Stimuli were added in 100 and 200 μL to yield a final concentration of 1× inhibitor and 1× stimulus, respectively.

Incubation in K^+-free medium

Cells were primed with 300 ng/mL LPS O55:B5 for 3 h and subsequently washed three times with Buffer A (4.2 mM Na_2CO_3, 0.8 mM Na_2HPO_4, 1.3 mM $CaCl_2$, 0.5 mM $MgCl_2$, 10 mM D-glucose monohydrate, pH 7.4) supplemented with 137 mM NaCl and 5 mM choline chloride. Nonstimulated controls were washed with Buffer A supplemented with 137 mM and 5 mM KCl. Cells were incubated for indicated times in respective buffers and inflammasome activation was determined as described above or K^+ concentrations were determined as described below.

Stimulation in high-K^+ medium

Prior to stimulation, cells were washed once with Buffer A (see above) supplemented with 137 mM NaCl and 5 mM KCl. Buffer A with 2× ion concentrations was added to respective wells—that is, supplemented with 274 mM NaCl and 10 mM KCl, 259 mM NaCl and 25 mM KCl, 234 mM NaCl and 50 mM KCl, 184 mM NaCl and 100 mM KCl. The stimulus was added in an equal volume of plain Buffer A to yield a final 1× concentration of respective ions and stimuli.

Intracellular K^+ measurements

Intracellular K^+ measurements were performed essentially as described [19]. BMDMs were seeded at a density of 0.2×10^6 per well of a 24-well plate and stimulated as described in the respective figure legend. After stimulation at 37°C 5% CO_2, the medium was removed until 270 μL were left and 30 μL of 10× staining solution (100 μM PBFI-AM, 25 mM Probenecid, 0.4% v/v Pluronic-123) was added per well and the plate was incubated for 45 min at room temperature in the dark. The plate was transferred on ice and washed once with ice-cold PBS, cells were stained with 1× PI (3.9 μM final) for 5 min on ice and lifted with a cell scraper and transferred to 5 mL FACS tube (BD) in 0.5 mL PBS, 2% FCS, 1 mM Probenecid. Cells were analyzed for PBFI fluorescence on a Fortessa Flow Cytometer (BD).

Statistical analysis

Statistical data analysis was done using Prism 5.0a (GraphPad Software). To evaluate the differences between two groups the Student's *t*-test was used.

Acknowledgments: We would like to thank Dr. Daniel Pinschewer, Kerstin Schmidt, and Sandra Kallert for access to the Flow Cytometry facilities and help with FACS analysis, and furthermore Dr. Jean Pieters for contribution of reagents. The study was supported by Swiss National Science Foundation funding (PP00P3_139120/1) to P.B. and a Werner Siemens Fellowship to (FFE Fellowship) S.R.

Conflict of interest: The authors declare no commercial or financial conflict of interests.

References

1 **von Moltke, J., Ayres, J. S., Kofoed, E. M., Chavarria-Smith, J. and Vance, R. E.**, Recognition of bacteria by inflammasomes. *Annu. Rev. Immunol.* 2013. **31**: 73–106.

2 **Broz, P., von Moltke, J., Jones, J. W., Vance, R. E. and Monack, D. M.**, Differential requirement for caspase-1 autoproteolysis in pathogen-induced cell death and cytokine processing. *Cell Host Microbe* 2010. **8**: 471–483.

3 **Lamkanfi, M., Vande Walle, L. and Kanneganti, T. D.**, Deregulated inflammasome signaling in disease. *Immunol. Rev.* 2011. **243**: 163–173.

4 **Jin, T., Perry, A., Jiang, J., Smith, P., Curry, J. A., Unterholzner, L., Jiang, Z. et al.**, Structures of the HIN domain: DNA complexes reveal ligand binding and activation mechanisms of the AIM2 inflammasome and IFI16 receptor. *Immunity* 2012. **36**: 561–571.

5 **Schroder, K. and Tschopp, J.**, The inflammasomes. *Cell* 2010. **140**: 821–832.

6 **Petrilli, V., Papin, S., Dostert, C., Mayor, A., Martinon, F. and Tschopp, J.**, Activation of the NALP3 inflammasome is triggered by low intracellular potassium concentration. *Cell Death Differ.* 2007. **14**: 1583–1589.

7 **Munoz-Planillo, R., Kuffa, P., Martinez-Colon, G., Smith, B. L., Rajendiran, T. M. and Nunez, G.**, K(+) efflux is the common trigger of NLRP3 inflammasome activation by bacterial toxins and particulate matter. *Immunity* 2013. **38**: 1142–1153.

8 **Hornung, V., Bauernfeind, F., Halle, A., Samstad, E. O., Kono, H., Rock, K. L., Fitzgerald, K. A. et al.**, Silica crystals and aluminum salts activate the NALP3 inflammasome through phagosomal destabilization. *Nat. Immunol.* 2008. **9**: 847–856.

9 **Halle, A., Hornung, V., Petzold, G. C., Stewart, C. R., Monks, B. G., Reinheckel, T., Fitzgerald, K. A. et al.**, The NALP3 inflammasome is involved in the innate immune response to amyloid-beta. *Nat. Immunol.* 2008. **9**: 857–865.

10 **Shimada, K., Crother, T. R., Karlin, J., Dagvadorj, J., Chiba, N., Chen, S., Ramanujan, V. K. et al.**, Oxidized mitochondrial DNA activates the NLRP3 inflammasome during apoptosis. *Immunity* 2012. **36**: 401–414.

11 **Zhou, R., Yazdi, A. S., Menu, P. and Tschopp, J.**, A role for mitochondria in NLRP3 inflammasome activation. *Nature* 2011. **469**: 221–225.

12 **Kayagaki, N., Warming, S., Lamkanfi, M., Vande Walle, L., Louie, S., Dong, J., Newton, K. et al.**, Non-canonical inflammasome activation targets caspase-11. *Nature* 2011. **479**: 117–121.

13 **Broz, P., Ruby, T., Belhocine, K., Bouley, D. M., Kayagaki, N., Dixit, V. M. and Monack, D. M.**, Caspase-11 increases susceptibility to Salmonella infection in the absence of caspase-1. *Nature* 2012. **490**: 288–291.

14 **Rathinam, V. A., Vanaja, S. K., Waggoner, L., Sokolovska, A., Becker, C., Stuart, L. M., Leong, J. M. et al.**, TRIF licenses caspase-11-dependent NLRP3 inflammasome activation by Gram-negative bacteria. *Cell* 2012. **150**: 606–619.

15 **Kayagaki, N., Wong, M. T., Stowe, I. B., Ramani, S. R., Gonzalez, L. C., Akashi-Takamura, S., Miyake, K. et al.**, Noncanonical inflammasome activation by intracellular LPS independent of TLR4. *Science* 2013. **341**: 1246–1249.

16 **Hagar, J. A., Powell, D. A., Aachoui, Y., Ernst, R. K. and Miao, E. A.**, Cytoplasmic LPS activates caspase-11: implications in TLR4-independent endotoxic shock. *Science* 2013. **341**: 1250–1253.

17 **Shi, J., Zhao, Y., Wang, Y., Gao, W., Ding, J., Li, P., Hu, L. et al.**, Inflammatory caspases are innate immune receptors for intracellular LPS. *Nature* 2014. **514**: 187–192.

18 **Arlehamn, C. S., Petrilli, V., Gross, O., Tschopp, J. and Evans, T. J.**, The role of potassium in inflammasome activation by bacteria. *J. Biol. Chem.* 2010. **285**: 10508–10518.

19 **Bortner, C. D., Hughes, F. M., Jr. and Cidlowski, J. A.**, A primary role for K^+ and Na^+ efflux in the activation of apoptosis. *J. Biol. Chem.* 1997. **272**: 32436–32442.

Abbreviations: **AIM2**: Absent in Melanoma 2 · **ASC**: Apoptosis-associated speck-like protein containing a CARD · **BMDM**: bone-marrow-derived macrophages · **CARD**: Caspase Recruitment Domain · **DSS**: disuccinimidyl suberate · **HMGB-1**: High-Mobility-Group-Protein B1 · **L/D**: live–dead · **LDH**: lactate dehydrogenase · **MAMP**: microbe-associated molecular pattern · **MCSF**: macrophage colony stimulating factor · **NAC**: N-acetyl-cysteine · **NEAA**: Non-essential aminoacids · **NLR**: NOD-like receptor · **PAM3CSK4**: Palmitoyl-3-cysteine-serine-lysine · **PBFI-AM**: Potassium Binding Fluorescent Indicator - acetoxymethyl ester · **PYHIN**: Pyrin and HIN-domain containing protein

Full correspondence: Dr. Petr Broz, Focal Area Infection Biology, Biozentrum, University of Basel, Klingelbergstrasse 50/70, CH-4056 Basel, Switzerland
Fax: +41-61-267-21-18
e-mail: petr.broz@unibas.ch

See accompanying articles:
http://dx.doi.org/10.1002/eji.201545655
http://dx.doi.org/10.1002/eji.201545523

See accompanying Commentary:
http://dx.doi.org/10.1002/eji.201545958

Received: 3/5/2015
Revised: 30/6/2015
Accepted: 10/7/2015
Accepted article online: 14/7/2015

4.2 Research Article II: GSDMD membrane pore formation constitutes the mechanism of pyroptotic cell death.

Lorenzo Sborgi[1,*], Sebastian Rühl[1,*], Estefania Mulvihill[2], Joka Pipercevic[1], Rosalie Heilig[1], Henning Stahlberg[1], Christopher J. Farady[3], Daniel J. Müller[2], Petr Broz[1] and Sebastian Hiller[1]

* these authors contributed equally

1 Biozentrum, University of Basel, Klingelbergstr. 70, 4056 Basel, Switzerland
2 Eidgenössische Technische Hochschule (ETH) Zurich, Department of Biosystems Science and Engineering, Mattenstr. 26, 4058 Basel, Switzerland
3 Novartis Institutes for BioMedical Research, Forum 1, Novartis Campus, 4002 Basel, Switzerland

Published online 14.07.2016 The EMBO Journal (2016) 35, 1766-1778

DOI 10.15252/embj.201694696

Statement of contribution:

I performed all experiments in macrophages and HEK293T cells (Figures 1, 2, S1 and S2) as well as complementation experiments described in Figure S4 C and D. I wrote the manuscript together with the other authors.

Published online: July 14, 2016

Article

SOURCE DATA | TRANSPARENT PROCESS | OPEN ACCESS

THE EMBO JOURNAL

GSDMD membrane pore formation constitutes the mechanism of pyroptotic cell death

Lorenzo Sborgi[1,†], Sebastian Rühl[1,†], Estefania Mulvihill[2], Joka Pipercevic[1], Rosalie Heilig[1], Henning Stahlberg[1], Christopher J Farady[3], Daniel J Müller[2], Petr Broz[1,*] & Sebastian Hiller[1,**]

Abstract

Pyroptosis is a lytic type of cell death that is initiated by inflammatory caspases. These caspases are activated within multi-protein inflammasome complexes that assemble in response to pathogens and endogenous danger signals. Pyroptotic cell death has been proposed to proceed via the formation of a plasma membrane pore, but the underlying molecular mechanism has remained unclear. Recently, gasdermin D (GSDMD), a member of the ill-characterized gasdermin protein family, was identified as a caspase substrate and an essential mediator of pyroptosis. GSDMD is thus a candidate for pyroptotic pore formation. Here, we characterize GSDMD function in live cells and *in vitro*. We show that the N-terminal fragment of caspase-1-cleaved GSDMD rapidly targets the membrane fraction of macrophages and that it induces the formation of a plasma membrane pore. *In vitro*, the N-terminal fragment of caspase-1-cleaved recombinant GSDMD tightly binds liposomes and forms large permeability pores. Visualization of liposome-inserted GSDMD at nanometer resolution by cryo-electron and atomic force microscopy shows circular pores with variable ring diameters around 20 nm. Overall, these data demonstrate that GSDMD is the direct and final executor of pyroptotic cell death.

Keywords atomic force microscopy; cell death; gasdermin; inflammasomes; inflammation; pyroptosis

Subject Categories Autophagy & Cell Death; Immunology

DOI 10.15252/embj.201694696 | Received 3 May 2016 | Revised 19 June 2016 | Accepted 28 June 2016 | Published online 14 July 2016

The EMBO Journal (2016) 35: 1766–1778

Introduction

Inflammatory caspases (caspase-1, human caspase-4, human caspase-5, and murine caspase-11) are a group of cysteine-dependent aspartate-directed proteases that is essential for host innate immune defense. Caspase-1 is activated within large multi-protein complexes termed inflammasomes, which are assembled by the protein pyrin or members of the NOD-like receptor (NLR) and PYHIN protein families (Latz *et al*, 2013; von Moltke *et al*, 2013). These proteins act as cytosolic pattern-recognition receptors (PRRs) and detect a variety of pathogen-associated molecular patterns (PAMPs) or endogenous danger signals (DAMPs). In contrast, the bacterial cell wall component lipopolysaccharide (LPS), one of the strongest immune-system activators, leads to the assembly of "non-canonical" inflammasomes through activation of caspase-4, caspase-5 or caspase-11 (Kayagaki *et al*, 2011, 2013; Hagar *et al*, 2013; Shi *et al*, 2014).

The downstream signaling pathways that follow the activation of inflammatory caspases and how the active caspases initiate these events are still poorly understood (Lamkanfi, 2011). Initial work has identified the pro-inflammatory cytokine interleukin (IL)-1β as a key substrate of caspase-1 (Thornberry *et al*, 1992). Subsequently, it was found that caspase-1, as well as caspase-11 and its human orthologs caspase-4 and caspase-5, induces a novel programmed cell death pathway that is characterized by cell swelling, lysis, and the release of cytoplasmic content (Fink & Cookson, 2007; Kayagaki *et al*, 2011; Shi *et al*, 2014), presumably as a result of the formation of membrane pores (Fink *et al*, 2008). Since this type of cell death is morphologically distinct from apoptosis and intrinsically pro-inflammatory, it was named pyroptosis, from the Greek *pyro* (fire or fever) and *ptosis* (to fall) (Bergsbaken *et al*, 2009). The physiological function of pyroptosis is thought to be the prevention of intracellular pathogen replication and to re-expose pathogens to extracellular killing mechanisms (Miao *et al*, 2010).

Several landmark studies have recently identified GSDMD (gasdermin D), a member of the gasdermin protein family, as an essential mediator of pyroptosis in human and murine cells (He *et al*, 2015; Kayagaki *et al*, 2015; Shi *et al*, 2015). GSDMD is required for pyroptosis induction after canonical and non-canonical inflammasome activation and is processed by caspase-1, caspase-11, caspase-4, and caspase-5, but not by apoptotic caspases. The N-terminal fragment of GSDMD ($GSDMD^{Nterm}$) was found sufficient to induce cell death with the morphological features of pyroptosis (Kayagaki *et al*, 2015; Shi *et al*, 2015), and overexpression of the C-terminal domain $GSDMD^{Cterm}$ was found to block $GSDMD^{Nterm}$-dependent cell death

1 Biozentrum, University of Basel, Basel, Switzerland
2 Department of Biosystems Science and Engineering, Eidgenössische Technische Hochschule (ETH) Zurich, Basel, Switzerland
3 Novartis Institutes for BioMedical Research, Forum 1, Basel, Switzerland
*Corresponding author. Tel: +41 6126 72342; E-mail: petr.broz@unibas.ch
**Corresponding author. Tel: +41 6126 72082; E-mail: sebastian.hiller@unibas.ch
†These authors contributed equally to this work

Published online: July 14, 2016

(Shi *et al*, 2015). These results gave rise to the hypothesis that caspase-dependent cleavage releases the N-terminal domain from an inhibitory interaction with the C-terminus, allowing $GSDMD^{Nterm}$ to induce cell death by a yet undefined mechanism. Since pyroptosis had long been speculated to involve the formation of a plasma membrane pore, immediate destruction of the electrochemical gradient, and subsequent osmotic lysis of the host cell (Lamkanfi, 2011), it is likely that $GSDMD^{Nterm}$ either promotes the formation of this pore or itself has pore-forming activity (Broz, 2015). Here, we investigate the functional role of $GSDMD^{Nterm}$ in live cells and *in vitro*. We demonstrate that after cleavage by caspase-1, $GSDMD^{Nterm}$ targets cellular membranes and that it induces the formation of a large permeability pore in the plasma membrane. *In vitro* experiments with purified recombinant GSDMD show that $GSDMD^{Nterm}$ forms large pores in liposomes. We visualize these with cryo-electron and atomic force microscopy. Overall, these results close the gaps in the pyroptotic signaling pathway by providing the proof that GSDMD is the final and direct executor of pyroptotic cell death.

Results

The N-terminal GSDMD fragment induces the formation of a large plasma membrane pore

Pyroptotic cell death involves the formation of a plasma membrane pore, cell swelling, and rupture of the plasma membrane. To investigate whether GSDMD, a recently identified mediator of pyroptosis, mediates pore formation directly, we developed a doxycycline-inducible system to express the N-terminal fragment ($GSDMD^{Nterm}$) of mouse GSDMD in HEK293T cells. Doxycycline treatment caused cell death in HEK293T cells harboring the $GSDMD^{Nterm}$-expressing plasmid, but not in cells harboring a vector control, in a concentration-dependent manner (Fig 1A). To characterize whether $GSDMD^{Nterm}$ expression induced a lytic type of cell death, characteristic for pyroptosis, we next measured the amount of LDH (lactate dehydrogenase) release after doxycycline-induced expression of the $GSDMD^{Nterm}$ (Fig 1B). Increasing levels of $GSDMD^{Nterm}$ expression resulted in increased levels of LDH release, indicating that ectopic expression of the $GSDMD^{Nterm}$ induced death through cell lysis. Microscopy analysis showed that $GSDMD^{Nterm}$-induced death had the morphological features of pyroptosis, *that is*, cell swelling and nuclear condensation. To estimate the size of the $GSDMD^{Nterm}$-induced plasma membrane pore, we next employed an osmoprotection assay based on the addition of polyethylene glycols (PEGs) of increasing molecular weight. Addition of these high-molecular polymers can prevent water influx through pores and the resulting swelling and osmotic lysis, if the molecular diameter of the agent is larger than the diameter of the pore (Appendix Fig S1A). We induced $GSDMD^{Nterm}$ expression by doxycycline addition in HEK293T cells in the presence of PEGs and measured LDH release as a readout for osmotic lysis and propidium iodide (PI) staining as a measure of plasma membrane pore formation (Fig 1C and D). Only the largest sized agent, PEG3000, was able to reduce LDH release partially, while smaller PEGs did not reduce cell lysis. Importantly, PEG3000 did not prevent PI influx, indicating that it does not block the pore directly, but functions as an osmoprotectant. PEGs in the range of 600–3,000 Da did not induce significant levels of cell death when added to cells (Appendix Fig S1B), but larger PEGs could not be used, since they proved to be cytotoxic.

Infection of primary murine bone marrow-derived macrophages (BMDMs) with *Salmonella enterica* serovar Typhimurium (*S. typhimurium*) activates the NLRC4 inflammasome (Mariathasan *et al*, 2004) and results in caspase-1- and GSDMD-dependent pyroptosis and cytokine release (Appendix Fig S1C and D). To estimate the size of the GSDMD-dependent plasma membrane pore in BMDMs, we measured cell lysis as a function of time in the presence of PEGs of increasing size (Fig 1E and F). Consistent with the osmoprotection experiment done in HEK293T cells, we observed that only PEG3000 had a small protective effect, while all smaller PEGs did not prevent pyroptosis. PI influx was not affected by any of the osmoprotectants. IL-1β release was also partially affected by PEG treatment (Appendix Fig S1E); consistent with the observation that pyroptosis is required for efficient release of the mature cytokine in BMDMs (Shi *et al*, 2015). Overall, these experiments suggest that GSDMD-dependent pyroptosis involves the formation of a plasma membrane pore with an inner diameter of over 3.5 nm, the estimated molecular size of PEG3000 (Scherrer & Gerhardt, 1971).

The N-terminal GSDMD fragment targets cellular membranes

$GSDMD^{Nterm}$ might itself form a pore in the plasma membrane or alternatively initiate other events that result in pore formation (Broz, 2015). To define the fate of $GSDMD^{Nterm}$ after caspase-1-dependent cleavage of GSDMD, we followed caspase-1 activation, GSDMD processing, and cell death over time in immortalized wild-type macrophages infected with *S. typhimurium* (Fig 2A, Appendix Fig S2A). The processed caspase-1 p20 fragment, an indicator of caspase-1 activation, appeared within 20 min after infection in the supernatant of macrophages. GSDMD processing correlated with caspase-1 activation and was detectable in the cell lysate as well as in the cell supernatant. LDH release was also detectable at the same time points (Fig 1F and Appendix Fig S1C). Based on these data, we decided to determine the subcellular localization of full-length GSDMD and $GSDMD^{Nterm}$ in either uninfected cells or in cells infected with *S. typhimurium* for 10 and 20 min. Cells were harvested at each of these time points and subjected to subcellular fractionation as outlined (Fig 2B). GSDMD full length was exclusively found in the cytosolic fraction (S150) in uninfected cells (Fig 2C and Appendix Fig S2B), in line with the notion that it is a soluble, cytosolic protein. After infection, full-length GSDMD, but very little $GSDMD^{Nterm}$ was detected in the S150 fraction. Instead, the majority of $GSDMD^{Nterm}$ was found in the P150 fraction and in the P10 fraction, correlating with the presence of the plasma membrane marker Na^+K^+ ATPase. The Na^+K^+ ATPase was also strongly present in the P10, presumably since it is secreted *via* the ER/Golgi pathway. The mitochondrial marker VDAC, a porin of the outer mitochondrial membrane, did not correlate with the $GSDMD^{Nterm}$ and was mainly found in the P0.7 and P10 fractions, but not in the P150 fraction. Overall, these results suggest that the $GSDMD^{Nterm}$ targets membranes after caspase-1-mediated cleavage. To characterize the interaction, we isolated plasma membrane fractions of BMDMs after *S. typhimurium* infection and subjected them to different treatments (Fig 2D). Conditions known to release membrane-associated proteins or destabilize protein–protein

Published online: July 14, 2016
The EMBO Journal The pyroptotic GSDMD pore *Lorenzo Sborgi et al*

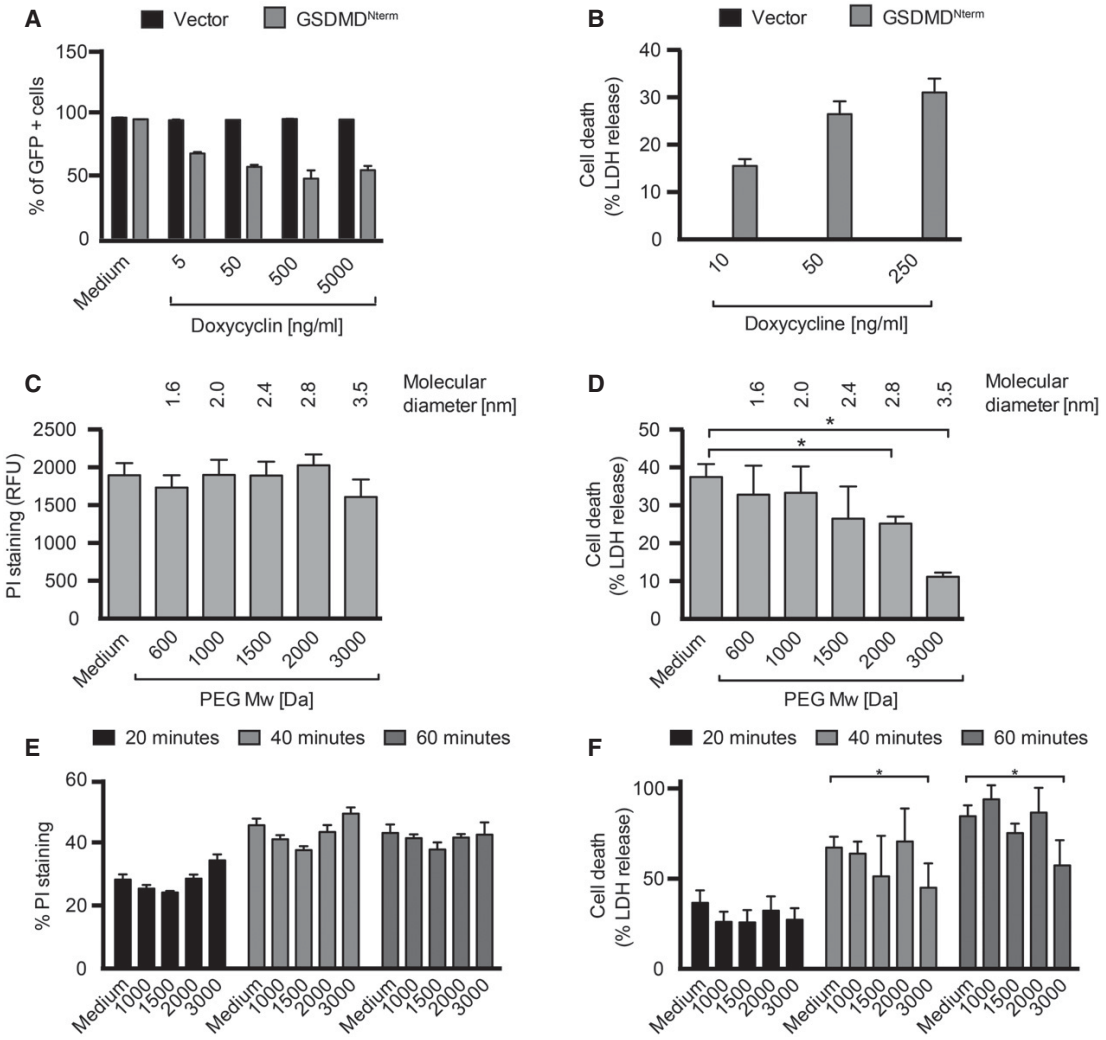

Figure 1. GSDMD^{Nterm} induces the formation of a large plasma membrane pore.

A Cell viability as assessed by GFP expression in HEK293T cells transfected with the pRetroX TetOne3G-eGFP plasmid only (vector) or pRetroX TetOne3G-eGFP harboring the N-terminal fragment of GSDMD. Cells were treated with the indicated concentrations of doxycycline 24 h post-transfection, and the percentage of GFP-positive cells was determined 16 h later by flow cytometry.

B LDH release from HEK293T cells transfected with the pRetroX TetOne3G-eGFP plasmid only (vector) or pRetroX TetOne3G-eGFP harboring the N-terminal fragment of GSDMD. At 24 h post-transfection, cells were treated with the indicated concentrations of doxycycline for 8 h and the percentage of LDH release was determined. Graphs show mean and s.d. of quadruplicate wells.

C, D PI staining of and LDH release from HEK293T cells transfected with pRetroX TetOne3G-eGFP harboring the N-terminal fragment of GSDMD in the presence of osmoprotectants. At 24 h post-transfection, PEGs of the indicated molecular weights were added to a final concentration of 30 mM, cells were treated with 250 ng ml^{-1} doxycycline for 8 h, and the level of PI staining (C) or LDH release (D) was determined.

E, F PI staining of and LDH release from LPS-primed primary BMDMs infected with log-phase *S. typhimurium* for the indicated time points in the presence of PEGs of the indicated molecular weight (numbers on the *x*-axis, 30 mM final concentration).

Data information: Graphs show mean and s.d. of quadruplicate wells (B–F) or the mean and s.d. of duplicate wells (A). *$P < 0.05$ as determined by Student's *t*-test. Data are representative of at least three independent experiments.

interactions (Gatfield & Pieters, 2000), such as high salt (1 M NaCl) and sodium carbonate (pH 11) did not solubilize GSDMD^{Nterm}. Extraction of the plasma membrane with 0.02% digitonin, a cholesterol-sequestering detergent, did not solubilize GSDMD^{Nterm} either. Only the disruption of the membrane with low concentrations of the detergent SDS (0.1%) was able to fully solubilize GSDMD^{Nterm}. Consistently, extraction of BMDMs membranes with 1% Triton was also able to partly solubilize GSDMD^{Nterm}

Published online: July 14, 2016

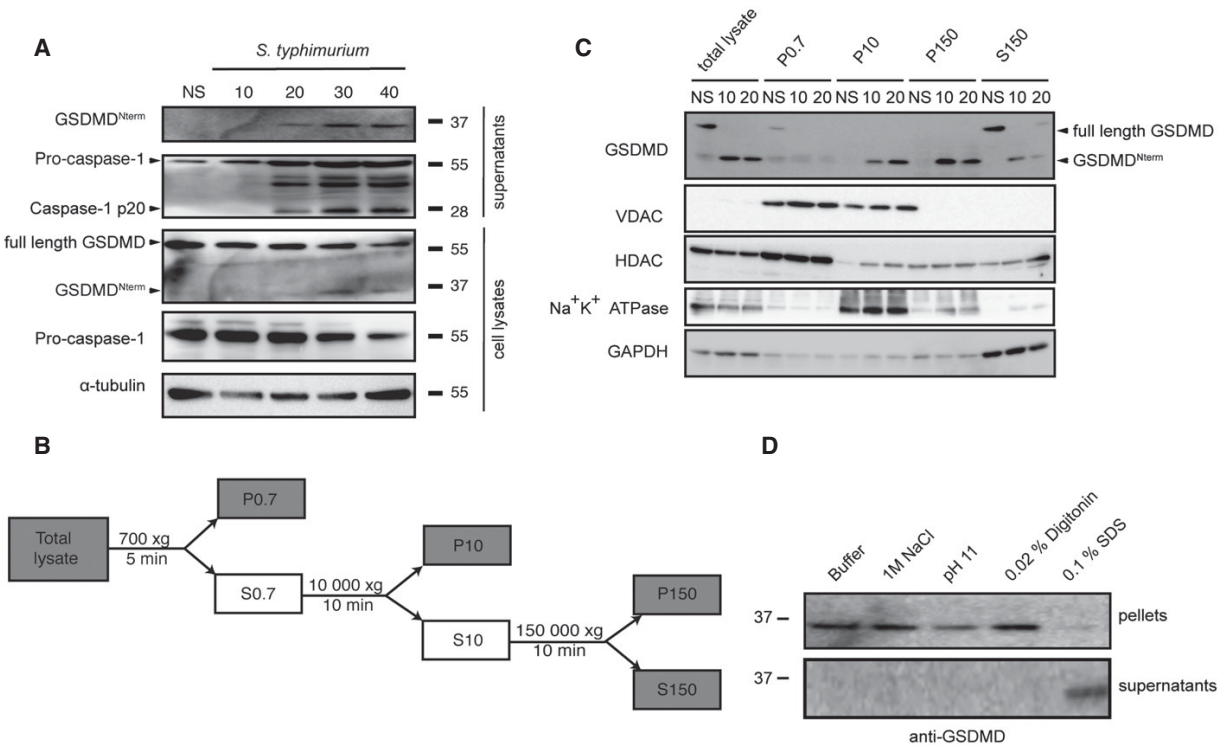

Figure 2. GSDMD^{Nterm} localizes to cellular membranes after inflammasome activation.

A Immunoblot analysis of cleaved GSDMD in culture supernatants and full-length GSDMD, cleaved GSDMD and α-tubulin in the cell lysates of immortalized LPS-primed WT macrophages left uninfected (NS) or infected for 10–40 min with log-phase *S. typhimurium* (MOI = 50).

B Schematic representation of the subcellular fractionation shown in (C).

C Fractionation and immunoblot analysis for GSDMD, Na^+K^+ ATPase, VDAC (voltage-dependent anion channel), HDAC1 (histone deacetylase 1), and GAPDH (glycerinaldehyd-3-phosphate dehydrogenase) of WT macrophages infected for 10 and 20 min with log-phase *S. typhimurium* (MOI = 50). Fractionation was carried out as described in the Materials and Methods section, and equivalent amount of protein was loaded per lane.

D Extraction of cleaved GSDMD from isolated membranes of WT macrophages infected for 10 min with log-phase *S. typhimurium* (MOI = 50). Extraction was carried in variable conditions as described in the Materials and Methods section.

Source data are available online for this figure.

(Appendix Fig S2C). Thus, GSDMD^{Nterm} integrates into cellular membranes in a cholesterol-independent manner, and this integration is associated with formation of a pore and cell lysis.

The N-terminal fragment of GSDMD associates to liposomes *in vitro*

These findings encouraged us to attempt the reconstitution of a possible pore-forming function of GSDMD^{Nterm} *in vitro*. We established recombinant expression for full-length human GSDMD in *E. coli* BL21(DE3) expression cells. The protein expressed well with yields of 1.5 mg l^{-1} cell culture. Notably, following the same protocol, GSDMD^{Nterm} did not express in *E. coli* BL21(DE3) cells to detectable levels by SDS–PAGE, in agreement with the hypothesis that the protein might have a toxic effect on the host cells. Full-length GSDMD was isolated and purified to homogeneity (Appendix Fig S3A). It elutes as a monodisperse, homogeneous elution peak from size exclusion chromatography, at the position of the expected monomeric species. Thermal denaturation showed a melting point of 43°C, indicating that the protein is folded and can be thermally denatured. Upon incubation with different human caspases, we confirmed that recombinant GSDMD is cleaved by caspase-1, but not by the apoptotic caspase-3 or caspase-8 (Shi *et al*, 2015). Recombinant GSDMD is thus a functional substrate of its native enzyme. Then, we characterized the time dependence of GSDMD cleavage (Fig 3A). About 5 nM of caspase-1 cleaves more than 50% of 2 μM of GSDMD in 40 min. GSDMD cleavage by caspase-1 results in a 30-kDa N-terminal (GSDMD^{Nterm}) and a 22-kDa C-terminal (GSDMD^{Cterm}) fragment. In aqueous solution in the absence of a lipidic phase, GSDMD^{Nterm} is not soluble and forms aggregates, as demonstrated in a cross-linking experiment (Fig 3B). After cleavage, the N-terminus is highly cross-linked by DSS (disuccinimidyl suberate), while the 22-kDa GSDMD^{Cterm} remains soluble. To determine whether the poorly soluble GSDMD^{Nterm} associates with lipids, GSDMD was incubated in the presence or absence of active caspase-1 with unilamellar liposomes made of either 1,2-dimyristoyl-sn-glycero-3-phosphocholine (DMPC) or from *E. coli* polar lipid extract. Ultracentrifugation allowed for separation of the

Published online: July 14, 2016
The EMBO Journal The pyroptotic GSDMD pore *Lorenzo Sborgi et al*

liposomes from the soluble fraction. Whereas full-length GSDMD did not associate with either the DMPC or the *E. coli* polar extract liposomes, the GSDMD^{Nterm} fully associated with either of the two membrane mimetics. GSDMD^{Cterm} did not associate with the liposomes (Fig 3C). Therefore, the soluble GSDMD^{Cterm} domain is acting in full-length GSDMD not only as an inhibitor of GSDMD^{Nterm} but also as a solubility tag for the intrinsically insoluble and lipophilic GSDMD^{Nterm}, preventing it from aggregation and membrane association. Once cleaved, GSDMD^{Nterm} associates strongly to available membranes. DMPC liposomes are made from a chemically pure compound, showing that membrane association by GSDMD^{Nterm} does not require any specific receptors in the membrane.

The N-terminal fragment of GSDMD forms pores in liposomes

Next, we asked whether liposome-associated GSDMD^{Nterm} forms transmembrane pores. Liposomes filled with a self-quenching concentration of the fluorophore 6-carboxyfluorescein were incubated with recombinant full-length GSDMD in the presence or absence of active caspase-1 (Fig 4). Release of the fluorophore from the liposome interior results in a strong reduction in the concentration-dependent self-quenching effect and consequently in an increase of the overall fluorescence signal, as demonstrated by chemical rupture of the liposomes with the detergent Triton X in a control experiment (Appendix Fig S5). Neither caspase-1 nor full-length GSDMD alone was able to release dye from the liposomes, but in the presence of both GSDMD and caspase-1, dye release was observed, indicating the formation of permeability pores with open diameters of at least the molecular size of 6-carboxyfluorescein (≈1 nm). The dye release reaction from liposomes includes at least three kinetic steps: the first step is the proteolytic cleavage of GSDMD by caspase-1, the second step is the membrane association, and the third step is pore formation of GSDMD^{Nterm}. Whereas the first step follows classical Michaelis–Menten kinetics, the reaction mechanisms of the second and third steps may include additional oligomerization steps with non-trivial concentration dependence. In an attempt to visualize the concentration dependence of the overall reaction, we measured the kinetics of dye release as a function of GSDMD concentration at a constant caspase-1 concentration of 5 nM (Fig 4A). At a GSDMD concentration of 520 nM, the dye release is very efficient so that in 20 min, already more than 90% of the total fluorescence signal is observed. With decreasing GSDMD concentration, the overall reaction rate decreases, but the overall dye release nonetheless reaches 100%, showing that sufficient GSDMD is available to permeate all liposomes. This conclusion breaks down at a GSDMD concentration of 65 nM, where only about 50% of the liposomes are permeated at late time points.

We then measured the kinetics of dye release as a function of the caspase-1 concentration in the range 1.2–15 nM, while keeping the GSDMD concentration constant at 130 nM (Fig 4B). In this experiment, by decreasing the concentration of caspase-1, we expect a reduction of the availability of cleaved GSDMD^{Nterm} by the initial protease cleavage step, and consequently, we observe a deceleration of the dye release reaction. The total amount of GSDMD is always sufficient to permeate all liposomes in the setup, and consequently, we observe 100% dye release levels in all measurements.

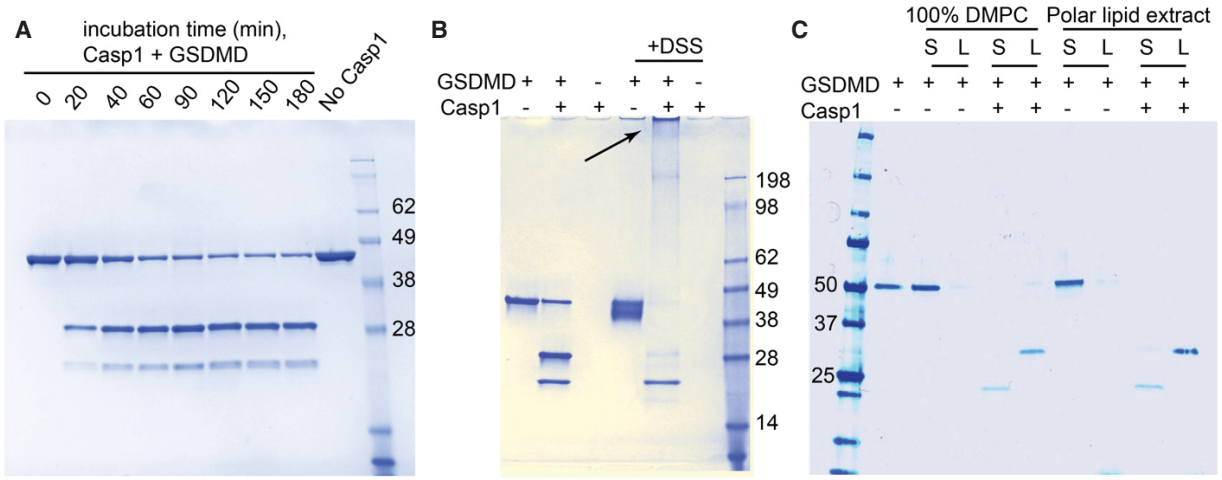

Figure 3. GSDMD^{Nterm} targets liposomes after caspase-1 cleavage.

A Human GSDMD at a concentration of 2 μM was incubated at room temperature with 5 nM caspase-1. The protein was cleaved in a time-dependent manner into two bands of 31 kDa (GSDMD^{Nterm}) and 22 kDa (GSDMD^{Cterm}).

B Cross-linking experiment of full-length and cleaved GSDMD. GSDMD at a concentration of 2 μM was incubated at room temperature with 5 nM caspase-1. After enzymatic cleavage, GSDMD^{Nterm} is highly cross-linked by DSS, resulting in the gel-impenetrating species highlighted by the arrow. GSDMD^{Cterm} is not cross-linked.

C GSDMD at a concentration of 1 μM was incubated at room temperature with 5 nM caspase-1 and liposomes composed of 4 mM DMPC or polar lipid extract derived from *E. coli*. After 2 h, the lipid fraction (L) was separated from the supernatant (S) by ultracentrifugation at 4°C for 1 h at 120,000 *g*.

Source data are available online for this figure.

Published online: July 14, 2016

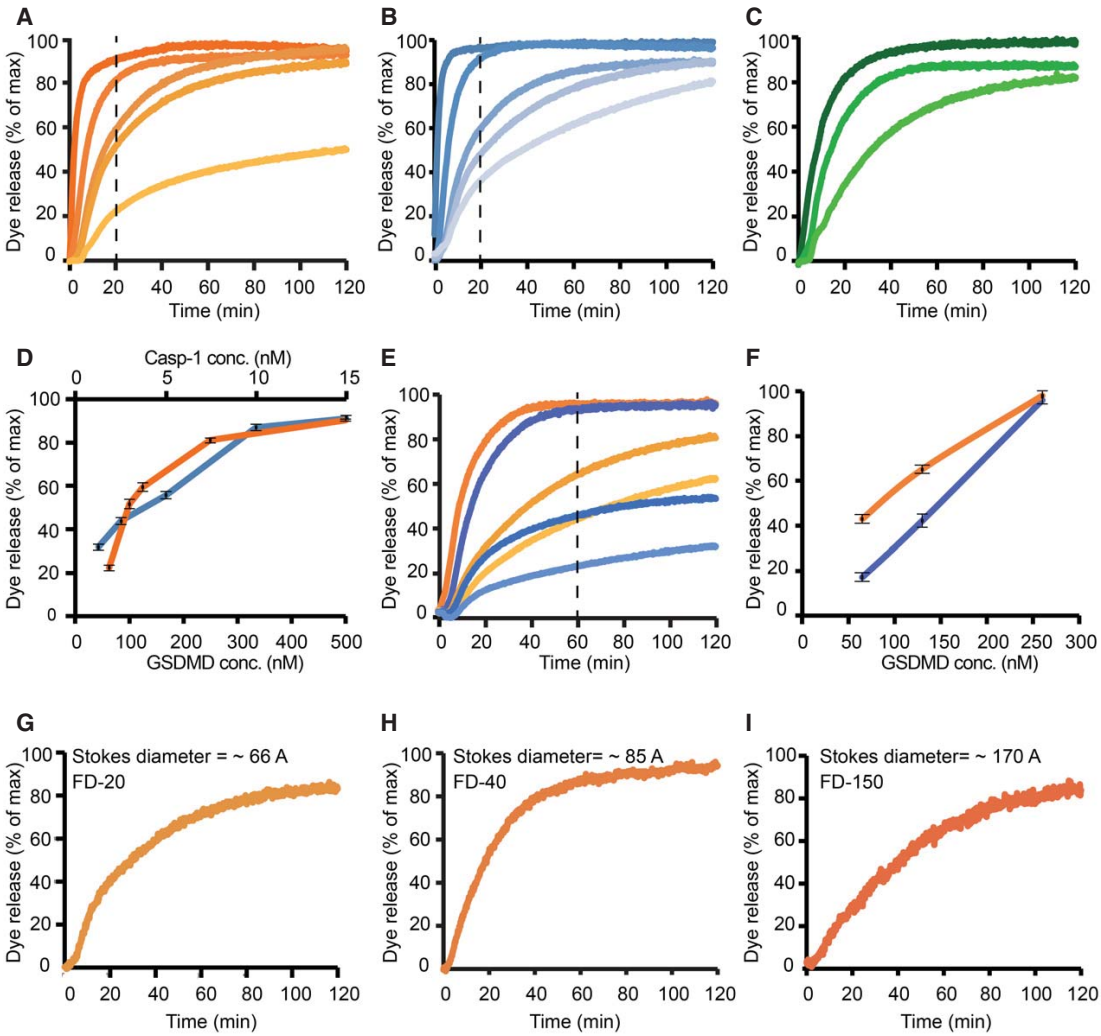

Figure 4. GSDMD^{Nterm} causes liposome permeability by pore formation.

A–I Dye release time courses from liposomes as a percentage of maximal release. (A) Five different reactions, where 5 nM caspase-1 and 400 μM 6-carboxyfluorescein-loaded liposomes prepared with *E. coli* polar lipids were incubated with GSDMD concentrations of (nM): 520, 260, 130, 100, 65 (colored dark to light orange). The time point of 20 min is highlighted by a vertical dashed line. (B) Five different reactions, where 130 nM of GSDMD and 400 μM 6-carboxyfluorescein-loaded liposomes prepared with *E. coli* extract polar lipid, were incubated with caspase-1 concentration of (nM): 15, 8, 5, 2.5, 1.2 (colored dark to light blue). The time point of 20 min is highlighted by a vertical dashed line. (C) Three different reactions, where 5 nM caspase-1 and 400 μM 6-carboxyfluorescein-loaded liposomes prepared with porcine brain total lipid extract, were incubated with GSDMD concentrations of (nM): 520, 260, 100 (colored dark to light green). (D) Dye release at 20-min reaction as a function of GSDMD (dark orange) and caspase-1 (dark blue) concentrations. Error bars for three independent experiments are shown. (E) Two different sets of reactions, where wild-type GSDMD (dark to light orange) and the mutant GSDMD^{I104N} (dark to light blue) were independently incubated at the concentrations of 260, 130, and 65 nM with 5 nM caspase-1 and 400 μM 6-carboxyfluorescein-loaded liposomes. The time point of 60 min is highlighted by a vertical dashed line. (F) Dye release at 60 min of reaction as a function of GSDMD wild-type (dark orange) and GSDMD^{I104N} (dark blue) concentration. Error bars for three independent experiments are shown. (G–I) Dye release from 400 μM liposomes loaded with the 6-carboxyfluorescein derivates FD-20, FD-40, and FD-150, with variable Stokes diameters, as indicated. 130 nM of GSDMD and 5 nM caspase-1 were incubated with the liposomes. For each experiment, a representative from three independent experiments is shown. The corresponding raw data are shown in Appendix Figure S5.

Importantly, GSDMD did not only permeate liposomes made of bacterial lipid extract (Fig 4A and B), but similarly also liposomes from a eukaryotic source (Fig 4C). In a next experiment, we examined the functionality of the I105N mutant of GSDMD. This mutant had played a key role in the discovery of GSDMD, since it had previously been identified as a loss-of-function mutant in mouse models (Kayagaki *et al*, 2015). We generated the analogous mutation I104N in GSDMD and expressed and purified the mutant protein with the same biochemical protocols as the wild-type protein. GSDMD^{I104N} is cleaved by caspase-1 with kinetics

Published online: July 14, 2016
The EMBO Journal The pyroptotic GSDMD pore *Lorenzo Sborgi et al*

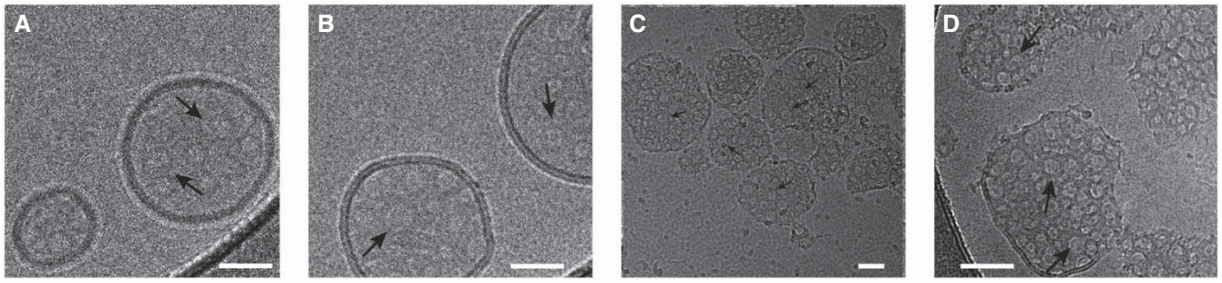

Figure 5. Visualization of GSDMD^{Nterm} pores in liposomes by cryo-electron microscopy.

A–C Cryo-electron micrographs of GSDMD^{Nterm} pores in *E. coli* polar lipid liposomes. The micrographs were acquired at protein/lipid molar ratios of 1/1,000, 1/500, and 1/100, respectively. Black arrows indicate ring-shaped structures corresponding to oligomeric GSDMD^{Nterm} pore forms. Scale bars = 80 nm.

D Proteoliposome with protein/lipid molar ratio of 1/100 at higher magnification. Black arrows indicate ring-shaped structures corresponding to oligomeric GSDMD^{Nterm} pore forms. Scale bar = 80 nm.

indistinguishable from wild-type GSDMD (Appendix Fig S4A and B). In the dye release assay, at high protein concentrations, GSDMD^{I104N} is able to form functional pores with only minor differences to the wild-type protein. At reduced proteins concentrations, however, it showed reduced activity compared to the wild-type protein (Fig 4E and F). Consistent with these data and previously published work (Kayagaki *et al*, 2015), we found that GSDMD^{I104N} could also induce cell death of HEK293T cells when expressed by a doxycycline-inducible promoter, although significantly less than the WT protein (Appendix Fig S4D). Similarly, expression of the I104N mutant of human GSDMD in immortalized *Gsdmd*-deficient mouse macrophages partially restored pyroptosis after *Salmonella* infection when compared to wild-type human GSDMD (Appendix Fig S4C). The quantitative differences observed here may well translate into an effective loss-of-function effect in whole animals, and our experiments thus confirm the functional deficiency of the mouse I105N mutant. As an additional control experiment, we verified that uncleaved GSDMD full length does not form pores in liposomes (Appendix Fig S5E and F). Next, we addressed the size of the GSDMD pore in liposomes by using carbohydrate-conjugated fluorophores as markers. These fluorophores have differently long carbohydrate chains attached, resulting in different overall Stokes radii. We selected three different fluorophores with Stokes radii of 33, 45, and 85 Å, but all of them were still released by the GSDMD pore (Fig 4G–I). This suggests that the pyroptosis pore formed by GSDMD^{Nterm} can reach diameters of at least 15 nm, in full agreement with the cellular experiments.

Visualization of GSDMD pores

We employed two methods to resolve pores of GSDMD^{Nterm} in liposomes at nanometer resolution. Cryo-electron micrographs of untreated liposomes show intact spherical shapes (Appendix Fig S6A). Also the incubation with full-length GSDMD in the absence of caspase-1 did not result in visual distortions of the liposomes (Appendix Fig S6B). However, upon addition of caspase-1 and subsequent incubation, large ruptures of the liposome structure were observed. In these preparations, the liposome surface features numerous large rings of dense material with inner diameters of ≈20 nm (Fig 5A–D and Appendix Fig S6C–E). These rings are formed by GSDMD^{Nterm} and although the liposomes appear completely covered by the assemblies, from the available contrast of the micrographs, it remains inconclusive, whether these rings are lipid-filled protrusions or actual transmembrane pores. The lack of contrast also did not allow for a clear identification of the different shapes of GSDMD oligomers. To characterize the assembly of the transmembrane pores convincingly, we thus imaged GSDMD oligomers and pore formation on liposomes by atomic force microscopy (AFM). In an initial control experiment, we adsorbed either GSDMD alone, or caspase-1 alone, or GSDMD and caspase-1 together to freshly cleaved mica, which we used as sample support in our AFM studies (Appendix Fig S7A–D). GSDMD and caspase-1 readily adsorbed to the negatively charged hydrophilic mica surface as monomers or small oligomers, but did not assemble into arcs or rings. After this, we incubated liposomes composed of *E. coli* polar lipids with GSDMD and caspase-1 for 90 min at 37°C and adsorbed the sample onto freshly cleaved mica. The AFM topographs recorded in buffer solution showed that upon adsorption to mica, the liposomes opened as single-layered membrane patches (Appendix Fig S7E). At higher resolution, the topographs showed GSDMD bound to the lipid membranes and forming arc-, slit- and ring-shaped oligomers (Fig 6A–E and Appendix Fig S7F). The height profile around the arc-, slit- and ring-like oligomers indicates that they protruded 4.3 ± 0.3 nm (average ± s.d.; n = 218) from the lipid surface and that each of them could form pores through the lipid membrane (Fig 6F and G). Occasionally, arcs and slits combined into ring-shaped structures, which were not yet perfectly circular and only partially associated with the formation of membrane pores. Several pore-forming toxins (PFTs) have shown the ability to bind to lipid membranes as oligomers forming arcs or slits that can dynamically rearrange on the membrane surface to form larger pores (Leung *et al*, 2014; Sonnen *et al*, 2014; Mulvihill *et al*, 2015; Podobnik *et al*, 2015). In agreement with this observation, GSDMD arcs and slits were found that presumably fused into perfect ring-shaped GSDMD^{Nterm} oligomers of variable diameters, with an average value of 21 nm (Fig 6F–H). These AFM topographs thus clearly show a structural variability of the GSDMD^{Nterm} assembly, which is, however, determined to eventually lead to the assembly of ring-like structures. These ring-like structures correspond to the pyroptotic membrane pores.

Published online: July 14, 2016

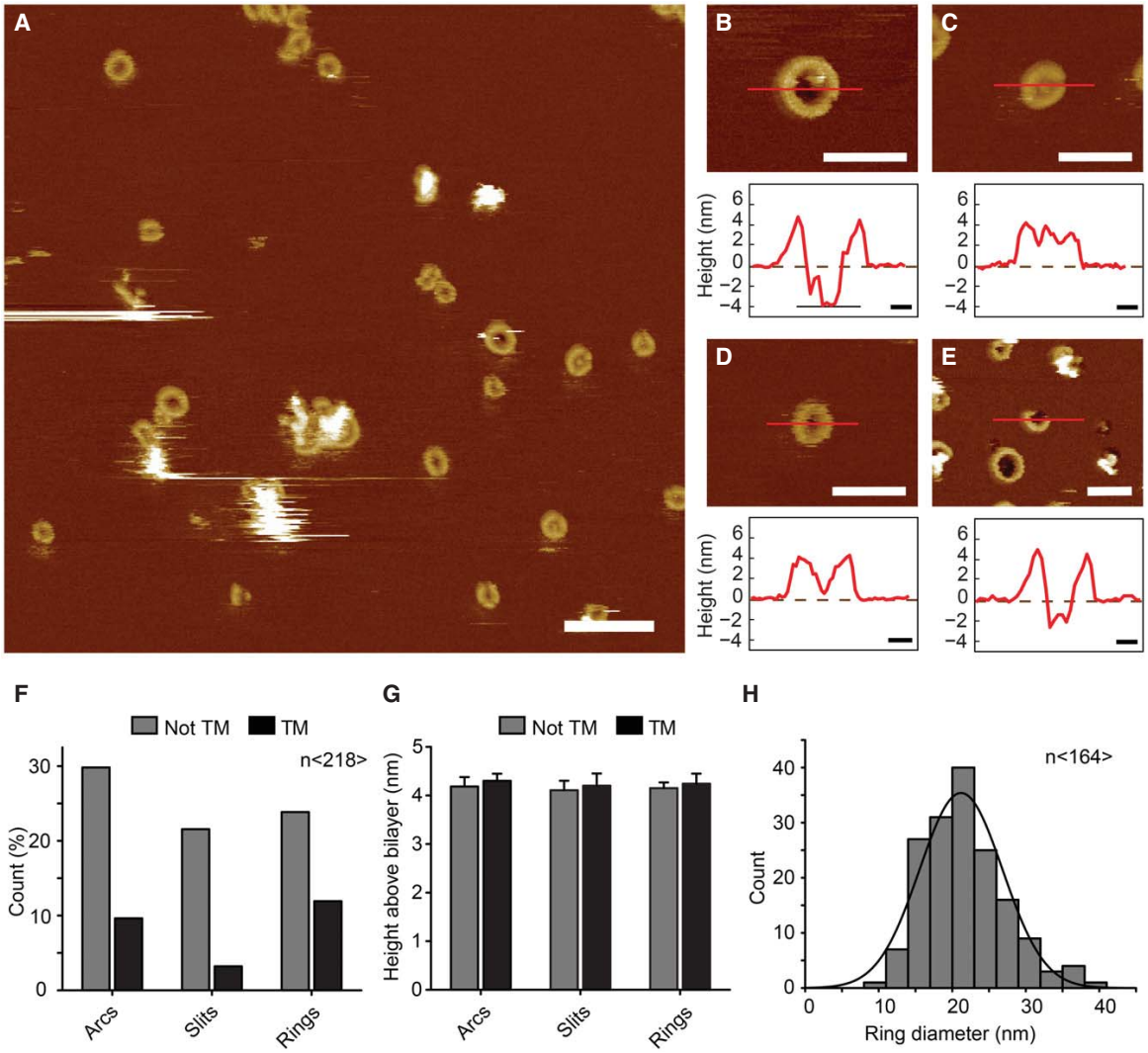

Figure 6. Characterization of GSDMD^{Nterm} pores by atomic force microscopy.

A AFM topograph of GSDMD^{Nterm} bound to lipid membranes of *E. coli* polar lipids. Overview topograph showing arc-, slit-, and ring-like GSDMD oligomers. Scale bar corresponds to 100 nm.

B–E High-resolution AFM topographs and height profiles of GSDMD^{Nterm} oligomers (red curves). Height profiles were measured along the red lines in the topographs. Dashed zero lines (0 nm) indicate the surface of the lipid membrane; heights of < −4 nm indicate that the oligomers formed transmembrane pores. Topographs were taken in buffer solution (150 NaCl, 20 mM Hepes, pH 7.8) at room temperature. The experiment was reproduced at least three times using independent liposome and GSDMD preparations. Scale bars of topographs correspond to 50 nm and of height profiles 10 nm. The full color range of the AFM topographs corresponds to a vertical scale (height) of 20 nm.

F–H Analysis of GSDMD^{Nterm} oligomers bound to lipid membranes of *E. coli* polar lipids. (F) GSDMD^{Nterm} oligomers assembled into arcs, slits, and rings leading to transmembrane (TM) pores or not transmembrane aggregate (n = 218). (G) Height of GSDMD^{Nterm} oligomers protruding from the lipid membrane. Bars represent mean, and error bars represent s.e.m. (n = 218). (H) Distribution of the diameters of rings formed by GSDMD^{Nterm} oligomers. The average distribution was 21.2 ± 5.6 nm (n = 164; average ± s.d.), and the bin size was 3 nm.

Discussion

Pyroptotic death is a defining feature of canonical and non-canonical inflammasome engagement and the final step associated with the activation of human and mouse caspase-1, but also mouse caspase-11 and human caspase-4/-5. Although the morphological features of pyroptotic cell death indicated the formation of a plasma membrane pore and subsequent lysis of the cell (Lamkanfi, 2011), the molecules involved in pyroptosis induction had remained elusive. The recent identification of GSDMD as an essential mediator of pyroptosis significantly expanded our understanding of pyroptotic cell death (He *et al*, 2015; Kayagaki *et al*, 2015; Shi *et al*, 2015), but

Published online: July 14, 2016
The EMBO Journal The pyroptotic GSDMD pore *Lorenzo Sborgi et al*

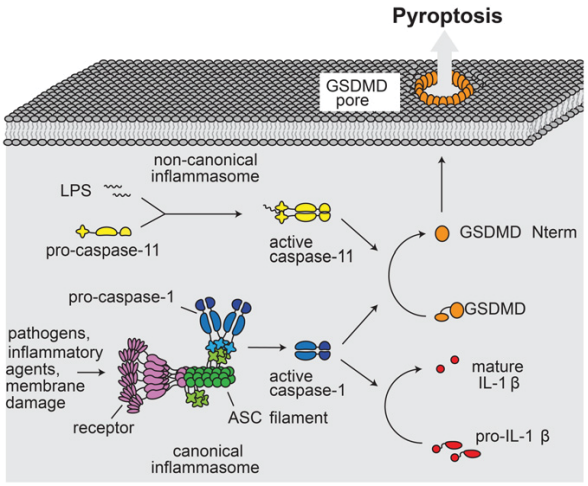

Figure 7. Model for GSDMD-mediated pyroptotic cell death.
Canonical inflammasomes act as sensors for a variety of pathogens and cellular insults. Assembly of these types of inflammasomes involves multimerization of the receptor (purple), which initiates filament formation of the adaptor protein ASC (green). ASC filaments act as activation platforms for caspase-1 (blue). In the noncanonical pathway, LPS is directly bound by caspase-11 (yellow), resulting in its activation. Caspase-1 processes interleukin IL-1β (red). Both caspase-1 and caspase-11 process GSDMD (orange), which results in release of the GSDMD^{Nterm} fragment. GSDMD^{Nterm} forms a large pore in the plasma membrane. Pore formation results in rapid loss of membrane integrity, the dissipation of the electrochemical gradient, and ultimately in cell death.

whether after cleavage by caspases GSDMD executes pyroptosis directly, or by initiating other signaling events remained unclear. In this work, we have shown that the N-terminal fragment of GSDMD, GSDMD^{Nterm}, can form pores with average diameters of 21 nm in artificial liposomes, as well as large pores in the plasma membrane of cells (Figs 5 and 6). GSDMD oligomers were found to form pre-pore states consisting of arcs, slits, and rings. Each of these oligomeric states had a certain probability to also show a pore state, among which the GSDMD rings with their variable diameter formed the largest transmembrane pores. The variable pore size suggests that GSDMD possesses an intrinsic high structural variability and that GSDMD arcs and slits represent intermediates that presumably may fuse toward the ring-shaped structures, similar to observations for several other pore-forming toxins (PFTs) that dynamically rearrange on the membrane surface (Leung *et al*, 2014; Sonnen *et al*, 2014; Mulvihill *et al*, 2015; Podobnik *et al*, 2015). Importantly, our *in vitro* assays show that the formation of the GSDMD pore does not require other proteins as co-factors or membrane receptors, demonstrating that GSDMD^{Nterm} is the sole and final executor of pyroptotic cell death (Fig 7). While this manuscript was in revision, other reports have been published that confirm our findings that the N-terminal fragment of GSDMD causes pyroptosis through the formation of a plasma membrane pore and that demonstrate that the N-terminal domains of other gasdermin family members share this pore-forming activity (Aglietti *et al*, 2016; Ding *et al*, 2016).

The placement and function of GSDMD in the canonical and non-canonical inflammasome pathway strongly resembles the placement and function of Bax (Bcl-2-associated X protein) in the apoptotic cell death pathways (Youle & Strasser, 2008). Bax is the final executor of apoptosis and forms a large pore in the mitochondrial outer membrane. Interestingly, whereas both proteins form large permeability pores in their respective target membranes, their mechanism of activation is entirely different. Whereas GSDMD is activated by proteolytic cleavage, Bax is activated by interactions within the Bcl-2 family of proteins (Gavathiotis *et al*, 2008; Czabotar *et al*, 2013). A strong difference can also be expected for the atomic structure of the two proteins. Bax features a bundle of nine α-helices (Suzuki *et al*, 2000), thereby burying the two presumed pore-forming helices in its central core. The prediction of secondary structure elements shows that GSDMD^{Nterm} consists mainly of β-strand secondary structure, whereas the soluble GSDMD^{Cterm} consists of α-helical secondary structure (Appendix Fig S8). Thus, while Bax resembles the bacterial pore-forming colicins, structural studies of the membrane-inserted form of GSDMD will be of highest interest.

Another functionally related pathway is necroptotic cell death, which is for instance initiated by TNF (tumor necrosis factor)-α or the engagement of Toll-like receptor (TLRs) in absence of caspase-8 activity (Pasparakis & Vandenabeele, 2015). Necroptosis involves the formation of the necrosome, a complex consisting of RIP (receptor serine–threonine–protein kinase)1, RIP3 and MLKL (mixed lineage kinase domain-like) and similarly to pyroptosis it is characterized by cell lysis (Pasparakis & Vandenabeele, 2015). Recent work has demonstrated that recruitment of MLKL to RIP3 and MLKL phosphorylation results in the conformational change that leads to the exposure of its four-helix bundle domain (FHBD) and oligomerization of MLKL (Murphy *et al*, 2013). Binding of the FHBD to negatively charged phosphatidylinositol phosphates has been proposed to recruit MLKL to the plasma membrane allowing it to directly permeabilize the membrane by forming a pore (Dondelinger *et al*, 2014; Su *et al*, 2014; Wang *et al*, 2014). Alternatively, it has been also proposed that plasma membrane-bound MLKL recruits Ca^{2+} or Na^{+} ion channels to permeabilize the membrane (Cai *et al*, 2014; Chen *et al*, 2014). Thus, although the steps leading up to necroptosis are markedly different from pyroptosis, the execution of both types of lytic cell death involves the formation of plasma membrane pores.

The fact that GSDMD targets membranes after cleavage by caspases and forms permeability pores also sheds some light on the function of the regulatory C-terminal domain. Cleavage of GSDMD by inflammatory caspases results in the release of the GSDMD C-terminal fragment (Kayagaki *et al*, 2015; Shi *et al*, 2015), but overexpression of GSDMD^{Cterm}, which was found to bind GSDMD^{Nterm}, results in the inhibition of cell death (Shi *et al*, 2015). This gave rise to a model in which cleavage releases an intramolecular autoinhibition exerted by GSDMD^{Cterm} on the GSDMD^{Nterm}, thus preventing GSDMD^{Nterm} to unleash its cytotoxic activity. Interestingly, we have observed that GSDMD^{Cterm} is a soluble protein, while GSDMD^{Nterm} is insoluble and aggregates, when GSDMD is cleaved in the absence of a target membrane (Fig 3). This result supports a slightly different model in which GSDMD^{Cterm} does not only act as an inhibitory domain, but simultaneously also as a solubility tag for the N-terminal domain, maybe by shielding certain hydrophobic or amphipathic segments required for membrane insertion. Based on these functions, the alternative names pore-forming domain (PFD) and solubilizing inhibitory domain (SID) appear well suited for the GSDMD^{Nterm} and GSDMD^{Cterm}, respectively.

Published online: July 14, 2016
Lorenzo Sborgi et al The pyroptotic GSDMD pore **The EMBO Journal**

The identification of GSDMD as an essential mediator of pyroptosis has shed light on the possible functions of other gasdermin family members in programmed cell death. All gasdermins (GSDMA, GSDMB, GSDMC, and GSDMD in humans; GSDMA1-3, GSDMC1-4, and GSDMD in mice) are composed of a distinct N-terminal and C-terminal domain (Tanaka *et al*, 2013), a feature shared by the extended gasdermin family members DFNA5 and DFNB59 (deafness, autosomal-dominant 5/autosomal-recessive 59). Several lines of evidence suggest that the N-terminal domain of other gasdermin family members is intrinsically cytotoxic (Saeki *et al*, 2007; Op de Beeck *et al*, 2011; Shi *et al*, 2015). Given the functional and sequence similarity between gasdermin N-terminal domains, it is not surprising that all gasdermins induce membrane permeability pores and subsequent cell death (Ding *et al,* 2016). Structural studies of GSDMD and other gasdermin family members in their full-length and membrane inserted forms as well as the stoichiometry of these pores will thus remain of high interest. Furthermore, it remains to be shown whether several gasdermins might cooperate in pore formation, given that caspase-1-dependent cell death does not solely rely on GSDMD (Kayagaki *et al*, 2015). Finally, to fully understand this emerging group of cell death effectors, it will be necessary to define how other gasdermin family members are activated and to identify the physiological context in which they induce cell death.

Materials and Methods

Cell culture and reagents

HEK293T were maintained in DMEM (Sigma), 10% FCS (Amimed), 1% penicillin/streptomycin (Amimed) and split, when they reached 90% confluency. Immortalized macrophages were obtained from R. Vance (UC Berkeley) and cultured in DMEM, 10% FCS, 1% PenStrep, 10 mM HEPES (Amimed), 1% non-essential amino acids (NEAA, Amimed). Polyethylenimine was from Polysciences Inc, LDH detection kit from Takara, IL-1β ELISA from eBiosciences, near IR live/dead marker from Thermo Scientific, propidium iodide from Santa Cruz Biotechnology, PEGs of different sizes from Merck. pRetroX TetONE3G-Puro was obtained from Clontech. The puromycin resistance cassette was replaced by an EGFP by standard cloning procedures yielding pRetroX TetONE-eGFP. $GSDMD^{Nterm}$ was amplified from murine cDNA and cloned into pRetroX TetONE-eGFP by standard cloning procedures. Anti-GSDMD and anti-GAPDH antibodies were from SCBT (both used at 1:250), anti-caspase-1 p20 from Adipogen (used at 1:4,000), anti-alpha tubulin from Abcam (used at 1:2,500), anti-VDAC, anti-HDAC1, and anti-Na^+/K^+ ATPase antibodies were from Cell Signaling Technologies (all at 1:1,000). HEK293T cells were seeded in 96-well plates (30,000 cells per well) 1 day prior to transfection. Cells were subsequently transfected with 300 ng of plasmid DNA and 3× (wt/vol) linear PEI (polyethylenimine). Twenty-four post-transfection cells were treated as indicated in the respective figures.

Generation of stable cell lines

For complementation of $Gsdmd^{KO}$ cell lines (Dick *et al,* 2016), human *Gsdmd* was amplified from HeLa cell cDNA (Clontech) and cloned into pLJM1 (addgene #19319) where the puromycin resistance cassette was replaced with a hygromycin resistance cassette. The I104N mutant was generated using the Q5 site-directed mutagenesis kit (NEB). To produce lentiviral particles, 1×10^6 HEK239T cells were transfected with the 2 μg lentiviral plasmid, 2 μg psPax2, and 0.4 μg VSV-G for 6 hrs. Medium was exchanged, and lentiviral particles were collected 24 h later. *Gsdmd*-deficient immortalized macrophages were spin-infected with these particles, and transduced cells were selected with Hygromycin (500 μg/ml, invivogen) for 7 days. Selected cells were used for experiments.

Macrophage infection

Immortalized macrophages were seeded the day before the experiment (30,000 cells per well of a 96-well plate, 1.5×10^6 cells per well of a 6-well plate). *S. typhimurium* (SL1344) was grown overnight in Luria broth (LB) medium. On the day of experiment, bacteria were subcultured 1:40 in LB and grown for 4 h to logarithmic phase to induce SPI-1 expression. Cells were washed once with PBS and infected at an MOI of 50 with *S. typhimurium* diluted in OptiMEM. LDH and IL-1β release was determined as described in the respective manufacturer's instructions. Cell lysates and supernatants were prepared for Western blot and analyzed by SDS–PAGE as described previously (Broz *et al*, 2012).

Subcellular fractionation and membrane extraction

About 1.5×10^7 million immortalized macrophages were seeded in 10-cm tissue culture-treated dishes the day before the experiment. The next day, cells were left either uninfected or infected with log-phase *S. Typhimurium* at a MOI of 50 for 10 and 20 min at 37°C. Cells were washed three times with homogenization buffer (10 mM Tris, 10 mM acetic acid, 1 mM EDTA, 7.5 mM $MgCl_2$, 250 mM sucrose), scraped, and homogenized using a syringe equipped with a 25G needle (30 strokes) (Total lysate). Samples were centrifuged for 700 *g* for 5 min; supernatants were transferred to a new tube and centrifuged the same way again. Combined pellets yielded the P0.7 fraction, while the remaining supernatant yielded the S0.7 fraction. Pellets were washed twice with homogenization buffer and lysed in RIPA buffer. Supernatants (S0.7) were centrifuged 10,000 *g* for 15 min; supernatant was transferred to new tube and centrifuged the same way again. Pellets (P10) were combined, washed twice with homogenization buffer, and resuspended in SOL buffer (50 mM Tris–HCl pH 6.8, 1 mM EDTA, 1% Triton X-100). Supernatants (S10) were centrifuged at 150,000 *g* for 30 min; supernatant was transferred to a new tube and centrifuged the same way again. Pellets were combined, washed again twice, and resuspended in SOL buffer (P150). The supernatants were analyzed as S150. Protein concentration of every sample was determined by BCA, and equal amounts were analyzed by SDS–PAGE. For extraction of membrane fractions, cells were infected for 15 min with log-phase *S. typhimurium*, homogenized as described above, and membrane preparation and extraction were performed as described in Gatfield and Pieters (2000).

Cloning, expression, and purification of GSDMD and caspases

cDNA coding for the full-length human *GSDMD* was cloned with an N-terminal His_6-SUMO-tag into a pET28a vector under control of a

Published online: July 14, 2016
The EMBO Journal

T7 promoter. Single amino acid point mutation I104N was generated by QuickChange site-directed mutagenesis kit (Stratagene). All plasmids were verified by DNA sequencing. The protein construct was transformed in BL21 (DE3) *E. coli* strains, and the protein was expressed by growing the cultures at 37°C to an OD_{600} of 0.7 and by inducing with 0.5 mM IPTG overnight at 18°C. The cells were harvested by centrifugation and the pellet was resuspended in 20 mM Tris buffer pH 7.5, 50 mM NaCl, 5 mM imidazole, 20 mM $MgCl_2$, 10 mM KCl, 0.5 mM TCEP, 0.1 mM protease inhibitor, and DNase I. The resuspended cells were disrupted by high-pressure microfluidization and centrifuged at 30,000 *g* at 4°C for 45 min. The supernatant was incubated for 2 h at room temperature with pre-equilibrated Ni-NTA affinity resin (Thermo Scientific) and then passed through a column for gravity flow purification. The column was washed with 20 column volumes of resuspension buffer containing 15 mM imidazole, and the fusion protein was eluted with 3 column volumes of the same buffer with 250 mM imidazole. SUMO-tag cleavage was achieved by addition of ULP1 protease to the solution and subsequent dialysis overnight at 4°C against 20 mM Tris buffer pH 7.5, 50 mM NaCl, 0.5 mM TCEP. GSDMD was eluted from a second round of purification through pre-equilibrated Ni-NTA affinity resin. The protein was further purified by Hi-trapQ ion-exchange and a Superdex 75 gel filtration column (GE Healthcare) pre-equilibrated with 20 mM Tris buffer pH 7.5, 50 mM NaCl, 0.5 mM TCEP. Purified GSDMD was frozen in small aliquots in liquid N_2. Human caspase-1, caspase-3, and caspase-8 were cloned into pET22 expression vectors, expressed as inclusion bodies in *E. coli*, and refolded as previously described (Ramage *et al*, 1995). Briefly, inclusion bodies were solubilized in 8M urea, and protein was refolded by rapid dilution; during which the enzymes autoactivated. A gel filtration column was run to purify the final product, and the concentration of active enzyme determined by active site titration.

Liposome preparation

The polar lipid extract derived from *E. coli*, total lipid extract derived from porcine brain, and DMPC were purchased from Avanti Polar Lipids, Inc. (Alabaster AL, USA). Chloroform lipid solutions at a concentration of 25 mg ml^{-1} were gently dried in a glass tube into a thin film under nitrogen flow and placed under vacuum overnight to further evaporate any residual solvent. The lipid layers were that rehydrated in 1 ml of 50 mM HEPES buffer, 150 mM NaCl, pH 7.5 under continuous shaking at 50°C for 2 h. The lipid dispersions were subjected to 10 freeze–thaw cycles, and the resultant liposomes were extruded 20 times through 100-nm polycarbonate membranes to form large unilamellar vesicles (LUV). The mean size diameter of the liposomes was verified by dynamic light scattering (DLS). To prepare dye-filled LUVs, the dry lipid film was hydrated with 0.5 ml of 50 mM HEPES buffer, 50 mM NaCl, 70 mM 6-carboxyfluorescein, 5 mM TCEP, pH 7.5) or by adding 100 mg ml^{-1} of fluorescein isothiocyanate dextran FD-20, FD-40, and FD-150. For the 6-carboxyfluorescein containing liposome, the removal of extra-vesicular dye was achieved by a purification step through a PD-10 column (GE Healthcare) pre-equilibrated with 50 mM HEPES buffer, 150 mM NaCl, 5 mM TCEP pH 7.5. The FD-20, FD-40, and FD-150 dye-filled liposomes were washed twice by ultracentrifugation at 4°C for 20 min at 100,000 *g* and then resuspended in 0.5 ml of the same isotonic solution. All liposomes were stored at 4°C and used within 24 h.

Liposome leakage assay

Membrane leakage experiments were performed using 6-carboxyfluorescein, FD-20, FD-40, and FD-150-filled liposomes composed of polar lipid extract derived from *E. coli* and total lipid extract derived from porcine brain. The samples were initially prepared by diluting 40 mM total lipid concentration in 100 µl solution of 50 mM HEPES buffer, 150 mM NaCl, 5 mM TCEP, pH 7.5 supplemented with different aliquots of a 2.6 µM GSDMD stock solution. The NaCl concentration in the reaction buffer outside the LUV was optimized to preserve caspase-1 activity and to minimize the dye release due to the osmotic pressure exerted by the dye on the membrane bilayer. To initiate the cleavage of GSDMD and the consequent pore formation reaction, different amounts of caspase-1 from a 12 µM stock solution were added to 100 µl of premixed LUV–GSDMD solution. The membrane leakage was detected by measuring the time-course increase in fluorescence resulting from the dye dilution and subsequent dequenching upon membrane pore formation. The experiments were carried out in a Corning 384-well non-binding surface plate, and the fluorescence was continuously recorded for 2 h at 10-s intervals using a Biotek Synergy 2 plate reader with excitation and emission wavelengths at 492 and 520 nm, respectively. At each time point, the percentage of dye release was calculated as:

$$\text{Dye release} = (I - I_0)/(I_{\max} - I_0)$$

where I is the emission intensity of the sample, I_0 is the emission intensity from an experiment with the liposome solution only (negative control), and $I_{\max}$ is the emission intensity from an experiment with added Triton X-100 to the liposome solution (positive control).

Gel-shift assays

Recombinant GSDMD was incubated with different caspases for the indicated time period in a reaction vessel in caspase activity buffer of 100 mM Hepes, pH 7.4, 0.5 mM EDTA, 50 mM NaCl, 0.1% CHAPS, 0.005% Novexin, and 5 mM TCEP. Final concentrations were 5 nM enzyme, 2 µM GSDMD. Reactions were quenched with 6xSDS loading buffer and analyzed by SDS–PAGE. For cross-linking experiments, 2 mM DSS (ThermoFisher) were added to the reaction, and protein was cross-linked for 30 min before quenching the reaction.

Thermofluor assay

To monitor GSDMD thermal stability, the protein was incubated with the fluorescent dye Sypro orange and the thermal shift assay was conducted in the CFX96 Real Time Detection System (Bio-Rad, Hercules, CA). Solutions of 2 µl of 2 µM GSDMD, 8 µl of 5× Sypro orange, 10 µl solution of screened condition were loaded to a 96-well plate. The plate was heated from 10 to 90°C with a heating rate of 0.5°C min^{-1}. The fluorescence intensity was measured with excitation and emission wave lengths of 490 and 530 nm, respectively.

Published online: July 14, 2016
Lorenzo Sborgi et al The pyroptotic GSDMD pore **The EMBO Journal**

Cryo-electron microscopy (cryo-EM)

Cryo-EM was used to visualize GSDMD-mediated pore on liposome surfaces. The samples were prepared by 2-h incubation of freshly prepared liposome (2 mM lipids) with 2.6 μM of GSDMD in the presence and the absence of catalytic amounts of caspase-1. All samples were adsorbed for 10 s on glow-discharged thin carbon film-coated 300-mesh lacey EM grids, blotted for 2 s, and plunge frozen in liquid ethane using a FEI Vitrobot MK4 (Vitrobot, Maastricht Instruments). Cryo-EM micrographs were acquired with a Philips CM200FEG transmission electron microscope operated at 200 kV and a nominal magnification of 66,000×. Images were recorded with a TVIPS F416 CMOS camera.

Liposome Preparation for atomic force microscopy (AFM)

Unilamellar liposomes were prepared at room temperature (≈23°C) by hydration of lipid films and extrusion through polycarbonate filters with 0.1-μm pore diameter (Nucleopore Polycarbonate, Whatman) according to the method described by Avanti Polar Lipids (www.avantilipids.com). The *E. coli* polar lipids and the extruding equipment used for liposome preparation were purchased from Avanti Polar Lipids. The liposomes were stored at −80°C in buffer solution (150 mM NaCl, 20 mM Hepes, pH 7.25). After incubation with 1 μM mM GSDMD and 0.2 μM caspase-1 for 90 min at 37°C in buffer solution (50 mM NaCl, 100 mM Hepes, 5 mM TCEP, pH 7.4), the liposomes were adsorbed onto freshly cleaved mica in buffer solution (50 mM NaCl, 20 mM Hepes, pH 7.4) (Muller *et al*, 1997). After an adsorption time of 30 min, the sample was washed several times with the AFM imaging buffer (150 mM NaCl, 20 mM Hepes, pH 7.8) to remove weakly adsorbed protein. Buffer solutions were freshly made using nanopure water (18.2 MΩ cm^{-1}) and pro-analysis (> 98.5%) purity grade reagents from Sigma-Aldrich and Merck. Each experimental condition characterized by AFM was reproduced at least three times. Liposomes made from *E. coli* polar lipids incubated in buffer solution but in the absence of GSDMD showed no arc-, slit- or ring-like structures when imaged by AFM (Mulvihill *et al*, 2015).

AFM

Force–distance curve-based AFM (FD-based AFM) (Dufrene *et al*, 2013) was performed using a Nanoscope Multimode 8 (Bruker, Santa Barbara, USA) operated in the PeakForce Tapping mode. The AFM was equipped with a 120-μm piezoelectric scanner and fluid cell. AFM cantilevers used (BioLever mini BL-AC40, Olympus Corporation, Tokyo, Japan) had a nominal spring constant of 0.1 N m^{-1}, a resonance frequency of ≈110 kHz in liquid and sharpened silicon tip with a nominal radius of 8–10 nm. The FD-based AFM topographs were recorded in AFM imaging buffer (150 mM NaCl, 20 mM Hepes, pH 7.8) and at room temperature as described (Pfreundschuh *et al*, 2014). The maximum force applied to image the samples was 70 pN, and the oscillation frequency and oscillation amplitude of the cantilever were set to 2 kHz and 40 nm, respectively. The AFM was placed inside a home-built temperature controlled acoustic isolation box. For data analysis, we took unprocessed AFM topographs. Diameters of ring-like GSDMD oligomers were measured from the highest protruding rim. Heights of GSDMD arcs, slits, and rings were measured from their highest protruding feature relative to the surface of the lipid membrane. GSDMD oligomers were classified to having formed transmembrane pores if the inside of the pore was at least 3.5 nm deeper compared to the surface of the surrounding lipid membrane.

Expanded View for this article is available online.

Acknowledgements
We thank Paul Erbel for help with the protein preparation. This work was supported by the European Research Council (FP7 contract MOMP 281764 to S.H.), the Swiss National Science Foundation (PP00P3_139120/1 to P.B.), and by the European Union Marie Curie Actions program through the ACRITAS Initial Training Network (FP7-PEOPLE-2012-ITN, Project 317348 to D.J.M.).

Author contributions
LS, SR, PB, SH designed the study. LS, SR, EM, JP, RH, CJF carried out research experiments. All authors (including HS) analyzed data. LS, SR, DJM, PB, SH wrote the paper.

Conflict of interest
The authors declare that they have no conflict of interest.

References

Aglietti RA, Estevez A, Gupta A, Ramirez MG, Liu PS, Kayagaki N, Ciferri C, Dixit VM, Dueber EC (2016) GsdmD p30 elicited by caspase-11 during pyroptosis forms pores in membranes. *Proc Natl Acad Sci USA* 113: 7858 – 7963

Bergsbaken T, Fink SL, Cookson BT (2009) Pyroptosis: host cell death and inflammation. *Nat Rev Microbiol* 7: 99 – 109

Broz P, Ruby T, Belhocine K, Bouley DM, Kayagaki N, Dixit VM, Monack DM (2012) Caspase-11 increases susceptibility to Salmonella infection in the absence of caspase-1. *Nature* 490: 288 – 291

Broz P (2015) Immunology: caspase target drives pyroptosis. *Nature* 526: 642 – 643

Cai Z, Jitkaew S, Zhao J, Chiang HC, Choksi S, Liu J, Ward Y, Wu LG, Liu ZG (2014) Plasma membrane translocation of trimerized MLKL protein is required for TNF-induced necroptosis. *Nat Cell Biol* 16: 55 – 65

Chen X, Li W, Ren J, Huang D, He WT, Song Y, Yang C, Li W, Zheng X, Chen P, Han J (2014) Translocation of mixed lineage kinase domain-like protein to plasma membrane leads to necrotic cell death. *Cell Res* 24: 105 – 121

Czabotar PE, Westphal D, Dewson G, Ma S, Hockings C, Fairlie WD, Lee EF, Yao S, Robin AY, Smith BJ, Huang DC, Kluck RM, Adams JM, Colman PM (2013) Bax crystal structures reveal how BH3 domains activate Bax and nucleate its oligomerization to induce apoptosis. *Cell* 152: 519 – 531

Dick MS, Sborgi L, Ruhl S, Hiller S, Broz P (2016) ASC filament formation serves as a signal amplification mechanism for inflammasomes. *Nat Commun* 7: 11929

Ding J, Wang K, Liu W, She Y, Sun Q, Shi J, Sun H, Wang DC, Shao F (2016) Pore-forming activity and structural autoinhibition of the gasdermin family. *Nature* 535: 111 – 116

Dondelinger Y, Declercq W, Montessuit S, Roelandt R, Goncalves A, Bruggeman I, Hulpiau P, Weber K, Sehon CA, Marquis RW, Bertin J, Gough PJ, Savvides S, Martinou JC, Bertrand MJ, Vandenabeele P (2014) MLKL compromises plasma membrane integrity by binding to phosphatidylinositol phosphates. *Cell Rep* 7: 971 – 981

Published online: July 14, 2016
The EMBO Journal The pyroptotic GSDMD pore *Lorenzo Sborgi et al*

Dufrene YF, Martinez-Martin D, Medalsy I, Alsteens D, Muller DJ (2013) Multiparametric imaging of biological systems by force-distance curve-based AFM. *Nat Methods* 10: 847 – 854

Fink SL, Cookson BT (2007) Pyroptosis and host cell death responses during Salmonella infection. *Cell Microbiol* 9: 2562 – 2570

Fink SL, Bergsbaken T, Cookson BT (2008) Anthrax lethal toxin and Salmonella elicit the common cell death pathway of caspase-1-dependent pyroptosis via distinct mechanisms. *Proc Natl Acad Sci USA* 105: 4312 – 4317

Gatfield J, Pieters J (2000) Essential role for cholesterol in entry of mycobacteria into macrophages. *Science* 288: 1647 – 1650

Gavathiotis E, Suzuki M, Davis ML, Pitter K, Bird GH, Katz SG, Tu HC, Kim H, Cheng EH, Tjandra N, Walensky LD (2008) BAX activation is initiated at a novel interaction site. *Nature* 455: 1076 – 1081

Hagar JA, Powell DA, Aachoui Y, Ernst RK, Miao EA (2013) Cytoplasmic LPS activates caspase-11: implications in TLR4-independent endotoxic shock. *Science* 341: 1250 – 1253

He WT, Wan H, Hu L, Chen P, Wang X, Huang Z, Yang ZH, Zhong CQ, Han J (2015) Gasdermin D is an executor of pyroptosis and required for interleukin-1beta secretion. *Cell Res* 25: 1285 – 1298

Kayagaki N, Warming S, Lamkanfi M, Vande Walle L, Louie S, Dong J, Newton K, Qu Y, Liu J, Heldens S, Zhang J, Lee WP, Roose-Girma M, Dixit VM (2011) Non-canonical inflammasome activation targets caspase-11. *Nature* 479: 117 – 121

Kayagaki N, Wong MT, Stowe IB, Ramani SR, Gonzalez LC, Akashi-Takamura S, Miyake K, Zhang J, Lee WP, Muszynski A, Forsberg LS, Carlson RW, Dixit VM (2013) Noncanonical inflammasome activation by intracellular LPS independent of TLR4. *Science* 341: 1246 – 1249

Kayagaki N, Stowe IB, Lee BL, O'Rourke K, Anderson K, Warming S, Cuellar T, Haley B, Roose-Girma M, Phung QT, Liu PS, Lill JR, Li H, Wu J, Kummerfeld S, Zhang J, Lee WP, Snipas SJ, Salvesen GS, Morris LX *et al* (2015) Caspase-11 cleaves gasdermin D for non-canonical inflammasome signalling. *Nature* 526: 666 – 671

Lamkanfi M (2011) Emerging inflammasome effector mechanisms. *Nat Rev Immunol* 11: 213 – 220

Latz E, Xiao TS, Stutz A (2013) Activation and regulation of the inflammasomes. *Nat Rev Immunol* 13: 397 – 411

Leung C, Dudkina NV, Lukoyanova N, Hodel AW, Farabella I, Pandurangan AP, Jahan N, Pires Damaso M, Osmanovic D, Reboul CF, Dunstone MA, Andrew PW, Lonnen R, Topf M, Saibil HR, Hoogenboom BW (2014) Stepwise visualization of membrane pore formation by suilysin, a bacterial cholesterol-dependent cytolysin. *elife* 3: e04247

Mariathasan S, Newton K, Monack DM, Vucic D, French DM, Lee WP, Roose-Girma M, Erickson S, Dixit VM (2004) Differential activation of the inflammasome by caspase-1 adaptors ASC and Ipaf. *Nature* 430: 213 – 218

Miao EA, Leaf IA, Treuting PM, Mao DP, Dors M, Sarkar A, Warren SE, Wewers MD, Aderem A (2010) Caspase-1-induced pyroptosis is an innate immune effector mechanism against intracellular bacteria. *Nat Immunol* 11: 1136 – 1142

von Moltke J, Ayres JS, Kofoed EM, Chavarria-Smith J, Vance RE (2013) Recognition of bacteria by inflammasomes. *Annu Rev Immunol* 31: 73 – 106

Muller DJ, Amrein M, Engel A (1997) Adsorption of biological molecules to a solid support for scanning probe microscopy. *J Struct Biol* 119: 172 – 188

Mulvihill E, van Pee K, Mari SA, Muller DJ, Yildiz O (2015) Directly Observing the Lipid-Dependent Self-Assembly and Pore-Forming Mechanism of the Cytolytic Toxin Listeriolysin O. *Nano Lett* 15: 6965 – 6973

Murphy JM, Czabotar PE, Hildebrand JM, Lucet IS, Zhang JG, Alvarez-Diaz S, Lewis R, Lalaoui N, Metcalf D, Webb AI, Young SN, Varghese LN, Tannahill GM, Hatchell EC, Majewski IJ, Okamoto T, Dobson RC, Hilton DJ, Babon JJ, Nicola NA *et al* (2013) The pseudokinase MLKL mediates necroptosis via a molecular switch mechanism. *Immunity* 39: 443 – 453

Op de Beeck K, Van Camp G, Thys S, Cools N, Callebaut I, Vrijens K, Van Nassauw L, Van Tendeloo VF, Timmermans JP, Van Laer L (2011) The DFNA5 gene, responsible for hearing loss and involved in cancer, encodes a novel apoptosis-inducing protein. *Eur J Hum Genet* 19: 965 – 973

Pasparakis M, Vandenabeele P (2015) Necroptosis and its role in inflammation. *Nature* 517: 311 – 320

Pfreundschuh M, Martinez-Martin D, Mulvihill E, Wegmann S, Muller DJ (2014) Multiparametric high-resolution imaging of native proteins by force-distance curve-based AFM. *Nat Protoc* 9: 1113 – 1130

Podobnik M, Marchioretto M, Zanetti M, Bavdek A, Kisovec M, Cajnko MM, Lunelli L, Dalla Serra M, Anderluh G (2015) Plasticity of listeriolysin O pores and its regulation by pH and unique histidine. *Sci Rep* 5: 9623

Ramage P, Cheneval D, Chvei M, Graff P, Hemmig R, Heng R, Kocher HP, Mackenzie A, Memmert K, Revesz L, Wishart W (1995) Expression, refolding, and autocatalytic proteolytic processing of the interleukin-1 beta-converting enzyme precursor. *J Biol Chem* 270: 9378 – 9383

Saeki N, Kim DH, Usui T, Aoyagi K, Tatsuta T, Aoki K, Yanagihara K, Tamura M, Mizushima H, Sakamoto H, Ogawa K, Ohki M, Shiroishi T, Yoshida T, Sasaki H (2007) GASDERMIN, suppressed frequently in gastric cancer, is a target of LMO1 in TGF-beta-dependent apoptotic signalling. *Oncogene* 26: 6488 – 6498

Scherrer R, Gerhardt P (1971) Molecular sieving by the Bacillus megaterium cell wall and protoplast. *J Bacteriol* 107: 718 – 735

Shi J, Zhao Y, Wang Y, Gao W, Ding J, Li P, Hu L, Shao F (2014) Inflammatory caspases are innate immune receptors for intracellular LPS. *Nature* 514: 187 – 192

Shi J, Zhao Y, Wang K, Shi X, Wang Y, Huang H, Zhuang Y, Cai T, Wang F, Shao F (2015) Cleavage of GSDMD by inflammatory caspases determines pyroptotic cell death. *Nature* 526: 660 – 665

Sonnen AF, Plitzko JM, Gilbert RJ (2014) Incomplete pneumolysin oligomers form membrane pores. *Open Biol* 4: 140044

Su L, Quade B, Wang H, Sun L, Wang X, Rizo J (2014) A plug release mechanism for membrane permeation by MLKL. *Structure* 22: 1489 – 1500

Suzuki M, Youle RJ, Tjandra N (2000) Structure of Bax: coregulation of dimer formation and intracellular localization. *Cell* 103: 645 – 654

Tanaka S, Mizushina Y, Kato Y, Tamura M, Shiroishi T (2013) Functional conservation of Gsdma cluster genes specifically duplicated in the mouse genome. *G3 (Bethesda)* 3: 1843 – 1850

Thornberry NA, Bull HG, Calaycay JR, Chapman KT, Howard AD, Kostura MJ, Miller DK, Molineaux SM, Weidner JR, Aunins J, Elliston KO, Ayala JM, Casano FJ, Chin J, Ding GJF, Egger LA, Gaffney EP, Limjuco G, Palyha OC, Raju SM *et al* (1992) A novel heterodimeric cysteine protease is required for interleukin-1 beta processing in monocytes. *Nature* 356: 768 – 774

Wang H, Sun L, Su L, Rizo J, Liu L, Wang LF, Wang FS, Wang X (2014) Mixed lineage kinase domain-like protein MLKL causes necrotic membrane disruption upon phosphorylation by RIP3. *Mol Cell* 54: 133 – 146

Youle RJ, Strasser A (2008) The BCL-2 protein family: opposing activities that mediate cell death. *Nat Rev Mol Cell Biol* 9: 47 – 59

4.3 Research Article III: ESCRT dependent membrane repair negatively regulates pyroptosis downstream of GSDMD activation

Sebastian Rühl[1], Rosalie Heilig[2] and Petr Broz[1,2,*]

1 Focal Area Infection Biology, Biozentrum, University of Basel, Klingelbergstrasse 50/70, 4056 Basel, Switzerland

2 Department of Biochemistry, University of Lausanne, Chemin des Boveresses 155, 1066 Epalinges, Switzerland

Running title: ESCRT repairs GSDMD-damaged membranes

Unpublished

Statement of contribution:

I performed all experiments described and wrote the manuscript together with Petr Broz. Rosalie Heilig generated the Dmrb-C1, pro-IL-1β transgenic HEK293T cells.

Abstract

Gasdermin-D is a new pore forming protein that is proteolytic processed and actiavted by inflammatory caspases. These caspases, caspase-1/11 in mice and caspase-1/-4/-5 in humans, are activated within canonical or non-canonical inflammasomes upon detection of host- or pathogen derived danger signals. Gasdermin-D pores target the cellular plasma membrane, disrupt the electrochemical gradient and thereby induce a lytic, inflammatory type of cell death referred to as pyroptosis, which involves the release of cytosolic content and pro-inflammatory cytokines like IL-1b and IL-18. Here we find that calcium influx through Gasdermin-D pores serves a signal for cells to repair damaged membrane areas and therefore delay or even prevent pyroptosis. We show that sensing of intracellular calcium ions is necessary for recruitment of the ESCRT-III machinery to the plasma membrane during pyroptosis. Inhibition of the ESCRT-III machinery strongly enhances pyroptosis in both human and murine cells and it enhances cytokine secretion in response to canonical and non-canonical inflammasome activators. Our results therefore not only attribute an anti-inflammatory role to membrane repair by the ESCRT-III system but also provide insight in general survival mechanisms during pyroptosis.

Main text

Introduction

Pyroptosis is a necrotic type of cell death initiated by inflammatory caspases (*1*). These caspases are activated within macromolecular signalling complexes known as inflammasomes (*2*). Canonical inflammasomes activate caspase-1 in both human and mouse cells and are assembled by cytoplasmic sensors - Pyrin and members of the PYHIN or the NLR (NOD-like receptor) family - that detect diverse pathogen- and host-derived danger signals. A ‘non-canonical inflammasome’ has been identified as well and shown to be assembled by the binding of the bacterial cell-wall component lipopolysaccharide (LPS) to caspase-4, -5 in humans or caspase-11 in mice (*2*). All inflammatory caspases share the ability to induce pyroptotic cell death. Caspase-1 however is unique as it can also process the pro-forms of interleukin (IL)-1b and IL-18 into their mature, bioactive forms.

Pyroptosis is characterised by a rounding of the nucleus, membrane blebbing and ballooning, cell swelling and ultimately results in cell lysis and the release of cytoplasmic content (*3-5*). Two landmark studies recently identified Gasdermin D (GSDMD), a member of the ill-characterized gasdermin protein family, as the sole executor of pyroptosis (*6, 7*). GSDMD is a 53 kDa protein that contains distinct N- and C-terminal domains connected by a linker. Inflammatory caspases cleave GSDMD at a conserved cleavage site within this linker, thus

liberating the N-terminal domain (GSDMDNT) from an inhibitory interaction with the C-term (GSDMDCT), and allowing the N-terminal part to induce pyroptosis (*6, 7*). Studies by us and others showed that GSDMDNT targets cellular membranes, among them the plasma membrane, and that it forms large pores with an internal diameter of 10-16 nm in liposomal membranes (*8-11*). Permeabilization of the plasma membrane by GSDMDNT pores dissipates the electrochemical gradient across the membrane (*5*), leading to the inability to maintain osmotic balance and to stabilize cell volume. This ultimately causes uncontrolled water influx, swelling and cell lysis. These findings however also raise the question if activation of inflammatory caspases always results in cell death or if cells feature mechanisms by which they can completely prevent or at least delay cell death. Indeed, several groups have reported that caspase-1 activation can result in pyroptosis- independent cytokine release, depending on stimulus or cell type (*12-15*).

Interestingly, damage of the plasma membrane does not necessarily result in death in all cases and muscle fibers for example repair large mechanical injuries in their plasma membrane in a Ca2+ dependent manner(*16-18*). Early studies postulated that this involves the fusion of large intracellular membrane patches to the site of injury, yet how these fusion events can mechanistically restore a functional lipid bi-layer could not be explained (*19, 20*). Later studies showed that stable trans- membrane pores, as assembled by bacterial pore forming toxins (PFTs) like Streptolysin O (SLO), are removed in a Ca2+-dependent manner, and proposed two mutually non-exclusive models. One mechanism involves the exocytosis of lysosomal acidic sphingomyelinase (ASM) at the site of injury, resulting in plasma membrane remodelling and subsequent endocytosis of damaged membrane parts (*21*). The other mechanism involves the shedding of damaged plasma membrane parts in form of ectosomes that are formed by the ESCRT machinery(*22, 23*). Both mechanisms are dependent on Ca2+ influx at the site of injury, confirming early observations that membrane repair by many cell types is dependent on extracellular calcium(*24*). ESCRT-mediated plasma membrane repair was mainly characterized in response to laser-induced damage, but recently Gong et al. demonstrated that the ESCRT machinery prevents premature cell death during necroptosis, therefore allowing the cells to produce more pro-inflammatory cytokines and signal to neighbouring cells(*25*).

In this study, we investigated if pyroptosis is an unavoidable consequence of inflammasome activation, or if cells have the ability to delay or prevent pyroptosis. We find that upon non-canonical inflammasome activation a sub-population of cells resists pyroptosis, and that this requires the detection of Ca2+ influx. Furthermore, pyroptosis induction leads to the

translocation of the ESCRT machinery to the plasma-membrane in a Ca2+-dependent manner, where the ESCRT components partially co- localize with GSDMDNT. Inactivation of the ESCRT machinery by expression of dominant-negative proteins resulted in highly enhanced pyroptotic cell death and cytokine release in a number of different cell types and in response to activators of both the canonical and non-canonical inflammasomes. Titration of inflammasome stimuli showed that an active ESCRT machinery was necessary for survival at sublytic levels of inflammasome activation. In conclusion, our findings indicate that membrane repair by the ESCRT machinery represents a universal mechanism how cells limit or even prevent cell death in response to inflammasome activation.

Results

Ca2+ chelation enhances cell death after non-canonical inflammasome activation In most cell types the activation of canonical or non-canonical inflammasomes results in incomplete lethality. Yet if the surviving cells fail to receive the stimulus or actively avoid cell death has not been examined so far. To investigate this question, we transfected primed bone marrow-derived macrophages (BMDMs) with LPS and monitored the disruption of the electrochemical gradient using the Ca2+ probe Fluo-8 and loss of membrane integrity (e.g. lysis) by propidium iodide (PI) staining in real-time. As expected we found that within 120 minutes post LPS transfection up to 50% of cells displayed strong PI staining (**Fig. 1A**). Single cell analysis showed that PI influx was preceded by a marked increase in Fluo-8 signal intensity that peaked immediately before cells lost membrane integrity and became PIhigh (**Fig. 1B-C, Movie 1**). Macrophages from *Casp11-/-* or *Gsdmd-/-* mice did not show an increase in Fluo-8 levels, nor did they acquire PI staining (**Fig. 1C, S1A, Movie 1**), confirming that the Ca2+ and PI influx was dependent on activation of the non-canonical pathway and the pyroptosis executor GSDMD. When examining the 40-50% cells that did not exhibiting strong Ca2+ influx (Fluo-8 increase) (**Fig. 1A**), we unexpectedly found that these cells also displayed a gradual increase in intracellular PI staining (**Fig. 1D and S1B**). The intensity of this PI signal was much lower than what could be observed in cells that completely lost membrane integrity, and only reached 1/10 of the signal 1.5 hours post LPS transfection. This low-level PI influx was however not due to plasma membrane leakage of PI into the cells, since it required stimulation by LPS transfection (**Fig. 1D**) (see Material and Methods section for calculation details), and was not observed in LPS transfected *Casp11-/-* or *Gsdmd-/-* cells (**Fig. 1C and S1B**). Altogether this analysis indicated that, depending on time point and amount of transfected LPS, GSDMDNT-induced pore formation leads to rapid

rise in intracellular Ca2+ concentrations in a majority of BMDMs, indicating a loss of the electrochemical gradient shorty before complete rupture of the plasma membrane. However, these data also show that a sizeable subset of LPS transfected BMDMs can by some means restore membrane integrity after GSDMD activation, thus acquiring PI staining gradually without apparent loss of the electrochemical gradient.

Since Ca2+ signalling controls cellular membrane repair mechanisms (*16*), we hypothesized that Ca2+ influx through the GSDMD pore serves indicates membrane permeabilization and that this initiates the repair of the affected plasma membrane area. Treatment with BAPTA-AM, a chelator of intracellular Ca2+ ions, has been widely used to study Ca2+-dependent membrane repair (*21, 24*). BMDMs were therefore pre-loaded with BAPTA-AM and transfected with LPS to test how the sensing of intracellular Ca2+ affects the level or speed of pyroptosis induction. BAPTA treatment increased the level of Lactate Dehydrogenase (a measure of cell death/lysis) release from LPS transfected WT BMDMs in a dose- dependent manner (**Fig. 1E**). Importantly, BAPTA treatment did not result in spontaneous LDH release, since LDH levels were not significantly altered in *Casp11–/–* BMDMs (**Fig. 1E**), thus confirming that the observed increase in cell death was specific to detecting Ca2+ influx. Ca2+ chelation robustly increased and accelerated cell death over a range of transfected LPS concentrations as shown by titration experiments (**Fig. S1C**). The most striking effects of BAPTA treatment were observed at very low levels

of LPS transfection, as cells transfected in medium were able to cope with caspase-11 activation and did not release LDH, while cells unable to detect Ca2+ influx failed to survive sub-lytic inflammasome activation and showed significant levels of cell death (**Fig. S1C**). Since Ca2+ chelation could increase the activity of the non-canonical inflammasome pathway by either enhancing the levels of LPS transfection, caspase-11 oligomerization or caspase-11 activity, we assessed the level of GSDMD processing as a proxy for altered levels of non-canonical inflammasome activation. Immortalized BMDMs expressing HA-tagged mouse GSDMD were transfected with different amounts of LPS in the presence or absence of BAPTA-AM, and the generation of the N-terminal p30 GSDMD fragment was assayed by immunoblotting. BAPTA treatment did not enhance GSDMD processing (**Fig. 1F**), suggesting that Ca2+ chelation did not modulate the assembly of the non-canonical inflammasome or caspase-11 activation, but acted downstream of GSDMD activation.

We next asked if the non-canonical inflammasome in human cells responds similarly to chelation of intracellular Ca2+ by examining HeLa cells infected with *ΔsifA S. enterica* serovar Typhimurium (*S. typhimurium*). Deficiency in the effector SifA results in an instable

Salmonella containing vacuole and entry of the bacteria into the cytosol, where LPS is detected by caspase-4 (NLRC4 is not present in HeLa cells)(*26, 27*). We observed a similar increase in LDH release upon treatment with BAPTA-AM compared to cells infected in medium (**Fig. 1G**), confirming the data obtained with primary mouse BMDMs. Ca2+ chelation did also not increase the levels of GSDMD processing in HeLa cells expressing FLAG-tagged human GSDMD (**Fig. 1H**). Overall, these findings suggested that chelating intracellular Ca2+ ions does not affect inflammasome assembly, caspase activation or GSDMD processing per se, but specifically enhances the levels of cell lysis, most likely by masking the signal (Ca2+ influx) necessary to initiate the repair of GSDMD-damaged plasma membrane regions.

ESCRT components translocate to the plasma membrane during pyroptosis

Ca2+ influx engages membrane repair programs, among them the shedding of damaged membrane areas in form of ectosomes that are formed with help of the ESCRT machinery (*22, 23*). To investigate if the ESCRT machinery is activated during upon pyroptosis induction, we made use of HeLa cells stably expressing near endogenous levels of CHMP4-GFP (*28*). Uninfected cells showed homogenous distribution of CHMP4-GFP in the cytoplasm and the nucleus, whereas upon activation of the non- canonical inflammasome by *ΔsifA S. typhimurium* infection, CHMP4-GFP formed multiple distinct puncta at the cell periphery, presumably at the plasma membrane (**Fig. 2A, arrowheads**). Similar puncta could also be observed in cells treated with pore forming toxin perforin (**Fig. 2A**), which has been shown to form pores in the plasma membrane (*24*). Furthermore, expression of GSDMDNT was sufficient to induce CHMP4-GFP puncta formation, supporting the notion that CHMP4-GFP aggregation was triggered by plasma membrane damage (**Fig. 2A**).

To confirm that CHMP4-GFP translocated to the plasma membrane upon GSDMD pore formation, we used the lipophilic probe FM 4-64FX that exhibits low fluorescence in water but fluoresces intensely upon binding the outer leaflet of the plasma membrane. Upon induction of GSDMDNT expression

CHMP4-GFP puncta localized with FM4-64FX stained membrane regions (**Fig. 2B**), confirming that during pyroptosis the ESCRT machinery is activated and localizes to the plasma membrane. Live cell microscopy of CHMP4-GFP puncta in cells induced for GSDMDNT expression further showed that CHMP4-GFP was dynamic, quickly assembling and disassembling at the cell periphery before cells lost membrane integrity (**Fig. 2C, Movie 2**). Interestingly, we also observed that in pyroptotic CHMP4-GFP HeLa cells the cytosolic

GFP signal was lost while peripheral GFP puncta were retained, suggesting that CHMP4-GFP complexes remain strongly associated with the plasma membrane after cell death (**Fig 2D**).

The translocation of ESCRTIII components to the plasma membrane in response to laser-induced damage or MLKL-induced damage requires the detection of Ca2+ influx into the cytosol and is effectively blocked by incubation in Ca2+ free medium or chelators like EDTA or BAPTA-AM (*22, 25*). We therefore assessed next if chelation of Ca2+ ions affects the number of CHMP4-GFP speckles after pyroptosis induction. HeLa CHMP4-GFP cells stably transduced with Dox-inducible GSDMDNT-mCherry, were pre- treated using medium, medium supplemented with BAPTA-AM or Ca2+-free medium (containing 2 mM EDTA). Cells were then either left untreated (control) or treated with Dox to induce GSDMDNT expression and subsequent pyroptosis, before quantifying the number of CHMP4-GFP specks by microscopy. Treatment with BAPTA-AM or incubation in Ca2+-free medium did not affect CHMP4-GFP localization in control cells, but significantly reduced the percentage of cells displaying CHMP4-GFP speckles after GSDMDNT induction (**Fig. 2E-F**). This finding demonstrated that detection of Ca2+ influx in response to GSDMD pore formation is necessary for the translocation of CHMP4-GFP and presumably other ESCRTIII components to the plasma membrane and suggested that the increase in cell death upon Ca2+ chelation (**Fig. 1, S1**) is linked to an inability to engage ESCRT-mediated membrane repair.

While clathrin, COPI and COPII coat promote the budding and pinching-off of vesicles towards the cytosol, the ESCRT machinery is the only mechanism known so far that allows vesicles to bud and pinch-off away from the cytosol (*29, 30*). This feature is necessary for example to form multi-vesicular bodies (MVBs), to release ectosomes or as part of viral budding, which incidentally involves the hijacking of the ESCRT machinery by the virus (*31*). In the context of ESCRT-mediated membrane repair these buds are thought to contain damaged plasma membrane areas. During necroptosis, which is delayed by ESCRT-mediated membrane repair, Annexin-V-positive bubbles appear at the plasma membrane(*25*), which might be ESCRT-induced structures, although their size (up to 500 nm in diameter) is larger than what has been reported for viral buds (approx. 100 nm in diameter). Examination of LPS transfected iBMDMs by electron microscopy revealed multiple vesicles budding off from the plasma membrane towards the extracellular space (**Fig. 2G**), while no such features could be found in untreated cells (**Fig. S2B**). These vesicles ranged in size between 50 and 100 nm often had a distinct neck region, reminiscent of ESCRT-induced HIV buds(*31*). In conclusion, our results showed that during GSDMDNT-induced pyroptosis cells respond by

initiating the formation of ectosomes and the recruitment of the ESCRT machinery to the plasma membrane, and that ESCRT recruitment requires
Ca2+ signalling. Thus, they support the notion that ESCRT-mediated membrane repair is engaged in response to GSDMD pore formation at the plasma membrane.

Expression of dominant-negative ESCRT-III components enhances pyroptosis

The ESCRT-III machinery is essential for cellular homeostasis (*29, 32*), and consequently knock-out or prolonged knock-down results in toxicity, for example due to uncontrolled basal levels of necroptosis(*25*). Previous studies have however shown that expression of dominant negative ESCRT- III proteins, such as truncated CHMP3 that lacks the regulatory C-terminal domain (CHMP31-179) or ATP-binding deficient VPS4a (VPS4aE228Q) leads to deregulated activation and impaired recycling of other ESCRT components, therefore effectively depleting the cytosolic pool of functional ESCRT components (*22*). To assess if an ESCRT-dependent membrane repair program regulates pyroptosis, we stably transduced HeLa cells with Dox-inducible wildtype human ESCRT-III proteins (CHMP3WT or VPS4aWT) or the respective dominant-negative versions (CHMP31-179 or VPS4aE228Q) (**Fig. S3A**). To assess the toxicity of these proteins we induced their expression for up to 24 hours. Immunoblot analysis showed that following Dox treatment WT and dominant-negative VPS4a and CHMP3 were expressed to comparable levels at all time points examined (**Fig. S3B**). Expression of VPS4aWT or CHMP3WT did not affect cell viability during the period examined, while both VPS4aE228Q or CHMP31-179 induced moderate cell death after 20 hours (**Fig. S3C**). This cell death, which is most likely caused by necroptosis (*25*), was even more prominent at 24 hours post induction (**Fig. S3C**). We therefore restricted the following experiments to the early period post induction (i.e. all experiments were terminated not later than 15 hours post Dox treatment) during which expression of dominant-negative proteins did not lead to increased frequency of dead cells nor changes in cell density or cell morphology, compared to cells expressing the WT protein. We next tested if induction of dominant-negative ESCRTIII components inactivates the ESCRT machinery. Induction of HA-tagged WT and dominant- negative VPS4a for 6 hours showed that while VPS4aWT localized evenly throughout the cytoplasm, VPS4aE228Q aggregated inside the cell (**Fig. 3A**). A similar pattern was observed with CHMP31-179, but required induction for 12 hours (**Fig. 3A**). These findings were in line with published observations (*33, 34*), and indicated that the dominant-negative proteins arrested the disassembly of the ESCRT machinery and thus depleted the cells of active ESCRT components.

We then assessed how depletion of active ESCRT components affected pyroptosis after non-canonical inflammasome activation in human and mouse cells. Expression of wildtype and dominant- negative VPS4a or CHMP3 was induced in the HeLa cells prior to infection with *ΔsifA S. typhimurium* to activate the non-canonical inflammasome. Consistent with an important role of the ESCRT machinery in controlling pyroptotic cell death in human cells, we observed that cell death was strongly enhanced in cells expressing either VPS4E228Q or CHMP31-179 compared to WT controls, independently of the multiplicity of infection (MOI) (**Fig 3B**). Immunoblotting for GSDMD processing demonstrated that inactivation of the ESCRT machinery through VPS4E228Q and CHMP31-179 expression did not change GSDMD processing even though it strongly enhanced cell death, suggesting that the ESCRT mediated

membrane repair acts downstream of caspase-4 and GSDMD activation (**Fig 3C**). As cells of the myeloid lineage respond to pathogen infection by activation of inflammasome, we tested if ESCRT dependent membrane repair has a role during pyroptosis in mouse macrophages by generating immortalized BMDMs stably transduced with Dox-inducible human VPS4WT or VPS4E228Q. The transgenic iBMDM lines were simultaneously treated for 6 hours with LPS to induce caspase-11 expression and doxycycline to induce expression of wildtype or dominant-negative VPS4a before transfection of LPS. Consistent with the results obtained in HeLa cells, we found that the wildtype protein localized evenly throughout cells, whereas the dominant-negative VPS4a clustered in iBMDMs (**Fig. S3D**). LPS transfection of these lines showed that expression of VPS4aE228Q more than doubled the levels of membrane permeabilization as judged by PI staining (**Fig. 3D-E**) as well as LDH release (**Fig. 3F**) compared to iBMDMs expressing VPS4aWT. These increased levels of cell death required the activation of the non-canonical inflammasome and GSDMD, as *Casp11-/-* or *Gsdmd-/-* iBMDMs expressing VPS4aWT or VPS4aE228Q only displayed basal levels of cell death when transfected with LPS (**Fig. 3G**). Immunoblots confirmed equal expression levels of VPS4aWT or VPS4aE228Q in all genotypes

(**Fig. 3H**). Next, we asked how ESCRT-III-mediated inhibition of cell death impacts on the release of mature

IL-1 cytokines. Since GSDMD pore formation and subsequent efflux of K+ is necessary to activate NLRP3 and caspase-1 in the non-canonical pathway (*35*), ESCRT inactivation could enhance cytokine release by enhancing the degree of K+ efflux due to prolonged GSDMD pore formation. Alternatively, accelerated cell lysis as a result of ESCRT inactivation could

also limit the time available for NLRP3 activation and IL-1b maturation and thus reduce the amount of mature cytokine that are released from dying cells. LPS-primed immortalized BMDMs expressing VPS4aE228Q or VPS4aWT were thus transfected with LPS and supernatants analysed for the release of mature IL-1b by ELISA. Significantly higher levels of mature IL-1b were found in the supernatants of VPS4aE228Q expressing BMDMs compared to VPS4aWT expressing controls (**Fig. 3I**), which was entirely dependent on the presence of caspase-11 and GSDMD (**Fig. 3J**). These findings are consistent with a model in which enhanced or prolonged GSDMD pore formation triggers increased K+ efflux and thus increased NLRP3 inflammasome activation, which was confirmed by the enhanced levels of processed, activated caspase-1 that were found in cells expressing VPS4aE228Q (**Fig. 3K**). Furthermore, inhibition of NLRP3 by MCC950 treatment or high extracellular K+ inhibited IL-1b release in cells expressing wild-type or dominant-negative VPS4a (**Fig. 3L, S3E)**. Immunoblotting revealed, that GSDMD processing was slightly enhanced in cells expressing VPS4aE228Q compared to iBMDMs expressing VPS4aWT (**Fig. 3M**). We postulated that this increase of GSDMD processing could be a consequence of enhanced NLRP3 inflammasome activation (**Fig. 3J-L**), and thus caspase-1-dependent. Consistent with this hypothesis, we found that GSDMD processing was unchanged between VPS4aE228Q and VPS4aWT expressing iBMDMs in the presence of MCC950 (**Fig. 3M**), confirming that in the non-canonical pathway ESCRT mediated regulation of pyroptosis is downstream of caspase-11 activation and GSDMD processing. Taken together these data show that inactivating the ESCRT machinery strongly enhances pyroptotic
cell death in human and mouse cells following non-canonical inflammasome activation, thus suggesting that ESCRT-dependent membrane repair is a conserved mechanism that counteracts cell death by reducing plasma membrane damage caused by GSDMD pore formation.

ESCRT controls cell death after canonical inflammasome activation

Given the strong effects of ESCRT inhibition of pyroptosis induced by the non-canonical inflammasome, we asked if cell death triggered by the canonical inflammasome pathway, which involves the activation of caspase-1 in human and mouse cells, is also negatively regulated by ESCRT-mediated membrane repair. We first examined the effect of Ca2+ chelation on pyroptosis induction after activation of the AIM2 inflammasome. Mouse BMDMs were primed, treated with BAPTA-AM and transfected with different concentrations of poly(dA:dT) (synthetic DNA), an AIM2 ligand. As observed for LPS

transfection (**Fig. 1**), intracellular Ca2+ chelation also significantly increased pyroptosis after AIM2 inflammasome activation (**Fig. 4A**). BAPTA treatment did not lead to spontaneous cell death, since BMDMs deficient in *Asc,* a critical adaptor protein of canonical inflammasomes, showed only basal levels of pyroptosis. Assessing caspase-1 activation by immunoblotting revealed that the generation of the caspase-1 p20 subunit was not enhanced by Ca2+ chelation, suggesting that BAPTA treatment did not enhance steps upstream of caspase-1 activation (**Fig. 4B**). These experiments (**Fig. 4B**) were conducted in BMDMs deficient in *Nlrp3* to exclude effects of secondary NLRP3 activation via GSDMD pore induced potassium efflux, and importantly, enhancement of cell death by calcium depletion was independent of NLRP3 (**Fig S4A**). Given the effects of Ca2+ sensing on canonical inflammasome activation, we next examined the effects of depleting the ESCRT machinery on cell death induction. Immortalized macrophages stably transduced with Dox-inducible VPS4aWT or VPS4aE228Q were treated with Dox to induce protein expression, primed and infected with different MOIs of log-phase *S. typhimurium* to activate the canonical NLRC4 inflammasome (*36*). Consistent with our previous findings, we observed an enhancement of cell death in cells expressing dominant-negative VPS4a despite unaltered levels of ASC speck formation or caspase-1 and GSDMD processing (**Fig. 4C-D and Fig. S4B**). This cell death was specific to the activation of the NLRC4 inflammasome, since it was not observed in *Gsdmd-/-* BMDMs (**Fig. S4C**). Increased cell death as a consequence of ESCRT inactivation also led to a slight increase in the release of mature IL-1b (**Fig. 4C**), suggesting that ESCRT-mediated membrane repair negatively regulates the levels of cytokines that are released in a GSDMD-dependent manner.

Although our experiments suggested that ESCRT-mediated membrane repair restricts caspase-1- induced cell death, the effects were much smaller compared to non-canonical inflammasome activation. A possible explanation could be that oligomerization of the receptors and the adaptor ASC, which have been proposed to amplify the signal generated by few active receptors (*37, 38*), produces too much active caspase-1 within a short period of time thereby quickly overwhelming membrane repair mechanisms. To investigate this possibility, we created HEK293T cells stably transduced with chemically dimerizable caspase-1 (DmrB-Casp1 HEK293T). Addition of B/B homodimerizer allows to induce the oligomerization of DmrB and thus the activation of caspase-1 in a controlled manner and without the need for receptor or adaptor proteins. DmrB-Casp1 HEK293T were co-transfected with human GSDMD and Dox-inducible constructs for wildtype and dominant-negative CHMP3/VPS4a proteins, respectively, and protein expression was induced with

Dox for 16 hours. Remarkably and unlike to what we had observed in HeLa cells, none of the dominant-negative proteins induced changes in cell appearance or induced cell death after 16 hours of expression in HEK 293T cells, most likely because of absence of a functional RIPK3/MLKL signalling axis(*39*) (**Fig. S4D**). We next examined the effects of ESCRT inactivation on caspase-1-induced pyroptosis by measuring PI influx over a period of 1.5 hours post B/B homodimerizer addition. PI influx increased faster in cells expressing dominant- negative ESCRT proteins compared to cells expressing wild-type ESCRT proteins (**Fig. S4E**), confirming that the ESCRT machinery restricts pyroptosis after caspase-1 activation. Nevertheless, even cells with an active membrane repair reached high levels of cell death after 2.5 hours, indicating that even chemically activated caspase-1 eventually overwhelms membrane repair mechanisms.

Treatment with washout compound allows to quickly disrupt B/B homodimerizer-induced DmrB oligomers and might thus allow to terminate DmrB-Casp-1 activity and create a limited amount of GSDMD pores. To test this, we activated DmrB-caspase-1 by B/B homodimerizer addition for 30 minutes in GSDMD expressing DmrB-Casp-1 HEK293T cells, before addition of a 50-fold excess of washout compound. Disruption of caspase-1 activity by washout compound treatment resulted in a significant reduction of cell death levels, while PI levels in cells that were only treated with B/B homodimerizer continued to rise (**Fig. 4E**). While washout compound treatment decreased cell death levels in cells expressing VPS4aWT and VPS4aE228Q, it however also strongly enhanced the difference in cell death levels between cells expressing VPS4aWT and VPS4aE228Q, indicating that an active ESCRT machinery plays a more important role in conditions where caspase-1 is activated at low level or for a limited time (compare **Fig 4E** to **Fig. S4E**). Titration of the B/B homodimerizer followed by washout treatment revealed that across a variety of concentrations, disruption of the ESCRT machinery by expression of dominant-negative proteins enhanced cell death strongly (**Fig 4F**, **Fig. S4F**), while processing of GSDMD by caspase-1 was not altered by expression of dominant-negative proteins compared to their wildtype counterparts (**Fig 4G**). Importantly, inhibition of ESCRT activity only enhanced cell death in Dmrb-Casp-1 HEK293T cells only when GSDMD was expressed, confirming that ESCRT-mediated membrane repair negatively regulates GSDMD-induced pyroptosis (**Fig. S4G**).

To confirm the impact of ESCRT-mediated membrane repair on cytokine secretion in DmrB-Casp1 HEK293T cells, we stably transduced these cells with pro-IL-1b (DmrB-Casp1 pro-IL-1b HEK293T). These cells were then transfected with Dox-inducible GSDMD and

dominant-negative CHMP3 and VPS4a respectively. Stimulation of these cells with B/B homodimerizer followed by treatment with washout compound resulted in the release of mature IL-1b, which was significantly higher in cells expressing CHMP31-179 or VPS4aE228Q (**Fig 4H and 4I**). Enhanced levels of IL-1b release correlated with enhanced cell death, consistent with the essential role of GSDMD pores in IL-1b release (Heilig et al. unpublished data, (*40*). Overall these experiments show that ESCRT mediated membrane repair not only dampens GSDMD pore mediated cell death but at the same time negatively affects IL-1b secretion

following canonical and non-canonical inflammasome activation, in a variety of cell lines and systems.

Discussion

Since the 1950 it has been known that various cells feature the ability to rapidly reseal damaged plasma membrane areas by mechanisms that strictly depends on the detection of Ca2+ influx. How membrane repair is initiated and executed has however only emerged recently, and two mutually non-exclusive mechanisms have been identified, relying either on lysosome exocytosis of ASM followed by internalization of damaged membrane regions or the removal of damaged membrane in form of ectosomes generated by the ESCRT machinery. While early reports suggested that such membrane repair is mainly regulating plasma membrane damage as a result of PFT or mechanical damage, it has now become evident that the ESCRT machinery also regulates host-signalling pathways, for example by enhancing survival of cells undergoing necroptosis and therefore increasing the potential to signal to neighbouring cells (*25*).

We now demonstrate that a Ca2+-dependent membrane repair by the ESCRT system negatively regulates GSDMD-induced pyroptosis in human and mouse cells, and in response to a variety of activators. We propose that the function of ESCRT in the context of pyroptosis is to remove GSDMD pores from the plasma membrane by removing permeabilized areas in form of ectosomes. We can however not exclude that another function of the ESCRT complex, for example in vesicular trafficking, restricts pyroptosis as well, nor do our findings exclude the possibility that other parallel mechanisms restrict pyroptotic cell death. ESCRT inhibition enhances IL-1b release after both canonical and non- canonical inflammasome activation and allows cell survival at sub-lytic levels of inflammasome stimulation, suggesting that membrane repair might be essential to protect the organism against low level spontaneous or uncontrolled inflammasome activation that could result in systemic inflammation. Unfortunately, due to the essential nature of the ESCRT machinery deletion of

ESCRT-III components are lethal, thus making it impossible to investigate the role of membrane repair *in vivo*.

Our results demonstrate the importance of calcium mediated membrane repair downstream of inflammasome assembly, caspase activation and GSDMD processing. It is however well established that membrane damage through pore forming toxins is an upstream signal that drives NLRP3 inflammasome assembly (*41*). Thus, it will be interesting to determine if and how membrane repair programs regulate NLRP3 activation triggered by pore forming toxins or during pathogen infection. recently it has also been demonstrated that disruption of the nuclear envelope results in release of DNA into the cytosol and the activation of the AIM2 inflammasome (*42*). As the ESCRT machinery mediates resealing of the nuclear envelope during upon mechanical stress (*43, 44*) or during the reformation of the nuclear envelop during telophase, it will be interesting to examine if inactivation of ESCRT-III results in higher levels of AIM2 activity during these events.

The release or secretion of mature IL-1b has debated for decades and several mechanisms were proposed. release within ectosomes or exosomes has been proposed to be one mechanism for how

IL-1b leaves the cells (*45*), and indeed several publications have reported that pyroptotic cells release microvesicles (*46-48*), even though the nature and source of these vesicles was unknown. Our findings thus provide an explanation why microvesicle shedding can be observed during inflammasome activation and implicate the ESCRT machinery in this process. It will be interesting to investigate if microvesicles released from pyroptotic cells contain mature GSDMD and possibly other factors know to be release during pyroptosis. Moreover, the function of these vesicles prior to pyroptosis or for cell to cell communication or as means of communication to more distant sites in the host remains to be elucidated.

Our findings could also have important implications for the mechanism of IL-1b release itself. While IL- 1b release has been shown to be GSDMD-dependent in macrophages and other cell types (*6, 7*), we have observed that GSDMD-dependent IL-1b release also happens if lysis is blocked (Heilig and Broz, EJI, in press) (*40*). While it is possible that IL-1b is released directly through the GSDMD pore under these circumstances, an alternative explanation would be that GSDMD pore formation triggers ESCRT activity that continuously releases IL-1b packed in ectosomes. Such a mechanism might also be mediating IL-1b release at sublytic levels of inflammasome activation (see **Fig. 4**) or in several systems that have been reported to result in cell death-independent IL-1b release, among these neutrophils (*13*), OxPAPC-treated DCs (*12*) and NAG-elicited activation of the NLRP3 inflammasome

(*14*). If lL-1b release in these systems requires GSDMD and the ESCRT machinery, and if it proceed through microvesicle shedding should be subject of further research.

Our results provide a conceptual insight into how the different cell types mentioned above resist pyroptosis and that regulation of inflammasome signalling is not necessarily dependent on expression and activation of components of the inflammasome but on the integration of inflammasome pathways with different host signalling pathways. These pathways may confer permanent resistance or transient persistence of cells against GSDMD mediated pyroptosis. It is important to note that plasma membrane repair in particular does not exclusively rely on the ESCRT system but can be mediated by ASM mediated endocytosis of pores. Both pathways are not mutually exclusive, however if they are connected yet needs to be determined. In addition, it was reported that caspase-1 activity induces the activation Sterol Regulatory Element Binding Proteins (SREBPs) (*49*), which can promote cell survival upon toxin challenge possibly by facilitating membrane repair. Therefore, further research is necessary to define membrane repair programs, cell type specific differences and if the engagement of the different programs changes the fate of cells subjected to inflammasome activation.

References

1. S. L. Fink, B. T. Cookson, Apoptosis, pyroptosis, and necrosis: mechanistic description of dead and dying eukaryotic cells. *Infect Immun* **73**, 1907-1916 (2005).
2. P. Broz, V. M. Dixit, Inflammasomes: mechanism of assembly, regulation and signalling. *Nat Rev Immunol* **16**, 407-420 (2016).
3. S. L. Fink, T. Bergsbaken, B. T. Cookson, Anthrax lethal toxin and Salmonella elicit the common cell death pathway of caspase-1-dependent pyroptosis via distinct mechanisms. *Proc Natl Acad Sci U S A* **105**, 4312-4317 (2008).
4. T. Bergsbaken, S. L. Fink, B. T. Cookson, Pyroptosis: host cell death and inflammation. *Nat Rev Microbiol* **7**, 99-109 (2009).
5. X. Chen *et al.*, Pyroptosis is driven by non-selective gasdermin-D pore and its morphology is different from MLKL channel-mediated necroptosis. *Cell Res* **26**, 1007-1020 (2016).
6. N. Kayagaki *et al.*, Caspase-11 cleaves gasdermin D for non-canonical inflammasome signalling. *Nature* **526**, 666-671 (2015).
7. J. Shi *et al.*, Cleavage of GSDMD by inflammatory caspases determines pyroptotic cell death. *Nature* **526**, 660-665 (2015).

8. J. Ding *et al.*, Pore-forming activity and structural autoinhibition of the gasdermin family. *Nature* **535**, 111-116 (2016).
9. X. Liu *et al.*, Inflammasome-activated gasdermin D causes pyroptosis by forming membrane pores. *Nature* **535**, 153-158 (2016).
10. L. Sborgi *et al.*, GSDMD membrane pore formation constitutes the mechanism of pyroptotic cell death. *EMBO J* **35**, 1766-1778 (2016).
11. R. A. Aglietti *et al.*, GsdmD p30 elicited by caspase-11 during pyroptosis forms pores in membranes. *Proc Natl Acad Sci U S A*, (2016).
12. I. Zanoni *et al.*, An endogenous caspase-11 ligand elicits interleukin-1 release from living dendritic cells. *Science* **352**, 1232-1236 (2016).
13. K. W. Chen *et al.*, The neutrophil NLRC4 inflammasome selectively promotes IL-1beta maturation without pyroptosis during acute Salmonella challenge. *Cell Rep* **8**, 570-582 (2014).
14. A. J. Wolf *et al.*, Hexokinase Is an Innate Immune Receptor for the Detection of Bacterial Peptidoglycan. *Cell* **166**, 624-636 (2016).
15. S. A. Conos, K. E. Lawlor, D. L. Vaux, J. E. Vince, L. M. Lindqvist, Cell death is not essential for caspase-1-mediated interleukin-1beta activation and secretion. *Cell Death Differ* **23**, 1827- 1838 (2016).
16. N. W. Andrews, P. E. Almeida, M. Corrotte, Damage control: cellular mechanisms of plasma membrane repair. *Trends Cell Biol* **24**, 734-742 (2014).
17. A. Draeger, R. Schoenauer, A. P. Atanassoff, H. Wolfmeier, E. B. Babiychuk, Dealing with damage: plasma membrane repair mechanisms. *Biochimie* **107 Pt A**, 66-72 (2014).
18. P. L. McNeil, R. Khakee, Disruptions of muscle fiber plasma membranes. Role in exercise- induced damage. *Am J Pathol* **140**, 1097-1109 (1992).
19. P. L. McNeil, S. S. Vogel, K. Miyake, M. Terasaki, Patching plasma membrane disruptions with cytoplasmic membrane. *J Cell Sci* **113 (Pt 11)**, 1891-1902 (2000).
20. T. Togo, J. M. Alderton, G. Q. Bi, R. A. Steinhardt, The mechanism of facilitated cell membrane resealing. *J Cell Sci* **112 (Pt 5)**, 719-731 (1999).

21. C. Tam *et al.*, Exocytosis of acid sphingomyelinase by wounded cells promotes endocytosis and plasma membrane repair. *J Cell Biol* **189**, 1027-1038 (2010).
22. A. J. Jimenez *et al.*, ESCRT machinery is required for plasma membrane repair. *Science* **343**, 1247136 (2014).
23. L. L. Scheffer *et al.*, Mechanism of Ca(2)(+)-triggered ESCRT assembly and regulation of cell membrane repair. *Nat Commun* **5**, 5646 (2014).
24. D. Keefe *et al.*, Perforin triggers a plasma membrane-repair response that facilitates CTL induction of apoptosis. *Immunity* **23**, 249-262 (2005).
25. Y. N. Gong *et al.*, ESCRT-III Acts Downstream of MLKL to Regulate Necroptotic Cell Death and Its Consequences. *Cell* **169**, 286-300 e216 (2017).
26. J. Shi *et al.*, Inflammatory caspases are innate immune receptors for intracellular LPS. *Nature*, (2014).
27. Y. Zhao *et al.*, The NLRC4 inflammasome receptors for bacterial flagellin and type III secretion apparatus. *Nature*, (2011).
28. I. Poser *et al.*, BAC TransgeneOmics: a high-throughput method for exploration of protein function in mammals. *Nat Methods* **5**, 409-415 (2008).
29. O. Schmidt, D. Teis, The ESCRT machinery. *Curr Biol* **22**, R116-120 (2012).
30. D. Teis, S. Saksena, S. D. Emr, SnapShot: the ESCRT machinery. *Cell* **137**, 182-182 e181 (2009).
31. E. Morita *et al.*, ESCRT-III protein requirements for HIV-1 budding. *Cell Host Microbe* **9**, 235- 242 (2011).
32. L. N. Ventimiglia, J. Martin-Serrano, ESCRT machinery: Damage control at the nuclear membrane. *Cell Res* **26**, 641-642 (2016).
33. N. Jouvenet, M. Zhadina, P. D. Bieniasz, S. M. Simon, Dynamics of ESCRT protein recruitment during retroviral assembly. *Nat Cell Biol* **13**, 394-401 (2011).
34. J. D. Dukes, J. D. Richardson, R. Simmons, P. Whitley, A dominant-negative ESCRT-III protein perturbs cytokinesis and trafficking to lysosomes. *Biochem J* **411**, 233-239 (2008).
35. S. Ruhl, P. Broz, Caspase-11 activates a canonical NLRP3 inflammasome by promoting K efflux. *Eur J Immunol*, (2015).
36. P. Broz *et al.*, Redundant roles for inflammasome receptors NLRP3 and NLRC4 in host defense against Salmonella. *J Exp Med* **207**, 1745-1755 (2010).

37. M. S. Dick, L. Sborgi, S. Ruhl, S. Hiller, P. Broz, ASC filament formation serves as a signal amplification mechanism for inflammasomes. *Nat Commun* **7**, 11929 (2016).
38. A. Lu *et al.*, Unified polymerization mechanism for the assembly of ASC-dependent inflammasomes. *Cell* **156**, 1193-1206 (2014).
39. S. He *et al.*, Receptor interacting protein kinase-3 determines cellular necrotic response to TNF- alpha. *Cell* **137**, 1100-1111 (2009).
40. C. L. Evavold *et al.*, The Pore-Forming Protein Gasdermin D Regulates Interleukin-1 Secretion from Living Macrophages. *Immunity*, (2017).
41. R. Munoz-Planillo *et al.*, K(+) efflux is the common trigger of NLRP3 inflammasome activation by bacterial toxins and particulate matter. *Immunity* **38**, 1142-1153 (2013).
42. A. Di Micco *et al.*, AIM2 inflammasome is activated by pharmacological disruption of nuclear envelope integrity. *Proc Natl Acad Sci U S A* **113**, E4671-4680 (2016).
43. M. Raab *et al.*, ESCRT III repairs nuclear envelope ruptures during cell migration to limit DNA damage and cell death. *Science* **352**, 359-362 (2016).
44. C. M. Denais *et al.*, Nuclear envelope rupture and repair during cancer cell migration. *Science* **352**, 353-358 (2016).
45. M. Monteleone, J. L. Stow, K. Schroder, Mechanisms of unconventional secretion of IL-1 family cytokines. *Cytokine* **74**, 213-218 (2015).
46. C. Pizzirani *et al.*, Stimulation of P2 receptors causes release of IL-1beta-loaded microvesicles from human dendritic cells. *Blood* **109**, 3856-3864 (2007).
47. C. Andrei *et al.*, The secretory route of the leaderless protein interleukin 1beta involves exocytosis of endolysosome-related vesicles. *Mol Biol Cell* **10**, 1463-1475 (1999).
48. A. MacKenzie *et al.*, Rapid secretion of interleukin-1beta by microvesicle shedding. *Immunity* **15**, 825-835 (2001).
49. L. Gurcel, L. Abrami, S. Girardin, J. Tschopp, F. G. van der Goot, Caspase-1 activation of lipid metabolic pathways in response to bacterial pore-forming toxins promotes cell survival. *Cell* **126**, 1135-1145 (2006).
50. P. Broz, J. von Moltke, J. W. Jones, R. E. Vance, D. M. Monack, Differential requirement for Caspase-1 autoproteolysis in pathogen-induced cell death and cytokine processing. *Cell Host Microbe* **8**, 471-483 (2010).

Acknowledgments

We thank Prof. Anthony Hyman (MPI-CBG, Dresden, Germany) for CHMP4-GFP HeLa cells, Prof. Andrew Oberst (University of Washington, Seattle, USA) for DmrB-caspase-1, the Biozentrum Imaging Core Facility, the C-CINA BioEM Lab for technical assistance. We especially thank J. Pieters (Biozentrum, Basel) for support and discussions. This work was supported by an SNSF project grant 310030_175576 to P.B. and Werner Siemens Fellowships (Fellowships for Excellence, University of Basel) to S.R. and R.H. .

Author Contributions

S.R. and P.B. designed the study, analysed data and wrote the manuscript. S.R. performed the experiments. R.H. contributed reagents. ***Conflict of interest statement*** The authors do not have any conflict of interest.

List of Supplementary material

Materials and Methods Fig S1 – S4 References (51) Multimedia files (3 Movies)

Figure 1. GSDMD-mediated calcium flux negatively regulates pyroptosis

A. Percentage of LPS-primed wildtype BMDMs displaying high PI levels after transfection with the indicated amount of LPS for 2 hours. Three fields of view were analyzed and PI^{high} cells enumerated manually. **B.** Live cell imaging of Ca^{2+} influx (Fluo-8) and membrane permeabilization (PI) in LPS-primed wildtype BMDMs after transfection of LPS. Scale bars are 5 μm. **C.** Single cell analysis of Ca^{2+} (Fluo-8) and PI influx in LPS-primed wildtype and *Casp11*$^{-/-}$ BMDMs either not stimulated or transfected with LPS. Graphs show data from 3 representative cells out of at least 30 analyzed per condition. **D**. PI influx in wildtype and *Casp11*$^{-/-}$ BMDMs not undergoing pyroptosis. Graphs show data from 6 representative cells out of at least 30 analyzed per condition. **E**. LDH release from untreated or BAPTA-AM treated wildtype and *Casp11*$^{-/-}$ BMDMs 2 hours after LPS transfection. **F.** Immunoblots for GSDMD processing in combined lysates and supernatants of LPS-primed immortalized BMDMs (expressing HA-tagged mGSDMD) after transfection with the indicated amounts of LPS in the presence or absence of BAPTA-AM. GAPDH serves as loading control. **G.** LDH release from BAPTA-AM treated HeLa cells (expressing Flag-hGSDMD-V5) 5 hours post infection with different multiplicities of infection (MOI) of Δ*sifA S. typhimurium.* **H.** Immunoblots for GSDMD processing in combined lysates and supernatants of BAPTA-AM treated HeLa cells (expressing Flag-hGSDMD-V5) 5 hours post infection with Δ*sifA S. typhimurium* at the indicated MOIs. Statistical analysis was done using unpaired student's t-test, * $p<0.05$, ** $p<0.01$, *** $p<0.001$. Results shown in **A-H** are representative of at least three independent experiments. Time is shown in hh:mm:ss.

Rühl et al. Figure 1

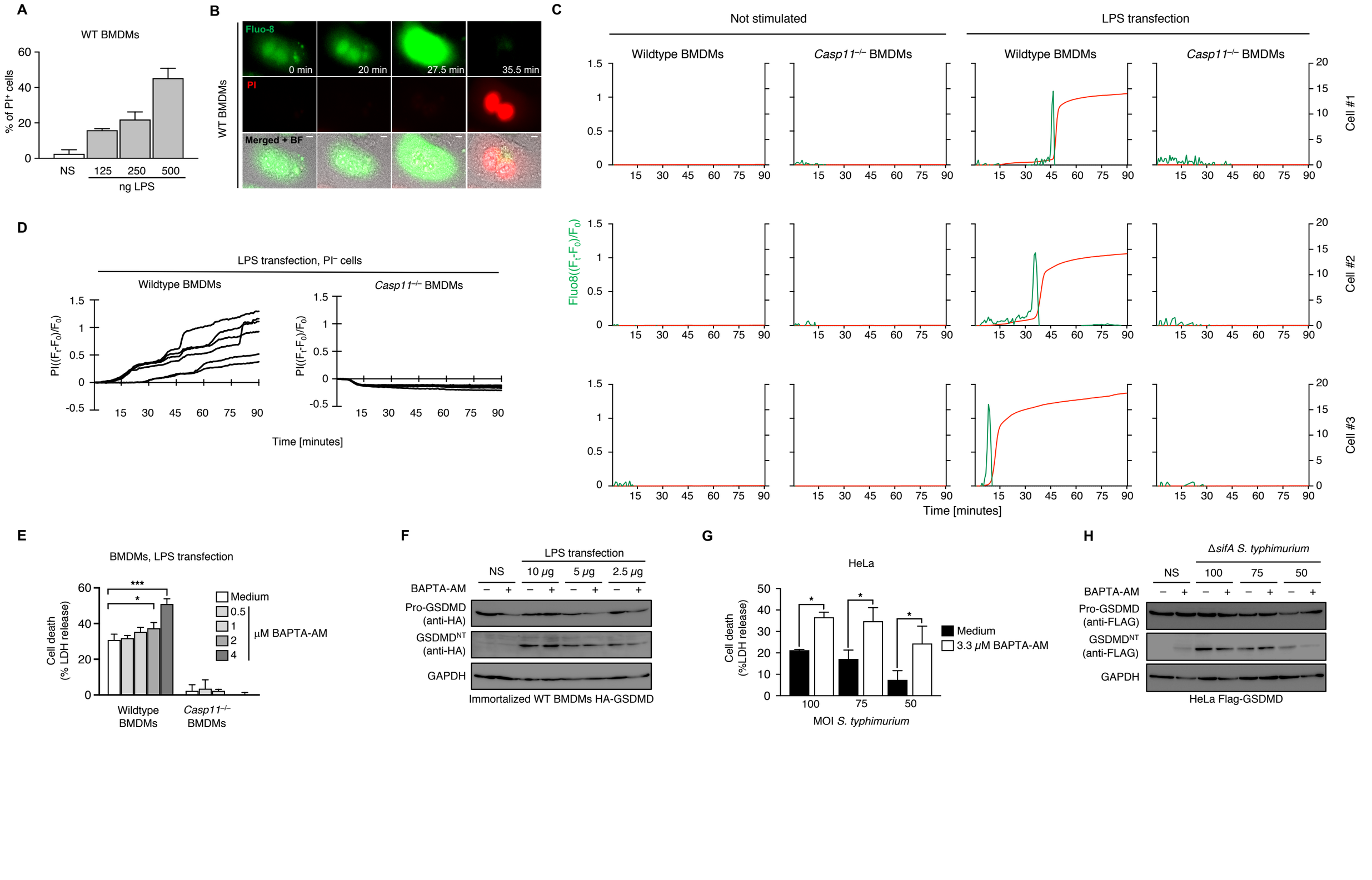

Figure 2. The ESCRT machinery translocates to the plasma membrane during pyroptosis

A. Microscopy images of CHMP4-GFP HeLa cells treated with medium only, perforin (200 µg/ml, 45 minutes) or infected with Δ*sifA S. typhimurium* (MOI 100, 5 hours), or CHMP4-GFP HeLa cells stably transduced with Dox-inducible $GSDMD^{NT}$-mCherry treated with Dox (1 µg/ml, 4 hours). Cells were fixed and analyzed by microscopy. **B.** Microscopy images of CHMP4-GFP HeLa cells stably transduced with Dox-inducible $GSDMD^{NT}$-mCherry 4.5 hours after Dox treatment. Cells were stained with FM4-64FX, fixed and analyzed by confocal microscopy. Inset shows co-localization CHMP4-GFP and FM4-64FX at the plasma membrane. **C-D.** Still images from time lapse movies of pyroptosis in CHMP4-GFP HeLa cells stably transduced with Dox-inducible $GSDMD^{NT}$-mCherry after Dox treatment. White arrows show peripheral ESCRT aggregates. Imaging was performed in the presence of PI to assess membrane integrity. Time is shown in mm:ss. Scale bars are 5 µm. **E-F.** Microscopy images and quantification of cells showing CHMP4 speckles. CHMP4-GFP HeLa cells stably transduced with Dox-inducible $GSDMD^{NT}$-mCherry were treated with 1 µg/ml Doxycycline for 4.5 hours in the presence of medium, 6 µM BAPTA-AM or 2 mM EDTA, fixed and analyzed by confocal microscopy. At least 100 cells per condition were analyzed for CHMP4 speckle formation. **G.** Electron microscopy of LPS-primed immortalized wildtype BMDMs, transfected with LPS for 1.5 hours. Insets show membrane buds emerging from the plasma membrane. Scale bar in left image is 1 µm, scale bars in insets corresponds to 100 nm. Result shown in **A-G** are representative of at least three independent experiments

Rühl et al. Figure 2

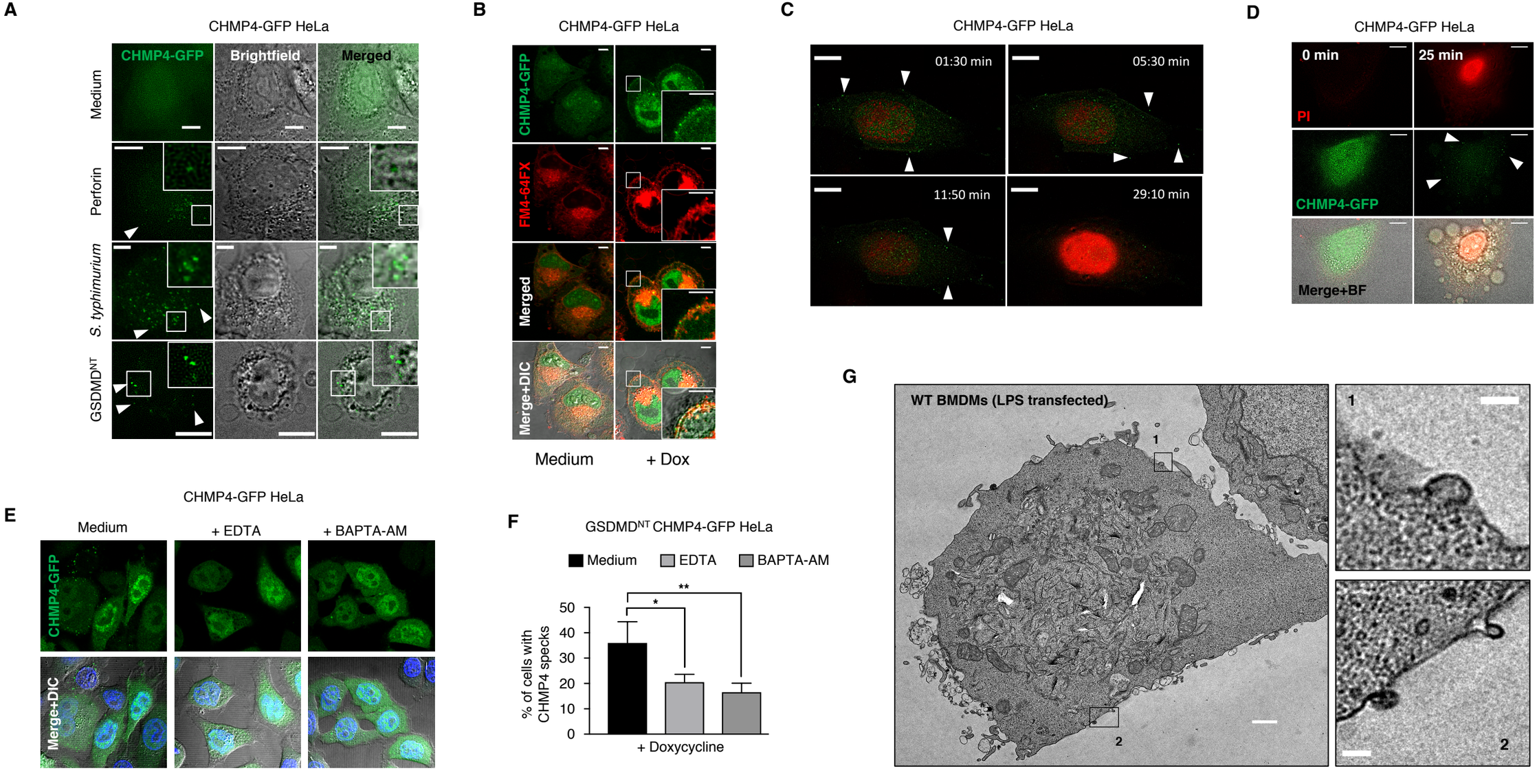

Figure 3 The ESCRT system negatively regulates gasdermin-D mediated pyroptosis

A. Subcellular distribution of wild-type and dominant-negative CHMP3 and VPS4a. HeLa cells stably transduced with HA-tagged Dox-inducible CHMP3 or VPS4 constructs were treated with 1 μg ml^{-1} Dox for 6 hours (VPS4a^{WT} and VPS4a^{E228Q}) or 12 hours (CHMP3^{WT} and CHMP3$^{1-179}$), fixed and stained for the HA-tag. Scale bar corresponds to 5 μm. **B-C.** LDH release (**B**) and GSDMD processing (**C**) after infection with varying MOI of Δ*sifA S. typhimurium* in HeLa cells stably transduced with HA-tagged Dox-inducible CHMP3 or VPS4 constructs. Protein expression was induced with 0.5 μg ml^{-1} Dox for 12 hours. GSDMD processing was analyzed in combined lysate and supernatant samples by immunoblotting. **D-E.** Immortalized wildtype BMDMs stably transduced with indicated Dox-inducible VPS4a constructs were primed with LPS (250 ng ml^{-1}) and Dox (1 μg ml^{-1}) for 4 and 6 hours and transfected with 5 μg ultrapure LPS /10^6 cells. PI staining was imaged (**D**) and counted (**E**) at 2 hours post transfection. **F and I.** LDH and IL-1β release from LPS-primed immortalized BMDMs stably transduced with indicated Dox-inducible VPS4 constructs after transfection with indicated amounts of LPS. **G and J.** LDH and IL-1β release from LPS-primed immortalized wildtype, *Casp11*$^{-/-}$ or *Gsdmd*$^{-/-}$ BMDMs expressing the respective Dox-inducible VPS4a constructs after transfection with LPS for 2 hours. **H.** Lysates of wildtype, *Casp11*$^{-/-}$ or *Gsdmd*$^{-/-}$ BMDMs from (**G**) were analyzed for expression of VPS4a proteins. **K.** Immunoblots from VPS4a transgenic immortalized macrophages treated as in **D**. Actin serves as loading control **L.** LDH and IL-1β release from LPS-primed immortalized BMDMs stably transduced with indicated Dox-inducible VPS4a constructs after transfection with indicated amounts of LPS in medium or medium supplemented with 2.5 μM MCC950. **M.** Immunoblots of combined lysate and supernatant samples from LPS-primed immortalized BMDMs stably transduced with indicated Dox-inducible VPS4a constructs after transfection with indicated amounts of LPS in medium or medium supplemented with 2.5 μM MCC950. Statistical analysis was done using unpaired student's t-test, *p<0.05, **p<0.01, ***p<0.001. Results shown in **A-M** are representative of at least three independent experiments.

Rühl et al. Figure 3

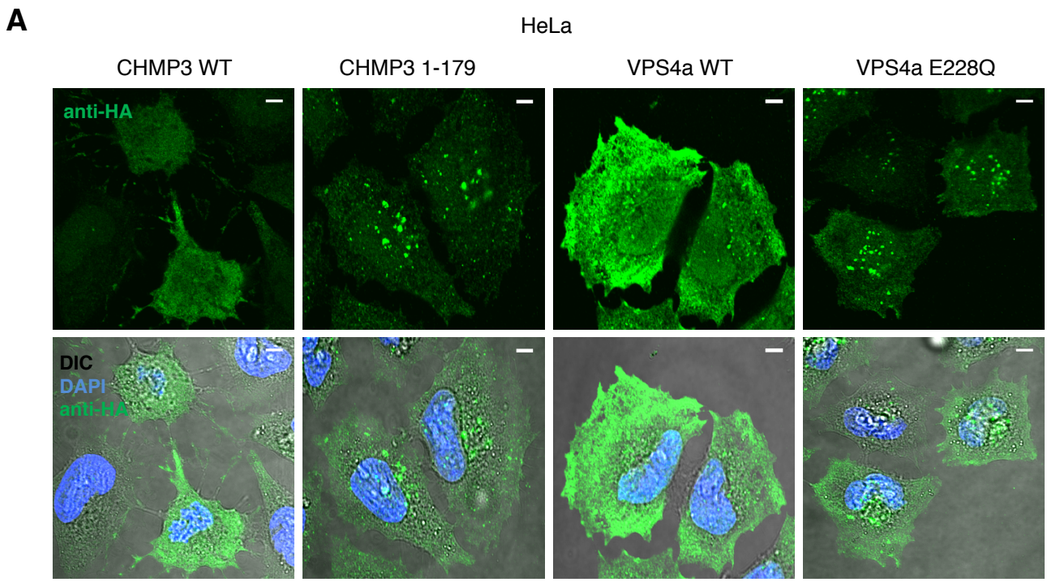

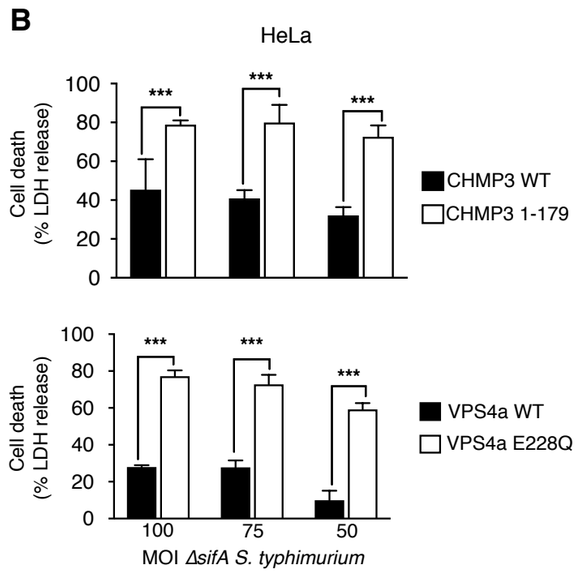

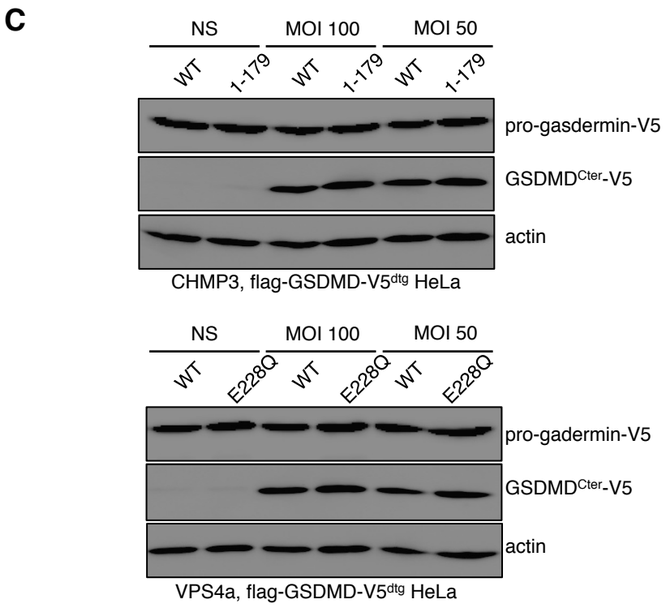

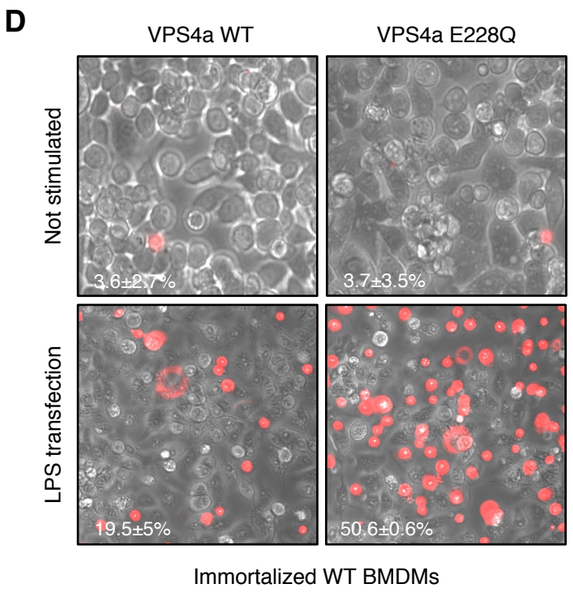

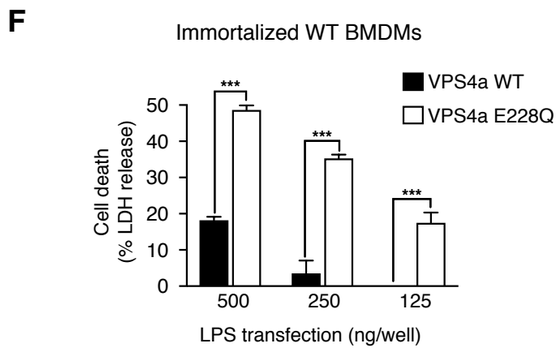

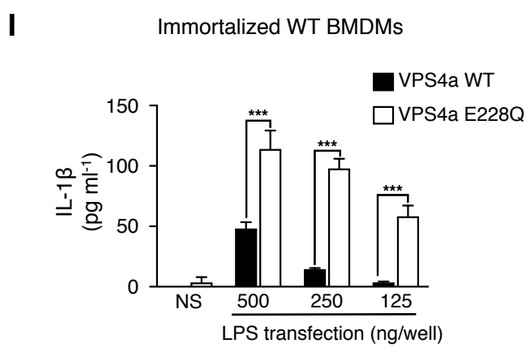

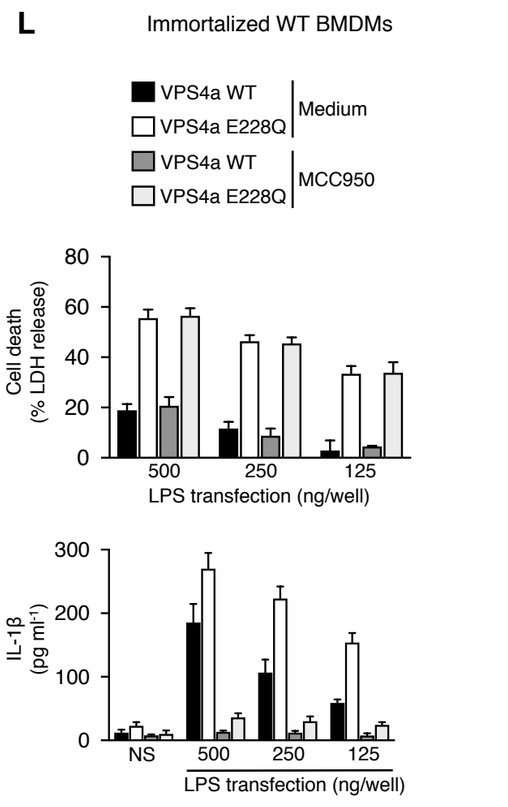

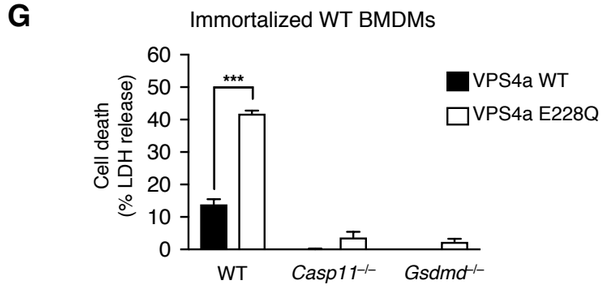

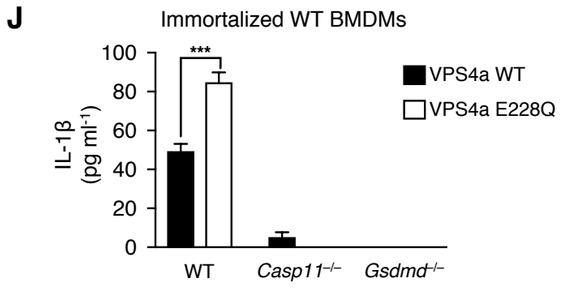

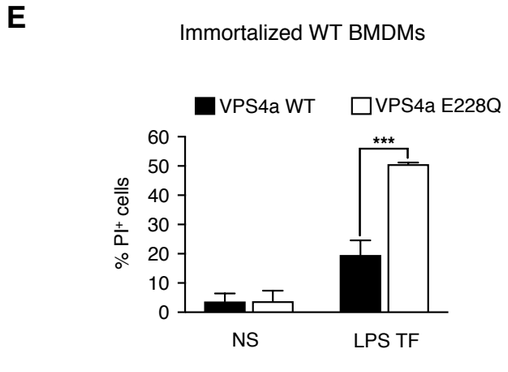

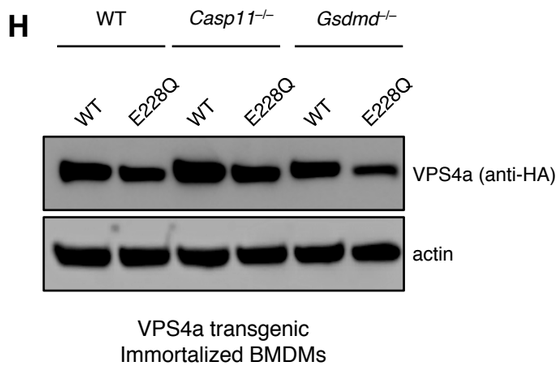

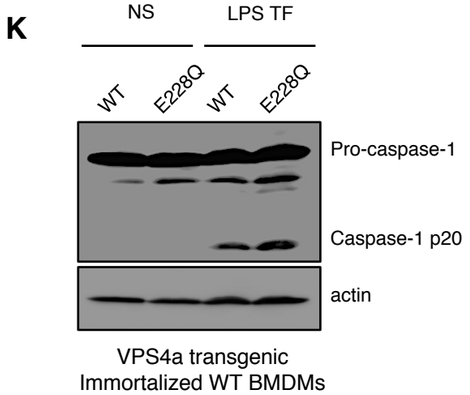

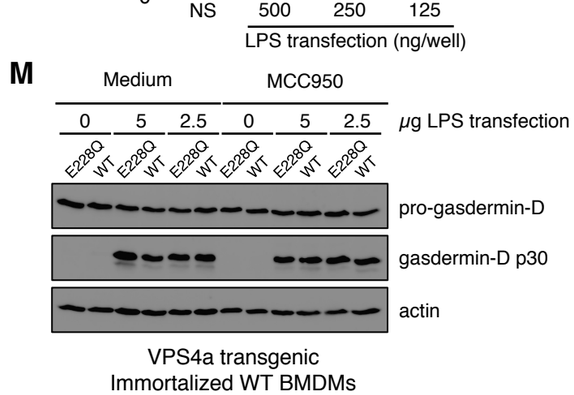

Figure 4. ESCRT negatively regulates pyroptosis and cytokines downstream of canonical inflammasomes.

A. LDH release from untreated or BAPTA-AM treated wildtype and *Asc*$^{-/-}$ BMDMs 2 hours after poly(dA:dT) transfection (500ng/5x10^4 cells). **B.** Immunoblots for pro-caspase-1 and caspase-1 p20 on combined supernatant and lysates samples of untreated or BAPTA-AM treated *Nlrp3*-deficient BMDMs 2 hours after poly(dA:dT) transfection. GAPDH serves as loading control. **C.** LDH and IL-1β release from immortalized wild-type BMDMs stably transduced with indicated Dox-inducible VPS4a constructs after infection with different MOI of *S. typhimurium* for 1 hour. **D.** Immunoblots for caspase-1 and GSDMD on combined supernatant and lysates samples from immortalized wild-type BMDMs stably transduced with indicated Dox-inducible VPS4a constructs after infection with different MOI of *S. typhimurium* for 1 hour. Actin serves as loading control. **E.** Time course of PI influx in DmrB-Casp1 HEK293T cells transfected with FLAG-hGSDMD-V5 and Dox-inducible VPS4a constructs (1:3). Cells were treated with 1 μg ml^{-1} doxycycline to induce ESCRT protein expression. Caspase-1 activation was induced by addition of 25 nM B/B homodimerizer (B/B HD) followed by addition of washout compound (1.25 μM final concentration or medium only) at 30 minutes. **F.** DmrB-Casp1 HEK293T were transfected as in **E**, treated with the indicated concentrations of B/B HD for 30 minutes and followed by washout compound at 50-fold excess. LDH release was analyzed 2 hours post stimulation. Immunoblots show equal expression levels of CHMP3 proteins. **G.** Immunoblots for full-length GSDMD and processed GSDMD^{CT} in combined supernatant and lysates from DmrB-Casp1 HEK293T cells treated for 60 minutes with 50 nM B/B homodimerizer (**F**). Actin serves as loading control. **H-I.** LDH and IL-1β release from DmrB-Casp1 pro-IL-1β HEK293T double transgenic cells transfected with FLAG-hGSDMD-V5 and Dox-inducible ESCRT constructs (1:3). Cells were treated with the indicated concentrations of B/B homodimerizer for 30 minutes and followed by washout compound at 50-fold excess. LDH and IL-1β release were measured at 90 minutes post treatment. Statistical significance was determined using unpaired student's t-test, * $p<0.05$, ** $p<0.01$, *** $p<0.001$. Each result is representative of at least three independent experiments

Rühl et al. Figure 4

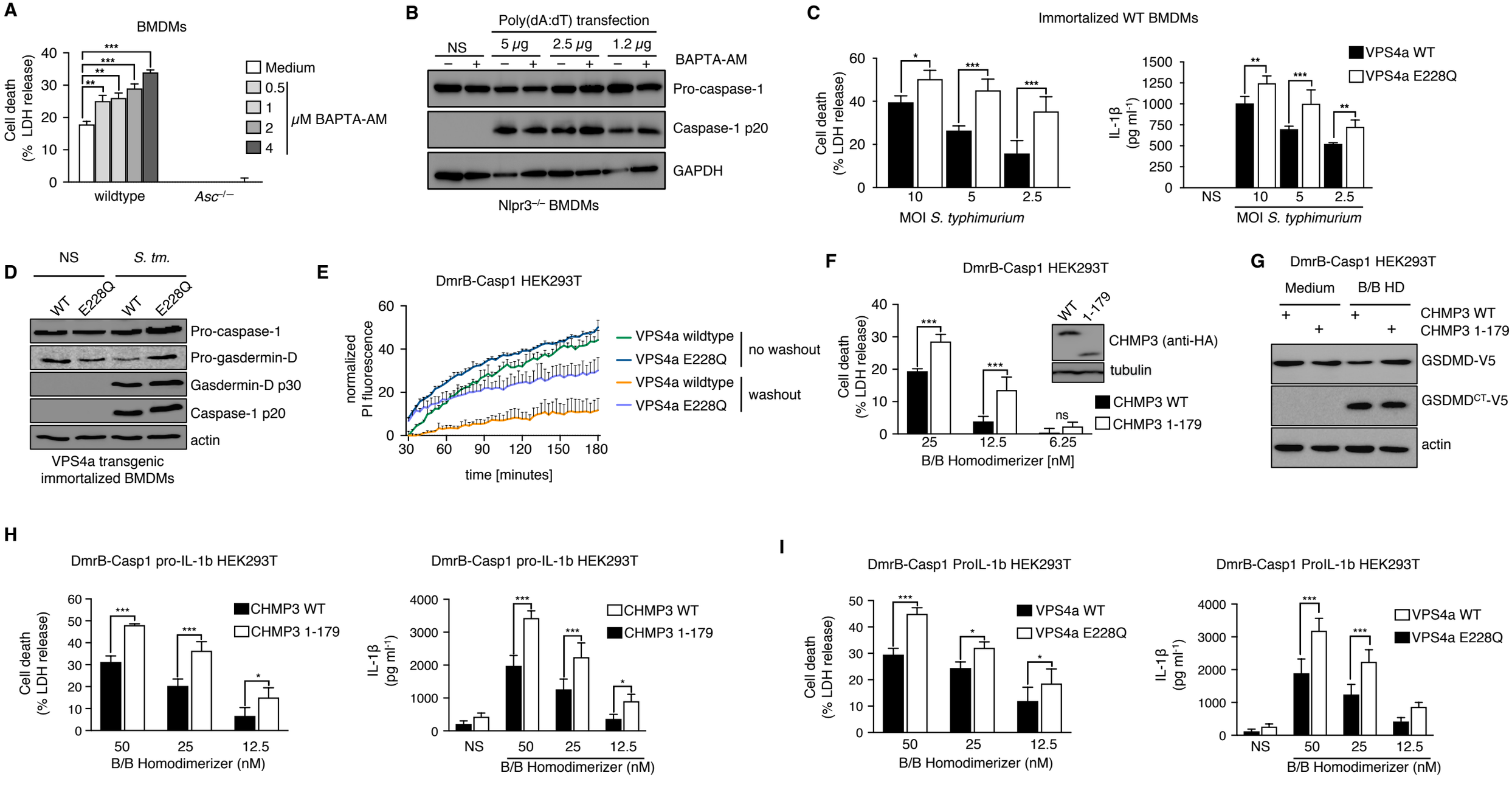

Figure S1 (related to Figure 1)

A. Single cell analysis of Ca^{2+} (Fluo-8) and PI influx in LPS-primed wildtype and *Gsdmd*$^{-/-}$ BMDMs left unstimulated or transfected with LPS. Graphs show data from 3 representative cells out of at least 30 analyzed per condition. **B**. PI influx in wildtype and *Gsdmd*$^{-/-}$ BMDMs not undergoing pyroptosis. Graphs show data from 8 representative cells out of at least 30 analyzed per condition. **C.** Time course analysis of LDH release from untreated or BAPTA-AM treated wildtype BMDMs transfected with the indicated amounts of LPS. Results shown in **A-C** are representative of three independent experiments

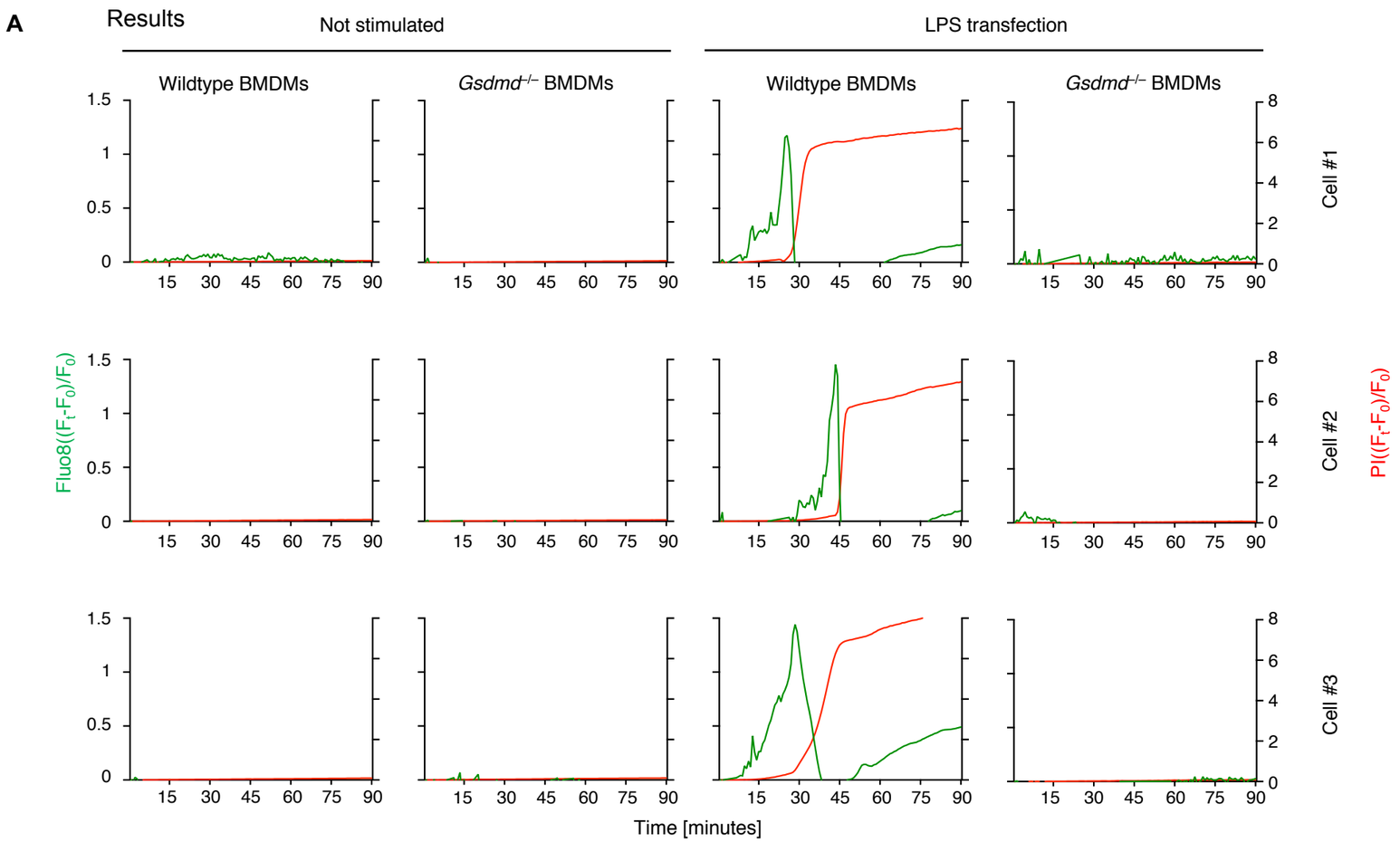

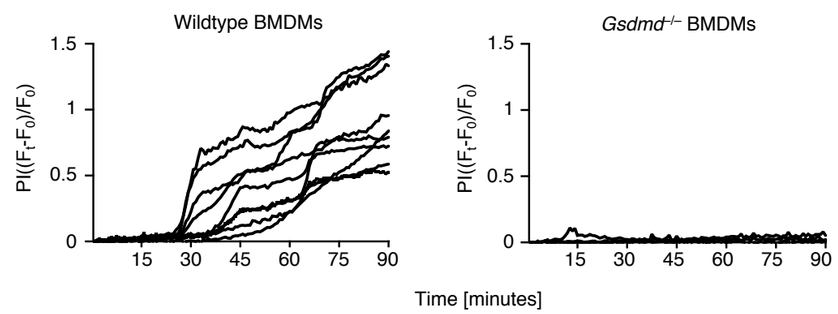

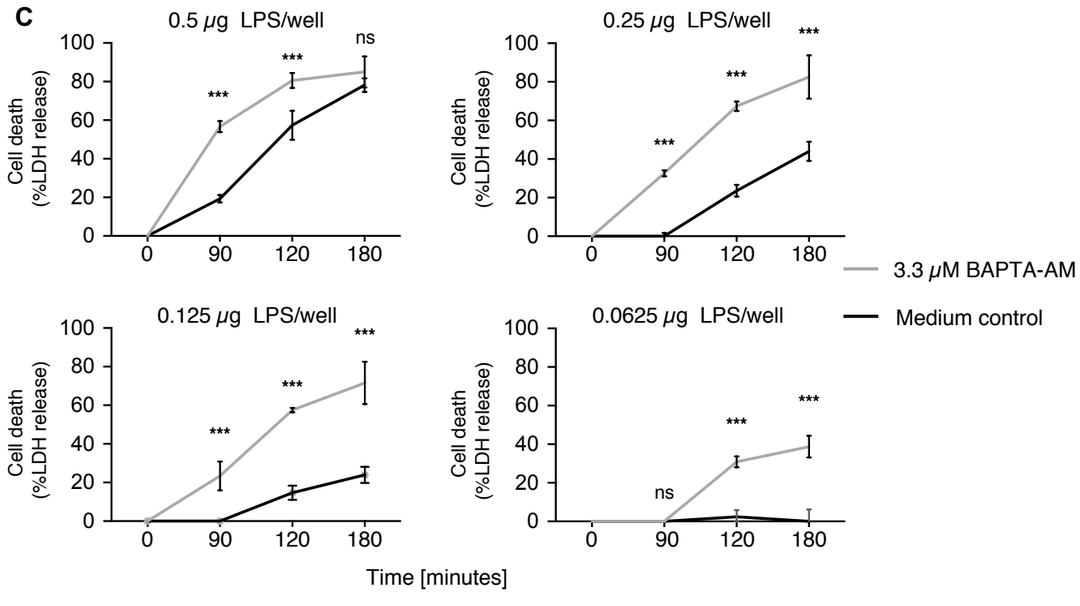

Rühl et al. Figure S1

Figure S2 (related to Figure 2)

A. Electron microscopy of LPS-primed immortalized wildtype BMDMs. Scale bar corresponds to 3 μm. Result shown are representative of at least three independent experiments.

Rühl et al. Figure S2

A

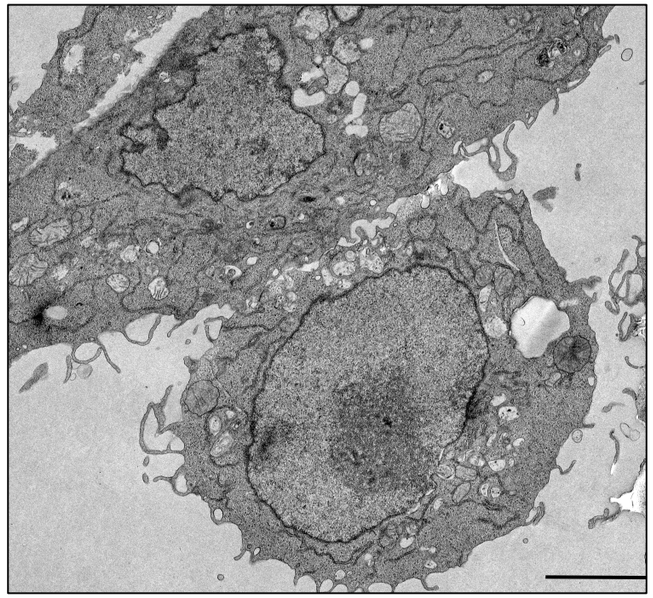

WT BMDMs (untreated)

Figure S3 (related to Figure 3)

A. Schematic outline of pRetroX-Tet-One plasmids used for Dox-induced expression of HA-tagged wild-type and dominant negative human CHMP3 and VPS4a, used in Figures 3, 4, S3 and S4. **B.** Time course of protein expression of HA-tagged $CHMP3^{WT}$, $CHMP3^{1-179}$, $VPS4a^{WT}$ or $VPS4a^{E228Q}$ in HeLa cells with HA-tagged Dox-inducible VPS4 or CHMP3 constructs after Dox treatment. Immunoblots show anti-HA and anti-actin (loading control). **C.** Cell viability measurement of HeLa stably transduced with Dox-inducible constructs for $CHMP3^{WT}$, $CHMP3^{1-179}$, $VPS4a^{WT}$ or $VPS4a^{E228Q}$ after Dox treatment for up to 25 hours. Cells were stained with a live/dead marker and cell death was quantified by flow cytometry analysis. **D.** Subcellular distribution of wild-type and dominant-negative VPS4a. Immortalized WT BMDMs stably transduced with HA-tagged Dox-inducible VPS4 constructs were treated with 1 μg ml^{-1} Dox for 6 hours, fixed and stained for the HA-tag. Scale bar corresponds to 5 μm. **E.** LDH and IL-1β release from LPS-primed immortalized BMDMs stably transduced with indicated Dox-inducible VPS4 constructs after transfection with indicated amounts of LPS in medium or medium supplemented with 55 mM KCl.

Rühl et al. Figure S3

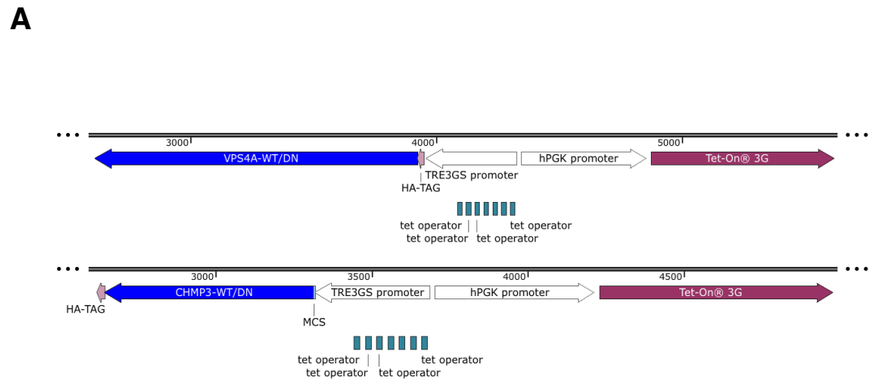

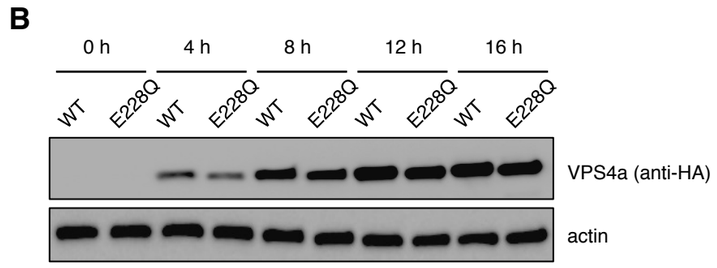

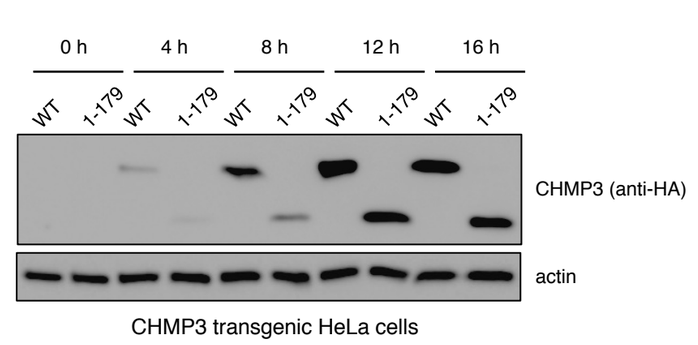

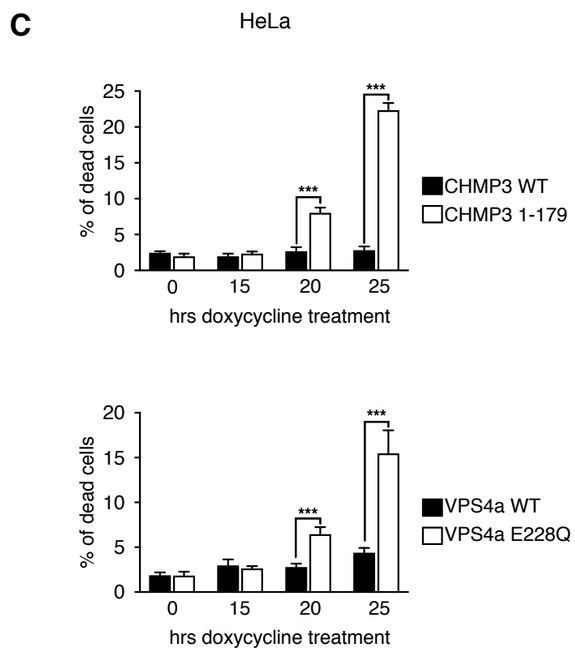

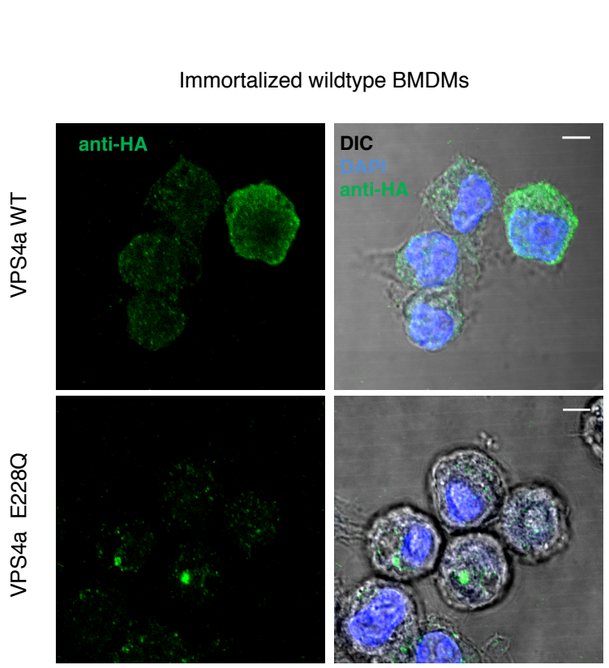

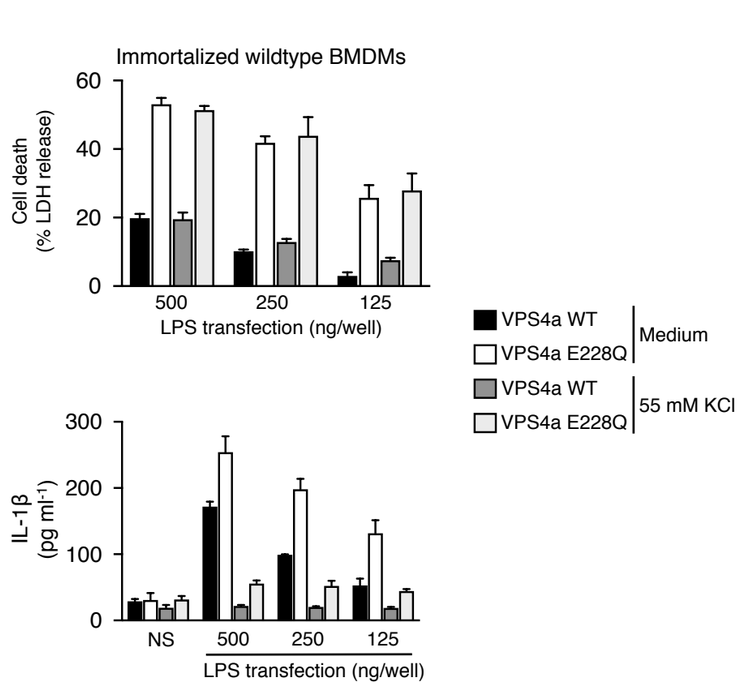

Figure S4 (related to Figure 4)

A LDH release 2 hours post stimulation of *Nlrp3*-deficient BMDMs transfected with the indicated amounts of poly(dA:dT) per $5x10^4$ cells in medium or in the presence of 3.3 μM BAPTA-AM **B.** VPS4a WT or E228Q expressing iBMDMs were primed with doxycycline and LPS for 6 and 4 hours and infected with *S. typhimurium* (MOI 10) for 1 hour. ASC specks were enumerated manually after immunofluorescence **C.** LDH release from immortalized wild-type or *Gsdmd*$^{-/-}$ BMDMs stably transduced with indicated Dox-inducible VPS4 constructs after infection with *S. typhimurium* (MOI 5) for 1 hour. **D.** PI levels in DmrB-Casp1 HEK293T cells transfected with Dox-inducible ESCRT constructs at 16 hours post Dox treatment. **E.** Time course of PI influx in DmrB-Casp1 HEK293T cells transfected with FLAG-hGSDMD-V5 and Dox-inducible ESCRT constructs (1:3). Cells were treated with 1 μg/ml doxycycline to induce ESCRT protein expression. Caspase-1 activation was induced by addition of 25 nM B/B homodimerizer (B/B HD and washout compound was added to a final concentration of 1.25 μM after 30 minutes. PI influx was measured on a multiplate reader. **F.** DrmB-Casp1 HEK293T were transfected as in **4C**, treated with the indicated concentrations of B/B HD for 30 minutes and followed by washout compound at 50-fold excess. LDH release was analyzed 1.5 hours post stimulation. Immunoblots show equal expression levels of VPS4a proteins. **G.** LDH release from DmrB-Casp1 HEK293T cells transfected with Luciferase or FLAG-hGSDMD-V5, and Dox-inducible ESCRT constructs (1:3). Cells were treated as in **Fig 4D**. Statistical significance was determined using unpaired student's t-test, * $p<0.05$, ** $p<0.01$, *** $p<0.001$. Each result is representative of at least three independent experiments

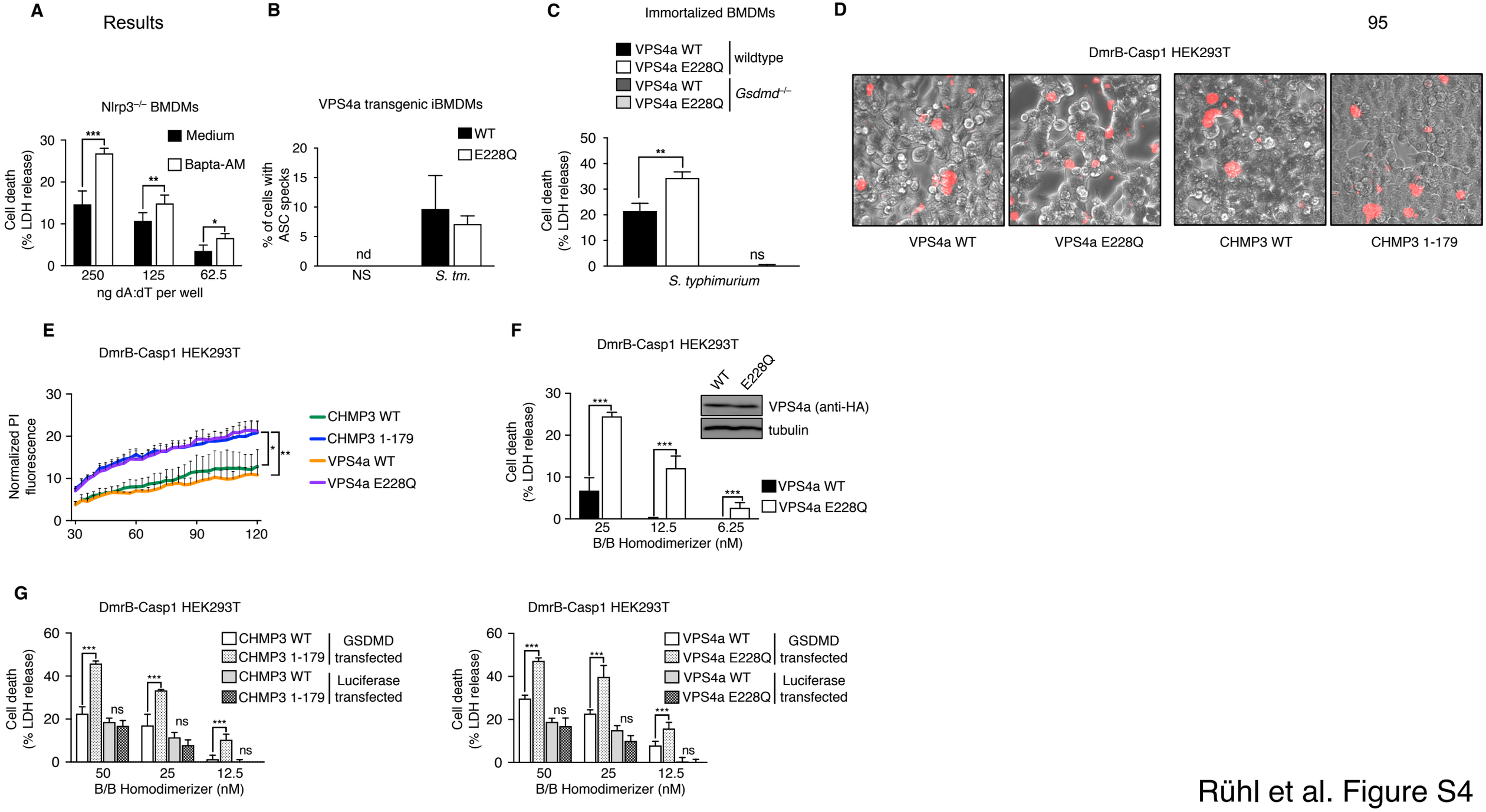

Rühl et al. Figure S4

4.4 Research Article IV: Guanylate-binding proteins promote activation of the AIM2 inflammasome during infection with Francisella novicida

Etienne Meunier [1,6], Pierre Wallet [2,6], Roland F Dreier [1], Stéphanie Costanzo [2], Leonie Anton [1], Sebastian Rühl [1], Sébastien Dussurgey [3], Mathias S Dick [1], Anne Kistner [1], Mélanie Rigard [2], Daniel Degrandi [4], Klaus Pfeffer [4], Masahiro Yamamoto [5], Thomas Henry [2]& Petr Broz [1]

1 Focal Area Infection Biology, Biozentrum, University of Basel, Basel, Switzerland.
2 Centre International de Recherche en Infectiologie, Inserm U1111, CNRS UMR 5308, Université Claude Bernard Lyon-1, Ecole Normale Supérieure, Lyon, France.
3 Structure Fédérative de Recherche Biosciences, UMS344/US8, Inserm, CNRS, Université Claude Bernard Lyon-1, Ecole Normale Supérieure, Lyon, France.
4 Institute of Medical Microbiology and Hospital Hygiene, Heinrich-Heine-University Duesseldorf, Duesseldorf, Germany.
5 Department of Microbiology and Immunology, Osaka University, Osaka, Japan.
6 These authors contributed equally to this work.

Published online 16 March 2015; Nature Immunology

doi:10.1038/ni.3119

Statement of contribution:

I performed optimizations of the F. novicida infection protocol. None of my results were included in the final manuscript.

ARTICLES

nature immunology

Guanylate-binding proteins promote activation of the AIM2 inflammasome during infection with *Francisella novicida*

Etienne Meunier[1,6], Pierre Wallet[2,6], Roland F Dreier[1], Stéphanie Costanzo[2], Leonie Anton[1], Sebastian Rühl[1], Sébastien Dussurgey[3], Mathias S Dick[1], Anne Kistner[1], Mélanie Rigard[2], Daniel Degrandi[4], Klaus Pfeffer[4], Masahiro Yamamoto[5], Thomas Henry[2] & Petr Broz[1]

The AIM2 inflammasome detects double-stranded DNA in the cytosol and induces caspase-1-dependent pyroptosis as well as release of the inflammatory cytokines interleukin 1β (IL-1β) and IL-18. AIM2 is critical for host defense against DNA viruses and bacteria that replicate in the cytosol, such as *Francisella tularensis* subspecies *novicida* (*F. novicida*). The activation of AIM2 by *F. novicida* requires bacteriolysis, yet whether this process is accidental or is a host-driven immunological mechanism has remained unclear. By screening nearly 500 interferon-stimulated genes (ISGs) through the use of small interfering RNA (siRNA), we identified guanylate-binding proteins GBP2 and GBP5 as key activators of AIM2 during infection with *F. novicida*. We confirmed their prominent role *in vitro* and in a mouse model of tularemia. Mechanistically, these two GBPs targeted cytosolic *F. novicida* and promoted bacteriolysis. Thus, in addition to their role in host defense against vacuolar pathogens, GBPs also facilitate the presentation of ligands by directly attacking cytosolic bacteria.

The innate immune system detects invading pathogens through membrane-bound and cytosolic pattern-recognition receptors, which recognize microbe- and damage-associated molecular patterns and induce conserved signaling pathways. Nucleic acids and their derivatives are detected by RIG-I-like receptors, cGAS, DAI and RNA polymerases, which results in the induction of type I interferons via the signaling molecule STING and the kinase TBK1 (refs. 1–3). Cytosolic microbial and host DNA also induces inflammasome formation through AIM2, a member of the PYHIN family of receptors[4–7]. AIM2 binds double-stranded DNA through its HIN-200 domain[8] and recruits the inflammasome adaptor ASC. ASC rapidly oligomerizes to form a macromolecular inflammasome complex known as an 'ASC speck', which activates caspase-1. Active caspase-1 promotes the maturation and release of the pro-inflammatory cytokines interleukin 1β (IL-1β) and IL-18. In addition, it induces pyroptosis, a lytic form of cell death that restricts pathogen replication. The AIM2 inflammasome mediates the recognition of DNA viruses as well as that of various Gram-negative and Gram-positive cytosolic bacteria, such as *Listeria monocytogenes*, *Legionella pneumophila, Mycobacterium* species and *Francisella tularensis* subspecies *novicida* (*F. novicida*)[8–14]. Notably, several studies have shown that activation of AIM2 by these bacteria requires bacteriolysis and the subsequent release of bacterial chromosomal DNA into the cytosol[10,12,15]. However, whether the bacteriolysis is accidental or is an active, host-directed mechanism has remained unclear.

The activation of AIM2 via the transfection of synthetic DNA or during infection with a DNA virus is independent of signaling via Toll-like receptors or interferons[9,13,16]. In contrast, the activation of AIM2 during infection with *F. novicida* requires the production of type I interferons, which are induced as a result of the recognition of an as-yet-undefined *F. novicida*–derived nucleic acid ligand in the cytosol[9,10,17–20]. Consistent with that, the activation of AIM2 inflammasomes in *F. novicida*–infected cells requires signaling through STING and the transcription factor IRF3 (refs. 9,10,17). It has been speculated that interferon signaling is necessary to increase cellular AIM2 for the detection of *F. novicida* DNA[9], yet interferon-mediated induction of AIM2 is contested, and even small amounts of transfected DNA efficiently trigger activation of AIM2 in an interferon-independent manner[9]. Therefore, it is likely that one or several interferon-inducible factor(s) is (are) required for efficient activation of AIM2 during bacterial infection.

Type I and type II interferons are potent cytokines that exert anti-microbial effects through the induction of a broad transcriptional program involving ~2,000 genes, the so-called 'interferon-stimulated genes' (ISGs), many of which remain uncharacterized.

[1]Focal Area Infection Biology, Biozentrum, University of Basel, Basel, Switzerland. [2]Centre International de Recherche en Infectiologie, Inserm U1111, CNRS UMR 5308, Université Claude Bernard Lyon-1, Ecole Normale Supérieure, Lyon, France. [3]Structure Fédérative de Recherche Biosciences, UMS344/US8, Inserm, CNRS, Université Claude Bernard Lyon-1, Ecole Normale Supérieure, Lyon, France. [4]Institute of Medical Microbiology and Hospital Hygiene, Heinrich-Heine-University Duesseldorf, Duesseldorf, Germany. [5]Department of Microbiology and Immunology, Osaka University, Osaka, Japan. [6]These authors contributed equally to this work. Correspondence should be addressed to T.H. (thomas.henry@inserm.fr) or P.B. (petr.broz@unibas.ch).

Received 11 November 2014; accepted 6 February 2015; published online 16 March 2015; doi:10.1038/ni.3119

Prominent among the products of these ISGs are several families of interferon-inducible GTPases, such as the 47-kilodalton immunity-related GTPases and the 65- to 73-kilodalton guanylate-binding proteins (GBPs)[21,22]. GBPs are conserved among vertebrates, with 11 GBPs in mice and 7 in humans, and exert anti-microbial effects on intracellular bacteria and protozoa[23]. GBP1 and GBP7 restrict *Mycobacterium bovis* bacillus Calmette-Guérin and *L. monocytogenes* by recruiting anti-microbial effectors to the pathogen-containing vacuole (PCV)[24]. Several GBPs are recruited onto the *Toxoplasma* parasitophorous vacuole[25], and most are also required for restricting the replication of *Toxoplasma gondii*[23,26–28]. In addition, GBPs encoded by genes on mouse chromosome 3 promote recognition of the vacuolar, Gram-negative bacterium *Salmonella typhimurium* by the innate immune system by destabilizing its PCV, which leads to egress of the bacteria into the cytosol and subsequent detection of its lipopolysaccharide (LPS) by the caspase-11 inflammasome[29]. In this study we found that GBPs encoded by genes on mouse chromosome 3 were a key factor for the activation of AIM2 during infection with *F. novicida*. In particular, GBP2 and GBP5 controlled the activation of AIM2 by targeting cytosolic *F. novicida* and inducing lysis of these bacteria by an as-yet-uncharacterized mechanism. We demonstrated that GBP-deficient mice were unable to control infection with *F. novicida in vivo*. Together our data reveal a function for GBPs during microbial infection, in that GBPs promoted bacteriolysis in the cytosol and the exposure of bacterial DNA to cytosolic sensors of the innate immune system.

RESULTS

AIM2 activation during *F. novicida* infection requires interferons

F. novicida is a facultative intracellular Gram-negative bacterium that avoids phagosomal degradation in phagocytes by escaping into the cytosol, a process that requires the *Francisella* pathogenicity island (FPI). After escaping from the phagosome, *F. novicida* replicates in the cytosol but also triggers AIM2-dependent activation of caspase-1 (refs. 10,13). Infection of mouse bone marrow–derived macrophages (BMDMs) with wild-type *F. novicida* resulted in cell death (pyroptosis; measured by the release of lactate dehydrogenase (LDH)) and the release of IL-1β dependent on AIM2, ASC and caspase-1, while a mutant lacking the FPI (ΔFPI) did not activate the inflammasome (**Fig. 1a**). STING is linked to the activation of AIM2 during infection with *F. novicida*[10,12]. Macrophages deficient in STING (via the 'goldenticket' (Gt) *N*-ethyl-*N*-nitrosourea–induced nonfunctional mutation of alleles encoding *Tmem173* (called '*Sting*$^{Gt/Gt}$' here)) had considerable attenuation of their ability to induce expression of type I interferons and activation of the AIM2 inflammasome upon infection with *F. novicida*[5] (**Fig. 1b** and **Supplementary Fig. 1a**). Consistent with a role for type I interferons in activation of the AIM2 inflammasome[17,19], macrophages from mice deficient in *Ifnar1*, which encodes the receptor for interferon-α (IFN-α) and IFN-β (IFNAR1), or *Stat1*, which encodes the transcription factor STAT1, displayed significantly less pyroptosis and release of IL-1β when infected with *F. novicida* than did their wild-type counterparts (**Fig. 1c**). To further confirm that activation of AIM2 during infection with *F. novicida* depended on signaling via type I interferons, we assessed whether exogenous interferons were able to restore inflammasome activation in STING-deficient BMDMs. As expected, IFN-β restored cell death and the release of cytokines in *Sting*$^{Gt/Gt}$ BMDMs (**Fig. 1d**). The addition of IFN-γ restored cell death and the release of cytokines in both *Sting*$^{Gt/Gt}$ BMDMs and *Ifnar1*$^{-/-}$ BMDMs (**Fig. 1d**), which indicated a requirement for a general interferon signature.

The induction of *Aim2* mRNA could explain the considerable dependence on type I interferons and signaling via STAT1 during infection with *F. novicida*[10]. However, activation of the AIM2 inflammasome by transfection of DNA or infection with DNA viruses is independent of interferon signaling[9,13,16]. In accordance with those reports, induction of cell death by transfection of the synthetic

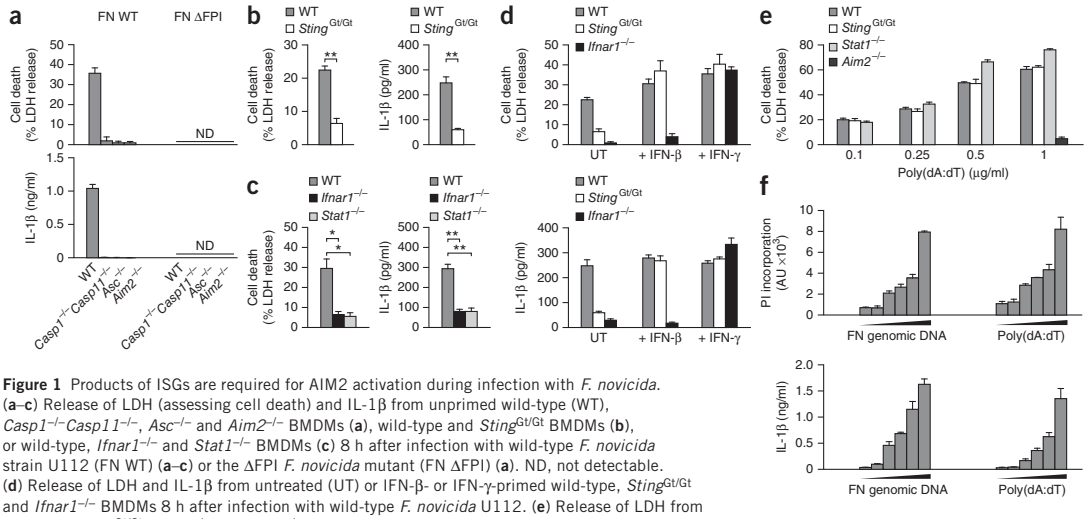

Figure 1 Products of ISGs are required for AIM2 activation during infection with *F. novicida*. (**a**–**c**) Release of LDH (assessing cell death) and IL-1β from unprimed wild-type (WT), *Casp1*$^{-/-}$*Casp11*$^{-/-}$, *Asc*$^{-/-}$ and *Aim2*$^{-/-}$ BMDMs (**a**), wild-type and *Sting*$^{Gt/Gt}$ BMDMs (**b**), or wild-type, *Ifnar1*$^{-/-}$ and *Stat1*$^{-/-}$ BMDMs (**c**) 8 h after infection with wild-type *F. novicida* strain U112 (FN WT) (**a**–**c**) or the ΔFPI *F. novicida* mutant (FN ΔFPI) (**a**). ND, not detectable. (**d**) Release of LDH and IL-1β from untreated (UT) or IFN-β- or IFN-γ-primed wild-type, *Sting*$^{Gt/Gt}$ and *Ifnar1*$^{-/-}$ BMDMs 8 h after infection with wild-type *F. novicida* U112. (**e**) Release of LDH from wild-type, *Sting*$^{Gt/Gt}$, *Stat1*$^{-/-}$ and *Aim2*$^{-/-}$ BMDMs transfected with increasing concentrations of poly(dA:dT) (horizontal axis). (**f**) Incorporation of propidium iodide (PI) (assessing cell death) and release of IL-1β by wild-type BMDMs primed with Pam_3CSK_4 and then transfected with increasing concentrations (wedges) of purified *F. novicida* (FN) genomic DNA or poly(dA:dT) (0, 20, 100, 250, 500 and 1000 ng/ml), assessed 1 h after transfection. $^*P < 0.01$ and $^{**}P < 0.001$ (two-tailed unpaired *t*-test). Data are representative of three (**a**,**c**,**e**) or two (**b**,**d**,**f**) independent experiments (mean and s.d. of quadruplicate wells).

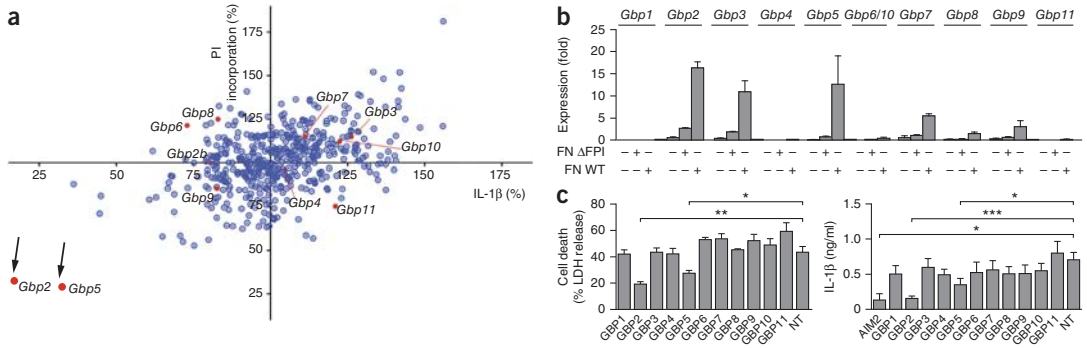

Figure 2 Screening by RNA-mediated interference identifies members of the GBP family as activators of AIM2. (**a**) Screening results for wild-type BMDMs treated with siRNA targeting various genes (red, genes encoding members of the GBP family; black arrows, *Gbp2* and *Gbp5*), presented as incorporation of propidium iodide and release of IL-1β, normalized to the average values obtained with all siRNA (set as 100%) and to the values obtained with *Aim2*-specific siRNA (set as 0%). (**b**) Expression of mRNA from various GBP-encoding genes (top) in wild-type BMDMs left uninfected (–) or infected (+) with wild-type *F. novicida* strain U112 or the ΔFPI mutant, assessed 8 h after infection. (**c**) Release of LDH and IL-1β from unprimed wild-type BMDMs pretreated with nontargeting control siRNA (NT) or with siRNA targeting genes encoding various GBPs (horizontal axis) 48 h before infection with wild-type *F. novicida* strain U112, assessed 8 h after infection. $^{*}P < 0.05$, $^{**}P < 0.01$ and $^{***}P < 0.001$ (two-tailed unpaired *t*-test). Data are representative of one experiment (**a**) or two (**b**) or three (**c**, LDH) independent experiments or are pooled from six independent experiments (**c**, IL-1β) (mean and s.d. of quadruplicate wells in **b**,**c**).

B-form double-stranded DNA poly(dA:dT) at a concentration of 1 μg/ml required AIM2 but was completely independent of STING and STAT1 (**Fig. 1e**). The transfection of large amounts of DNA might overload the system and render it independent of interferon signaling. To rule out this possibility, we 'titrated down' the amount of transfected DNA. The activation of AIM2 remained interferon independent even upon the transfection of small quantities of DNA (**Fig. 1e**). These results indicated that basal AIM2 was sufficient to initiate inflammasome activation[9,13]. Indeed, we observed only weak induction of *Aim2* mRNA following infection with *F. novicida* (**Supplementary Fig. 1b**).

Finally, we confirmed that *F. novicida* genomic DNA was as stimulatory as synthetic DNA by transfecting increasing amounts of each into macrophages that had been primed with the synthetic lipopeptide Pam_3CSK_4 to induce expression of pro-IL-1β. Both types of DNA triggered similar cell death and release of IL-1β (**Fig. 1f**), which excluded the possibility that *F. novicida* DNA had properties that allowed it to evade recognition by AIM2. Together these results indicated that one (or several) IFN-β- or IFN-γ-inducible gene(s) was (were) needed to activate AIM2 specifically during bacterial infection.

Identification of the GBP family by genetic screening

To identify ISGs encoding products involved in *F. novicida*–mediated activation of the AIM2 inflammasome, we screened BMDMs by RNA-mediated interference with small interfering RNA (siRNA). We selected 443 genes with at least twofold higher expression in *F. novicida*–infected wild-type macrophages than in *F. novicida*–infected *Ifnar1*$^{-/-}$ macrophages[17] and selected 40 additional genes on the basis of published reports[9,10,17,18] (data not shown and **Supplementary Table 1**). At 48 h after transfection of siRNA specific for those genes, we infected macrophages with *F. novicida* and monitored inflammasome activation by measuring the release of IL-1β and incorporation of propidium iodide (as a measure of cell death). Knockdown of most of the 483 genes did not substantially affect the release of IL-1β or cell death (**Fig. 2a**). In contrast, knockdown of *Gbp2* or *Gbp5* resulted in much less *F. novicida*–mediated release of IL-1β and macrophage death than that of cells treated with nontargeting siRNA, while knockdown of other GBP-encoding genes showed no comparable effect (**Fig. 2a**). *Gbp2* and *Gbp5* had the highest expression among the GBP-encoding genes in macrophages and were substantially and specifically induced upon infection with wild-type *F. novicida* in a STING- and IFNAR-dependent manner but independently of Toll-like receptor 2 and MyD88 (**Fig. 2b** and **Supplementary Fig. 1c–e**). We confirmed by RT-PCR the efficiency of siRNA-mediated knockdown of GBP-encoding genes expressed during infection with *F. novicida* (**Supplementary Fig. 2a**). We next confirmed the screening results by knocking down all 11 mouse GBP-encoding genes individually and measuring cell death and IL-1β release (**Fig. 2c**). Knockdown of *Gbp2* and *Gbp5* specifically decreased the *F. novicida*–mediated release of IL-1β and cell death, as assessed by two different techniques (**Fig. 2c** and **Supplementary Fig. 2b**). In conclusion, our screening approach identified GBP2 and GBP5 as two possible ISG products that controlled the activation of AIM2 during infection with *F. novicida*.

AIM2 activation requires GBP-encoding genes on chromosome 3

To confirm our screening data, we obtained macrophages from wild-type mice, mice deficient in both caspase-1 and caspase-11 (*Casp1*$^{-/-}$*Casp4*$^{-/-}$; called '*Casp1*$^{-/-}$*Casp11*$^{-/-}$' here) or mice that lack the locus on chromosome 3 encoding GBP1, GBP2, GBP3, GBP5 and GBP7 (called '*Gbp*^{chr3}' here)[23] and infected naive or primed macrophages with *F. novicida*. Consistent with defective activation of the AIM2 inflammasome, *Gbp*^{chr3}-deficient BMDMs displayed a significant reduction in cell death and cytokine release and had a diminished abundance of processed caspase-1 p20 compared with that of their wild-type counterparts, even though their expression of pro-caspase-1, ASC and AIM2 protein was similar to that of wild-type cells (**Fig. 3a**,**b** and **Supplementary Fig. 3a**). Measuring the incorporation of propidium iodide in real time following infection showed that *Gbp*^{chr3}-deficient BMDMs died with delayed kinetics compared with that of wild-type cells and similar to that of *Ifnar1*$^{-/-}$ BMDMs (**Supplementary Fig. 3b**). To determine if GBPs encoded by genes on

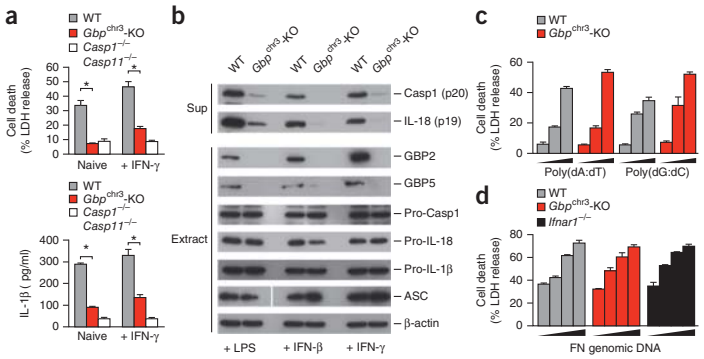

Figure 3 Macrophages from *Gbp*^{chr3}-deficient mice have deficient activation of AIM2 in response to *F. novicida*. (**a**) Release of LDH and IL-1β from naive or IFN-γ-primed wild-type, *Gbp*^{chr3}-deficient (*Gbp*^{chr3}-KO) and *Casp1*$^{-/-}$*Casp11*$^{-/-}$ BMDMs 8 h after infection with wild-type *F. novicida* strain U112. (**b**) Immunoblot analysis of cleaved caspase-1 (p20) and IL-18 (p19) in culture supernatants (Sup), and of GBP2, GBP5, pro-caspase-1 (Pro-Casp1), pro-IL-18, pro-IL-1β, ASC and β-actin (loading control) in extracts (Extract), of wild-type and *Gbp*^{chr3}-deficient BMDMs primed with LPS, IFN-β or IFN-γ (below blots) and then infected with wild-type *F. novicida* strain U112, assessed 8 h after infection. (**c**) Release of LDH from wild-type and *Gbp*^{chr3}-deficient BMDMs 8 h after transfection of increasing concentrations (wedges) of poly(dA:dT) or poly(dG:dC) (0.25, 0.5 or 1 μg/ml). (**d**) Release of LDH from wild-type, *Gbp*^{chr3}-KO and *Ifnar1*$^{-/-}$ BMDMs 8 h after transfection of increasing concentrations (wedges) of *F. novicida* genomic DNA (0.1, 0.25, 0.5 or 1 μg/ml). $^{*}P < 0.001$ (two-tailed unpaired *t*-test). Data are representative of six (**a**) three (**b**,**c**) or two (**d**) independent experiments (mean and s.d. of quadruplicate wells in **a**,**c**,**d**).

chromosome 3 were directly involved in the activation of AIM2, we engaged AIM2 by transfecting synthetic DNA into unprimed wild-type and *Gbp*^{chr3}-deficient macrophages. Cytosolic DNA triggered LDH release to a similar extent in both groups of cells, even when the amount of transfected DNA was 'titrated down' (**Fig. 3c**). Wild-type, *Gbp*^{chr3}-deficient and *Ifnar1*$^{-/-}$ cells also responded similarly to the transfection of purified *F. novicida* genomic DNA (**Fig. 3d**). Thus, GBPs were not required in the context of DNA transfection, which suggested that they functioned upstream of AIM2-mediated DNA detection.

GBP2 and GBP5 direct parallel pathways of AIM2 activation

Since our screening data suggested that mainly GBP2 and GBP5 were required for the activation of AIM2 (**Fig. 2a**), we infected BMDMs from wild-type, *Casp1*$^{-/-}$*Casp11*$^{-/-}$, *Gbp*^{chr3}-deficient, *Gbp2*$^{-/-}$ or *Gbp5*$^{-/-}$ mice with *F. novicida* and measured activation of the AIM2 inflammasome. *Gbp2*$^{-/-}$ BMDMs displayed less death and cytokine release than did wild-type BMDMs (**Fig. 4a**,**b**). Similarly, *Gbp5*$^{-/-}$ BMDMs also displayed attenuated inflammasome activation when infected with *F. novicida* relative to that of their wild-type counterparts (**Fig. 4a**,**b**). Deficiency in *Gbp2* or *Gbp5* did not affect cell death in response to DNA transfection, even when we used very small amounts of DNA (**Fig. 4c**). To determine if expression of GBP2 or GBP5 could restore activation of the AIM2 inflammasome in *Ifnar1*$^{-/-}$ cells, we retrovirally transduced macrophages with constructs expressing GBP2 or GBP5 or with an empty vector (control) and infected them with *F. novicida*. Such ectopic expression was not able to complement the deficiency in inflammasome activation (**Supplementary Fig. 4a–c**), which suggested that other products of ISGs might be required for the function of GBP2 and GBP5, in line with data showing that GBPs are active and correctly targeted only in the context of the interferon response[25].

Single deficiency in *Gbp2* or *Gbp5* did not reduce the activation of AIM2 during infection with *F. novicida* as much as *Gbp*^{chr3} deficiency did (**Fig. 4a**,**b**), which suggested that GBP2 and GBP5 promoted activation of AIM2 through independent pathways. To investigate whether GBP2 and GBP5 acted sequentially or in parallel, we knocked down *Gbp2* expression in wild-type, *Gbp2*$^{-/-}$ and *Gbp5*$^{-/-}$ BMDMs (control

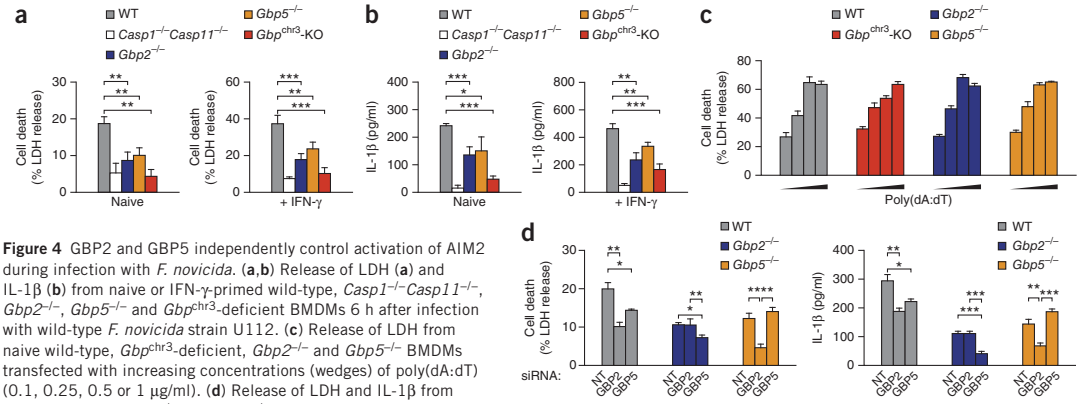

Figure 4 GBP2 and GBP5 independently control activation of AIM2 during infection with *F. novicida*. (**a**,**b**) Release of LDH (**a**) and IL-1β (**b**) from naive or IFN-γ-primed wild-type, *Casp1*$^{-/-}$*Casp11*$^{-/-}$, *Gbp2*$^{-/-}$, *Gbp5*$^{-/-}$ and *Gbp*^{chr3}-deficient BMDMs 6 h after infection with wild-type *F. novicida* strain U112. (**c**) Release of LDH from naive wild-type, *Gbp*^{chr3}-deficient, *Gbp2*$^{-/-}$ and *Gbp5*$^{-/-}$ BMDMs transfected with increasing concentrations (wedges) of poly(dA:dT) (0.1, 0.25, 0.5 or 1 μg/ml). (**d**) Release of LDH and IL-1β from naive wild-type, *Gbp2*$^{-/-}$ and *Gbp5*$^{-/-}$ BMDMs treated with nontargeting control siRNA or siRNA specific for the gene encoding GBP2 or GBP5 (horizontal axis), then, 22 h later, infected with wild-type *F. novicida* U112, assessed 8 h after infection. $^{*}P < 0.05$, $^{**}P < 0.01$ and $^{***}P < 0.001$ (two-tailed unpaired *t*-test). Data are representative of four (**a**,**b**), three (**c**) or two (**d**) independent experiments (mean and s.d. of quadruplicate wells).

of siRNA knockdown efficacy, **Supplementary Fig. 4d**) and measured inflammasome activation after infection with *F. novicida*. Knockdown of *Gbp2* reduced cell death and release of IL-1β in wild-type BMDMs but not in *Gbp2*-deficient BMDMs (**Fig. 4d**). Treatment with *Gbp2*-specific siRNA also significantly reduced inflammasome activation in *Gbp5*$^{-/-}$ BMDMs (**Fig. 4d**), which demonstrated that in *Gbp5*-deficient cells, GBP2 was still active and was able to promote activation of AIM2. Consistent with that, knockdown of *Gbp5* reduced activation of the inflammasome in both wild-type BMDMs and *Gbp2*$^{-/-}$ BMDMs (**Fig. 4d**). In conclusion, our data suggested that the interferon-inducible GTPases GBP2 and GBP5 controlled non-redundant, parallel pathways that promoted activation of AIM2 during infection with *F. novicida*.

Escape of *F. novicida* from phagosomes is GBP independent

Since cytosolic localization of *F. novicida* is required for the activation of AIM2 and since GBPs promote the destabilization of phagosomes and/or pathogen-containing vacuoles of protozoan parasites or bacteria[23,27,29], we speculated that GBPs might facilitate the escape of *F. novicida* from phagosomes. We used a phagosome-protection assay[29,30] based on selective permeabilization of the plasma membrane with digitonin to assay the escape of *F. novicida* from phagosomes. As reported before[30], we observed that 90–95% of wild-type *F. novicida* escaped from phagosomes within a few hours of infection, but this frequency was similar for wild-type BMDMs and *Gbp*^{chr3}-deficient BMDMs at various time points after infection (**Fig. 5a**). In contrast, ΔFPI *F. novicida* remained in the phagosome (data not shown).

F. novicida is naturally resistant to β-lactam antibiotics and secrete the β-lactamase FTN_1072. Taking advantage of this, we developed an alternative assay to detect cytosolic bacteria based on cleavage of the FRET (Förster resonance energy transfer) reporter probe CCF4 by FTN_1072, which leads to a loss of FRET activity[31,32] (**Supplementary Fig. 5**). We preloaded wild-type, *Gbp2*$^{-/-}$ and *Gbp*^{chr3}-deficient BMDMs with CCF4-AM, the membrane-permeable form of the reporter, and subsequently infected the cells with wild-type *F. novicida*, an FTN_1072-deficient strain (the β-lactamase mutant Δbla) or the ΔFPI mutant. We observed no difference among wild-type, *Gbp2*$^{-/-}$ or *Gbp*^{chr3}-deficient BMDMs in terms of FRET activity after infection with wild-type *F. novicida* (**Fig. 5b** and **Supplementary Fig. 5**). The ΔFPI and Δbla mutant strains did not produce any significant FRET signals, similar to the signaling of uninfected macrophages (**Supplementary Fig. 5**). Thus, we concluded that GBPs did not control the activation of AIM2 by promoting the escape of *F. novicida* from phagosomes but that they were active after *F. novicida* reached the cytosol. This was consistent with our data showing that in unprimed cells, *F. novicida*–induced expression of GBP-encoding mRNA was dependent on the FPI and on the escape from phagosomes (**Fig. 2b**) and that cytosolic recognition was required for interferon induction (**Supplementary Fig. 1a**).

GBPs promote cytosolic lysis of *F. novicida*

To identify the mechanism by which GBPs controlled the activation of AIM2 during infection with *F. novicida*, we investigated the subcellular localization of GBPs in infected cells. GBPs are known to co-localize with vacuolar pathogens such as *S. typhimurium*, *M. bovis* bacillus Calmette-Guérin and *T. gondii*, consistent with the ability of GBPs to recruit anti-microbial effector mechanisms to the pathogen and to destabilize PCVs[24,27,29]. We observed that both GBP2 and GBP5 were targeted to intracellular *F. novicida* (**Fig. 6a**). Closer examination of GBP-positive *F. novicida* revealed that GBPs localized to different spots close to or onto the surface of the bacterium (data not shown). However, it was unclear if GBPs targeted the bacterium directly or

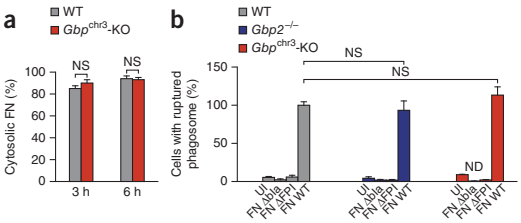

Figure 5 The escape of *F. novicida* from phagosomes is GBP independent. (**a**) Frequency of cytosolic *F. novicida* (FN) among total bacteria at 3 h and 6 h after infection of wild-type and *Gbp*^{chr3}-deficient BMDMs with wild-type *F. novicida* strain U112, assessed by phagosome-protection assay. (**b**) Quantification of cells with ruptured phagosomes at 16 h after infection of wild-type, *Gbp2*$^{-/-}$ and *Gbp*^{chr3}-deficient BMDMs with wild-type *F. novicida* U112, the β-lactamase-deficient mutant Δbla or the ΔFPI mutant or in uninfected cells (UI), assessed with the β-lactamase-cleavable FRET probe CCF4 and presented relative to that of wild-type cells infected with wild-type *F. novicida*. NS, not significant (two-tailed unpaired *t*-test). Data are pooled from four independent experiments with 300 bacteria counted in each (**a**; mean and s.d.) or three independent experiments with 1.5×10^5 cells counted three times in each (**b**; mean and s.d.).

targeted remnants of the host membrane (i.e., lysed phagosomes) or another closely associated membrane compartment.

Since the irregular shape of GBP-positive bacteria suggested that they were lysed, we next determined if wild-type and *Gbp*^{chr3}-deficient cells differed in the abundance of lysed intracellular *F. novicida*. Viable and lysed intracellular bacteria can be quantified on the basis of propidium iodide staining, since intact bacteria remain protected from the influx of propidium iodide[33] (**Fig. 6b**). We tested the assay by quantifying lysed bacteria in wild-type BMDMs infected with wild-type *F. novicida* or an *F. novicida* mutant in which the gene encoding the outer membrane protein FopA is deleted (Δ*fopA*) and thus it has lower membrane stability that results in increased intracellular lysis and hyperactivation of the AIM2 inflammasome[15]. We detected significantly larger amounts of propidium iodide–positive Δ*fopA F. novicida* than wild-type *F. novicida* (**Fig. 6c**), which confirmed the validity of our assay. We next compared the frequency of lysed bacteria in wild-type and *Gbp*^{chr3}-deficient macrophages. The *Gbp*^{chr3}-deficient BMDMs had a significantly lower frequency of lysed bacteria (positive for staining with antibodies to *F. novicida* and propidium iodide) (23% on average) than the wild-type BMDMs had (40% on average) (**Fig. 6c**).

The macromolecular inflammasome complex known as the 'ASC speck' assembles on genomic DNA released from lysed cytosolic *F. novicida*[10]. Immunofluorescence analysis revealed mostly irregularly shaped *F. novicida* in the vicinity of ASC specks (**Fig. 6d**). These bacteria released DNA and were often also positive for GBP staining (**Fig. 6d** and **Supplementary Fig. 6**). Consistent with that, the number of ASC speck-containing cells was significantly lower in GBP-deficient (*Gbp2*$^{-/-}$, *Gbp5*$^{-/-}$ or *Gbp*^{chr3}-deficient) BMDMs than in wild-type BMDMs (**Fig. 6e**). In conclusion, these findings indicated that GBPs associated with cytosolic *F. novicida* and, by an as-yet-undefined mechanism, induced lysis of the bacterium, which resulted in DNA release and detection by the cytosolic DNA sensor AIM2, followed by oligomerization of ASC.

GBPs control *F. novicida* replication

Inflammasome-induced cell death (pyroptosis) restricts intracellular bacteria by removing their replicative niche and reexposing

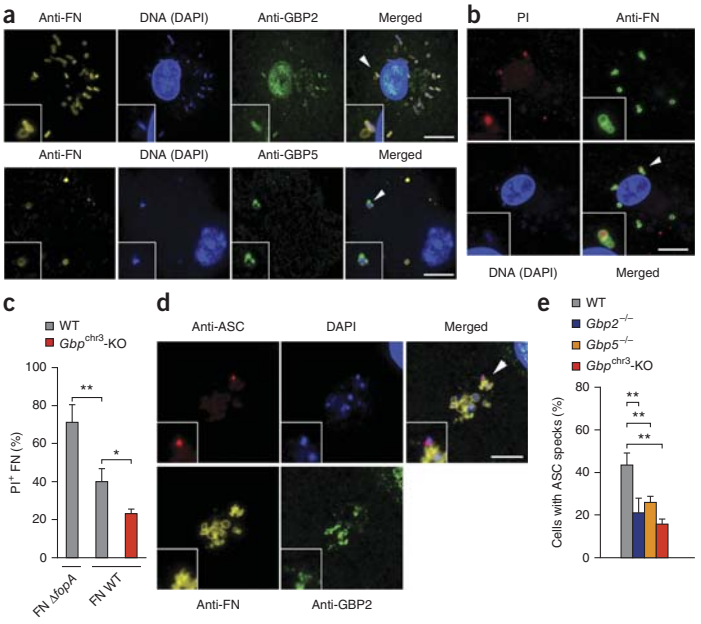

Figure 6 GBPs promote the activation of AIM2 by inducing bacteriolysis. (**a**) Immunostaining with antibody to *F. novicida* (anti-FN), antibody to GBP2 (anti-GBP2) and anti-GBP5, and staining with the DNA-binding dye DAPI, in IFN-γ-primed wild-type BMDMs 8 h after infection with wild-type *F. novicida*. (**b**) Microscopy of lysed (propidium iodide–positive) *F. novicida* in IFN-γ-primed wild-type BMDMs 8 h after infection with wild-type *F. novicida*. (**c**) Quantification of lysed (propidium iodide–positive) *F. novicida* (PI+ FN) in IFN-γ-primed wild-type and Gbp^{chr3}-deficient BMDMs 8 h after infection with wild-type *F. novicida* (FN WT) or the Δ*fopA* mutant (FN Δ*fopA*). (**d**) Immunostaining of ASC, GBP2 and *F. novicida* in IFN-γ-primed wild-type BMDMs 8 h after infection with wild-type *F. novicida*. (**e**) Quantification of ASC speck formation in IFN-γ-primed wild-type, $Gbp2^{-/-}$, $Gbp5^{-/-}$ and Gbp^{chr3}-deficient BMDMs 8 h after infection with wild-type *F. novicida*. Outlined areas (**a**,**b**,**d**) contain 2× enlargement of areas marked by arrowheads. Scale bars (**a**,**b**,**d**), 10 μm. $^*P < 0.05$ and $^{**}P < 0.01$ (two-tailed unpaired *t*-test). Data are representative of three independent experiments (**a**,**b**,**d**) or are pooled from three independent experiments with 300 bacteria (**c**) or cells (**e**) counted in each (mean and s.d.).

them to extracellular immunological mechanisms[34]. Cell-autonomous immunity, on the other hand, relies on cell-intrinsic mechanisms to restrict bacterial growth without the need for killing the host cell[21]. To determine whether GBPs restricted *F. novicida* growth through cell-autonomous mechanisms or inflammasome-dependent mechanisms, we infected wild-type, $Aim2^{-/-}$, Gbp^{chr3}-deficient and $Ifnar1^{-/-}$ BMDMs with wild-type *F. novicida* expressing green fluorescent protein (GFP) and used flow cytometry to quantify infected cells (more than two bacteria per cell, our specific fluorescence-detection threshold) among the live cell population. We observed a significantly higher percentage of live infected $Aim2^{-/-}$, Gbp^{chr3}-deficient and $Ifnar1^{-/-}$ BMDMs than live infected wild-type BMDMs (**Fig. 7a**). This suggested that deficiency in *Ifnar1* or Gbp^{chr3}, similar to deficiency in *Aim2*, resulted in a reduction in inflammasome-mediated killing of host cells upon infection.

Cell-autonomous growth restriction is an interferon-induced mechanism that is at least partially independent of inflammasome-mediated cell death[35,36]. Therefore, we next determined if Gbp^{chr3}-deficient BMDMs and *Ifnar1*-deficient BMDMs also had a defect in restricting intracellular bacterial replication. We infected macrophages with GFP+ *F. novicida* and quantified bacteria (per cell) by both automated microscopy in flow and microscopy at various

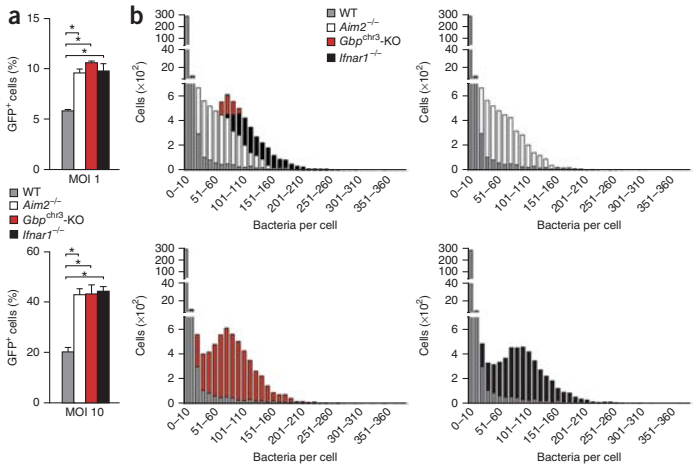

Figure 7 GBPs restrict the intracellular replication of *F. novicida*. (**a**) Flow cytometry–based quantification of infected (GFP+) cells among live wild-type, $Aim2^{-/-}$, Gbp^{chr3}-deficient and $Ifnar1^{-/-}$ BMDMs 12 h after infection with GFP-expressing wild-type *F. novicida* at a multiplicity of infection (MOI) of 1 (top) or 10 (bottom). $^*P < 0.001$ (two-tailed unpaired *t*-test). (**b**) Quantification of bacterial loads in single cells among wild-type, $Aim2^{-/-}$, Gbp^{chr3}-deficient and $Ifnar1^{-/-}$ BMDMs 12 h after infection with GFP-expressing wild-type *F. novicida* at a multiplicity of infection of 10, assessed by high-resolution microscopy in flow and presented as a comparison of all four genotypes (top left) or a comparison of wild-type cells with each other genotype, with bacteria-per-cell values grouped by increments of 10 (horizontal axes). $P < 0.0001$, wild-type versus $Aim2^{-/-}$, wild-type versus Gbp^{chr3}-deficient, and wild-type versus $Ifnar1^{-/-}$ (Kolmogorov-Smirnov test with Bonferroni correction). Data are representative of three independent experiments (**a**; mean and s.d. of triplicate wells) or are pooled from three independent experiments (**b**).

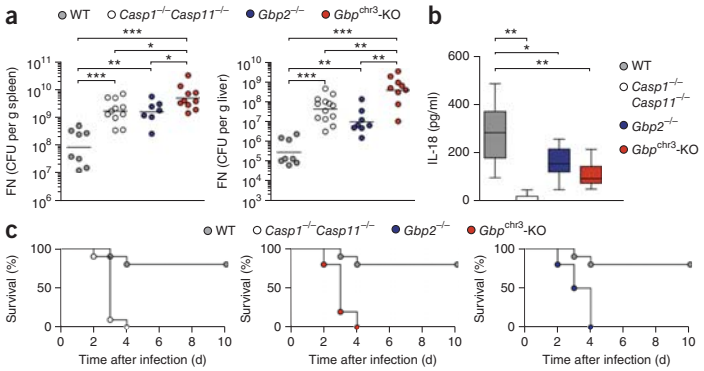

Figure 8 GBPs control host defense against *F. novicida in vivo*. (**a**) Bacterial burden (as colony-forming units (CFU) of *F. novicida* (FN) per gram tissue) in the liver and spleen at day 2 after subcutaneous infection of wild-type, *Casp1*$^{-/-}$*Casp11*$^{-/-}$, *Gbp2*$^{-/-}$ and *Gbp*^{chr3}-deficient mice with 5×10^3 wild-type *F. novicida*. Each symbol represents an individual mouse ($n = 8$ (wild-type), 10 (*Casp1*$^{-/-}$*Casp11*$^{-/-}$), 7 (*Gbp2*$^{-/-}$) and 10 (*Gbp*^{chr3}-deficient) (spleen), or $n = 8$ (wild-type), 13 (*Casp1*$^{-/-}$*Casp11*$^{-/-}$), 8 (*Gbp2*$^{-/-}$) and 9 (*Gbp*^{chr3}-deficient) (liver)); small horizontal lines indicate the mean. $^*P < 0.05$, $^{**}P < 0.01$ and $^{***}P < 0.001$ (Mann-Whitney test). (**b**) IL-18 in serum obtained from wild-type mice ($n = 12$), *Casp1*$^{-/-}$*Casp11*$^{-/-}$ mice ($n = 11$), *Gbp2*$^{-/-}$ mice ($n = 12$) and *Gbp*^{chr3}-deficient mice ($n = 14$) 16 h after subcutaneous infection with 1.5×10^5 wild-type *F. novicida*. $^*P < 0.01$ and $^{**}P < 0.001$ (Mann-Whitney test). (**c**) Survival of wild-type, *Casp1*$^{-/-}$*Casp11*$^{-/-}$, *Gbp2*$^{-/-}$ and *Gbp*^{chr3}-deficient mice ($n = 10$ per genotype) after subcutaneous infection with 5×10^3 wild-type *F. novicida*. $P < 0.0001$, wild-type versus *Casp1*$^{-/-}$*Casp11*$^{-/-}$ or wild-type versus *Gbp*^{chr3}-deficient, and $P = 0.0005$, wild-type versus *Gbp2*$^{-/-}$ (log-rank (Mantel-Cox) test). Data are representative of two independent experiments (**a**,**c**) or are pooled from two individual experiments (**b**; with 10th–90th percentiles).

time points after infection. Wild-type macrophages efficiently controlled intracellular replication, but *Aim2*$^{-/-}$ BMDMs contained large numbers of intracellular *F. novicida* (30 or more per cell) (**Fig. 7b** and **Supplementary Fig. 7a**,**b**), consistent with a loss of inflammasome-mediated killing of host cells. Bacterial loads were even higher in *Gbp*^{chr3}-deficient or *Ifnar1*-deficient BMDMs, with many cells containing up to 100 bacteria (**Fig. 7b** and **Supplementary Fig. 7a**,**b**). The production of reactive oxygen species and nitric oxide is a potent cell-intrinsic anti-microbial mechanism that can also be activated in an interferon-dependent manner. GBP7 has been shown to recruit subunits of the NADPH oxidase to intracellular *L. monocytogenes* and *M. bovis* bacillus Calmette-Guérin[24], and inducible nitric oxide synthase can restrict bacterial growth in a cell-intrinsic manner[21]. However, deficiency in these mechanisms achieved through the use of BMDMs deficient in both inducible nitric oxide synthase and Nox2 did not significantly alter bacteriolysis and inflammasome activation after infection with *F. novicida* ($P = 0.3081$, $P = 0.2786$ and $P = 0.0529$; **Supplementary Fig. 8a**,**b**). Overall, these data indicated that GBPs encoded by the locus on chromosome 3 participated in growth restriction in two ways: directly, by promoting the lysis of intracellular bacteria by an as-yet-unknown mechanism; and indirectly, by promoting the inflammasome-mediated killing of host cells, thereby removing the intracellular replicative niche of *F. novicida*.

GBPs control *F. novicida* replication *in vivo*

AIM2, ASC and caspase-1 control the replication of *F. novicida in vivo* in mice[9,10,37]. Since GBPs are required for inflammasome activation *in vitro*, we investigated whether these proteins also have a physiological role in host defense. We infected age- and sex-matched wild-type, *Casp1*$^{-/-}$*Casp11*$^{-/-}$, *Gbp2*$^{-/-}$ and *Gbp*^{chr3}-deficient mice subcutaneously with 5×10^3 colony-forming units of wild-type *F. novicida* strain U112 and measured the bacterial burden in the liver and spleen at 2 d after infection. As published before[37], *Casp1*$^{-/-}$*Casp11*$^{-/-}$ mice displayed a significantly higher bacterial burden in the liver and spleen than that of wild-type mice (**Fig. 8a**). Similarly, *Gbp2*$^{-/-}$ and *Gbp*^{chr3}-deficient mice showed higher bacterial counts than wild-type mice, similar to or even higher than those of *Casp1*$^{-/-}$*Casp11*$^{-/-}$ mice (**Fig. 8a**). Consistent with diminished inflammasome activation *in vivo*, we detected a significantly lower serum concentration of IL-18 in *Casp1*$^{-/-}$*Casp11*$^{-/-}$, *Gbp2*$^{-/-}$ and *Gbp*^{chr3}-deficient mice than in wild-type mice (**Fig. 8b**). To further assess the effects of GBP deficiency *in vivo*, we analyzed survival. Within 4 d of infection, all *Casp1*$^{-/-}$*Casp11*$^{-/-}$, *Gbp2*$^{-/-}$ and *Gbp*^{chr3}-deficient mice died, while most wild-type mice survived until the end of the experiment (day 10) (**Fig. 8c**). These results confirmed the relevance of our *in vitro* data and demonstrated that GBPs encoded by the locus on chromosome 3 were important for inflammasome activation and host defense against *F. novicida in vivo*.

DISCUSSION

Since the activation of AIM2 during infection with the cytosolic pathogen *F. novicida* required interferon signaling, we investigated the role of the products of ISGs in this process. Our results showed that the interferon-inducible GTPases GBP2 and GBP5 promoted *F. novicida*–mediated activation of the AIM2 inflammasome but were dispensable for the activation of AIM2 upon transfection of DNA. Members of the GBP family take part in interferon-induced cell-autonomous immunity and are known to induce disruption of the PCVs of vacuolar bacteria and parasites[23,27,29]. However, the cytosolic localization of *F. novicida* was similar in wild-type and *Gbp*^{chr3}-deficient cells, which indicated that GBPs must have been involved later during infection, after the bacteria had entered the cytosol. This was consistent with results showing that the escape from phagosomes is an interferon-independent process[36] and that cytosolic localization of *F. novicida* is a prerequisite for interferon induction[17]. Since the activation of AIM2 during infection with *F. novicida* or *L. monocytogenes* is known to require cytosolic bacteriolysis[12,15], we investigated whether GBPs controlled the bacteriolysis and replication of *F. novicida* in the cytosol. Significantly fewer lysed and more overall *F. novicida* were present in cells deficient in GBP-encoding genes or *Ifnar1* than in wild-type cells, which indicated that GBPs were required for interferon-mediated cell-autonomous immunity to the pathogen. Furthermore, our results demonstrated that in addition to their known function in destabilizing PCVs, GBPs can also promote the lysis of cytosolic bacteria.

GBPs are also critical for the cytosolic recognition of LPS and for activation of the caspase-11 inflammasome pathway. In this context, they act by promoting the release of vacuolar *S. typhimurium* into the cytosol or by promoting activation of caspase-11 during infection with *L. pneumophila*[29,38]. At present, no model fully explains how GBPs restrict pathogen growth during infection with microbes or protozoa

and at the same time control inflammasome signaling. It is, however, conceivable that the membrane-destabilizing activity of GBPs in combination with their bacteriolytic activity could not only result in the entry of bacteria into the cytosol but also release microbe-associated molecular patterns (for example, LPS and DNA) directly. Such a model might explain their effect on both the caspase-11 pathway[38] and the AIM2 pathway in response to cytosolic bacteria. Thus, bacteriolysis would also release *F. novicida* LPS into the cytosol. However, since *F. novicida* LPS is tetra-acylated, it does not trigger caspase-11 activation[39]. Conversely, we would expect GBPs to lyse cytosolic *Salmonella* or *Legionella*, which would result in activation of AIM2. But in this case, activation of AIM2 is most probably masked by a high degree of caspase-11-dependent cell death and cytokine release.

GBP-mediated bacteriolysis might also be expected to release DNA and amplify the production of type I interferons via STING. Notably, what triggers initial STING signaling and the induction of GBP-encoding genes during infection with *F. novicida* is still undefined, but two possibilities exist. One is the direct activation of STING via a secreted bacterial cyclic nucleotide, analogous to infection with *L. monocytogenes*[40], and another is activation of the DNA sensor cGAS by *F. novicida* DNA and subsequent production of the cyclic dinucleotide cGAMP[41,42]. Lysis of *F. novicida* within the phagosome followed by translocation of its DNA into the cytosol could trigger interferon production[9]. Alternatively, low levels of *F. novicida* extracellular DNA could reach the cytosol by sticking to the surface of the infecting bacteria, as suggested for infection with *M. tuberculosis*[43]. Finally, small amounts of spontaneous bacteriolysis might occur in the host-cell cytosol. If DNA indeed triggers initial STING-mediated production of interferons, it remains to be shown why it is insufficient to trigger activation of AIM2. Additional experiments are needed to determine the relative DNA-binding affinities of cGAS and AIM2 and how their signaling hierarchy is controlled.

Our results have revealed an underappreciated, close connection between cell-autonomous immunity and recognition by the innate immune system. The attack of GBPs on PCVs or pathogens liberates microbe-associated molecular patterns and thus ensures subsequent immunological recognition of the pathogen, which explains the role of interferon signaling in the detection of bacterial DNA by AIM2 or LPS from vacuolar bacteria by the caspase-11 pathway[9,10,13,44,45]. Additional questions remain, such as how GBP targeting is regulated and how GBPs act mechanistically. Ectopic expression of GBP2 or GBP5 did not 'rescue' the inflammasome deficiency of *Ifnar1*$^{-/-}$ cells, which suggests that other products of ISGs are necessary for proper targeting and activity of GBPs[24,25]. Indeed, members of the IRGM family, a subclass of the immunity-related GTPases, can act as guanine-dissociation inhibitors and control the targeting of both immunity-related GTPases and GBPs to pathogen-containing vacuoles, yet the molecular mechanism of this is still unclear[46–49]. Additional biochemical studies are needed to define the mechanism of GBP targeting and action during bacterial infection and how this promotes the exposure of bacterial ligands to cytosolic recognition pathways.

METHODS

Methods and any associated references are available in the online version of the paper.

Note: Any Supplementary Information and Source Data files are available in the online version of the paper.

ACKNOWLEDGMENTS

We thank N. Gekara (Umea University) for *Sting*$^{Gt/Gt}$ mice; M. Roth and S. Hofer for support with mouse experiments; D. Monack (Stanford University) for chicken antibody to *F. novicida*; N. Kayagaki (Genentech) and V. Dixit (Genentech) for *Gbp5*$^{-/-}$ and *Aim2*$^{-/-}$ mice, rat antibody to ASC and rat antibody to caspase-1; L. Gallagher and C. Manoil (University of Washington) for plasmid pFFlp; O. Allatif for statistical analysis; the Imaging and FACS Core Facilities of the Biozentrum, University of Basel, for technical assistance; and the Plateau de Biologie Expérimentale de la Souris and the flow cytometry platform of SFR Biosciences Gerland-Lyon Sud. Supported by Swiss National Science Foundation (PP00P3_139120/1 to P.B.), the University of Basel (ID2153162 to P.B.), the European Research Council (311542 to T.H.) and the Déléguation Générale de l'Armement (M.R.).

AUTHOR CONTRIBUTIONS

E.M., P.W., T.H. and P.B. conceived of the research; E.M., P.W., R.F.D., S.C., L.A., S.R., S.D., M.S.D., A.K., M.R., T.H. and P.B. performed experiments; D.D., K.P. and M.Y. provided reagents; and T.H. and P.B. wrote the manuscript.

COMPETING FINANCIAL INTERESTS

The authors declare no competing financial interests.

1. Paludan, S.R. & Bowie, A.G. Immune sensing of DNA. *Immunity* **38**, 870–880 (2013).
2. Ishikawa, H., Ma, Z. & Barber, G.N. STING regulates intracellular DNA-mediated, type I interferon-dependent innate immunity. *Nature* **461**, 788–792 (2009).
3. Sauer, J.D. *et al.* The *N*-ethyl-*N*-nitrosourea-induced Goldenticket mouse mutant reveals an essential function of Sting in the in vivo interferon response to *Listeria monocytogenes* and cyclic dinucleotides. *Infect. Immun.* **79**, 688–694 (2011).
4. Hornung, V. *et al.* AIM2 recognizes cytosolic dsDNA and forms a caspase-1-activating inflammasome with ASC. *Nature* **458**, 514–518 (2009).
5. Fernandes-Alnemri, T., Yu, J.W., Datta, P., Wu, J. & Alnemri, E.S. AIM2 activates the inflammasome and cell death in response to cytoplasmic DNA. *Nature* **458**, 509–513 (2009).
6. Roberts, T.L. *et al.* HIN-200 proteins regulate caspase activation in response to foreign cytoplasmic DNA. *Science* **323**, 1057–1060 (2009).
7. Bürckstümmer, T. *et al.* An orthogonal proteomic-genomic screen identifies AIM2 as a cytoplasmic DNA sensor for the inflammasome. *Nat. Immunol.* **10**, 266–272 (2009).
8. Ge, J., Gong, Y.N., Xu, Y. & Shao, F. Preventing bacterial DNA release and absent in melanoma 2 inflammasome activation by a Legionella effector functioning in membrane trafficking. *Proc. Natl. Acad. Sci. USA* **109**, 6193–6198 (2012).
9. Fernandes-Alnemri, T. *et al.* The AIM2 inflammasome is critical for innate immunity to *Francisella tularensis*. *Nat. Immunol.* **11**, 385–393 (2010).
10. Jones, J.W. *et al.* Absent in melanoma 2 is required for innate immune recognition of *Francisella tularensis*. *Proc. Natl. Acad. Sci. USA* **107**, 9771–9776 (2010).
11. Kim, S. *et al. Listeria monocytogenes* is sensed by the NLRP3 and AIM2 inflammasome. *Eur. J. Immunol.* **40**, 1545–1551 (2010).
12. Sauer, J.D. *et al. Listeria monocytogenes* triggers AIM2-mediated pyroptosis upon infrequent bacteriolysis in the macrophage cytosol. *Cell Host Microbe* **7**, 412–419 (2010).
13. Rathinam, V.A. *et al.* The AIM2 inflammasome is essential for host defense against cytosolic bacteria and DNA viruses. *Nat. Immunol.* **11**, 395–402 (2010).
14. Briken, V., Ahlbrand, S.E. & Shah, S. *Mycobacterium tuberculosis* and the host cell inflammasome: a complex relationship. *Front. Cell. Infect. Microbiol.* **3**, 62 (2013).
15. Peng, K., Broz, P., Jones, J., Joubert, L.M. & Monack, D. Elevated AIM2-mediated pyroptosis triggered by hypercytotoxic Francisella mutant strains is attributed to increased intracellular bacteriolysis. *Cell. Microbiol.* **13**, 1586–1600 (2011).
16. Muruve, D.A. *et al.* The inflammasome recognizes cytosolic microbial and host DNA and triggers an innate immune response. *Nature* **452**, 103–107 (2008).
17. Henry, T., Brotcke, A., Weiss, D.S., Thompson, L.J. & Monack, D.M. Type I interferon signaling is required for activation of the inflammasome during Francisella infection. *J. Exp. Med.* **204**, 987–994 (2007).
18. Cole, L.E. *et al.* Macrophage proinflammatory response to *Francisella tularensis* live vaccine strain requires coordination of multiple signaling pathways. *J. Immunol.* **180**, 6885–6891 (2008).
19. Cole, L.E. *et al.* Toll-like receptor 2-mediated signaling requirements for *Francisella tularensis* live vaccine strain infection of murine macrophages. *Infect. Immun.* **75**, 4127–4137 (2007).
20. Jones, J.W., Broz, P. & Monack, D.M. Innate immune recognition of *Francisella tularensis*: activation of type-I interferons and the inflammasome. *Front Microbiol* **2**, 16 (2011).
21. Kim, B.H., Shenoy, A.R., Kumar, P., Bradfield, C.J. & MacMicking, J.D. IFN-inducible GTPases in host cell defense. *Cell Host Microbe* **12**, 432–444 (2012).
22. Howard, J.C., Hunn, J.P. & Steinfeldt, T. The IRG protein-based resistance mechanism in mice and its relation to virulence in *Toxoplasma gondii*. *Curr. Opin. Microbiol.* **14**, 414–421 (2011).
23. Yamamoto, M. *et al.* A cluster of interferon-γ-inducible p65 GTPases plays a critical role in host defense against *Toxoplasma gondii*. *Immunity* **37**, 302–313 (2012).

24. Kim, B.H. *et al.* A family of IFN-gamma-inducible 65-kD GTPases protects against bacterial infection. *Science* **332**, 717–721 (2011).
25. Degrandi, D. *et al.* Extensive characterization of IFN-induced GTPases mGBP1 to mGBP10 involved in host defense. *J. Immunol.* **179**, 7729–7740 (2007).
26. Kresse, A. *et al.* Analyses of murine GBP homology clusters based on in silico, in vitro and in vivo studies. *BMC Genomics* **9**, 158 (2008).
27. Degrandi, D. *et al.* Murine guanylate binding protein 2 (mGBP2) controls *Toxoplasma gondii* replication. *Proc. Natl. Acad. Sci. USA* **110**, 294–299 (2013).
28. Kravets, E. *et al.* The GTPase activity of murine guanylate-binding protein 2 (mGBP2) controls the intracellular localization and recruitment to the parasitophorous vacuole of *Toxoplasma gondii*. *J. Biol. Chem.* **287**, 27452–27466 (2012).
29. Meunier, E. *et al.* Caspase-11 activation requires lysis of pathogen-containing vacuoles by IFN-induced GTPases. *Nature* **509**, 366–370 (2014).
30. Checroun, C., Wehrly, T.D., Fischer, E.R., Hayes, S.F. & Celli, J. Autophagy-mediated reentry of *Francisella tularensis* into the endocytic compartment after cytoplasmic replication. *Proc. Natl. Acad. Sci. USA* **103**, 14578–14583 (2006).
31. Nothelfer, K., Dias Rodrigues, C., Bobard, A., Phalipon, A. & Enninga, J. Monitoring *Shigella flexneri* vacuolar escape by flow cytometry. *Virulence* **2**, 54–57 (2011).
32. Juruj, C. *et al.* Caspase-1 activity affects AIM2 speck formation/stability through a negative feedback loop. *Front. Cell. Infect. Microbiol.* **3**, 1–11 (2013).
33. Chong, A. *et al.* Cytosolic clearance of replication-deficient mutants reveals *Francisella tularensis* interactions with the autophagic pathway. *Autophagy* **8**, 1342–1356 (2012).
34. Miao, E.A. *et al.* Caspase-1-induced pyroptosis is an innate immune effector mechanism against intracellular bacteria. *Nat. Immunol.* **11**, 1136–1142 (2010).
35. Zhou, H. *et al.* Genome-wide RNAi screen in IFN-γ-treated human macrophages identifies genes mediating resistance to the intracellular pathogen *Francisella tularensis*. *PLoS ONE* **7**, e31752 (2012).
36. Edwards, J.A., Rockx-Brouwer, D., Nair, V. & Celli, J. Restricted cytosolic growth of *Francisella tularensis* subsp. tularensis by IFN-γ activation of macrophages. *Microbiology* **156**, 327–339 (2010).
37. Mariathasan, S., Weiss, D.S., Dixit, V.M. & Monack, D.M. Innate immunity against *Francisella tularensis* is dependent on the ASC/caspase-1 axis. *J. Exp. Med.* **202**, 1043–1049 (2005).
38. Pilla, D.M. *et al.* Guanylate binding proteins promote caspase-11-dependent pyroptosis in response to cytoplasmic LPS. *Proc. Natl. Acad. Sci. USA* **111**, 6046–6051 (2014).
39. Hagar, J.A., Powell, D.A., Aachoui, Y., Ernst, R.K. & Miao, E.A. Cytoplasmic LPS activates caspase-11: implications in TLR4-independent endotoxic shock. *Science* **341**, 1250–1253 (2013).
40. Woodward, J.J., Iavarone, A.T. & Portnoy, D.A. c-di-AMP secreted by intracellular *Listeria monocytogenes* activates a host type I interferon response. *Science* **328**, 1703–1705 (2010).
41. Sun, L., Wu, J., Du, F., Chen, X. & Chen, Z.J. Cyclic GMP-AMP synthase is a cytosolic DNA sensor that activates the type I interferon pathway. *Science* **339**, 786–791 (2013).
42. Li, X.D. *et al.* Pivotal roles of cGAS-cGAMP signaling in antiviral defense and immune adjuvant effects. *Science* **341**, 1390–1394 (2013).
43. Manzanillo, P.S., Shiloh, M.U., Portnoy, D.A. & Cox, J.S. *Mycobacterium tuberculosis* activates the DNA-dependent cytosolic surveillance pathway within macrophages. *Cell Host Microbe* **11**, 469–480 (2012).
44. Broz, P. *et al.* Caspase-11 increases susceptibility to Salmonella infection in the absence of caspase-1. *Nature* **490**, 288–291 (2012).
45. Rathinam, V.A. *et al.* TRIF licenses caspase-11-dependent NLRP3 inflammasome activation by gram-negative bacteria. *Cell* **150**, 606–619 (2012).
46. Martens, S. *et al.* Disruption of *Toxoplasma gondii* parasitophorous vacuoles by the mouse p47-resistance GTPases. *PLoS Pathog.* **1**, e24 (2005).
47. Howard, J.C., Hunn, J.P. & Steinfeldt, T. The IRG protein-based resistance mechanism in mice and its relation to virulence in *Toxoplasma gondii*. *Curr. Opin. Microbiol.* **14**, 414–421 (2011).
48. Bekpen, C. *et al.* The interferon-inducible p47 (IRG) GTPases in vertebrates: loss of the cell autonomous resistance mechanism in the human lineage. *Genome Biol.* **6**, R92 (2005).
49. Haldar, A.K. *et al.* IRG and GBP host resistance factors target aberrant, "non-self" vacuoles characterized by the missing of "self" IRGM proteins. *PLoS Pathog.* **9**, e1003414 (2013).

ONLINE METHODS

Bacterial strains and plasmids. *F. novicida* strain U112 and isogenic ΔFPI mutants have been published[10]. Where applicable, strains were transformed with the plasmid pKK219-GFP (**Supplementary Table 2**). The β-lactamase mutant Δ*bla* was generated by PCR-mediated homologous recombination with a kanamycin selection cassette through use of the following primers (upper case indicates *F. novicida* sequence; lower case indicates the kanamycin-resistance casette sequence): ForUpstream, GTCGAGTACGCT AATATAAAAATTCTAAAAA; RevUpstream, gcttatcgataccgtcgaccctcGGGA TTAATGATAAAGTTGTAACTAATATACGC; ForDownstream, gatatcgat cctgcagctatgcCACTTATAAATAAGCGGTACGCCAC; and RevDownstream, AAGACGGTGATGTACCATTTGTCTATAG. The kanamycin-resistance casette was removed by transformation of the mutant obtained with the thermosensitive plasmid pFFlp (provided by L. Gallagher and C. Manoil) encoding the recombinase Flp. Following loss of the plasmid, genomic deletion was verified by sequencing.

Mice. *Gbp*^{chr3}-deficient, *Gbp2*$^{-/-}$, *Gbp5*$^{-/-}$, *Nos2*$^{-/-}$*Cybb*$^{-/-}$, *Casp1*$^{-/-}$*Casp11*$^{-/-}$ ('caspase-1-knockout'), *Asc*$^{-/-}$, *Aim2*$^{-/-}$, *Stat1*$^{-/-}$, *Ifnar1*$^{-/-}$, *Sting*$^{Gt/Gt}$, *Tlr2*$^{-/-}$ and *Myd88*$^{-/-}$ mice have been described[3,10,23,27,29,44]. Mice were bred in the animal facilities of the University of Basel or at the Plateau De Biologie Expérimentale De La Souris.

Animal infection. All animal experiments were approved (license 2535, Kantonales Veterinäramt Basel-Stadt and ENS_2012_061) and were performed according to local guidelines (Tierschutz-Verordnung, Basel-Stadt and CECCAPP, Lyon) and the Swiss animal protection law (Tierschutz-Gesetz). Age- and sex-matched mice (8–10 weeks of age) were infected subcutaneously with 5×10^3 or 1.5×10^5 colony-forming units of stationary-phase wild-type *F. novicida* strain U112 in 50 µl PBS. Mice were killed at the appropriate time point after infection. No randomization or 'blinding' of researchers to sample identity was used.

Cell culture and infection. BMDMs were differentiated in DMEM (Invitrogen) with 10% vol/vol FCS (Thermo Fisher Scientific), 10% MCSF (supernatants of L929 mouse fibroblasts), 10 mM HEPES (Invitrogen) and nonessential amino acids (Invitrogen). 1 d before infection, macrophages were seeded into 6-, 24- or 96-well plates at a density of 1.25×10^6, 2.5×10^5 or 5×10^4 cells per well. Where required, macrophages were pre-stimulated with Pam_3CSK_4 (tripalmitoyl cysteinyl seryl tetralysine), LPS (from *Escherichia coli* strain O111:B4 (InvivoGen)), mouse IFN-β or mouse IFN-γ (eBioscience). For infection with *F. novicida*, bacteria were grown overnight at 37 °C with aeration in brain-heart–infusion medium or tryptic soy broth. The bacteria were added to the macrophages at a multiplicity of infection of 100 or the appropriate value. The plates were centrifuged for 15 min at 500*g* to ensure similar adhesion of the bacteria to the cells and were incubated for 120 min at 37 °C. Next, cells were washed and fresh medium with 10 µg/ml gentamycin (Invitrogen) was added to kill extracellular bacteria, then plates were incubated for the desired length of time. Transfection with poly(dA:dT) or poly(dG:dC) was done as described[29] or as indicated in the figures and legends (**Figs. 1** and **3**).

siRNA-mediated knockdown. Genes were knocked down with GenMute (SignaGen Laboratories) and siRNA pools (siGenome; Dharmacon). Wild-type BMDMs were seeded into 24- or 96-well plates at a density of 1.5×10^5 or 3×10^4 cells per well. siRNA complexes were prepared at a concentration of 25 nM siRNA in GenMute Buffer according to the manufacturer's instructions for forward knockdown (SignaGen laboratories). siRNA complexes were mixed with BMDM medium (described above) and were added onto the cells. After 22–48 h of gene knockdown, BMDMs were infected with *F. novicida* at a multiplicity of infection of 100:1 and were analyzed for inflammasome activation as outlined below. siRNA pools targeted the following genes (numbers in parentheses indicate Dharmacon reference): *Aim2* (M-044968-01), *Casp11* (that is, *Casp4*) (M-042432-01), Gbp1 (M-040198-01), Gbp2 (M-040199-00), Gbp3 (M-063076-01), Gbp4 (M-047506-01), Gbp5 (M-054703-01), Gbp6 (M-041286-01), Gbp7 (M- 061204-01), Gbp8 (M-059726-01), Gbp9 (M-052281-01), Gbp10 (M-073912-00), Gbp11 (M-079932-00) and NT (non-targeting) pool 2 (D-001206-14).

siRNA screening. Knockdown of the 483 selected genes was performed as described above in the 36 central wells of 96-well plates; this included the nontargeting control siRNA and siRNA specific for *Asc* and *Aim2* on each plate. Macrophages were infected with *F. novicida* at a multiplicity of infection of 100:1 and, following a wash at 1 h after infection, cells were incubated with medium supplemented with propidium iodide at 5 µg/ml. At 6 h after infection, the fluorescence of propidium iodide was determined on a plate reader (Tecan) and supernatants were collected for analysis of the release of IL-1β by enzyme-linked immunosorbent assay (DuoSet; R&D Systems). The fluorescence of propidium iodide and concentration of IL-1β in cells transfected with each siRNA were normalized to the average value of the full plate set, set as 100, and to the value obtained with *Aim2*-specific siRNA, set as 0, with the following calculation (for gene 'X'): normalized value obtained with X-specific siRNA = (value obtained with X-specific $siRNA_x$ – value obtained with *Aim2*-specific siRNA) / (average value obtained with siRNA – value obtained with *Aim2*-specific siRNA). All the siRNA presenting variation of more than 50% in either one of the two parameters have been retested two or three times. Average normalized values are presented in the display items.

Ectopic expression of GBP2 and GBP5. Mouse *Gbp2* and *Gbp5* were cloned into the lentiviral plasmid TRIP iziE-SSFV-GFP with the following primers and restriction enzymes (upper case indicates gene sequence; lower case indicates restriction site (underlined) and four bases flanking in the 5′ direction): For_mGBP2_AvrII, attacctaggGACATGGCCTCAGAGATCCACATG; Rev_mGBP2_EcoRV, aatagataTCAGAGTATAGTGCACTTCCCAGACG; For_mGBP5_AvrII, aaatcctagGACATGGCCCCAGAGATTCACATG; and Rev_mGBP5_HpaI, atttgttaacTTAGCTTATAACACAGTCATGATGATGT CTAC. The production of lentiviruses in 293T human embryonic kidney cells and the transduction of primary BMDMs were performed by standard methods. IFNAR1-deficient macrophages were transduced after 8 d of differentiation by spin-inoculation (1,500*g* for 2 h at room temperature). Transduced macrophages were infected 48 h later. Transduction frequency was determined by flow cytometry based on GFP expression. Specific ectopic expression was checked by quantitative RT-PCR.

Cytokine and LDH release measurement. IL-1β, IL-18 and tumor-necrosis factor were measured by enzyme-linked immunosorbent assay (eBioscience). LDH was measured with an LDH Cytotoxicity Detection Kit (Clontech). To normalize for spontaneous lysis, the percentage of LDH release was calculated as follows: (LDH infected – LDH uninfected) / (LDH total lysis – LDH uninfected) × 100.

Immunoblot analysis. Immunoblot analysis was done as described[29]. Antibodies used were rat anti–mouse caspase-1 (1:1,000 dilution; 4B4; Genentech), rabbit anti-IL-1α (1:1,000 dilution; ab109555; Abcam), rabbit anti-IL-18 (1:500 dilution; 5180R; Biovision), goat anti–mouse IL-1β (1:500 dilution; AF-401-NA; R&D Systems), rabbit anti-GBP2 (1:1,000 dilution; 11854-1-AP; Proteintech) and rabbit anti-GBP5 (1:1,000 dilution; 13220-1-AP; Proteintech). Cell lysates were probed with monoclonal anti-β-actin (1:2,000 dilution; AC-15; A1978; Sigma). Secondary antibodies were as follows (all conjugated to horseradish peroxidase and all at a dilution of 1:3,000): goat anti-rat (NA935V; GE Healthcare), goat anti-rabbit (G21234; Invitrogen), rabbit anti-goat (811620; Invitrogen) and rabbit anti-mouse (816720; Invitrogen).

Real-time PCR. Primers used for mRNA quantification are in **Supplementary Table 3**. Experiments were performed with an iCycler (Bio-Rad) and SYBR green (Applied Biosystems) with standard protocols.

Statistical analysis. Prism 5.0a software (GraphPad Software) was used for statistical analysis of data. For evaluation of the differences between two groups (cell death, cytokine release, flow cytometry, colony-forming units and immunofluorescence-based counts), a two-tailed *t*-test was used. The Kolmogorov-Smirnov test was used for comparison of the cell distribution as determined by ImageStream microscopy in flow. *P* values were adjusted for multiple comparisons with the Bonferroni correction approach. Animal experiments were evaluated with the Mann-Whitney or log-rank Cox-Mantel test.

Immunofluorescence. Macrophages were seeded on glass coverslips and were infected as described above. At the desired time points, cells were washed three times with PBS and were fixed for 15 min at 37 °C with 4% paraformaldehyde. Following fixation, coverslips were washed, and the fixative was quenched for 10 min at room temperature with 0.1 M glycine. Coverslips were stained for 16 h at 4 °C with primary antibodies (identified below), then were washed with PBS and then incubated for 1 h at room temperature with the appropriate Alexa Fluor–conjugated secondary antibodies (identified below) (1:500 dilution; Invitrogen), then were washed with PBS and mounted on glass slides with Vectashield containing DAPI (6-diamidino-2-phenylindole; Vector Labs). Antibodies used were chicken anti–*F. novicida* (1:1,000 dilution; a gift from D. Monack), rat anti-ASC (1:1,000 dilution; Genentech), rabbit anti-GBP2 (1:100 dilution; 11854-1-AP; Proteintech) and rabbit anti-GBP5 (1:100 dilution; 13220-1-AP; Proteintech). Secondary antibodies used were as folllows (all at a dilution of 1:500 and all from Life Technologies): goat anti-rat coupled to Alexa Fluor 488 (A11006), Alexa Fluor 568 (A11077) or Alexa Fluor 633 (A21094); goat anti-rabbit coupled to Alexa Fluor 488 (A11008) or Alexa Fluor 568 (A10042); and goat anti-chicken coupled to Alexa Fluor 488 (A11032), Alexa Fluor 568 (A11047) or Alexa Fluor 633 (A21103). Coverslips were imaged on a Zeiss LSM700 or a Leica SP8 at a magnification of ×63 and vacuolar versus cytosolic bacteria, total intracellular bacteria or ASC specks were quantified as described in the figure legends.

Phagosome protection assay. For quantification of cytoplasmic and vacuolar bacteria, macrophages were infected with GFP$^+$ *F. novicida* as described above. At the desired time point, cells were washed with KHM buffer (110 mM potassium acetate, 20 mM HEPES and 2 mM MgCl2, pH 7.3), followed by incubation for 1 min in KHM buffer with 50 μg/ml digitonin (Sigma). Cells were immediately washed three times with KHM buffer and then were stained for 12 min with Texas Red–coupled chicken antibody to *F. novicida* (identified above) in KHM buffer with 2% BSA. Cells were washed with PBS, then were fixed and analyzed by microscopy. Controls were included in every assay as described[29].

Intracellular viability measurement. For measurement of the intracellular lysis of *F. novicida*, we adapted a published propidium iodide–staining method[33]. Infected BMDMs were incubated for 12 min at 37 °C with Alexa Fluor 488–conjugated mouse antibody to *F. novicida* (identified above) and 2.6 μM propidium iodide (Sigma) in KHM buffer (described above) for labeling of accessible cytosolic bacteria and compromised bacteria, respectively, in permeabilized cells. Cells were fixed and imaged as described above.

CCF4 measurements. Quantification of escape from vacuoles with the β-lactamase–CCF4 assay was performed following manufacturer's instructions (Life Technologies). Macrophages seeded onto non-treated plates were infected for 1 h as described above, washed and then incubated for 1 h at room temperature in CCF4 in the presence of 2.5 mM probenicid (Sigma). Live (propidium iodide–negative) cells were used for quantification of cells containing cytosolic *F. novicida*, with excitation at 405 nm and detection at 450 nm (cleaved CCF4) or 510 nm (intact CCF4).

Flow cytometry. For assessment of bacterial replication by flow cytometry, macrophages seeded onto untreated plates were infected as described above with GFP-expressing *F. novicida* strains. At 8 h after infection, cells were lifted with trypsin and were immediately analyzed by flow cytometry on a FACSCanto II cytometer (BD Biosciences). Dead cells were excluded on the basis of staining with propidium iodide.

ImageStream flow cytometry. Macrophages infected with GFP-expressing bacteria were fixed in 4% PFA and were analyzed on an ImageStream X Mark II (Amnis; EMD-Millipore) with Inspire software, with the extended depth-of-field function activated to increase the accuracy of spot counts. Images of single cells were analyzed with Ideas software (Amnis; EMD-Millipore) with the following steps (each step being confirmed by visualization of at least 20 single cells). Doublets and debris were excluded by morphological parameters (aspect ratio and area in the brightfield channel). Defocused images were eliminated by the Gradient RMS function of the brightfield function. For spot counts and definition of the mean fluorescence of single bacterium, the specific GFP fluorescence signal was defined by application of a mask combining an intensity threshold and a spot to cell background ratio (peak) function. Automatic spot counts were performed with the mask described above. Cells containing a single spot (either a single bacterium or a tight cluster of several bacteria) were gated. The area of the specific signal was analyzed in single cells on the gated population. For the exclusion of bacterial clusters and quantification of the fluorescence of single bacterium, the mean fluorescence intensity was calculated on the GFP$^+$ signal covering an area of 1 ± 0.5 μm^2 in 1,599 cells.

Bacteria in single cells were quantified by the automatic spot count function or their numbers were calculated based on the fluorescence of single bacterium. The quantification was identical for cells containing fewer than seven bacteria ($R^2 > 0.99$). For higher intracellular burden, the spot-count function largely underestimated the number of bacteria per cell due to the difficulty to discriminate bacterial cluster. We thus relied on the specific fluorescence of the bacteria within the cells as defined by the mask described above and the calculated fluorescence value of single intracellular bacterium to quantify bacteria per cell. The mask was applied to at least 10,000 images of single cells per sample to extract the specific fluorescence of the intracellular bacteria in single cells.

doi:10.1038/ni.3119

4.5 Research Article V: ASC filament formation serves as a signal amplification mechanism for inflammasomes

M. S. Dick [1], L. Sborgi [2], S. Rühl [1], S. Hiller [2] and P. Broz [1].

1 Focal Area Infection Biology, Biozentrum, University of Basel, Klingelbergstrasse 50/70, 4056 Basel, Switzerland.
2 Focal Area Structural Biology, Biozentrum,
University of Basel, Klingelbergstrasse 50/70, 4056 Basel, Switzerland.

Published: Nature Communications2016 June 22; 7:11929.

doi: 10.1038/ncomms11929.322

Statement of contribution:

I cloned the CRISPR plasmids targeting caspase-1 and gasdermin-D

nature COMMUNICATIONS

ARTICLE

Received 23 Nov 2015 | Accepted 11 May 2016 | Published 22 Jun 2016

DOI: 10.1038/ncomms11929 OPEN

ASC filament formation serves as a signal amplification mechanism for inflammasomes

Mathias S. Dick[1], Lorenzo Sborgi[2], Sebastian Rühl[1], Sebastian Hiller[2] & Petr Broz[1]

A hallmark of inflammasome activation is the ASC speck, a micrometre-sized structure formed by the inflammasome adaptor protein ASC (apoptosis-associated speck-like protein containing a CARD), which consists of a pyrin domain (PYD) and a caspase recruitment domain (CARD). Here we show that assembly of the ASC speck involves oligomerization of ASC^{PYD} into filaments and cross-linking of these filaments by ASC^{CARD}. ASC mutants with a non-functional CARD only assemble filaments but not specks, and moreover disrupt endogenous specks in primary macrophages. Systematic site-directed mutagenesis of ASC^{PYD} is used to identify oligomerization-deficient ASC mutants and demonstrate that ASC speck formation is required for efficient processing of IL-1β, but dispensable for gasdermin-D cleavage and pyroptosis induction. Our results suggest that the oligomerization of ASC creates a multitude of potential caspase-1 activation sites, thus serving as a signal amplification mechanism for inflammasome-mediated cytokine production.

[1] Focal Area Infection Biology, Biozentrum, University of Basel, Klingelbergstrasse 50/70, 4056 Basel, Switzerland. [2] Focal Area Structural Biology, Biozentrum, University of Basel, Klingelbergstrasse 50/70, 4056 Basel, Switzerland. Correspondence and requests for materials should be addressed to P.B. (email: petr.broz@unibas.ch).

Detection of pathogens by the innate immune system relies on germline-encoded pattern recognition receptors (PRRs), which recognize a variety of pathogen-derived molecules, known as pathogen-associated molecular patterns (PAMPs), and host-derived danger signals, known as danger-associated molecular patterns[1]. Although most PRRs initiate transcriptional responses, such as the expression of cytokines[2,3], a subset of cytosolic PRRs promote the assembly of inflammasome complexes and subsequent activation of the cysteine protease caspase-1 (refs 4,5). To date, only members of the NOD-like receptor (NLR) family, the PYHIN protein family and PYRIN were shown to assemble inflammasomes in response to different cytosolic PAMPs or danger-associated molecular patterns[5,6]. A unifying feature of all these receptors is either a pyrin domain (PYD) or a caspase recruitment domain (CARD), both of which belong to the death-fold domain superfamily. On the basis of the presence of these domains, the receptors can be classified as PYD-containing receptors (NLRP3: NLR family, PYD containing 3; AIM2: absent in myeloma 2; pyrin) or CARD-containing receptors (NLRC4: NLR family, CARD containing 4; NLRP1: NLR family, PYD containing 1). After receptor activation and oligomerization, these domains recruit the adaptor protein ASC (apoptosis-associated speck-like protein containing a CARD) and pro-caspase-1 into the complex through homotypic domain–domain interactions. Within the inflammasome, pro-caspase-1 is activated by dimerization and auto-proteolysis, and the proteolytically active hetero-tetramer is released[7]. Several substrates of caspase-1 have been identified, among them the pro-forms of the cytokines interleukin (IL)-1β and IL-18 (refs 7–9). Another consequence of inflammasome activation is the induction of a pro-inflammatory cell death called pyroptosis[10]. Pyroptosis is driven by the amino-terminal cleavage fragment of gasdermin-D, a protein cleaved by caspase-1, and results in the lysis of the host cell and subsequent release of cytoplasmic content, among them processed IL-1β and IL-18 (refs 11,12).

Recent studies have started to elucidate the role of the inflammasome adaptor protein ASC[13–15], a bipartite protein composed of a PYD and a CARD, also known as PYCARD[16,17]. ASC has previously been regarded as a simple adaptor protein that links PYD-containing receptors to the CARD-containing caspase-1, via homotypic PYD–PYD and CARD–CARD interactions[18]. However, its role appears to be more complex, as on receptor activation ASC also forms the so-called ASC speck, a macromolecular form of the inflammasome with a diameter of ~1–2 μm[19,20]. Formation of the ASC speck is independent of caspase-1 activity, but requires the oligomerization of ASC into large insoluble aggregates[20,21]. These ASC aggregates are stable and have even been shown to be released into the extracellular space, after pyroptosis induction, where they can trigger prolonged inflammasome activation in phagocytic cells[22,23]. Analyses of stimulated emission depletion microscopy images and electron micrographs suggest an irregular, filamentous shape[22,23]. Consistently, we and others have shown that ASC oligomerizes into long helical filaments via its PYD[13–15]. Despite the advances regarding the atomic structure of the ASC filament, whether the ASC speck is the functional unit of the inflammasome is unclear. Several inflammasome receptors (for example, NLRC4 and mouse Nlrp1b) contain a CARD instead of a PYD and are able to recruit caspase-1 even in the absence of ASC. Indeed, we and others have shown that ASC is not required for cell death induction by these receptors[24–28]. Nonetheless, activation of CARD-containing receptors results in ASC speck formation in wild-type (WT) cells, but how their CARD initiates ASC filaments is unknown. Furthermore, it is unclear whether ASC oligomerization itself is required for inflammasome signalling. Previous mutagenesis studies of ASC could not address the role of ASC oligomerization in signalling, as they were based on overexpression of ASC mutants in HEK293 cells, which is prone to artefact generation and lacks the means to study the effects on downstream signalling[13,29,30].

Here we use retroviral expression of ASC mutants in *Asc*-deficient immortalized mouse macrophages, to address the mechanism of ASC speck formation and the functional relevance of ASC filament formation for inflammasome signalling. Our results reveal an architectural role for the ASC^{CARD}, showing that it is required to link individual ASC filaments towards forming the dense ASC speck. Furthermore, we show that ASC bridging molecules are necessary to allow CARD-containing receptors the initiation of ASC filament formation. Finally, we use site-directed mutagenesis of the ASC^{PYD}–ASC^{PYD} interaction interfaces to identify mutations that disrupt ASC filament formation without affecting the interaction to receptor PYDs. Surprisingly, such ASC mutants are still able to initiate caspase-1-dependent gasdermin-D maturation and subsequent cell death, but lack the ability to form filaments, to assemble ASC specks and to process IL-1β, thus uncoupling the two major downstream signalling pathways. In conclusion, our data show that the ASC speck has a function in inflammasome signalling and support a model in which the rapid oligomerization of ASC via its PYD creates a multitude of potential caspase-1 activation sites, thus serving as a signal amplification mechanism for inflammasome signalling.

Results

Distinct roles for the ASC^{PYD} and ASC^{CARD} in speck assembly. Although ASC is the main structural component of the ASC speck[20,24], conflicting reports have implicated either the ASC^{PYD} or the ASC^{CARD} in speck assembly[13,31,32]. To address the role of the ASC^{PYD} and the ASC^{CARD} in speck formation and downstream signalling, we transduced immortalized $Asc^{-/-}$ murine bone marrow-derived macrophages (BMDMs) with fluorescently tagged full-length ASC (ASC^{FL}) or ASC^{PYD} and ASC^{CARD} alone (Fig. 1a). As overexpression of ASC^{FL} can result in aggregation even in the absence of activated receptor[19], we selected individual clonal lines that did not display any autoactivation when unstimulated (Supplementary Fig. 1a). To test the functionality of these constructs, cells were primed with lipopolysaccharide (LPS) and transfected with the synthetic DNA analogue poly(deoxyadenylic-deoxythymidylic) acid (poly(dA:dT)), an activator of AIM2 (refs 33,34). mCherry-tagged ASC^{FL}, expressed in $Asc^{-/-}$ cells, promoted pyroptosis (as measured by the release of lactate dehydrogenase (LDH)) and IL-1β release (measured by enzyme-linked immunosorbent assay (ELISA)), to levels seen in immortalized WT macrophage controls (Fig. 1b). We also observed comparable levels of IL-1β/-18 and caspase-1 processing and release by western blotting (Supplementary Fig. 1b). In contrast, neither the ASC^{PYD} nor ASC^{CARD} restored cell death, IL-1β/-18 secretion or caspase-1 cleavage on AIM2 activation (Fig. 1b and Supplementary Fig. 1b). Similarly, expression of the individual domains did not restore inflammasome signalling in response to extracellular ATP, an NLRP3 activator[35] (Supplementary Fig. 1c,d).

Heterologous expression of ASC^{PYD} and ASC^{CARD} or CARDs of mitochondrial antiviral-signalling protein (MAVS), retinoic acid-inducible gene 1 (RIG-I) and pro-caspase-1 results in the formation of filaments of varying length in different cell types and *in vitro*[13,36–40]. However, it is possible that such ASC^{PYD} or ASC^{CARD} filaments are overexpression artefacts, as ASC^{FL} normally forms a distinct dense speck structure[20]. To assess the ability of ASC^{PYD} and ASC^{CARD} to form macromolecular assemblies, we examined the above described cell lines by

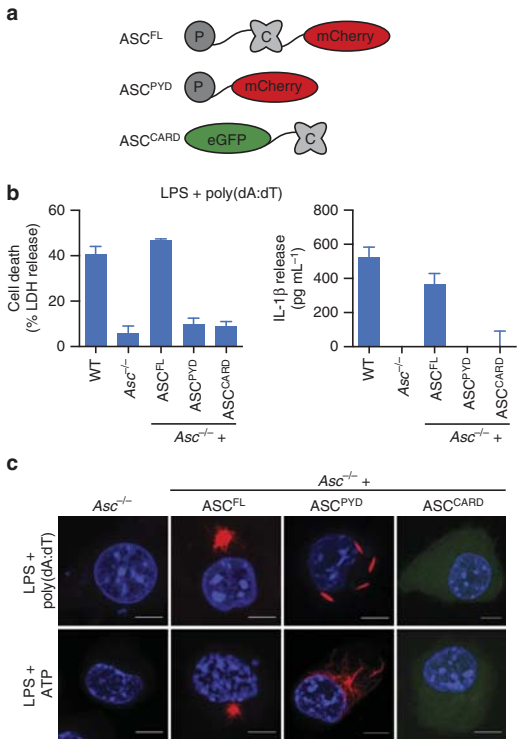

Figure 1 | Both domains of ASC are required for signalling. (**a**) Schematic representation of the domain organization of fluorophore-tagged (mCherry or enhanced GFP (eGFP)) WT ASC (ASC^{FL}), ASC^{PYD} and ASC^{CARD} constructs. (**b**) Release of LDH (assessing cell death) and IL-1β from LPS-primed immortalized WT, $Asc^{-/-}$ or $Asc^{-/-}$ BMDMs expressing ASC^{FL}, ASC^{PYD} or ASC^{CARD} 3 h after poly(dA:dT) transfection (1 μg ml^{-1}). (**c**) Representative images of cell lines from (**b**) 3 h after poly(dA:dT) transfection (1 μg ml^{-1}) or 1 h after ATP treatment (5 mM). DNA (blue, Hoechst), ASC^{FL} or ASC^{PYD} (red) and ASC^{CARD} (green). Scale bars, 10 μm. Data (**b**,**c**) are representative of three independent experiments. Graphs show the mean and s.d. from quadruplicate wells. See also Supplementary Fig. 1.

microscopy, following inflammasome stimulation. As expected, activation of AIM2 or NLRP3 induced the formation of perinuclear specks in cells expressing mCherry-tagged ASC^{FL} (Fig. 1c and Supplementary Fig. 1e,f). In line with the reported ability of ASC to form filaments[13,15], specks formed by ASC^{FL} had a dense core with emanating filaments (Fig. 1c). Instead of forming similarly dense specks, the ASC^{PYD} assembled into filaments on the engagement of NLRP3 or AIM2 (Fig. 1c). Of note, filaments formed after NLRP3 or AIM2 activation differed in their appearance, possibly due to distinct modes of how NLR and PYHIN family members assemble complexes and initiate ASC filaments[13,41]. Remarkably, these filaments had varying lengths and widths, with some appearing clearly thicker than 90 Å, the reported diameter of an ASC^{PYD} filament[13,15]. Unlike reported before, we observed that the ASC^{CARD} was not able to form macromolecular assemblies (Fig. 1c and Supplementary Fig. 1e,f). Taken together, these data suggest that although both domains of ASC are necessary for signalling, only the ASC^{PYD} forms filaments on inflammasome activation. This is consistent with reports by us and others showing that full-length ASC forms helical filaments *in vitro* via the ASC^{PYD} (refs 13,15), whereas the ASC^{CARD} is exposed on the surface and not involved in ASC filament formation[15]. As straight filaments are formed by ASC^{PYD} and compact specks are formed by ASC^{FL}, our data also suggest that the ASC^{CARD} must contribute significantly to the macroscopic structure of the ASC speck.

ASC^{CARDs} condense ASC^{PYD} filaments into ASC specks. To test whether ASC^{CARD} is required to form ASC specks, we generated immortalized $Asc^{-/-}$ macrophage lines expressing ASC^{D130R} or ASC^{D134R} (Fig. 2a and Supplementary Fig. 2a), two mutations in surface-exposed residues of the ASC^{CARD} that abrogate interaction of the ASC^{CARD} with the pro-caspase-1^{CARD} (ref. 31). As expected, $Asc^{-/-}$ macrophages expressing ASC^{D130R} or ASC^{D134R} did not activate caspase-1, release mature IL-1β or undergo pyroptosis in response to DNA transfection or ATP treatment (Fig. 2b and Supplementary Fig. 2b–d). ASC^{D130R} and ASC^{D134R} formed long filaments rather than dense ASC specks in response to AIM2 and NLRP3 activation (Fig. 2c,d and Supplementary Fig. 2e,f), similar to the ASC^{PYD} alone, thus supporting our hypothesis that a functional ASC^{CARD} is required to assemble ASC^{PYD} filaments into a speck. To confirm that these mutations not only disrupt ASC^{CARD}–pro-caspase-1^{CARD} interactions but also ASC^{CARD}–ASC^{CARD} interactions, we expressed enhanced green fluorescent protein (eGFP)-tagged ASC^{CARD} in the presence of reconstituted inflammasomes, formed by co-transfection of AIM2 with mCherry-tagged ASC^{FL}, ASC^{PYD}, ASC^{D130R} or ASC^{D134R} in HEK293T cells. Co-localization and co-immunoprecipitation assays demonstrated that GFP-ASC^{CARD} was only able to interact with WT ASC and not with ASC^{D130R} or ASC^{D134R}, confirming that the two mutations blocked ASC^{CARD}–ASC^{CARD} interaction (Supplementary Fig. 2g,h).

If the ASC^{CARD} organizes ASC filaments into dense specks, we speculated that increasing levels of ASC^{CARD} mutants would disrupt specks formed by WT ASC, resulting in larger but less dense ASC specks. Therefore, we retrovirally transduced various ratios of mCherry-tagged WT and mCherry-tagged ASC^{D130R} into primary WT C57BL/6 macrophages (containing endogenous ASC) and measured median speck size on the activation of AIM2 by poly(dA:dT) transfection or NLRP3 by Nigericin, a pore-forming toxin[35]. Indeed, increasing levels of ASC^{D130R} resulted in a significant increase in ASC speck size (Fig. 2e,f). As expected, microscopy analysis of these large ASC specks showed that they were also less dense and had a filamentous nature (Fig. 2g). Taken together, these results support a model in which the ASC speck observed in WT cells is composed of individual ASC filaments that are formed via their PYDs and cross-linked to each other via their CARDs (Supplementary Fig. 3a).

NLRC4 oligomerizes ASC via a bridging ASC molecule. Most inflammasome-forming receptors contain a PYD and initiate ASC filaments directly by homotypic PYD–PYD interactions. Notable exceptions are NLRC4 and mouse Nlrp1b, which contain a CARD and thus might recruit and activate caspase-1 directly[42,43]. Nevertheless, ASC promotes caspase-1 processing and efficient IL-1β/-18 release after NLRC4 and Nlrp1b activation[26,44]. ASC specks can be observed after NLRC4 activation, but how CARD-containing receptors initiate oligomerization of ASC is unknown. Theoretically, NLRC4 could initiate ASC oligomerization either by (i) $NLRC4^{CARD}$–ASC^{CARD} interaction and ASC^{CARD} oligomerization, (ii) heterotypic interaction between related death-fold domains, that is,

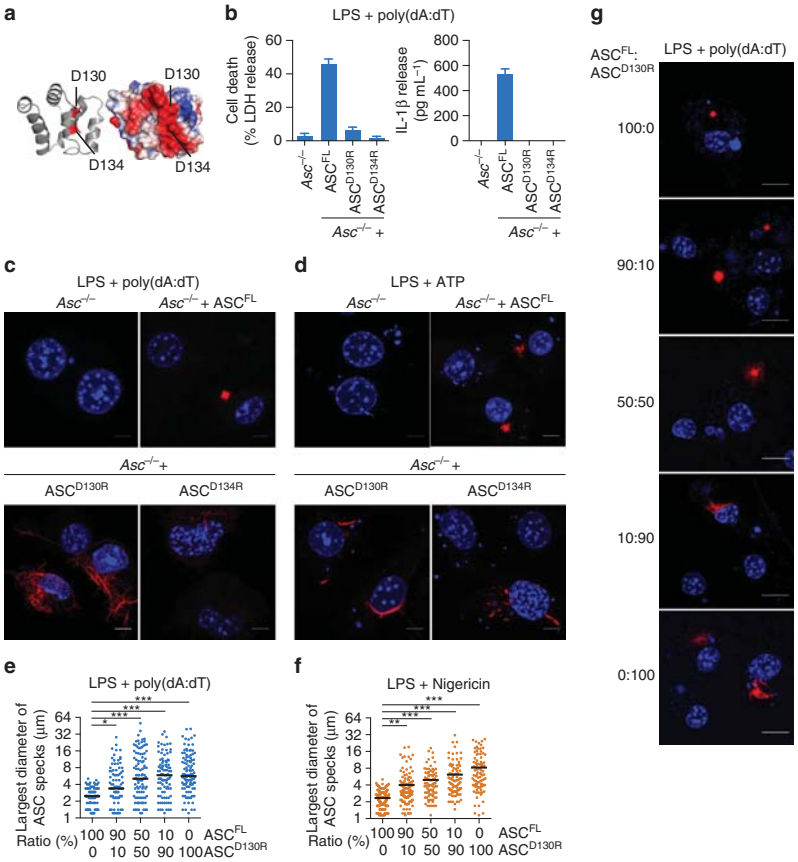

Figure 2 | The CARD of ASC condenses PYD filaments into the speck. (**a**) Structural model of the mouse ASC^{CARD} based on the human homologue (PDB 2KN6 (ref. 67)). The structure is shown in ribbon (left) and electrostatic surface representation (right, blue, positive charge; red, negative charge). Residues D130 and D134, involved in the interaction with pro-caspase-1, are highlighted[31]. (**b**) Release of LDH and IL-1β from LPS-primed immortalized $Asc^{-/-}$ BMDMs and $Asc^{-/-}$BMDMs expressing ASC^{FL}, ASC^{D130R} or ASC^{D134R} 3 h after poly(dA:dT) transfection (1 μg ml^{-1}). (**c**,**d**) Representative images of cell lines from (**b**) 3 h after poly(dA:dT) transfection (1 μg ml^{-1}) (**c**) or 1 h after ATP treatment (5 mM) (**d**). DNA was stained with Hoechst (blue) and ASC (red). Scale bars, 10 μm. (**e**,**f**) Measurement of the ASC speck diameter in primary C57BL/6 BMDMs transduced with the indicated ratio of mCherry-tagged ASC^{FL} or ASC^{D130R} and transfected with poly(dA:dT) (3 h at 1 μg ml^{-1} (**e**)) or treated with nigericin (1 h, 20 μM (**f**)) after LPS priming. (**g**) Representative images from **e**. DNA was stained with Hoechst (blue) and ASC (red). Scale bars, 5 μm. Data are representative of three (**b**–**d**) independent experiments. Graphs show the mean and s.d. from quadruplicate wells (**b**) or triplicate coverslips (**e**,**f**). The numbers of specks measured were 99, 92, 104, 94 and 108 in (**e**) and 149, 134, 85, 98 and 95 in (**f**). $^{*}P<0.05$, $^{**}P<0.01$ and $^{***}P<0.001$ (one-way analysis of variance). See also Supplementary Figs 2 and 3.

by a non-canonical $NLRC4^{CARD}$–ASC^{PYD} interaction or (iii) via bridging ASC molecules that would be linked with NLRC4 via CARD–CARD interactions and provide their free PYDs as seeds for ASC^{PYD} filament formation. To determine which domain of ASC was necessary for ASC speck formation after NLRC4 activation, we infected the above described cell lines harbouring the single domains of ASC with log-phase *Salmonella enterica* serovar Typhimurium SL1344 (*Salmonella* Typhimurium), a robust activator of NLRC4 (refs 45,46). Consistent with published reports[24,27,47], immortalized $Asc^{-/-}$ BMDMs still induced cell death, whereas efficient IL-1β processing and release required ASC (Fig. 3a). Expression of ASC^{FL} in $Asc^{-/-}$ cells restored IL-1β release, but neither the ASC^{PYD} nor ASC^{CARD} alone were able to functionally restore inflammasome activation (Fig. 3a). We next analysed whether the ASC^{PYD} or ASC^{CARD} would form specks or filaments after NLRC4 activation by microscopy. Although ASC^{FL} formed specks, ASC^{PYD} alone did not initiate filaments following activation of NLRC4 (Fig. 3b,c), which was in contrast to what we had observed for PYD-containing receptors (Fig. 1c). In addition, cells expressing ASC^{CARD} alone did not form any specks or macromolecular filaments, again suggesting that the ASC^{CARD} in the endogenous setting is not able to form filaments (Fig. 3b,c). These results exclude the possibilities that ASC specks form via CARD oligomerization after NLRC4 activation, or that a heterotypic $NLRC4^{CARD}$–ASC^{PYD} interaction initiates ASC filament formation. Instead, they suggest that one or several bridging molecules of ASC are required to initiate ASC filament formation

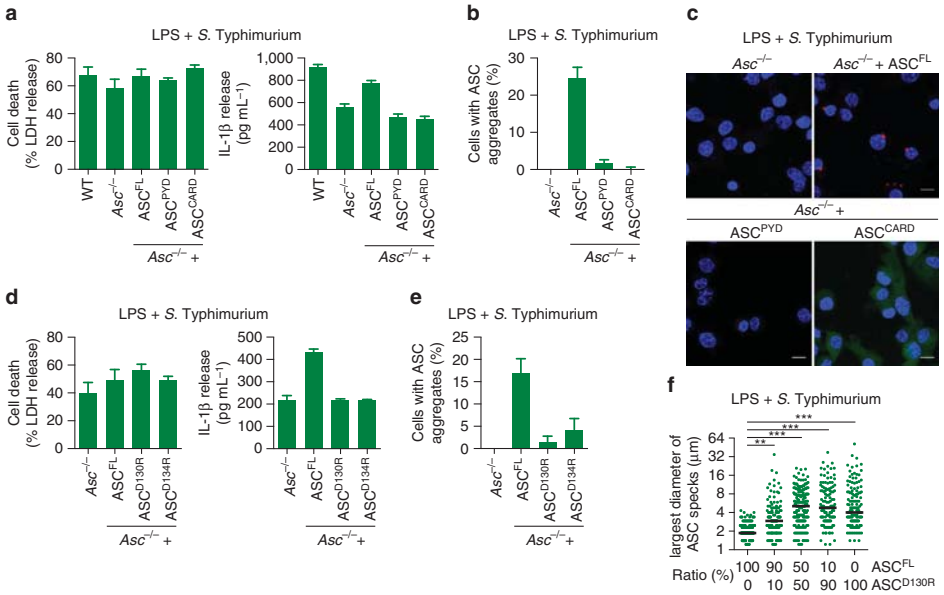

Figure 3 | A bridging ASC molecule is required for ASC speck formation after NLRC4 activation. (**a**) Release of LDH and IL-1β from LPS-primed immortalized WT, *Asc*$^{-/-}$ or *Asc*$^{-/-}$ BMDMs expressing ASC^{FL}, ASC^{PYD} or ASC^{CARD} after infection with log-phase WT *S.* Typhimurium SL1344 (multiplicity of infection (MOI) 10 for 1 h). (**b**) Quantification of the percentage of cells from **a** with ASC specks or filaments (collectively referred to as ASC aggregates). (**c**) Representative images of cell lines from **b**. DNA (blue, Hoechst) and ASC (red). Scale bars, 10 μm. (**d**) Release of LDH and IL-1β from LPS-primed *Asc*$^{-/-}$ BMDMs and *Asc*$^{-/-}$ BMDMs expressing ASC^{FL}, ASC^{D130R} or ASC^{D134R} after infection with log-phase WT *S.* Typhimurium SL1344 (MOI 10 for 1 h). (**e**) Quantification of the percentage of cells with ASC aggregates from **d**. (**f**) Measurement of the ASC speck diameter in primary C57BL/6 BMDMs transduced with the indicated ratio of mCherry-tagged ASC^{FL} or ASC^{D130R} and infected with log-phase WT *S.* Typhimurium SL1344 (MOI 10 for 1 h) after LPS priming. Data are representative of three (**a**–**e**) independent experiments. Graphs show the mean and s.d. from quadruplicate wells in (**a**,**c**–**e**) and triplicate coverslips in **f**. The numbers of specks measured were 194, 134, 184, 128 and 141 in **f**. $^{*}P<0.05$, $^{**}P<0.01$ and $^{***}P<0.001$ (one-way analysis of variance). See also Supplementary Fig. 3.

after NLRC4 activation, and that in these conditions ASC oligomerization into filaments and specks also proceeds via the ASC^{PYD}.

We also examined cells expressing ASC^{D130R} and ASC^{D134R} mutants, which are defective for CARD–CARD interactions (Supplementary Fig. 2g,h (ref. 31)). As expected, expression of these mutants in *Asc*$^{-/-}$ macrophages did not complement the release of mature IL-1β after NLRC4 activation (Fig. 3d). Furthermore, we did not observe the formation of filaments or specks in cells expressing ASC^{D130R} or ASC^{D134R} (Fig. 3e), confirming the requirement for a functional ASC^{CARD} for ASC oligomerization by NLRC4. Finally, we also tested our notion that the ASC^{CARD} is required to condense ASC filaments into a speck in the context of NLRC4 activation. Primary WT C57BL/6 BMDMs (containing endogenous ASC, thus enabling initiation of ASC oligomerization) were retrovirally transduced with varying ratios of mCherry-tagged ASC^{FL} or ASC^{D130R} and the speck diameter was measured on *S.* Typhimurium infection (Fig. 3f). The increase in speck size concurring with increasing concentrations of the ASC^{D130R} mutant indicated that also in the NLRC4 inflammasome the ASC^{CARD} condenses the ASC filaments into the speck. In conclusion, our results suggested a triple functional role for ASC^{CARD} in the NLRC4 inflammasome: (1) mediating the interaction with pro-caspase-1 (refs 17,31), (2) condensing ASC^{PYD} filaments into the speck and (3) initiating ASC oligomerization through bridging ASC molecules (Supplementary Fig. 3b).

Pyroptosis induction is independent of ASC oligomerization. Having elucidated the general architecture of the ASC speck, we next investigated whether the ASC speck constitutes the active, signalling-competent inflammasome. Higher-order signalosomes were reported for other innate immune signalling pathways (Toll-like receptors, receptor-interacting serine/threonine-protein kinase 2 (RIP2K) and MAVS) and could promote signal amplification and digital all-or-nothing responses[48], leading us to hypothesize that ASC oligomerization and filament formation might have a similar function for inflammasome signalling.

Within the ASC^{PYD} filaments that form the backbone of ASC specks in human and murine cells (Supplementary Fig. 4a (refs 13,15)), individual ASC^{PYDs} interact with other six adjacent ASC^{PYDs} through three asymmetric interfaces, types I–III (Fig. 4a). Mutations targeting these interfaces can abrogate ASC filament formation *in vitro* or in cell overexpression systems[13,29,49]. As these mutations also most probably abrogate the interaction between the receptor^{PYD} and ASC^{PYD}, and/or were only tested in an artificial overexpression system, a definite confirmation that ASC filament formation is required for inflammasome signalling is still missing[50]. Identification of mutations that abrogate ASC oligomerization but leave ASC–receptor interaction intact allowed us to characterize the role of ASC filaments in inflammasome signalling. Therefore, we generated a number of clonal immortalized *Asc*$^{-/-}$ macrophage lines expressing different mCherry-tagged ASC mutants targeting all three interaction interfaces (Fig. 4a and Supplementary

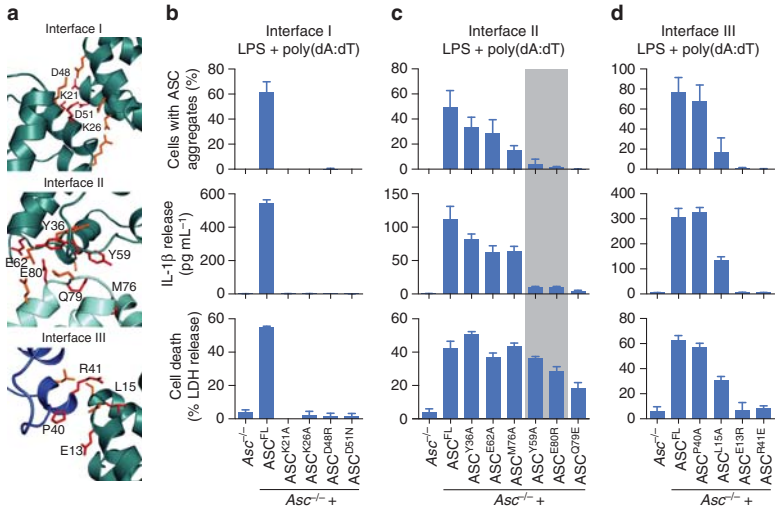

Figure 4 | Mutations in interface II uncouple speck formation and IL-1β release from cell death. (**a**) Detailed view of the three interaction interfaces forming the ASC^{PYD} filament (PDB 2N1F (ref. 15), shown in Supplementary Fig. 4a). The polypeptide backbones are shown in ribbon representation. All amino acid side chains involved in intersubunit contacts are shown as stick models. Residues mutated in this study are coloured red with their sequence label. (**b**–**d**) Quantification of ASC aggregates or the release of LDH and IL-1β from LPS-primed immortalized *Asc*$^{-/-}$ BMDMs and *Asc*$^{-/-}$ BMDMs expressing ASC^{FL} or the indicated ASC mutants 3 h after poly(dA:dT) transfection (1 μg ml^{-1}). ASC^{Y59A} and ASC^{E80R} are highlighted in grey. Graphs show means and s.d. from quadruplicate wells or ten random fields of view. Data are representative of at least three independent experiments. See also Supplementary Figs 4 and 6.

Fig. 4b–d). Next, we assessed the effects of these mutations on ASC speck/filament formation on AIM2 activation by poly(dA:dT) transfection. Mutations targeting interface I (that is, K21A, K26A, D48N and D51R) completely abrogated the filament formation as determined by microscopy (Fig. 4b upper panel and Supplementary Fig. 4e). This is consistent with interface I being the most extensive interface and required for the propagation of single layers of the filament[13,15]. In contrast, mutations in interfaces II and III displayed a larger variability, ranging from no defect in ASC speck formation (Y36A, E62A (interface II) or P40A (interface III)), intermediate phenotypes (M76A (interface II) or L15A (interface III)) to complete abrogation in ASC speck formation (Y59A, Q79E, E80R (interface II) or E13R and R41E (interface III)) (Fig. 4c,d upper panels and Supplementary Fig. 4e). Taken together, these data suggest that the formation of ASC specks requires all three interfaces of ASC^{PYD}.

We next tested how these mutations affect downstream inflammasome signalling by measuring IL-1β secretion (Fig. 4b–d middle panels) and pyroptosis (Fig. 4b–d lower panels). In line with the loss of ASC speck formation, interface I proved to be essential for induction of downstream inflammasome signalling (Fig. 4b). Macrophages expressing mutants in interface III of ASC^{PYD} displayed similar phenotypes as interface I mutations: the ability to form ASC specks correlated with both IL-1β secretion and pyroptosis, that is, mutants either lost all inflammasome signalling (E13R and R41E), were partially affected (L15A) or not affected at all (P40A) (Fig. 4d). These results show that interface III is important for induction of downstream inflammasome signalling, albeit some mutations are tolerated.

Mutants in interface II displayed a differential signalling phenotype (Fig. 4c). Although some mutations had no or only a very small effect on inflammasome signalling (Y36A, E62A and M76A) or abrogated inflammasome signalling altogether (Q79E), we identified two mutations (Y59A and E80R) that retained the ability to induce cell death, while losing the ability to release mature IL-1β and to form ASC specks in response to AIM2 stimulation (Fig. 4c middle and lower panels, highlighted in grey). Of note, the ELISA assay displays a higher sensitivity for the mature form of IL-1β than the pro-form, thus pro-IL-1β, which is potentially released into the supernatant by pyroptosis, is poorly detected (Supplementary Fig. 5). To test whether the phenotype of the different mutants is specific to the AIM2 inflammasome, we analysed ASC speck formation, secretion of mature IL-1β and pyroptosis in response to NLRP3 stimulation by ATP treatment. *Asc*$^{-/-}$ macrophages expressing the ASC interface I, II and III mutants showed the same phenotype for NLRP3 stimulation as for AIM2 stimulation (Supplementary Fig. 6a–c). Importantly, also ASC^{Y59A} and ASC^{E80R} mutations abrogated speck formation and IL-1β secretion but still promoted pyroptosis on NLRP3 stimulation (Supplementary Fig. 6b, highlighted in grey). Finally, we also examined IL-1β release and pyroptosis of macrophages expressing interface II mutants treated with *Clostridium difficile* Toxin B (TcdB). TcdB was recently described to activate the pyrin inflammasome, which senses modifications of Rho GTPases[6]. Again, *Asc*$^{-/-}$ macrophages expressing ASC^{Y59A} or ASC^{E80R} were competent for cell death induction but could not efficiently release IL-1β (Supplementary Fig. 6d, highlighted in grey). In conclusion, our site-directed mutagenesis approach identified two mutations, Y59A and E80R, in the inflammasome adaptor ASC that uncouple pyroptosis from ASC speck formation and cytokine secretion.

ASC oligomerization mutants maintain receptor interaction. As cell death was still observed in cells expressing ASC^{Y59A} and ASC^{E80R}, we speculated that the mutant proteins retained the ability to interact with the PYD of the receptor, but lost the

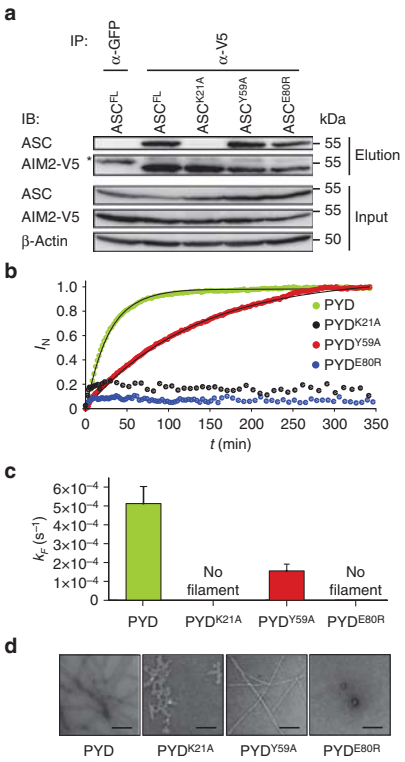

Figure 5 | ASC–receptor interaction and ASC filament formation can be uncoupled genetically. (**a**) Western blot analysis of the interaction of AIM2 with ASC^{FL} or the indicated ASC mutants. AIM2-V5 was immunoprecipitated from lysates of HEK293T cells co-transfected with AIM2-V5 and the indicated ASC mutants. Co-immunoprecipitating proteins were identified using anti-ASC and anti-V5. *Immunoglobulin heavy chain. Results shown are representative from two independent experiments. (**b**) Filament formation of WT ASC^{PYD} and its single amino-acid variants K21A, Y59A and E80R *in vitro* monitored by dynamic light scattering. Normalized growth signals (I_N) are reported as a function of time for one representative experiment for each variant (dots). Best fits to single exponential functions are shown with solid lines. (**c**) Kinetic rate constants k_F of filament formation obtained from three independent experiments. (**d**) Representative negative-stained TEM micrographs of filament formed by ASC^{PYD} and its variants after 350 min of incubation at physiological pH condition. Scale bars, 200 nm. See also Supplementary Figs 7 and 9.

ability to oligomerize into ASC filaments. To investigate this, we reconstituted the AIM2 inflammasome by co-expressing V5-tagged AIM2 with ASC^{FL} or the ASC^{K21A}, ASC^{Y59A} or ASC^{E80R} mutants in HEK293T cells. AIM2 interactors were then immunoprecipitated using an anti-V5 antibody and analysed by western blotting (Fig. 5a). Consistent with our notion, ASC^{Y59A} and ASC^{E80R} retained the ability to interact with AIM2, similar to WT ASC. In contrast, ASC^{K21A} did not interact with AIM2, possibly explaining the clear-cut phenotypes of interface I mutants (Fig. 4b and Supplementary Fig. 6b).

Given that ASC^{Y59A} and ASC^{E80R} mutants still interacted with the receptor (Fig. 5a), but did not form any ASC filaments/specks (Fig. 4c and Supplementary Fig. 4e), we speculated that the mutations abolished or reduced the ability of ASC to organize itself into filaments following the recruitment to the activated receptor. Based on our previous observation that purified ASC^{PYD} or ASC^{FL} form filaments *in vitro*[15], we established an assay to monitor the kinetics of this oligomerization process by dynamic light scattering and analysed the kinetics of filament formation for WT ASC^{PYD} and the above-mentioned mutants (Fig. 5b,c and Supplementary Fig. 7a,b). Although WT PYD rapidly formed well-structured filaments, the K21A mutant was no longer able to oligomerize correctly and formed unspecific aggregates (Fig. 5d). Interestingly, E80R also lost the ability to oligomerize into ordered filaments, whereas the Y59A mutant formed well-ordered filaments, but at a much slower rate than the WT protein (Fig. 5b–d and Supplementary Fig. 7a,b). Thus, these results confirmed that the ASC–receptor interaction and the ASC filament formation can be uncoupled, and that the ability to rapidly form filaments/specks strongly correlates with the levels of cytokine production but not cell death.

Gasdermin-D cleavage is independent of ASC oligomerization. The observation that even in the absence of ASC oligomerization inflammasome activation still promotes cell death but not cytokine release (Fig. 4c, Supplementary Fig. 4e) was reminiscent of NLRC4 activation in *Asc*$^{-/-}$ macrophages[24]. In the absence of ASC, NLRC4 interacts with pro-caspase-1 to initiate cell death but not efficient caspase-1 autoprocessing and cytokine secretion. We therefore examined to what level ASC^{Y59A} and ASC^{E80R} were able to promote caspase-1 autoprocessing on activation of the AIM2 inflammasome. In contrast to cells expressing ASC^{FL}, macrophages expressing the mutant proteins displayed significantly reduced levels of caspase-1 processing, as determined by western blotting for the released p20 subunit (Fig. 6a). Furthermore, caspase-1 autoprocessing correlated with the amount of released bioactive IL-1β (Figs 4c and 6a), but not with the induction of cell death (Fig. 4c) and the release of the danger signal high mobility group box 1 (HMGB1) into the cell supernatants (Fig. 6a), an alternative marker for cell lysis during inflammasome activation[51]. Similarly, results were obtained on activation of the NLRP3 inflammasome (Supplementary Fig. 8a). To exclude the possibility that the observed cell death is induced through caspase-1-independent pathways, we knocked out *Casp1* by CRISPR-Cas9-mediated gene targeting[52,53] in the cell lines expressing ASC^{FL}, ASC^{Y59A} or ASC^{E80R}. Western blotting for pro-caspase-1 confirmed successful targeting (Supplementary Fig. 8b). *Casp1* deficiency significantly abrogated pyroptosis induction in cells expressing ASC^{FL}, ASC^{Y59A} or ASC^{E80R} (Fig. 6b), thus confirming that the cell death observed in the parental cell lines was caspase-1 dependent. Taken together, these data confirm that caspase-1 processing is not a prerequisite for induction of cell death, expanding previous findings from CARD-containing inflammasome receptors[24] to PYD-containing receptors.

Recent reports showed that a major substrate of caspase-1 responsible for pyroptosis is gasdermin-D, and that *Gsdmd*-deficiency abrogates pyroptosis[11,12]. Caspase-1 cleaves full-length gasdermin-D, whereby the active N-terminal fragment (gasdermin-D^{Nterm}) is generated (Supplementary Fig. 8c,d), which induces pyroptotic cell death[11,12]. Consistently, CRISPR-Casp9-mediated *Gsdmd* knockout (Supplementary Fig. 8e) reduced cell death significantly in response to AIM2 and NLRP3 activation (Supplementary Fig. 8f,g). As ASC^{Y59A} and ASC^{E80R} mutants induced cell death, we speculated that gasdermin-D is still processed in cells expressing these mutant forms of ASC. Indeed, although gasdermin-D was not processed in *Asc*$^{-/-}$ macrophages on stimulation of AIM2 or NLRP3, we observed gasdermin-D processing to its 30 kDa gasdermin-D^{Nterm} fragment in *Asc*$^{-/-}$

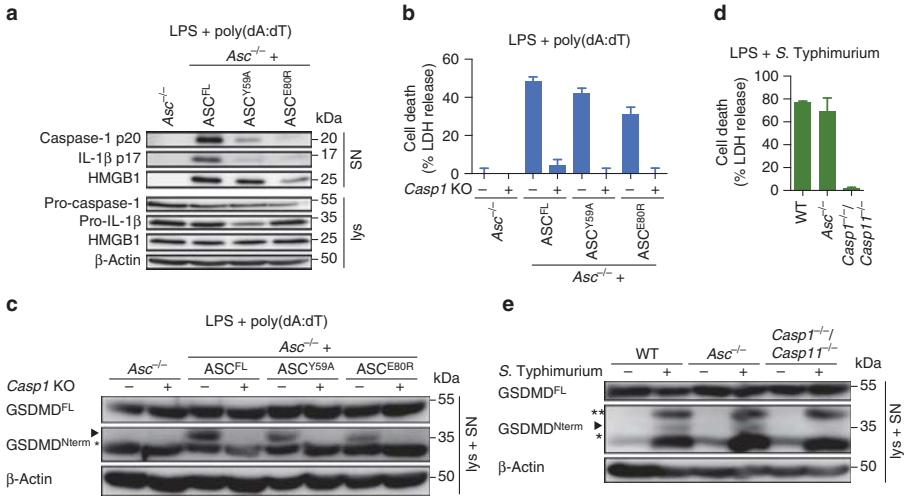

Figure 6 | Caspase-1 but not gasdermin-D processing depends on ASC oligomerization. (**a**) Western blot analysis for cleaved caspase-1 p20, IL-1β p17, and HMGB-1 in cell supernatants (SN) and pro-caspase-1, pro-IL-1β and HMGB-1 in cell lysates (lys) of LPS-primed immortalized *Asc*$^{-/-}$ BMDMs or *Asc*$^{-/-}$ BMDMs expressing ASC^{FL}, ASC^{Y59A} or ASC^{E80R} 3 h after poly(dA:dT) transfection (1 μg ml^{-1}). (**b**) Release of LDH from LPS-primed immortalized *Asc*$^{-/-}$ BMDMs or *Asc*$^{-/-}$ BMDMs expressing ASC^{FL}, ASC^{Y59A} or ASC^{E80R}, or derived *Casp1* knockouts 3 h after poly(dA:dT) transfection (1 μg ml^{-1}). (**c**) Western blot analysis for processing of full-length gasdermin-D (GSDMD^{FL}) into the active N-terminal fragment (GSDMD$^{N\text{-}term}$) in combined lysates and supernatants (lys + SN) of LPS-primed immortalized *Asc*$^{-/-}$ BMDMs expressing ASC^{FL}, ASC^{Y59A} or ASC^{E80R}, or derived *Casp1* knockouts 3 h after poly(dA:dT) transfection (1 μg ml^{-1}). Arrowhead, gasdermin-D^{Nterm} p30; *a cross-reacting band. (**d**) Release of LDH from LPS-primed primary C57BL/6 WT (WT), *Casp1*$^{-/-}$/*Casp11*$^{-/-}$ or *Asc*$^{-/-}$ BMDMs infected with *S.* Typhimurium (multiplicity of infection (MOI) = 10, 1 h). (**e**) Western blot analysis for processing of full-length gasdermin-D (GSDMD^{FL}) into the active N-terminal fragment (GSDMD$^{N\text{-}term}$) in combined lysates and supernatants (lys + SN) of LPS-primed primary C57BL/6 WT (WT), *Casp1*$^{-/-}$/*Casp11*$^{-/-}$ or *Asc*$^{-/-}$ BMDMs infected with *S.* Typhimurium (MOI = 10, 1 h) or left uninfected. Arrowhead, gasdermin-D^{Nterm} p30; *a cross-reacting band; ** a *S.* Typhimurium-specific cross-reactive band. See also Supplementary Figs 8 and 9.

macrophages expressing ASC^{FL}, ASC^{Y59A} and ASC^{E80R} (Fig. 6c and Supplementary Fig. 8h). Furthermore, processing of gasdermin-D on AIM2 stimulation is dependent on caspase-1 in cells harbouring oligomerization-deficient ASC mutants, as *Casp1* deficiency abrogated gasdermin-D cleavage (Fig. 6c). These results indicated that gasdermin-D^{Nterm} causes the cell death observed in these mutations. As significant levels of cell death can be observed in *Asc*-deficient macrophages after NLRC4 activation[24], but caspase-1 processing is reduced below detection levels, we next determined whether gasdermin-D is processed under these conditions. Indeed, we found that the induction of cell death in *S.* Typhimurium-infected WT, *Asc*$^{-/-}$ and *Casp1*$^{-/-}$/*Casp11*$^{-/-}$ macrophages (Fig. 6d) correlated with detectable levels of processed gasdermin-D (Fig. 6e). Furthermore, CRISPR-Cas9-mediated *Gsdmd* knockout confirmed that gasdermin-D played an essential role in inducing pyroptosis during *S.* Typhimurium infections (Supplementary Fig. 8i). Taken together, these results confirm that even the smallest amounts of active caspase-1, as judged by the amount of processed caspase-1 p20 subunits, are sufficient to efficiently process gasdermin-D and trigger gasdermin-D-induced cell death. On the other hand, large amounts of processed, active caspase-1 are required to produce detectable amounts of mature, bioactive IL-1β as seen by the direct correlation of the level of caspase-1 processing with the levels of cytokine release. Importantly, the ability of ASC to form filaments and ASC specks correlates with caspase-1 activation and cytokine processing, thus supporting a model in which the rapid formation of ASC filaments acts as a signal amplification mechanism for inflammasomes, generating a multitude of caspase-1 activation sites and thus enabling the cells to rapidly mature IL-1β before the onset of pyroptosis.

Discussion

The formation of higher-order signalling machineries, signalosomes, for transmission of receptor activation information to cellular responses is an emerging theme in signal transduction[48]. It is particularly important in innate immune signalling, where the signal generated by a few ligand–receptor interactions needs to trigger an appropriate cellular response. Formation of oligomers has been reported for different signalling adaptors, for example, B-cell lymphoma/leukemia 10 (Bcl10) or MAVS filaments, the Myddosome[36,54,55] and others. However, the archetypical supramolecular assembly formed during inflammasome activation, the ASC speck, has remained relatively poorly understood. Here we present evidence that the formation of ASC speck by oligomerization of the inflammasome adaptor protein ASC acts as a signal amplification mechanism for inflammasomes (Fig. 7), as the rapid formation of ASC^{PYD} filaments that expose ASC^{CARD} on their surface creates a multitude of pro-caspase-1 recruitment and activation sites. We speculate that such a system might therefore be able to detect the smallest amounts of PAMPs in the host cell cytosol, as recent reports have shown that a single ligand molecule (flagellin, PrgJ) is sufficient to initiate assembly of a NLR family, apoptosis inhibitory protein (NAIP) and 10–12 NLRC4 proteins into a wheel-shaped receptor oligomer that acts as seed for ASC oligomerization[39,56].

Our result reveals that this signal amplification mechanism only applies to cytokine maturation, whereas gasdermin-D-

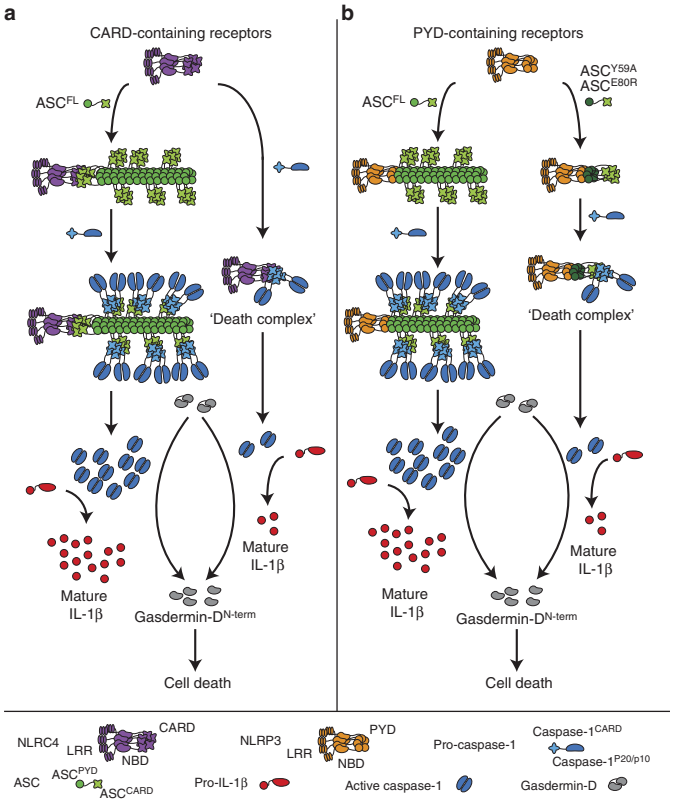

Figure 7 | Model of signal amplification by ASC filaments. (**a**) CARD-containing receptors recruit the adaptor protein ASC via homotypic CARD–CARD interactions, that is, a bridging ASC molecule. This step nucleates the ASC^{PYD} of several bridging ASC molecules, leading to the formation of an ASC^{PYD} filament, which is condensed into the ASC speck by the ASC^{CARD}. Filament formation promotes the activation of large quantities of caspase-1, thus promoting the proteolytic maturation of large amounts of cytokines (pro-IL-1β). In the absence of ASC, CARD-containing receptors directly interact with pro-caspase-1, leading to the formation of so-called 'death complexes'. In these small complexes, only few molecules of caspase-1 are activated and pro-caspase-1 processing might not happen. The few molecules of caspase-1 are sufficient to effectively induce pyroptosis, but cytokine processing is reduced. (**b**) PYD-containing receptors can directly interact with ASC via homotypic PYD–PYD interactions, leading to ASC^{PYD} filaments and finally the ASC speck. As for CARD-containing receptors, this leads to caspase-1 activation and subsequent cytokine processing and pyroptosis. Mutations blocking or slowing ASC filament formation (for example, ASC^{E80R} or ASC^{Y59A}) only allow for few molecules of caspase-1 being activated. This is sufficient to induce pyroptosis, but insufficient to produce large amounts of mature cytokines before the cell lyses.

induced pyroptotic cell death could be observed even in the absence of ASC oligomerization. Why would cells need to amplify the receptor-generated signal to process IL-1β/-18? We speculate that a cell will inevitably progress towards pyroptosis, once a few molecules of caspase-1 have been activated, given the rapid kinetics by which gasdermin-D is processed[57] and the strong toxicity of the gasdermin-D^{Nterm} fragment[11,12]. This fate leaves a limited time window to mature the pro-forms of IL-1β/-18 to their bioactive form. As processing of IL-1β/-18 occurs with slow kinetics, increasing the amount of active caspase-1 is a means to generate large amounts of bioactive IL-1β/-18 in the available time window. Consistent with this notion we have observed that gasdermin-D processing does not correlate with the overall level of active caspase-1. Furthermore, pyroptosis has been observed to occur within 30–60 min in stimulated cells, whereas ASC speck formation was reported to proceed much faster[23,58], with all cytosolic ASC being incorporated into a speck in <3 min[20,59]. Thus, ASC speck formation might serve to activate sufficient amounts of caspase-1 to generate enough bioactive cytokines before the cell lyses and releases its intracellular content, including proteolytically matured cytokines.

Although recent studies revealed that ASC specks are filamentous in nature[22,23], consistent with recently reported structures of human and murine ASC^{PYD} filaments[13,15], it was so far unknown how these filaments assemble into a speck. Our mutagenesis studies indicates that the clustering of ASC^{PYD} filaments and finally their condensation into a dense ASC speck structure is mediated by the ASC^{CARD}, which, as we have shown[15], is exposed on the surface of the ASC^{PYD} filament. These results have uncovered a function for the ASC^{CARD} in ASC speck formation, beyond its role as adaptor domain between receptor and caspase-1. How ASC^{CARDs} condense ASC^{PYD} filaments is unknown, but it can be assumed that either dimeric interactions between ASC^{CARDs} or limited oligomerization of ASC^{CARD} from different filaments could build lattices interconnecting the ASC^{PYD} filaments. Interestingly, the same residues in ASC^{CARD}

that are required for ASC–pro-caspase-1 interaction are also needed for ASC speck formation. Notably, it has previously been shown that phosphorylation of the ASC^{CARD} at Y144/Y146 is not only required for caspase-1 activation, but also for ASC speck formation[60,61] Our model of the ASC speck, which includes interactions between the ASC^{CARD} domains, now provides a structural rationale for these data. To which extent ASC filaments are still formed in the absence of ASC^{CARD} phosphorylation remains to be determined.

Recently, a unified assembly mechanism was proposed for the PYD-containing receptors AIM2 and NLRP3: the receptors nucleate clusters of ASC through PYD–PYD interactions, which in turn nucleate caspase-1 filaments[13]. In analogy, it was proposed that the CARD-containing receptor NLRC4 directly nucleates caspase-1 filaments[13,39], as in theory CARD-containing receptors do not require ASC for caspase-1 recruitment. Although direct recruitment of pro-caspase-1 to NLRC4 might indeed happen in *Asc*-deficient cells as we hypothesized before[24], it does not seem to efficiently activate caspase-1, because we and others have reported that caspase-1 processing into its p20/p10 subunits and the levels of released mature cytokines are reduced. Furthermore, a large number of ASC specks can be observed in WT cells on NLRC4 activation[24–28], indicating that ASC nevertheless plays an important role in NLRC4 signalling. Our results now indicate that the ASC^{CARD} lacks the ability to form higher-order oligomers at physiological concentrations, and that even on NLRC4 activation ASC speck formation relies on the ASC^{PYD}. Our data thus support a model in which CARD-containing receptors initiate ASC speck formation with the help of ASC bridging molecules, and that the PYDs of these ASC molecules nucleates an ASC^{PYD} filament. Thus, the ASC^{CARD} can have a triple function in inflammasome signalling on CARD-receptor activation.

In conclusion, our study gives insights into the architecture of the ASC speck and the mechanism by which ASC filaments assemble this structure. Furthermore, we provide experimental evidence that ASC filament formation serves as an amplification mechanism in inflammasome signalling, and that this amplification serves to generate sufficient mature cytokines before the onset of pyroptotic cell death. Nevertheless, important questions remain; the higher-resolution structure of the activated NLRC4 receptor has been recently reported[39,56], yet how exactly such receptor complexes with C_{10}–C_{12} stoichiometry initiate the 3-start ASC^{PYD} filaments is still unknown. Furthermore, the structure of the whole ASC speck assembly, including receptor, ASC and caspase-1, is still lacking and it remains unknown whether other proteins participate in its formation. Finally, additional theoretical and experimental approaches will be necessary to understand if and how ASC speck formation might impart threshold responses, reduce biological noise and control temporal and spatial control of inflammasome signalling.

Methods

Cell culture. Immortalized BMDM cell lines were generated from bone marrow using infection with a v-myc/v-raf-expressing J2 retrovirus[24,62]. WT and *Asc*$^{-/-}$ immortalized murine BMDMs were cultured in DMEM (Sigma) supplemented with 10% FCS (Bioconcept) and 10% 3T3-MCSF supernatant, and incubated at 37 °C with 5% CO_2.

Generation of monoclonal cell lines with mutations in ASC. Murine *Asc*^{FL} and *Asc*^{PYD} were cloned with a carboxy-terminal mCherry tag and *Asc*^{CARD} with an N-terminal enhanced GFP tag into V48, a derivative of the replication-defective murine stem cell retroviral construct pMSCV2.2 (excision of the IRES-GFP by EcoRI digestion, gift from Thomas Henry). Mutations were introduced by SOE PCR using appropriate oligonucleotides (Supplementary Table 1) and cloned into V48. GP2 packaging cells were transfected with the individual vectors (9 µg per 1.5×10^6 cells) and the lentviral envelope vector VSV-G (Addgene, 6 µg per 1.5×10^6 cells), and the retroviral particles were used to transduce *Asc*$^{-/-}$ iBMDMs (10^6 cells). Seven days later, the transduced iBMDMs were sorted into single cells based on the mCherry or enhanced GFP expression (FACS) and grown up to clonal cell lines. Up to ten clones of each cell line were tested for inflammasome activation and the level of ASC expression was assessed by western blotting and a representative clone was selected for further analysis.

Retroviral transduction of primary BMDMs. For transduction of primary bone marrow cells, retroviral particles were generated in Phoenix-Eco packaging cells and used to transduce WT C57BL/6 bone marrow cells after 48 and 72 h of culture in medium with 10% 3T3-MCSF supernatant. Inflammasome stimulation was performed 4 days after the first transduction[24].

Inflammasome stimulation. Immortalized BMDMs (seeded at 250 000 cells per ml in 96-well plates) were primed for 4 h with 100 ng ml^{-1} LPS O55:B5 (Invivogen). The NLRP3 inflammasome was triggered by addition of 5 mM extracellular ATP (Sigma-Aldrich) for 60 min. The AIM2 inflammasome was triggered by transfection of 1 µg ml^{-1} of the synthetic DNA analogue poly(dA:dT) (Invivogen) using Lipofectamine 2000 (Invitrogen), according to the manufacturer's protocol, in OptiMEM (Gibco) for 3 h. The NLRC4 inflammasome was triggered by infection of the cells with *S. enterica* serovar Typhimurium SL1344 at a multiplicity of infection of 10. The infection was synchronized by centrifugation and continued for 60 min. The pyrin inflammasome was triggered by addition of 1 µg ml^{-1} (final concentration) of *C. difficile* toxin B (CdtB, Enzo Biotech) for 2.5 h.

Cell death and IL-1β release measurements. IL-1β release was measured by ELISA (eBiosciences). Cell death was quantified by measuring LDH release using the LDH Cytotoxicity detection kit (TaKaRa Clontech). To normalize for spontaneous cell lysis, the percentage of cell death was calculated as follows: [(LDH sample) − (LDH negative control)]/[(LDH positive control) − (LDH negative control)] × 100.

Imaging and quantification of ASC speck formation. Cells were seeded on coverslips (150 000 cells per coverslip) and treated as described above with the addition of 25 µM Z-VAD-fmk (Bachem) to prevent detachment of pyroptotic cells and therefore loss of cells with ASC specks. Coverslips were fixed with 4% paraformaldehyde (PFA) (15 min, 37 °C, Alfa Aesar) and washed with PBS. Nuclei were stained with Hoechst 33342 (Life Technologies) for 10 min and the slides mounted using Vectashield (Vector Laboratories). For quantifications of ASC aggregates (specks or filaments), ten random regions of interest were imaged at × 20 magnification (Leica DMI3000B inverted fluorescence microscope, HCX PL FLUOTAR objective, Leica DFC3000G camera and LAS AF Version 3 software) and the number of ASC aggregates and cells were counted. For representative images, the slides were imaged at × 63 magnification (Leica point scanning confocal 'SP8', HC PL APO CS2 × 63 objective, Leica AF software version 3). For measurements of speck sizes, random regions of interest were images at × 63 magnification (Leica point scanning confocal 'SP8') and the largest diameters of individual specks were measured using Fiji[63].

Western blotting. For western blotting of supernatant and lysate samples, cells were seeded at 10^6 cells per well in six-well plates and treated as described above. Supernatants were precipitated with 10% trichloracetic acid, precipitates washed with acetone and resuspended in 40 µl 1 × SDS–PAGE sample buffer and boiled at 95 °C for 10 min. Cells were lysed with 200 µl 1 × RIPA (50 mM Tris-HCl pH 7.5, 150 mM NaCl, 0.1% SDS, 0.5% sodium deoxycholate, 1% NP-40, 1 × protease inhibitor cocktail (Roche)) for 30 min on ice. Lysates were re-suspended in 5 × SDS–PAGE sample buffer and boiled at 95 °C for 10 min[64]. For combined supernatant and lysates, samples were prepared as above, but supernatant precipitates were resuspended in lysate samples. Samples were run on 14% (supernatants or lysates) or 12% (combined SN + lysates) acrylamide gels (1 h, 170 V, 40 mA per gel), transferred to polyvinylidene difluoride membranes (1 h, 100 V constant), blocked in 5% milk in Tris-buffered saline + Tween-20 (TBS-T) and incubated with primary antibodies in 5% BSA–TBS-T for 16 h at 4 °C or 2 h at room temperature with agitation. Secondary antibodies were diluted 1:5,000 in 5% milk–TBS-T and incubated for 1 h at room temperature. The membranes were developed using either LumiGLO (KPL) or LumiGLO Reserve (KPL). The following antibodies and dilutions were used: rat anti-Caspase-1 p20 (Genentech, 1:1,000; Supplementary Figs 1b,d and 2c,d) or mouse anti-Caspase 1 p20 (1:4,000, AG20B-0042, AdipoGen; Fig. 6a and Supplementary Fig. 8a), rat anti-ASC (Genentech, 1:2,000; Fig. 5a and Supplementary Fig. 2a,h) or rabbit anti-ASC (1:1,000, AG25B-006, Adipogen, all other figures), rabbit anti-IL-18 (5180R-100, Biovision, 1:1,000), goat anti-IL-1β (AF-401-NA, R&D, 1:1,000), mouse anti-GFP (632381, Clontech, 1:1,000), mouse anti-mCherry (ab125096, Abcam, 1:1,000), mouse anti-V5 (R960-25, Invitrogen, 1:1,000), rabbit anti-HMGB1 (GTX-101277, Genetex, 1:1,000), mouse anti-gasdermin-D (GSDMDC1 (A-7), Santa Cruz Biotechnology, 1:1,000; Supplementary Fig. 7), rabbit anti-gasdermin-D (1:2,000, G7422, Sigma, all other figures) and mouse anti-β-actin (A1987, Sigma, 1:1,000).

Co-immunoprecipitation. Co-immunoprecipitation was done according to a modified protocol published previously[49]. For assessment of ASC/AIM2 interactions, 3 × 800,000 HEK293T cells were transfected with 2 µg per well AIM2-V5 and ASC-mCherry (ASC^{FL}, ASC^{K21A}, ASC^{Y59A} or ASC^{E80R}) encoding plasmids at a ratio of 1:4 using linear polyethylenimine (PEI, Polysciences) at a ratio DNA:PEI of 1:4 (refs 65,66). Twenty-four hours after transfection, the cells were washed twice with ice-cold 1 × PBS and lysed using HEK lysis buffer (20 mM HEPES pH 7.4, 10 mM KCl, 1 mM EDTA, 0.1 mM phenylmethylsulfonyl fluoride, 1 mM Na_3VO_4, 5 mM NaF, 0.5 % Nonidet P-40 and 1 × protease inhibitor cocktail (Roche)). Lysates were sonicated for 5 × 7 s before removing debris and non-lysed cells by centrifugation (10,000 *g*, 15 min, 4 °C). The samples were incubated with 1 µg mouse anti-V5 antibody (R960-25, Invitrogen) or a control antibody (mouse anti-GFP, 632381, Clontech) with agitation for 16 h at 4 °C. For assessment of ASC^{CARD}/ASC^{CARD} interactions, 3 × 800 000 HEK293T cells were transfected with 1 µg per well ASC-mCherry (ASC^{FL}, ASC^{PYD}, ASC^{D130R} or ASC^{D134R}), 1 µg per well ASC^{CARD}-GFP and 0.2 µg AIM2-V5, to initiate ASC/ASC interactions using linear PEI. Forty hours after transfection, the cells were washed, lysed and sonicated as described above. The samples were then incubated with 1 µg mouse anti-mCherry antibody (ab125096, Abcam) or a control antibody (mouse anti-HA, MMS-101R-200, Covance). The samples were then incubated with agitation for 2 h at 4 °C with 25 µl Pierce Protein A Plus Agarose bead slurry (22810, Thermo Scientific). Beads were washed three times with lysis buffer (centrifugation 1 min 1,000 *g*, 4 °C), resuspended in 2 × SDS–PAGE sample buffer (30 µl) and boiled at 95 °C, before analysing the eluted proteins by western blotting as described above.

CRISPR-Cas9-mediated *Caspase1* and *Gasdermin-D* knockout. Two guide RNAs[52] targeting exon 4 of *Casp1* (5′-gagggcaagacgtgtacgag-3′ and 5′-cgagtgg ttgtattcattat-3′) and one guide RNA targeting exon 2 of *Gsdmd* (5′-ggtca agaatgtgatcaagg-3′) were cloned into lentiCRISPRv2 harbouring a puromycin resistance cassette (Addgene[53]). These constructs were transfected into HEK293T cells using PEI (as described above) together with the lentiviral packaging vector PsPax2 (Addgene) and the lentviral envelope vector VSV-G (Addgene). Sixteen hours after transfection, medium was exchanged with macrophage medium and incubated at 37 °C for 2 days to produce lentiviral particles. The lentiviral particles were used to transfect the immortalized macrophage cell lines (800,000 cells per well in 6-well plates) using polybrene (Merck) to favour virus attachment. Two days after viral transduction, the macrophages were expanded. Attached macrophages were then treated with 10 µg ml^{-1} puromycin (Gibco) for 6 days to select for successful lentiviral transduction. After puromycin selection, the cells were tested for successful knockout by western blotting.

Expression and purification of ASC^{PYD}. The ASC^{PYD} (residues 1–91) was cloned with a C-terminal His_6 tag into the pET28a vector under the control of a T7 promoter. Protein expression was induced by isopropyl-β-D-thiogalactopyranosid addition in BL21(DE3) *Escherichia coli* at an OD_{600} of 0.8 for 4 h at 37 °C. Bacteria were harvested by centrifugation and resuspended in 50 mM phosphate buffer pH 7.5, 300 mM NaCl, with Complete protease inhibitor (Roche). Resuspended bacteria were incubated for 1 h at room temperature with DNase I, sonicated on ice and centrifuged at 20,000 *g* at 4 °C for 30 min. The pellet, including ASC^{PYD}-containing inclusion bodies, was solubilized in 50 mM phosphate buffer pH 7.5, 300 mM NaCl, 6 M guanidinium hydrochloride and centrifuged at 20,000 *g* at 4 °C for 30 min. The supernatant was incubated for 2 h at room temperature with pre-equilibrated Ni-NTA affinity resin (Thermo Scientific) and then passed through a plastic body column for gravity flow purification. The column was washed with 20 column volumes of solubilization buffer containing 20 mM imidazole and eluted with 3 column volumes of solubilization buffer with 500 mM imidazole. The pH of the elution fraction was decreased to 3.8 and dialysed against 50 mM glycine buffer pH 3.8, 150 mM NaCl. The protein was further purified on a pre-equilibrated Superdex 75 gel filtration column (GE Healthcare). This gel-filtration step removed traces of pre-existing aggregates and yielded highly pure, monomeric soluble form of ASC^{PYD}. Samples were either used immediately or stored after flash-freezing in small aliquots in liquid N_2.

Measurements of ASC^{PYD} filament formation kinetics *in vitro*. Immediately before the experiments, samples of monomeric soluble ASC^{PYD} were centrifuged at 20,000 *g* at 4 °C for 30 min and filtered with 0.1 µM filter (Millipore). The protein concentration was adjusted to 25 µM by dilution from a higher-concentrated stock solution. Filament formation was triggered by rapid dilution to neutral pH. Thereby, 70 µl of monomeric ASC^{PYD} was mixed with 0.45 µl of 2.75 M NaOH solution to a reach the pH of 7.5. The solution was mixed at room temperature by careful pipetting, to avoid introduction of air bubbles, and immediately transferred to a quartz cuvette with 1 cm path length. Between runs, cuvettes were carefully cleaned with 1 M Hellmanex solution (Sigma-Aldrich) to avoid cross-seeding effects between sequential measurements. Filament growth was monitored by dynamic light scattering with a Malvern Zetasizer Nano ZS series instrument. The laser focal spot was positioned in the middle of the cuvette and maintained fixed for all the measurements. To maximize the intensity of the scattered light, the minimal attenuation level was used. Data were acquired in 60 s intervals by averaging three runs of 20 s, until a total time of 350 min. Afterwards, the protein solution was blotted on EM grids, negatively stained and imaged with transmission electron microscopy to visualize filament formation.

Data analysis. Filament growth was modelled assuming pseudo-first-order kinetics where the filament propagation step occurs by the addition of monomers to the initial growth centre. The time-dependent growth signal I was fitted independently for each measurement by a single exponential function,

$$I(t) = I_{\infty}\left(1 - e^{(-k_F t)}\right)$$

where I_{∞} corresponds to the signal at time t and at infinitive time, respectively, and k_F is the first-order rate constant. Fits were done with nonlinear least-square minimization.

Data availability. The data that support the findings of this study are available from the corresponding author upon request.

References

1. von Moltke, J., Ayres, J. S., Kofoed, E. M., Chavarría-Smith, J. & Vance, R. E. Recognition of bacteria by inflammasomes. *Annu. Rev. Immunol.* **31,** 73–106 (2013).
2. Philpott, D. J., Sorbara, M. T., Robertson, S. J., Croitoru, K. & Girardin, S. E. NOD proteins: regulators of inflammation in health and disease. *Nat. Rev. Immunol.* **14,** 9–23 (2014).
3. Franchi, L., Warner, N., Viani, K. & Nuñez, G. Function of Nod-like receptors in microbial recognition and host defense. *Immunol. Rev.* **227,** 106–128 (2009).
4. Martinon, F., Burns, K. & Tschopp, J. The inflammasome: a molecular platform triggering activation of inflammatory caspases and processing of proIL-beta. *Mol. Cell* **10,** 417–426 (2002).
5. Schroder, K. & Tschopp, J. The inflammasomes. *Cell* **140,** 821–832 (2010).
6. Xu, H. *et al.* Innate immune sensing of bacterial modifications of Rho GTPases by the Pyrin inflammasome. *Nature* **513,** 237–241 (2014).
7. Thornberry, N. A. *et al.* A novel heterodimeric cysteine protease is required for interleuking-1β processing in monocytes. *Nature* **356,** 768–774 (1992).
8. Gu, Y. *et al.* Activation of interferon-gamma inducing factor mediated by interleukin-1beta converting enzyme. *Science* **275,** 206–209 (1997).
9. Ghayur, T. *et al.* Caspase-1 processes IFN-γ-inducing factor and regulates LPS-induced IFN-γ production. *Nature* **386,** 619–623 (1997).
10. Fink, S. L. & Cookson, B. T. Apoptosis, pyroptosis , and necrosis: mechanistic description of dead and dying eukaryotic cells. *Infect. Immun.* **73,** 1907–1916 (2005).
11. Kayagaki, N. *et al.* Caspase-11 cleaves gasdermin D for non-canonical inflammasome signaling. *Nature* **526,** 666–671 (2015).
12. Shi, J. *et al.* Cleavage of GSDMD by inflammatory caspases determines pyroptotic cell death. *Nature* **526,** 660–665 (2015).
13. Lu, A. *et al.* Unified polymerization mechanism for the assembly of ASC-dependent inflammasomes. *Cell* **156,** 1193–1206 (2014).
14. Cai, X. *et al.* Prion-like polymerization underlies signal transduction in antiviral immune defense and inflammasome activation. *Cell* **156,** 1207–1222 (2014).
15. Sborgi, L. *et al.* Structure and assembly of the mouse ASC inflammasome by combined NMR spectroscopy and cryo-electron microscopy. *Proc. Natl Acad. Sci. USA* **112,** 13237–13242 (2015).
16. Martinon, F., Burns, K. & Tschopp, J. The inflammasome: a molecular platform triggering activation of inflammatory caspases and processing of proIL-beta. *Mol. Cell* **10,** 417–426 (2002).
17. Srinivasula, S. M. *et al.* The PYRIN-CARD protein ASC is an activating adaptor for caspase-1. *J. Biol. Chem.* **277,** 21119–21122 (2002).
18. Stehlik, C. *et al.* Apoptosis-associated speck-like protein containing a caspase recruitment domain is a regulator of procaspase-1 activation. *J. Immunol.* **171,** 6154–6163 (2003).
19. Masumoto, J. *et al.* ASC, a novel 22-kDa protein, aggregates during apoptosis of human promyelocytic leukemia HL-60 cells. *J. Biol. Chem.* **274,** 33835–33838 (1999).
20. Fernandes-Alnemri, T. *et al.* The pyroptosome: a supramolecular assembly of ASC dimers mediating inflammatory cell death via caspase-1 activation. *Cell Death Differ.* **14,** 1590–1604 (2007).
21. Broz, P. *et al.* Redundant roles for inflammasome receptors NLRP3 and NLRC4 in host defense against *Salmonella*. *J. Exp. Med.* **207,** 1745–1755 (2010).
22. Franklin, B. S. *et al.* The adaptor ASC has extracellular and 'prionoid' activities that propagate inflammation. *Nat. Immunol.* **15,** 727–737 (2014).
23. Baroja-Mazo, A. *et al.* The NLRP3 inflammasome is released as a particulate danger signal that amplifies the inflammatory response. *Nat. Immunol.* **15,** 738–748 (2014).
24. Broz, P., von Moltke, J., Jones, J. W., Vance, R. E. & Monack, D. M. Differential requirement for Caspase-1 autoproteolysis in pathogen-induced cell death and cytokine processing. *Cell Host Microbe* **8,** 471–483 (2010).

25. Case, C. L., Shin, S. & Roy, C. R. Asc and Ipaf Inflammasomes direct distinct pathways for caspase-1 activation in response to *Legionella pneumophila*. *Infect. Immun.* **77,** 1981–1991 (2009).
26. Mariathasan, S. *et al.* Differential activation of the inflammasome by caspase-1 adaptors ASC and Ipaf. *Nature* **430,** 213–218 (2004).
27. Suzuki, T. *et al.* Differential regulation of caspase-1 activation, pyroptosis, and autophagy via Ipaf and ASC in *Shigella*-infected macrophages. *PLoS Pathog.* **3,** e111 (2007).
28. Guey, B., Bodnar, M., Manié, S. N., Tardivel, A. & Petrilli, V. Caspase-1 autoproteolysis is differentially required for NLRP1b and NLRP3 inflammasome function. *Proc. Natl. Acad. Sci. USA* **111,** 17254–17259 (2014).
29. Moriya, M. *et al.* Role of charged and hydrophobic residues in the oligomerization of the PYRIN domain of ASC. *Biochemistry* **44,** 575–583 (2005).
30. Sahillioglu, A. C., Sumbul, F., Ozoren, N. & Haliloglu, T. Structural and dynamics aspects of ASC speck assembly. *Structure* **22,** 1–13 (2014).
31. Proell, M., Gerlic, M., Mace, P. D., Reed, J. C. & Riedl, S. J. The CARD plays a critical role in ASC foci formation and inflammasome signalling. *Biochem. J.* **449,** 613–621 (2013).
32. Masumoto, J., Taniguchi, S. & Sagara, J. Pyrin N-terminal homology domain- and caspase recruitment domain-dependent oligomerization of ASC. *Biochem. Biophys. Res. Commun.* **280,** 652–655 (2001).
33. Hornung, V. *et al.* AIM2 recognizes cytosolic dsDNA and forms a caspase-1-activating inflammasome with ASC. *Nature* **458,** 514–518 (2009).
34. Fernandes-Alnemri, T., Yu, J.-W., Datta, P., Wu, J. & Alnemri, E. S. AIM2 activates the inflammasome and cell death in response to cytoplasmic DNA. *Nature* **458,** 509–513 (2009).
35. Mariathasan, S. *et al.* Cryopyrin activates the inflammasome in response to toxins and ATP. *Nature* **440,** 228–232 (2006).
36. Xu, H. *et al.* Structural basis for the prion-like MAVS filaments in antiviral innate immunity. *Elife* **2014,** 1–25 (2014).
37. Peisley, A., Wu, B., Xu, H., Chen, Z. J. & Hur, S. Structural basis for ubiquitin-mediated antiviral signal activation by RIG-I. *Nature* **509,** 110–114 (2014).
38. Hou, F. *et al.* MAVS forms functional prion-like aggregates to activate and propagate antiviral innate immune response. *Cell* **146,** 448–461 (2011).
39. Zhang, L. *et al.* Cryo-EM structure of the activated NAIP2- NLRC4 inflammasome reveals nucleated polymerization. *Science* **4,** 12–14 (2015).
40. Vajjhala, P. R. *et al.* The inflammasome adaptor ASC induces procaspase-8 death effector domain filaments. *J. Biol. Chem.* **290,** 687731 (2015).
41. Lu, A. *et al.* Plasticity in PYD assembly revealed by cryo-EM structure of the PYD filament of AIM2. *Cell Discov.* **1,** 15013 (2015).
42. Nour, A. M. *et al.* Anthrax lethal toxin triggers the formation of a membrane-associated inflammasome complex in murine macrophages. *Infect. Immun.* **77,** 1262–1271 (2009).
43. Poyet, J. L. *et al.* Identification of Ipaf, a human caspase-1-activating protein related to Apaf-1. *J. Biol. Chem.* **276,** 28309–28313 (2001).
44. Faustin, B. *et al.* Reconstituted NALP1 inflammasome reveals two-step mechanism of caspase-1 activation. *Mol. Cell* **25,** 713–724 (2007).
45. Franchi, L. *et al.* Cytosolic flagellin requires Ipaf for activation of caspase-1 and interleukin 1beta in salmonella-infected macrophages. *Nat. Immunol.* **7,** 576–582 (2006).
46. Miao, E. A. *et al.* Cytoplasmic flagellin activates caspase-1 and secretion of interleukin 1beta via Ipaf. *Nat. Immunol.* **7,** 569–575 (2006).
47. Miao, E. A. *et al.* Caspase-1-induced pyroptosis is an innate immune effector mechanism against intracellular bacteria. *Nat. Immunol.* **11,** 1136–1142 (2010).
48. Kagan, J. C., Magupalli, V. G. & Wu, H. SMOCs: supramolecular organizing centres that control innate immunity. *Nat. Rev. Immunol.* **14,** 821–826 (2014).
49. Vajjhala, P. R., Mirams, R. E. & Hill, J. M. Multiple binding sites on the pyrin domain of ASC protein allow self-association and interaction with NLRP3 protein. *J. Biol. Chem.* **287,** 41732–41743 (2012).
50. Elliott, E. I. & Sutterwala, F. S. Initiation and perpetuation of NLRP3 inflammasome activation and assembly. *Immunol. Rev.* **265,** 35–52 (2015).
51. Lamkanfi, M. *et al.* Inflammasome-dependent release of the alarmin HMGB1 in endotoxemia. *J. Immunol.* **185,** 4385–4392 (2010).
52. Cong, L. *et al.* Multiplex genome engineering using CRISPR/Cas systems. *Science* **339,** 819–823 (2013).
53. Sanjana, N. E., Shalem, O. & Zhang, F. Improved vectors and genome-wide libraries for CRISPR screening. *Nat. Methods* **11,** 783–784 (2014).
54. Qiao, Q. *et al.* Structural architecture of the CARMA1/Bcl10/MALT1 signalosome: nucleation-induced filamentous assembly. *Mol. Cell* **51,** 766–779 (2013).
55. Lin, S.-C., Lo, Y.-C. & Wu, H. Helical assembly in the MyD88-IRAK4-IRAK2 complex in TLR/IL-1R signalling. *Nature* **465,** 885–890 (2010).
56. Hu, Z. *et al.* Structural and biochemical basis for induced self-propagation of NLRC4. *Science* **350,** 1–11 (2015).
57. Agard, N. J., Maltby, D. & Wells, J. A. Inflammatory stimuli regulate caspase substrate profiles. *Mol. Cell. Proteomics* **9,** 880–893 (2010).
58. Sagoo, P. *et al. In vivo* imaging of inflammasome activation reveals a subcapsular macrophage burst response that mobilizes innate and adaptive immunity. *Nat. Med.* **22,** 64–71 (2015).
59. Cheng, J. *et al.* Kinetic properties of ASC protein aggregation in epithelial cells. *J. Cell. Physiol.* **222,** 738–747 (2010).
60. Hara, H. *et al.* Phosphorylation of the adaptor ASC acts as a molecular switch that controls the formation of speck-like aggregates and inflammasome activity. *Nat. Immunol.* **14,** 1247–1255 (2013).
61. Lin, Y.-C. *et al.* Syk is involved in NLRP3 inflammasome-mediated caspase-1 activation through adaptor ASC phosphorylation and enhanced oligomerization. *J. Leukoc. Biol.* **97,** 1–11 (2015).
62. Blasi, E. *et al.* Selective immortalization of murine macrophages from fresh bone marrow by a raf/myc recombinant murine retrovirus. *Nature* **318,** 667–670 (1985).
63. Schindelin, J. *et al.* Fiji: an open-source platform for biological-image analysis. *Nat. Methods* **9,** 676–682 (2012).
64. Broz, P. & Monack, D. M. Measuring inflammasome activation in response to bacterial infection. *Methods Mol. Biol.* **1040,** 65–84 (2013).
65. Reed, S. E., Staley, E. M., Mayginnes, J. P., Pintel, D. J. & Tullis, G. E. Transfection of mammalian cells using linear polyethylenimine is a simple and effective means of producing recombinant adeno-associated virus vectors. *J. Virol. Methods* **138,** 85–98 (2006).
66. Tang, Y., Garson, K., Li, L. & Vanderhyden, B. Optimization of lentiviral vector production using polyethylenimine-mediated transfection. *Oncol. Lett.* **9,** 55–62 (2014).
67. de Alba, E. Structure and interdomain dynamics of apoptosis-associated speck-like protein containing a CARD (ASC). *J. Biol. Chem.* **284,** 32932–32941 (2009).

Acknowledgements

We thank V. Dixit (Genentech) for the rat antibody to ASC and rat antibody to caspase-1 p20; Vesna Oliveri, Tim Sharpe, the Imaging Core Facility, FACS Core Facility, Biophysics Core Facility and the Microscopy Center of the Biozentrum, University of Basel, for technical assistance. Work was supported by the Swiss National Science Foundation (PP00P3_139120/1 to P.B).

Author contributions

M.S.D., L.S., S.H. and P.B. designed research. M.S.D., L.S., S.R. and P.B. performed experiments. M.S.D., L.S., S.H. and P.B. analysed data and wrote the manuscript.

Additional information

Supplementary Information accompanies this paper at http://www.nature.com/naturecommunications

Competing financial interests: The authors declare no competing financial interests.

Reprints and permission information is available online at http://npg.nature.com/reprintsandpermissions/

How to cite this article: Dick, M. S. *et al.* ASC filament formation serves as a signal amplification mechanism for inflammasomes. *Nat. Commun.* 7:11929 doi: 10.1038/ncomms11929 (2016).

nature COMMUNICATIONS

DOI: 10.1038/ncomms15030 OPEN

Corrigendum: ASC filament formation serves as a signal amplification mechanism for inflammasomes

Mathias S. Dick, Lorenzo Sborgi, Sebastian Rühl, Sebastian Hiller & Petr Broz

Nature Communications 7:11929 doi: 10.1038/ncomms11929 (2016); Published 22 Jun 2016; Updated 17 Mar 2017

In this Article, residues D128 and D132 of ASC are consistently referred to incorrectly as D130 and D134, respectively. These errors appear in the Results, Methods, Fig. 2, Fig. 3 and Supplementary Fig. 1.

4.6 Review: The gasdermin-D pore: Executor of pyroptotic cell death

Sebastian Rühl [1] and Petr Broz [1]

1 Biozentrum Universität Basel, Klingelbergstrasse 50/70, 4056 Basel

Published: August 19th 2016, Oncotarget

https://doi.org/10.18632/oncotarget.11421

Statement of contribution:

I wrote the article with Petr Broz

www.impactjournals.com/oncotarget/ Oncotarget, Vol. 7, No. 36

Editorial: Autophagy and Cell Death

The gasdermin-D pore: Executor of pyroptotic cell death

Sebastian Rühl and Petr Broz

Pyroptosis is a lytic type of programmed cell death that is initiated in response to pathogen- or host-derived perturbations of the cytosol. It is characterized by cell swelling, lysis, and the release of cytoplasmic content; thus restricting the replication of intracellular pathogens and attracting effector cells of the immune system. The name pyroptosis derives from the Greek pyro (fire or fever) and ptosis (to fall), illustrating its intrinsic pro-inflammatory properties. Pyroptosis is induced by a dedicated set of proteases, the so-called inflammatory caspases, such as caspase-1, -4 and -5 in humans, and caspase-1 and -11 in mice. These caspases are activated within inflammasomes, multi-protein complexes that are assembled by cytosolic pattern-recognition receptors upon recognition various cytosolic danger- or pathogen-associated molecular patterns [1]. While the basis of inflammasome assembly and caspase activation has been well established, the exact mechanism of pyroptosis remained unclear for over a decade.

This picture changed dramatically in 2015 when Shi et al. and Kayagaki et al. independently discovered that the orphan protein gasdermin D (GSDMD) was the central mediator of pyroptotic cell death downstream of both caspase-1 and caspase-11 [2, 3]. The two groups also found that GSDMD is cleaved by these caspases into a 31 kDa N-terminal fragment ($GSDMD^{Nterm}$) and a 22 kDa C-terminal fragment ($GSDMD^{Cterm}$), and that the N-terminus by itself had the ability to induce pyroptosis when expressed ectopically. A series of papers by us and other groups has now shown that the cytotoxicity of this N-terminal fragment is due to its ability to target, insert and permeabilize cellular membranes, therefore representing a novel class of pore forming proteins (Figure 1) [4, 5, 6, 7].

To understand how the $GSDMD^{Nterm}$ induces pyroptosis, we started by investigating its subcellular localization using biochemical fractionation and membrane extraction methods. We found that that

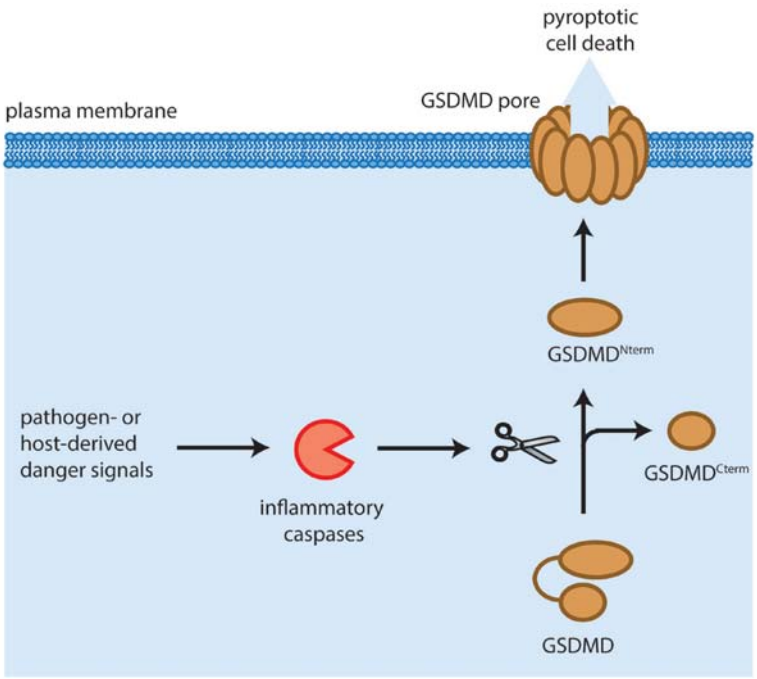

Figure 1: Mechanism of GSDMD-induced pyroptosis. Pathogen- or host-derived signals induce the activation of inflammatory caspases, such as caspase-1 in humans and mice, caspase-4 and -5 in humans and caspase-11 in mice. These caspases cleave gasdermin D (GSDMD) resulting in the separation of the N- and C-terminal domains ($GSDMD^{Nterm}$, $GSDMD^{Cterm}$). The $GSDMD^{Nterm}$ assembles large permeability pores in the plasma membrane which in a lytic type of cell death, known as pyroptosis.

after caspase cleavage the cytotoxic GSDMD$^{N\text{-}term}$ re-localized to cellular membranes and inserted into these, while the GSDMD$^{C\text{-}term}$ remained soluble. Strikingly, the generation of the GSDMD^{Nterm} also correlated with the appearance of large plasma membrane pores and cell lysis, a characteristic feature of pyroptosis. These results indicated that GSDMD^{Nterm} either forms a pore in the host cell plasma membrane or interacts with additional proteins to promote assembly of such a pore.

To demonstrate that the GSDMD^{Nterm} is the sole executor of pyroptosis and that it has intrinsic pore forming ability, we next established a liposome-based *in vitro* assay to measure membrane permeabilization. Incubation of purified full-length GSDMD with recombinant caspase-1 in the presence of dye-loaded liposomes of different lipid compositions showed that GSDMD^{Nterm} targets membranes, whereas GSDMD^{Cterm} and full-length GSDMD remained soluble. Furthermore, this interaction resulted in a rapid release of the dye from the liposomes, indicating that the GSDMD^{Nterm} can by itself permeabilize membranes.

How does the GSDMD^{Nterm} permeabilize liposomes? To visualize the morphology of the permeabilized liposomes and possibly any pore-like structures formed by the GSDMD^{Nterm}, we used a combination of Cryo-electron microscopy and atomic force microscopy (AFM). Indeed, liposomes incubated with cleaved GSDMD were covered with multiple trans-membrane holes or pores, which were as large as 20 nm in diameter, confirming our hypothesis that pyroptotic cell death is the result of the formation of a large permeability pore by GSDMD in plasma membrane of host cells.

GSDMD is just one member of the ill-characterized Gasdermin protein family that features 6 members in humans and nine in mice. Intriguingly, all gasdermin family members share similar N-terminal domains and these domains all exhibit comparable pore forming activity [2, 5]. While the exact stoichiometry and structure of the GSDMD pore has not yet been determined, Ding et al. were recently able to show that the pore formed by mouse GSDMA3 contains 16 symmetric protomers and has an inner diameter of 10-14 nm[5]. Moreover the high-resolution crystal structure of mouse gasdermin A3 revealed the structural basis for the auto-inhibitory mechanism by which the mainly α-helical C-terminus prevents the activity of the N-terminus, an architecture that is most likely conserved in the gasdermin family.

Gasdermins have emerged as a family of new class of cell death inducers, but many questions remain unanswered. For example, it is still unclear how other family members beside GSDMD are activated and how this is regulated on the post-translation level. Furthermore, if and how these proteins are implicated in physiological and pathological cell death pathways, will be an extremely interesting question to address. As caspase-11 and GSDMD were shown to be the central mediators in a murine model of sepsis, the GSDMD pore might also be a possible target for treating symptoms of septic shock. Beyond that, pyroptotic activity of all gasdermin family members could be a useful tool or target to modulate cell death across different fields of cell biology.

Petr Broz: Focal Area Infection Biology, Biozentrum, University of Basel, Basel, Switzerland

Correspondence to: *Petr Broz*, ***email*** *petr.broz@unibas.ch*

Keywords: cell death, caspases

Received: *August 11, 2016*

Published: *August 19, 2016*

REFERENCES

1. Broz, P. et al. Nature reviews Immunology. 2016; 16: 407-20.
2. Shi, J. et al. Nature. 2015; 526: 660-5.
3. Kayagaki, N. et al. Nature. 2015; 526: 666-71.
4. Sborgi, L. et al. The EMBO journal 2016; doi:10.15252/embj.201694696.
5. Ding, J. et al. Nature. 2016; 535: 111-116.
6. Liu, X. et al. Nature. 2016; 535: 153-8.
7. Aglietti, R. A. et al. Proceedings of the National Academy of Sciences of the United States of America. 2016; 113: 7858-63.

4.7 CRISPR-Cas9 screen for novel regulators of the non-canonical inflammasome pathway

4.7.1 Intro

In recent years the development of novel genome editing tools has facilitated the identification and study of unknown genes tremendously. The discovery of the CRISPR Cas9 system represented probably the most important advancement in the field of gene editing. This system is found in several bacteria where it acts as a defence mechanism against bacteriophages through degradation of foreign DNA elements (Pourcel *et al*, 2005),(Mojica *et al*). The development of CRISPR as a genome editing tool was pioneered by several groups(Jinek *et al*, 2012),(Le Cong *et al*, 2013). The CRISPR Cas9 system relies on two major components for its function. The Cas9 nuclease, which is proficient in inducing breaks in double stranded DNA and the guideRNA (gRNA), which is capable of directing the Cas9 protein to virtually any DNA sequence of interest by using a complementary 20bp DNA sequence. As these components can be functionally expressed independently from each other, this allows for design of any gRNA to direct the Cas9 nuclease to any (genomic) DNA sequence desired. Upon induction of the double strand break in the genomic DNA by Cas9, eukaryotic cells will repair the damage by 2 possible mechanisms 1) non-homologous end joining (NHEJ) or 2) homology directed repair. NHEJ is not always correct therefore leading to insertions or deletions (INDELs) at the cutting site, which can lead to frameshift mutations and can be employed to render a gene of interest non-functional. Homology directed repair instead by default uses the second allele of the gene as a correction template, however this mechanism can be exploited by providing a template of interest, allowing the generation of a knock-in around the Cas9 cutting site. Further applications of the CRISPR system are reviewed in(Sander & Joung, 2014), and include among other CRISPR silencing.

As mentioned above, single gRNAs are sufficient to direct the Cas9 to a gene of interest, so this made it possible to design libraries containing several guide RNAs against all genes in the genome (Shalem *et al*, 2014). Generation of these libraries allowed forward genetic screens by means of negative selection, making studies of different cell death pathways particularly amenable to these negative selection screen (Sanjana *et al*, 2014). Shortly after the introduction of these CRISPR Cas9 libraries along with $Cas9^{tg}$ mice (Platt *et al*, 2014) it became apparent that these screens could also be used in primary cells and were not limited

to negative selection by cell death (Parnas *et al*, 2015). Nevertheless, meaningful results, like the discovery of gasdermin-D describe above, could be obtained using cell death based CRISPR Cas9 screens(Shi *et al*, 2015a). However, the complete spectrum of genes involved in promoting survival during non-canonical inflammasome activation was not disclosed in the study by Shi et al. We therefore sought to investigate the non-canonical inflammasome pathway using a negative selection based CRISPR/Cas9 screen to find previously unknown regulators of this pathway.

4.7.2 Experimental design

Following established protocols(Sanjana *et al*, 2014),(Shi *et al*, 2015a) we obtained the murine GeCKO V2 library from addgene containing 130 000 gRNAs, amplified and purified the plasmids from *E. Coli* and produced lentiviral particles in HEK293T cells. The titer of the obtained viral supernatant was determined by transducing primary BMDMs and assessing puromycin resistance post transduction. Immortalized, $Cas9^{tg}$ BMDMs were transduced at a low MOI and transduced cells were selected using puromycin. A sample of cells was collected as a not stimulated reference to verify representation of the gRNAs present. To stimulate the non-canonical inflammasome pathway, cells were electroporated with LPS. Surviving cells were grown and genomic DNA was prepared for three independent experiments. The gRNA sequences were amplified using specific primers, purified and submitted for next-generation-sequencing (NGS).

4.7.3 Results

Analysis of the NGS results obtained revealed that representation of all gRNAs prior to stimulation was comparable across all biological repeats. Unfortunately, only replicate two showed and enrichment of a small number of gRNAs and a depletion of a majority of genes, which is the desired result for a cell death-based screen as the majority of cell should succumb to the cell death stimulus. The other two replicates showed incomplete selection of a subpool of gRNAS most likely due to high survival (i.e. too little cell death) of cells. However, replicate two revealed caspase-11 as a top hit, serving as a positive control. Why exactly gasdermin-D as another known essential component was not found enriched after LPS electroporation remains unclear.

To reduce the amount of hits we eliminated all genes, where only one gRNA was found and considered only genes with a p value higher than 0.01 for further analysis. 287 genes matched these criteria (**Supplementary Table 1**). Using KEGG pathway analysis, 11 pathways were detected, which contained more than 3 proteins present. These pathways with the proteins present are summarized in table 1. TLR2 and TLR4 were prominent hits, potentially indicating that our experimental setup used, induced TLR dependent cell death, which might be due to prolonged LPS exposure over 10 days. It has actually been shown that the non-canonical inflammasome pathway is independent of TLR4 ((Kayagaki *et al*, 2013; Hagar *et al*, 2013). There were some histone proteins detected, which were previously implicated in the necroptotic pathway. Multiple gRNAs of all members were detected, potentially indicating that the whole histone cluster could be important for pyroptosis induction. Lama2 is a member of the extracellular matrix proteins and implicated in the activation of the PI3K/AKT pathway, which is crucial for cell survival and proliferation. Another hit, Gngt2, potentially also acts in this pathway (**Table 3**). It might be conceivable that cells lacking these proteins had a significant growth advantage during the experiment, however it might be worth investigating the importance of the AKT pathway during caspase-11 mediated pyroptosis, especially as there are highly potent and specific pharmacological inhibitors for this pathway.

Pathway	Number of proteins	Gene_IDs; name
Metabolism/ Biosynthetic pathway	8	• Acly; ATP citrate lyase • Anpep; alanyl (membrane) aminopeptidase • Cbr3; carbonyl reductase 3 • Ctps; cytidine 5'-triphosphate synthase • Fut1; fucosyltransferase 1 • Mboat2; membrane bound O-acyltransferase domain containing 2 • Piga; phosphatidylinositol glycan anchor biosynthesis, class A • pigyl; phosphatidylinositol glycan anchor biosynthesis, class Y-like
Olfactory transduction	7	• Cnga4; cyclic nucleotide gated channel alpha 4 • Olfr1037; olfactory receptor 1037 • Olfr1094; olfactory receptor 1094 • Olfr1314; olfactory receptor 1314 • Olfr1450; olfactory receptor 1450 • Olfr389; olfactory receptor 389 • Olfr799; olfactory receptor 799
Necroptosis	4	• Hist1h2ad; histone cluster 1, H2ad • Hist1h2ai; histone cluster 1, H2ai • Hist1h2an; histone cluster 1, H2an • Tlr4; toll-like receptor 4

Pathway	Number of proteins	Gene_IDs; name
PIK3/AKT	4	• Gngt2; guanine nucleotide binding protein (G protein), gamma transducing activity polypeptide 2 • Lama2; laminin, alpha 2 • Tlr2; toll-like receptor 2 • Tlr4; toll-like receptor 4
Alcohol abuse	4	• Gngt2; guanine nucleotide binding protein (G protein), gamma transducing activity polypeptide 2 • Hist1h2ad; histone cluster 1, H2ad • Hist1h2ai; histone cluster 1, H2ai • Hist1h2an; histone cluster 1, H2an
Tuberculosis	3	• Coro1a; coronin, actin binding protein 1A • Tlr2; toll-like receptor 2 • Tlr4; toll-like receptor 4
SLE	3	• Hist1h2ad; histone cluster 1, H2ad • Hist1h2ai; histone cluster 1, H2ai • Hist1h2an; histone cluster 1, H2an
RNA transport	3	• Gm8994; predicted gene 8994 • Nup50; nucleoporin 50 • Prmt5; protein arginine N-methyltransferase 5

Pathway	Number of proteins	Gene_IDs; name
Toxplasmosis	3	• Tlr2; toll-like receptor 2 • Tlr4; toll-like receptor 4 • Lama2; laminin, alpha 2
Amoebiasis	3	• Tlr2; toll-like receptor 2 • Tlr4; toll-like receptor 4 • Lama2; laminin, alpha 2
Phagosome	3	• Coro1a; coronin, actin binding protein 1A • Tlr2; toll-like receptor 2 • Tlr4; toll-like receptor 4

Table 3 Enriched pathways after NGS sequencing of surviving cells upon LPS electroporation

4.7.4 Discussion

Although we tested repeatedly the efficiency of cell death upon LPS electroporation, the induction of cell death across all biological replicates using one round of LPS electroporation was not sufficient to obtain consistent enrichment of the genes known to be involved in the non-canonical inflammasome pathway. Further CRISPR-Cas9 screen need to be performed using a stimulus, which is applied for multiple rounds to ensure complete depletion of insignificant gRNAs from the pool. The procedure furthermore should be optimized using recently published protocols and guidelines for genetic forward CRISPR screens(Joung *et al*, 2017). These guidelines include for example a more sophisticated and precise protocol for determination of viral titers as well as technical considerations for performance of CRISPR/Cas9 based screen.

Potentially other interesting screens to be performed using the cell lines generated might include screening for essential genes involved in activation of the pyrin inflammasome, as this inflammasome is probably the least well understood. Delivery of bacterial effectors that modify RhoA using the anthrax lethal factor-protective antigen (LF-PA) could be evaluated as potential stimuli.

4.7.5 Material and Methods

Preparation and amplification of library

The GeCKOv2 library comes in two half libraries (A and B). They need to be amplified separately. The steps described below are representative for ONE half library. The library was diluted to 50 ng/ml and 2 µl of this solution was added to 25 µl of Lucigen Endura electrocompetent cells. Bacteria were electroporated and recovered in 2 ml of media. This was repeated for a total of 4 electroporations and the bacteria were put on a rotating wheel at 37 °C for 1 hour. 8 ml of bacterial solution were plated on 20 pre-warmed 10 cm agar plates + ampicillin. To estimate transformation efficiency the bacterial suspension was diluted 1:100 in LB (10 µl in 1ml) and 20 µl of this dilution (40 000-fold final dilution) was plated as well. Plates were grown overnight at 32 °C. Bacteria were scraped off in LB and pelleted by centrifugation. 6 endotoxin free maxipreps (Qiagen) were performed per half library, dilution of DNA solution was adjusted to 1 µg/µl and 50 µl aliquots were frozen to -80 °C.

Transduction of macrophages

To prepare viral particles, HEK293T cells were seeded at a density of 5 million per 10 cm dish one day prior to transfection. Cells were transfected with GeCKO plasmids, PsPax2 and VSV-G at a ratio of 9:9:1 µg and 60 µl of linear PEI. Medium was exchanged 8 hours post transfection, viral particles were collected after 36 hours and aliquots were frozen to -80 °C. To estimate viral titers, primary wildtype BMDMs were differentiated for 6 days and transduced with different volumes of the viral supernatant by spin transduction (1900 *xg* 90 min). After 2 days cells were treated with 5 µg/ml puromycin for 6 days and number of surviving cells was enumerated using flow cytometry. Immortalized $Cas9^{tg}$ BMDMs were seeded at a density of 400’000 cells per well of a 12 well plate (24 wells in total). Cells were transduced at a MOI of 0.3 by spin infection and transduced cells were selected after 48 hours with 10 µg/ml puromycin for 6 days.

Electroporation

Prior to electroporation $4x10^7$ cells were pelleted by centrifugation and frozen to -80 °C as a not stimulated reference. Before electroporation, cells were washed 3 times with PBS and counted whereafter they were electroporated with $1\mu g/10^6$ cells LPS O111:B4 using the NEON electroporation system (settings: 1300 volts/20 ms width/2 pulses) and recovered in medium without antibiotics. After cells had grown to confluency (approximately 10 days), 4×10^7 cells were pelleted by centrifugation and frozen to -80 °C.

Genomic DNA prep and PCR amplification

Genomic DNA was isolated using the Qiagen DNeasy Blood and Tissue kit according to the manufacturer's instructions. Two elutions per column were performed in the end to enhance the amount of recovered DNA. DNA was precipitated using sodium acetate and isopropanol. 1/5 5M sodium acetate of the volume of the DNA solution was added and the solution was vortexed well. An equal volume of isopropanol was added to precipitate the gDNA. Samples were centrifuged at 21 000 *xg*, 4 °C for 15 minutes, washed once with 70% Ethanol and centrifuged again as described above. Samples were resuspended to approximately 4-5 µg/µl. Next gRNAs were amplified by PCR. Per screen, at least 200 µg of DNA (approx. 30 Million cells), divided into 6x50 µl PCR reactions were used for amplification of gRNA sequences.
Primers flanking the gRNA
FW:
TCGTCGGCAGCGTCAGATGTGTATAAGAGACAGtcttgtggaaaggacgaaacaccg.
REV:
GTCTCGTGGGCTCGGAGATGTGTATAAGAGACAGTCTACTATTCTTTCCCCTGCA
CTGT
were used for PCR amplification. Reactions were prepared using the NEBNext Ultra Q5 2x Master Mix. The following protocol was used:
95°C 60s, 40 cycles of [94°C for 30s,55°C for 10s and 72°C for 10s] and final 2-min extension at 72°C. PCR reactions were combined and loaded on a 1% agarose gel, separated by electrophoresis and purified using a commercial gel extraction kit. PCR products were stored at -20 °C and submitted for NGS.

4.7.6 Supplementary Table 1

Gene_ID	Number of gRNAs	p value	detected gRNAs
Casp4	6	2.25E-05	5
mmu-mir-1943	4	6.52E-05	2
Ctps	6	6.84E-05	5
Olfr1314	6	0.0001002	6
Ceacam10	6	0.00011792	5
Lama2	6	0.00013246	4
Pnma3	6	0.00013564	3
Vmn2r46	6	0.00021289	6
D830030K20Rik	6	0.00022697	6
Olfr1109	6	0.0002347	3
Mup7	6	0.00029604	6
LOC100048884	6	0.00029604	5
Mup9	6	0.00029604	5
Mup19	6	0.00029604	5
Gm2083	6	0.00029604	5
Mup10	6	0.00029604	5
Mup16	6	0.00029604	5
Gart	6	0.00033103	2
Trp53rk	6	0.0003583	3
Six4	6	0.00038783	3
Vmn2r30	6	0.00039874	6
Vmn2r37	6	0.00039874	6
Vmn2r47	6	0.00039874	6
Dzip1l	6	0.00039919	6
Krtap31-2	6	0.00044009	4
Cbr3	6	0.00046508	5
4833423E24Rik	6	0.00047508	6
Hs3st3b1	6	0.00052688	2
Gm2863	6	0.00053461	5
Zbtb45	6	0.00056369	6
Rpa2	6	0.00057959	5
Igf2r	6	0.00070728	4
Piga	6	0.00071182	4
4930447A16Rik	6	0.00077771	2
Rhox3g	6	0.00086995	5
Gm3763	6	0.00087132	4
Amacr	6	0.00090994	3
Zfp760	6	0.0010454	6

Gene_ID	Number of gRNAs	p value	detected gRNAs
Hist1h2an	6	0.0010894	5
Zbtb7a	6	0.001173	2
Emilin1	6	0.0011912	4
Stab2	6	0.0012444	6
Gm17019	6	0.0012848	6
Chst2	6	0.0012907	4
Cst11	6	0.0013148	3
Gm2933	6	0.0013439	5
Gm21951	6	0.0013439	5
Styk1	6	0.0013603	4
Rars	6	0.001388	3
Fbxw7	6	0.0014434	2
Scgb2b12	6	0.0015588	3
Fermt3	6	0.0015752	3
Zfp72	6	0.0016193	5
Fam102a	6	0.0016274	5
Olfr95	6	0.0017433	2
Dnpep	6	0.001781	2
Vmn2r42	6	0.0018601	6
Cxx1a	6	0.001866	5
Cxx1b	6	0.001866	5
Tmem141	6	0.0018842	3
Gm4305	6	0.0019164	5
Gm4302	6	0.0019164	5
Gm4303	6	0.0019164	5
Gm4307	6	0.0019164	5
Kif26b	6	0.0019305	5
Klhl33	6	0.0019346	4
Tlr4	6	0.0020041	4
Ska3	6	0.002065	4
Gm8994	6	0.0020928	5
Ctr9	6	0.0021396	4
Pcdhgb5	6	0.0022722	6
Mup17	6	0.0023145	5
Tor1a	6	0.0023145	4
Aspdh	6	0.0023622	2
Ildr2	6	0.0023763	3
6030468B19Rik	6	0.002474	3
Vmn1r142	6	0.002504	6
Vmn1r127	6	0.002504	6

Gene_ID	Number of gRNAs	p value	detected gRNAs
Gm4216	6	0.002504	6
Gm4177	6	0.002504	6
Vmn1r94	6	0.002504	6
Prmt5	6	0.0025415	4
AU022751	6	0.0025567	2
Cd300e	6	0.0026439	2
Olfr1094	6	0.0026653	4
1700008P02Rik	6	0.0026771	4
Anpep	6	0.0027294	5
Lce1a2	6	0.0027553	6
Irgc1	6	0.0027621	3
Dcun1d1	6	0.0027685	3
Rtel1	6	0.0027685	5
Olfr628	6	0.0027807	3
Egr4	6	0.0027998	3
Foxh1	6	0.0028957	2
Ddx55	6	0.0029234	4
Gtf3c1	6	0.0029275	3
Sigirr	6	0.0029289	4
Srgn	6	0.0029548	2
Cntnap5a	6	0.0029616	6
Rtbdn	6	0.002972	5
Fam132a	6	0.0029793	4
Grhl3	6	0.0029947	6
Amph	6	0.0030234	3
Fam83f	6	0.0030488	4
Mrgpre	6	0.003112	4
Gm17252	6	0.0031474	2
Slc35f1	6	0.0031706	4
mmu-mir-493	4	0.0031829	2
Chml	6	0.0032574	5
Gm14479	6	0.0032869	5
Gm14484	6	0.0032869	5
Gm14474	6	0.0032869	5
Gm14475	6	0.0032869	5
Gm14501	6	0.0032869	5
Gm14478	6	0.0032869	5
Gm14476	6	0.0032869	5
Gm14477	6	0.0032869	5
Gm14482	6	0.0032869	5

Gene_ID	Number of gRNAs	p value	detected gRNAs
Gm14483	6	0.0032869	5
Apopt1	6	0.0033142	5
Tlr2	6	0.0033546	4
Fadd	6	0.0034746	2
Coro1a	6	0.0034955	4
Pou1f1	6	0.0035064	4
Csrp3	6	0.0035114	5
Defb25	6	0.0035169	3
Bzw1	6	0.0035341	2
Acly	6	0.0037288	4
Vmn2r36	6	0.0037559	5
Sypl	6	0.003819	5
Esyt1	6	0.003859	3
Glt25d1	6	0.0038613	2
Ccdc41	6	0.0039317	2
Ptpn20	6	0.0039494	3
mmu-mir-7647	4	0.0039722	3
Cltc	6	0.0040431	4
Fjx1	6	0.0040612	4
Synb	6	0.0041267	2
Cnga4	6	0.0041385	5
Slc25a29	6	0.0041457	4
Zcchc8	6	0.0041798	3
Pigyl	6	0.0042734	5
Scgb2b20	6	0.004303	5
Stard7	6	0.0043816	2
Sipa1l1	6	0.0043911	5
Kng1	6	0.0044075	4
Prkacb	6	0.0044234	3
Gm14436	6	0.0044288	4
Gm14306	6	0.0044288	4
Olfr1450	6	0.004542	5
Proc	6	0.0045597	4
Cyp2c54	6	0.0045806	3
Gm10142	6	0.0046415	4
Gm527	6	0.0046588	3
Igf2bp1	6	0.0046933	5
mmu-mir-6952	4	0.0047465	3
Ripk2	6	0.004781	3
Polg	6	0.004898	3

Gene_ID	Number of gRNAs	p value	detected gRNAs
Hist1h2ad	6	0.0049191	5
Gria4	6	0.0049355	4
Npl	6	0.0049419	5
Lsp1	6	0.0050118	3
Psmd9	6	0.005192	2
Gm10408	6	0.0052818	5
Gm5795	6	0.0052818	5
Gm10413	6	0.0052818	5
Spag1	6	0.0053054	3
Cyp3a16	6	0.0053926	3
Ovol1	6	0.0054108	2
Tgfa	6	0.0054122	3
Dgkh	6	0.0054326	2
Tmem39b	6	0.0054617	3
Zfp516	6	0.005503	5
Fcrla	6	0.0055412	4
Olfr799	6	0.0055671	4
Kctd16	6	0.0056035	2
Lingo4	6	0.0056053	5
1700065D16Rik	6	0.0056235	2
Tmco1	6	0.005648	2
Pura	6	0.0056953	5
Morc2b	6	0.0058107	3
Tnfrsf14	6	0.0058852	3
Cpeb2	6	0.0059206	4
Nup50	6	0.0059261	4
Gm2825	6	0.0060024	5
Gm14346	6	0.0060024	5
Gm14374	6	0.0060024	5
Gm14345	6	0.0060024	5
Gm14347	6	0.0060024	5
Gm14351	6	0.0060024	5
Gm10922	6	0.0060024	5
Olfr389	6	0.0060497	5
Tgif2	6	0.0061338	3
Car4	6	0.0061715	4
Dnaja3	6	0.0061824	3
Tmem219	6	0.0062265	4
Wdr77	6	0.0062674	3
Vmn1r48	6	0.0062896	3

Gene_ID	Number of gRNAs	p value	detected gRNAs
Lrrc4c	6	0.0063264	4
Pbld1	6	0.0063787	5
Tmem167b	6	0.0064355	5
A330070K13Rik	6	0.0064846	2
Tekt5	6	0.0064986	3
Krtap5-5	6	0.0065459	5
Ogg1	6	0.0066168	2
Gm5916	6	0.006635	2
Rnf145	6	0.0066677	5
Pcdha5	6	0.0066999	5
Hist1h2ai	6	0.0067227	4
Pum2	6	0.0067663	2
Gtf2h3	6	0.0068172	2
Rapgef6	6	0.0068958	4
Casp12	6	0.0069894	3
Repin1	6	0.0069989	2
Olfr1037	6	0.0070576	4
Gm6370	6	0.0070607	5
Gm3415	6	0.0070607	5
Gm3402	6	0.0070607	5
4930449I24Rik	6	0.0070607	5
mmu-mir-6336	4	0.0071344	3
Enpp1	6	0.0071484	3
Lamtor4	6	0.0071812	4
Mboat2	6	0.0072461	4
Rilpl1	6	0.0072461	3
Pcdhgb6	6	0.007257	5
Pcdhga9	6	0.007257	5
Abcc3	6	0.0073347	4
Mrpl20	6	0.0074565	3
Oplah	6	0.0074702	3
Krtap5-3	6	0.0074788	5
Phc1	6	0.0074924	2
Vmn2r39	6	0.0075515	5
Aifm3	6	0.0075651	4
Rnf2	6	0.0075951	2
Laptm4a	6	0.0077074	2
Rad54l2	6	0.0077573	5
Tm9sf1	6	0.007801	4
Trim61	6	0.0078396	5

Gene_ID	Number of gRNAs	p value	detected gRNAs
mmu-mir-3081	4	0.0079709	2
Vmn1r103	6	0.0080323	4
Vmn1r151	6	0.0080323	4
Slc12a9	6	0.0080641	5
Dnah9	6	0.0082604	4
Vmn2r41	6	0.0082717	5
Vmn2r48	6	0.0082717	5
Vmn2r91	6	0.0082776	4
mmu-mir-8120	4	0.0083149	3
Kctd18	6	0.008354	4
Slc35a1	6	0.0084299	3
Ceacam9	6	0.0084303	4
Acer1	6	0.0084426	3
Brd1	6	0.0084967	2
Gngt2	6	0.0086398	4
Sval2	6	0.0086566	5
Bri3	6	0.0086961	3
Vmn2r87	6	0.008697	4
Ncbp1	6	0.0087139	2
9930111J21Rik1	6	0.0087311	3
Ung	6	0.0088852	5
Mkrn3	6	0.008897	4
Trim43b	6	0.0089402	2
Trim43c	6	0.0089402	2
Wt1	6	0.0089538	4
Nlgn1	6	0.0089742	5
Fxn	6	0.0090528	3
Slc6a14	6	0.0090797	5
Cbll1	6	0.0091106	2
Gm2799	6	0.0091355	4
Gmcl1l	6	0.0091355	4
Bcas3	6	0.0091555	3
Ptprk	6	0.0092442	4
Arsg	6	0.0093014	3
Park7	6	0.0093278	3
Aff4	6	0.0093382	4
Gucy2c	6	0.0095086	4
Micalcl	6	0.0095168	3
Syp	6	0.0096222	4
Reps1	6	0.0096886	4

Gene_ID	Number of gRNAs	p value	detected gRNAs
Lyst	6	0.0097086	3
Fut1	6	0.0097604	4
Rxfp1	6	0.0097713	4
5031410I06Rik	6	0.0097958	5
37135	6	0.0098072	4
Vmn2r44	6	0.0098376	4
Vmn2r38	6	0.0098376	4
Vmn2r33	6	0.0098376	4
Chd5	6	0.0099912	5

5 Discussion

5.1 Regulation of immunity by ectosomes

A direct membrane contact is the easiest and most apparent way of two neighbouring cells to communicate. For longer distances in turn, soluble proteins like interleukins, chemokines, cytokines and bioactive mediators are needed for efficient transmission of information in the body. In recent years the shedding of extracellular microvesicles (EVs) from cells has been brought forward as an alternative for intermediate to long distance communications (Johnstone, 2006; Théry *et al*, 2009; Cocucci *et al*, 2009). EVs can be classified into exosomes, ectosomes or shedding microvesicles (SMVs) and apoptotic bodies(Kalra *et al*, 2016). They share the common trait that they are vesicles, surrounded by a lipid bi-layer and encapsulating cellular content, whereas they are very heterogeneous in size, ranging from 1-100 nm for exosomes, 50-1000 nm for ectosomes and up to 5 µm for apoptotic bodies. Exosomes are the best studied type of EVs(Mathivanan *et al*, 2010) and the term exosome refers actually to intraluminal vesicles (ILVs) of MVB that are released to the extracellular space when an MVB fuses with the PM. ILV require the ESCRT machinery for formation, by budding into the MVB luminal space(Colombo *et al*, 2013). MVB trafficking to the cell periphery and fusion with the PM requires multidimensional changes in the actin cytoskeleton, actin-PM interactions, local enzymatic degradation and activation of the membrane fusion machinery (Simons & Raposo, 2009). As mentioned above, ectosomes are more heterogeneous in terms of size distribution. Shedding of these microvesicles happens at sites of Ca^{2+} influx, which leads to rearrangement of the actin cytoskeleton and exposure of phosphatidylserine (PS) through the action of the calcium dependent scramblase TMEM16F (Suzuki *et al*, 2010). Generation of lipid asymmetry primes the PM for curvature to the outside, however the generation and pinching off of the ectosomes strictly requires the ESCRT-III machinery(Nabhan *et al*, 2012; Jimenez *et al*, 2014; Scheffer *et al*, 2014).

Interestingly ectosomes shed by human polymorphonuclear neutrophils (hPMNs) upon stimulation with LPS or N-formyl-methionyl-leucyl-phenylalanine (fMLP) are PS positive (Zwaal & Schroit, 1997; Hess *et al*, 1999). To date, we know that human monocytes undergo inflammasome dependent IL-1β secretion without pyroptosis(Gaidt *et al*, 2016), which might be gasdermin-D dependent. It has been observed that Annexin-V staining on stimulated PMNs is patchy(Frasch *et al*, 2004) and although we lack thorough analysis about the

distribution of PS on the PM membrane during inflammasome stimulation in murine BMDMs or human monocytes one can easily imagine, that the patchy Annexin-V staining is the result of ESCRT-III mediated membrane shedding is response to gasdermin-D pore formation. More research will be required to determine the spatiotemporal assembly of ESCRT during inflammasome signalling and possibly visualize ectosome shedding.
One of the main challenges in the future will be to develop reliable isolation methods for ectosomes. As ectosomes are, both in size and composition, a very heterogeneous population of EVs, it will be important to define transmembrane antigens, common to ectosomes, which will allow affinity based isolation of these vesicles(Kalra *et al*, 2016).
Ectosomes from PMNs, probably due to their high concentration of PS (Refs), have been shown act in an anti-inflammatory manner (Gasser & Schifferli, 2004) by inhibiting cytokine secretion from activated macrophages .
In case future research will be able to demonstrate, that cells which undergo inflammasome activation secrete ectosomes in a significant quantity, it will be of interest if (a) these ectosomes are comparable to the vesicles discovered in PMN in terms of composition and (b) what the effect of these vesicle on other immune and non-immune cells are.

5.2 Gasdermin-D mediated pore formation as the mechanism of unconventional secretion

Since its discovery by Dinarello et al in 1984, IL-1β has been of great interest for immunologists and cell biologists. Over time the IL-1 family grew and to date consists of 11 members and most of them, although being released to the extracellular environment do not have a signal sequence, which directs them to the conventional ER-GOLGI mediated secretion. Therefore, multiple pathways of ‘unconventional secretion’ for mature IL-1β have been proposed(Monteleone *et al*, 2015). ‘Unconventional secretion’ is a catch-all term for different models ranging from secretion in secretory lysosomes, to autophagy mediated secretion, transport across a hyperpermeable membrane, release by PM pores and release by passive lysis. All models proposed suffer from incomplete data and most importantly genetics to prove one or the other mechanism as a valid pathway of IL-1β secretion (discussed in Monteleone et al., 2015). The discovery of gasdermin-D for the first time allowed researchers to uncouple cell death from IL-1β secretion(Shi *et al*, 2015a; Kayagaki *et al*, 2015; He *et al*, 2015). Our results and studies from several other groups (Aglietti *et al*, 2016; Chen *et al*, 2016b; Ding *et al*, 2016; Sborgi *et al*, 2016; Liu *et al*, 2016) for the first time defined a

possible mechanism for lysis independent release of IL-1β mechanism, by showing that the $GSDMD^{Nterm}$ forms pore of a certain range of sizes in the PM prior to pyroptosis. Follow up studies from our lab(Heilig *et al*, 2017) proved this hypothesis by showing that blocking cell lysis, does not reduce gasdermin-D dependent IL-1β secretion and that gasdermin-D pores allow the passage of mature IL-1β in liposomes. Evavold *et al.* confirmed these findings further characterizing the role of gasdermin-D mediated pore formation during a process they call macrophage (or DC) 'hyperactivation'(Evavold *et al*, 2017). Macrophage or DC hyperactivation is characterized by IL-1β secretion, stimulated by inflammasome activation, without detectable cell death and lysis. Several stimuli in different cell types have been proposed to lead to IL-1β secretion without detectable levels of cell lysis. These were for example the aforementioned stimulation of human monocytes with LPS, which mediates IL-1β release through a TRIF/RIPK1/CASP8/Nlrp3 dependent signalling axis(Gaidt *et al*, 2016) or stimulation of murine cells with PGN(Wolf *et al*, 2016)or OxPAPC(Zanoni *et al*, 2016). Both studies show that IL-1β release during stimulation of DCs or macrophages with PGN and OxPAPC is gasdermin-D dependent. These studies therefore suggest convincingly for the first time by genetic means that release of IL-1β through gasdermin-D pores is one, if not the only mechanism of cytokine release in the absence of cell lysis. It should be noted that both, *in vitro* and *in vivo*, the contribution of pyroptosis to IL-1β release is much higher than the release through gasdermin-D pores without pyroptosis. This means that the relative cytokine levels measured in the absence of pyroptosis are much lower than the levels of IL-1β elicited by stimuli, which induce pyroptosis (Zanoni *et al*, 2017). It remains to be investigated if the alternative inflammasome pathway in human monocytes also relies on gasdermin-D mediated pore formation for IL-1β secretion.

These results lead to several questions, one of them being: How do cells manage to survive in the face of gasdermin-D pore formation? Our results provide an answer to this question, suggesting that membrane repair mechanisms allow cells to survive during hyperactivation without succumbing to gasdermin-D pore formation but mediating IL-1β release at the same time via GSDMD pores. Furthermore, as the ESCRT-III machinery leads to budding of ectosomes at the site of PM injury(Jimenez *et al*, 2014; Scheffer *et al*, 2014) one could hypothesize that these ectosomes might contain IL-1β and that ectosome release also contributes to unconventional IL-1β secretion, in line with previous reports that suggested that IL-1b is released within vesicles. I think this rather unlikely because our data suggest that upon inactivation of the ESCRT machinery, IL-1β secretion is enhanced during canonical and

non-canonical inflammasome stimulation. However, since ESCRT inactivation enhances the levels of GSDMD pores formed in the PM and cell lysis, most IL-1 is then released in a manner dependent on lysis. Thus, by only inhibiting ESCRT it is difficult to unravel the contribution of each possible pathway to the overall level of IL-1 release. One goal for future research will be to develop more sophisticated methods of ectosome isolation to clarify the question if mature IL-1β is contained within these or other extracellular vesicles.

6 References

Aglietti RA, Estevez A, Gupta A, Ramirez MG, Liu PS, Kayagaki N, Ciferri C, Dixit VM & Dueber EC (2016) GsdmD p30 elicited by caspase-11 during pyroptosis forms pores in membranes. *Proc. Natl. Acad. Sci. U.S.A.* **113:** 7858–7863

Akira S & Takeda K (2004) Toll-like receptor signalling. *Nature reviews. Immunology* **4:** 499–511

Amulic B, Cazalet C, Hayes GL, Metzler KD & Zychlinsky A (2012) Neutrophil Function: From Mechanisms to Disease. *http://dx.doi.org/10.1146/annurev-immunol-020711-074942* **30:** 459–489

Andrews NW, Almeida PE & Corrotte M (2014) Damage control: cellular mechanisms of plasma membrane repair. *Trends Cell Biol.* **24:** 734–742

Babiychuk EB, Monastyrskaya K & Draeger A (2008) Fluorescent Annexin A1 Reveals Dynamics of Ceramide Platforms in Living Cells. *Traffic* **9:** 1757–1775

Baker PJ, Boucher D, Bierschenk D, Tebartz C, Whitney PG, D'Silva DB, Tanzer MC, Monteleone M, Robertson AAB, Cooper MA, Alvarez-Diaz S, Herold MJ, Bedoui S, Schroder K & Masters SL (2015) NLRP3 inflammasome activation downstream of cytoplasmic LPS recognition by both caspase-4 and caspase-5. *European Journal of Immunology* **45:** 2918–2926

Barbalat R, Lau L, Locksley RM & Barton GM (2009) Toll-like receptor 2 on inflammatory monocytes induces type I interferon in response to viral but not bacterial ligands. *Nature Immunology* **10:** 1200–1207

Barnich N, Aguirre JE, Reinecker H-C, Xavier R & Podolsky DK (2005) Membrane recruitment of NOD2 in intestinal epithelial cells is essential for nuclear factor–κB activation in muramyl dipeptide recognition. *J Cell Biol* **170:** 21–26

Bi GQ, Alderton JM & Steinhardt RA (1995) Calcium-regulated exocytosis is required for cell membrane resealing. *J Cell Biol* **131:** 1747–1758

Bischoff AMLC, Luijendijk MWJ, Huygen PLM, van Duijnhoven G, De Leenheer EMR, Oudesluijs GG, van Laer L, Cremers FPM, Cremers CWRJ & Kremer H (2004) A novel mutation identified in the DFNA5 gene in a Dutch family: a clinical and genetic evaluation. *AUD* **9:** 34–46

Boehme KW, Guerrero M & Compton T (2006) Human Cytomegalovirus Envelope Glycoproteins B and H Are Necessary for TLR2 Activation in Permissive Cells. *J. Immunol.* **177:** 7094–7102

Borregaard N (2010) Neutrophils, from Marrow to Microbes. *Immunity* **33:** 657–670

Bratton SB & Salvesen GS (2010) Regulation of the Apaf-1–caspase-9 apoptosome. *Journal of Cell Science* **123:** 3209–3214

Brinkmann V & Zychlinsky A (2007) Beneficial suicide: why neutrophils die to make NETs. *Nature Reviews Microbiology* **5:** 577–582

Brown GD, Herre J, Williams DL, Willment JA, Marshall ASJ & Gordon S (2003) Dectin-1 Mediates the Biological Effects of β-Glucans. *The Journal of experimental medicine* **197:** 1119–1124

Brown V, Brown RA, Ozinsky A, Hesselberth JR & Fields S (2006) Binding specificity of Toll-like receptor cytoplasmic domains. *European Journal of Immunology* **36:** 742–753

Broz P & Dixit VM (2016) Inflammasomes: mechanism of assembly, regulation and signalling. *Nature reviews. Immunology* **16:** 407–420

Broz P, Moltke von J, Jones J & Vance R (2010) Differential requirement for Caspase-1 autoproteolysis in pathogen-induced cell death and cytokine processing. *Cell host &***:** 1–13

Brubaker SW, Bonham KS & Zanoni I (2015) Innate Immune Pattern Recognition: A Cell Biological Perspective. *Annual review of ...*

Brydges SD, Mueller JL, McGeough MD, Pena CA, Misaghi A, Gandhi C, Putnam CD, Boyle DL, Firestein GS, Horner AA, Soroosh P, Watford WT, O'Shea JJ, Kastner DL & Hoffman HM (2009) Inflammasome-Mediated Disease Animal Models Reveal Roles for Innate but Not Adaptive Immunity. *Immunity* **30:** 875–887

Burdette DL, Monroe KM, Sotelo-Troha K, Iwig JS, Eckert B, Hyodo M, Hayakawa Y & Vance RE (2011) STING is a direct innate immune sensor of cyclic di-GMP. *Nature* **478:** 515–518

Buwitt-Beckmann U, Heine H, Wiesmüller K-H, Jung G, Brock R, Akira S & Ulmer AJ (2006) TLR1- and TLR6-independent recognition of bacterial lipopeptides. *J. Biol. Chem.* **281:** 9049–9057

Cader MZ & Kaser A (2013) Recent advances in inflammatory bowel disease: mucosal immune cells in intestinal inflammation. *Gut* **62:** 1653–1664

Cai Z, Jitkaew S, Zhao J, Chiang H-C, Choksi S, Liu J, Ward Y, Wu L-G & Liu Z-G (2014) Plasma membrane translocation of trimerized MLKL protein is required for TNF-induced necroptosis. *Nature Cell Biology, Published online: 15 July 2002; | doi:10.1038/ncb822* **16:** 55–65

Carlton JG & Martin-Serrano J (2007) Parallels Between Cytokinesis and Retroviral Budding: A Role for the ESCRT Machinery. *Science* **316:** 1908–1912

Chamaillard M, Hashimoto M, Horie Y, Masumoto J, Qiu S, Saab L, Ogura Y, Kawasaki A, Fukase K, Kusumoto S, Valvano MA, Foster SJ, Mak TW, Núñez G & Inohara N (2003) An essential role for NOD1 in host recognition of bacterial peptidoglycan containing diaminopimelic acid. *Nature Immunology* **4:** 702–707

Chang S, Dolganiuc A & Szabo G (2007) Toll-like receptors 1 and 6 are involved in TLR2-mediated macrophage activation by hepatitis C virus core and NS3 proteins. *Journal of Leukocyte Biology* **82:** 479–487

Chao KL, Kulakova L & Herzberg O (2017) Gene polymorphism linked to increased asthma and IBD risk alters gasdermin-B structure, a sulfatide and phosphoinositide binding protein. *Proc. Natl. Acad. Sci. U.S.A.* **114:** E1128–E1137

Chen G, Shaw MH, Kim Y-G & Núñez G (2009) NOD-Like Receptors: Role in Innate Immunity and Inflammatory Disease. *http://dx.doi.org/10.1146/annurev.pathol.4.110807.092239* **4:** 365–398

Chen KW, Groß CJ, Sotomayor FV, Stacey KJ, Tschopp J, Sweet MJ & Schroder K (2014) The neutrophil NLRC4 inflammasome selectively promotes IL-1β maturation without pyroptosis during acute Salmonella challenge. *Cell Rep* **8:** 570–582

Chen Q, Sun L & Chen ZJ (2016a) Regulation and function of the cGAS-STING pathway of cytosolic DNA sensing. *Nature Immunology* **17:** 1142–1149

Chen X, He W-T, Hu L, Li J, Fang Y, Wang X, Xu X, Wang Z, Huang K & Han J (2016b) Pyroptosis is driven by non-selective gasdermin-D pore and its morphology is different from MLKL channel-mediated necroptosis. *Cell Res.* **26:** 1007–1020

Chipuk JE, Moldoveanu T, Llambi F, Parsons MJ & Green DR (2010) The BCL-2 family reunion. *Mol. Cell* **37:** 299–310

Cho Y, Challa S, Moquin D, Genga R, Ray TD, Guildford M & Chan FK-M (2009) Phosphorylation-Driven Assembly of the RIP1-RIP3 Complex Regulates Programmed Necrosis and Virus-Induced Inflammation. *Cell* **137:** 1112–1123

Choi YJ, Jung J, Chung HK, Im E & Rhee SH (2012) PTEN regulates TLR5-induced intestinal inflammation by controlling Mal/TIRAP recruitment. *The FASEB Journal* **27:** 243–254

Christofferson DE & Yuan J (2010) Necroptosis as an alternative form of programmed cell death. *Current Opinion in Cell Biology* **22:** 263–268

Cocucci E, Racchetti G & Meldolesi J (2009) Shedding microvesicles: artefacts no more. *Trends Cell Biol.* **19:** 43–51

Colombo M, Moita C, van Niel G, Kowal J, Vigneron J, Benaroch P, Manel N, Moita LF, Théry C & Raposo G (2013) Analysis of ESCRT functions in exosome biogenesis, composition and secretion highlights the heterogeneity of extracellular vesicles. *Journal of Cell Science* **126:** 5553–5565

Corrotte M, Fernandes MC, Tam C & Andrews NW (2012) Toxin Pores Endocytosed During Plasma Membrane Repair Traffic into the Lumen of MVBs for Degradation. *Traffic* **13:** 483–494

Costantini C, Calzetti F, Perbellini O, Micheletti A, Scarponi C, Lonardi S, Pelletier M, Schakel K, Pizzolo G, Facchetti F, Vermi W, Albanesi C & Cassatella MA (2011) Human neutrophils interact with both 6-sulfo LacNAc+ DC and NK cells to amplify NK-derived IFN{gamma}: role of CD18, ICAM-1, and ICAM-3. *Blood* **117:** 1677–1686

Costantini C, Micheletti A, Calzetti F, Perbellini O, Pizzolo G & Cassatella MA (2010) Neutrophil activation and survival are modulated by interaction with NK cells. *Int. Immunol.* **22:** 827–838

Crawford ED & Wells JA (2011) Caspase Substrates and Cellular Remodeling. *http://dx.doi.org/10.1146/annurev-biochem-061809-121639* **80:** 1055–1087

da Silva Correia J, Soldau K, Christen U, Tobias PS & Ulevitch RJ (2001) Lipopolysaccharide Is in Close Proximity to Each of the Proteins in Its Membrane Receptor Complex TRANSFER FROM CD14 TO TLR4 AND MD-2. *J. Biol. Chem.* **276:** 21129–21135

Dandekar T & Argos P (2008) A novel heterodimeric cysteine protease is required for interleukin 1ß processing in monocytes.

Declercq W, Vanden Berghe T & Vandenabeele P (2009) RIP kinases at the crossroads of cell death and survival. *Cell* **138:** 229–232

Delmaghani S, Defourny J, Aghaie A, Beurg M, Dulon D, Thelen N, Perfettini I, Zelles T, Aller M, Meyer A, Emptoz A, Giraudet F, Leibovici M, Dartevelle S, Soubigou G, Thiry M, Vizi ES, Safieddine S, Hardelin J-P, Avan P, et al (2015) Hypervulnerability to Sound Exposure through Impaired Adaptive Proliferation of Peroxisomes. *Cell* **163:** 894–906

Delmaghani S, del Castillo FJ, Michel V, Leibovici M, Aghaie A, Ron U, van Laer L, Ben-Tal N, Van Camp G, Weil D, Langa F, Lathrop M, Avan P & Petit C (2006) Mutations in the gene encoding pejvakin, a newly identified protein of the afferent auditory pathway, cause DFNB59 auditory neuropathy. *Nature Genetics 1998 20:2* **38:** 770–778

Denais CM, Gilbert RM, Isermann P, McGregor AL, Lindert te M, Weigelin B, Davidson PM, Friedl P, Wolf K & Lammerding J (2016) Nuclear envelope rupture and repair during cancer cell migration. *Science* **352:** 353–358

Deretic V, Saitoh T & Akira S (2013) Autophagy in infection, inflammation and immunity. *Nature reviews. Immunology* **13:** 722–737

Dewson G, Kratina T, Czabotar P, Day CL, Adams JM & Kluck RM (2009) Bak Activation for Apoptosis Involves Oligomerization of Dimers via Their α6 Helices. *Mol. Cell* **36:** 696–703

Di Micco A, Frera G, Lugrin J, Jamilloux Y, Hsu E-T, Tardivel A, De Gassart A, Zaffalon L, Bujisic B, Siegert S, Quadroni M, Broz P, Henry T, Hrycyna CA & Martinon F (2016) AIM2 inflammasome is activated by pharmacological disruption of nuclear envelope integrity. *Proc. Natl. Acad. Sci. U.S.A.* **113:** E4671–80

Dick MS, Sborgi L, Rühl S, Hiller S & Broz P (2016) ASC filament formation serves as a signal amplification mechanism for inflammasomes. *Nat Commun* **7:** 11929

Dickens LS, Powley IR, Hughes MA & MacFarlane M (2012) The 'complexities' of life and death: Death receptor signalling platforms. *Experimental Cell Research* **318:** 1269–1277

Dietrich N, Lienenklaus S, Weiss S & Gekara NO (2010) Murine Toll-Like Receptor 2 Activation Induces Type I Interferon Responses from Endolysosomal Compartments. *PLOS ONE* **5:** e10250

Dihlmann S, Erhart P, Mehrabi A, Nickkholgh A, Lasitschka F, Böckler D & Hakimi M (2014a) Increased expression and activation of absent in melanoma 2 inflammasome components in lymphocytic infiltrates of abdominal aortic aneurysms. *Mol. Med.* **20:** 230–237

Dihlmann S, Tao S, Echterdiek F, Herpel E, Jansen L, Chang-Claude J, Brenner H, Hoffmeister M & Kloor M (2014b) Lack of Absent in Melanoma 2 (AIM2) expression in tumor cells is closely associated with poor survival in colorectal cancer patients. *Int. J. Cancer* **135:** 2387–2396

Ding J, Wang K, Liu W, She Y, Sun Q, Shi J, Sun H, Wang D-C & Shao F (2016) Pore-forming activity and structural autoinhibition of the gasdermin family. *Nature*

Dixit E, Boulant S, Zhang Y, Lee ASY, Odendall C, Shum B, Hacohen N, Chen ZJ, Whelan SP, Fransen M, Nibert ML, Superti-Furga G & Kagan JC (2010) Peroxisomes Are Signaling Platforms for Antiviral Innate Immunity. *Cell* **141:** 668–681

Dombrowski Y, Peric M, Koglin S, Kammerbauer C, Göss C, Anz D, Simanski M, Gläser R, Harder J, Hornung V, Gallo RL, Ruzicka T, Besch R & Schauber J (2011) Cytosolic DNA triggers inflammasome activation in keratinocytes in psoriatic lesions. *Science Translational Medicine* **3:** 82ra38–82ra38

Drummond RA & Brown GD (2011) The role of Dectin-1 in the host defence against fungal infections. *Current Opinion in Microbiology* **14:** 392–399

Dzopalic T, Rajkovic I, Dragicevic A & Colic M (2012) The response of human dendritic cells to co-ligation of pattern-recognition receptors. *Immunologic Research* **52:** 20–33

Eckelman BP, Salvesen GS & Scott FL (2006) Human inhibitor of apoptosis proteins: why XIAP is the black sheep of the family. *EMBO Rep.* **7:** 988–994

Eckert JK, Kim YJ, Kim JI, Gürtler K, Oh D-Y, Sur S, Lundvall L, Hamann L, van der Ploeg A, Pickkers P, Giamarellos-Bourboulis E, Kubarenko AV, Weber AN, Kabesch M, Kumpf O, An H-J, Lee J-O & Schumann RR (2013) The Crystal Structure of Lipopolysaccharide Binding Protein Reveals the Location of a Frequent Mutation that Impairs Innate Immunity. *Immunity* **39:** 647–660

Enokizono Y, Kumeta H, Funami K, Horiuchi M, Sarmiento J, Yamashita K, Standley DM, Matsumoto M, Seya T & Inagaki F (2013) Structures and interface mapping of the TIR domain-containing adaptor molecules involved in interferon signaling. *PNAS* **110:** 19908–19913

Erridge C (2010) Endogenous ligands of TLR2 and TLR4: agonists or assistants? *Journal of Leukocyte Biology* **87:** 989–999

Eskes R, Desagher S, Antonsson B & Martinou JC (2000) Bid induces the oligomerization and insertion of Bax into the outer mitochondrial membrane. *Mol. Cell. Biol.* **20:** 929–935

Evavold CL, Ruan J, Tan Y, Xia S, Wu H & Kagan JC (2017) The Pore-Forming Protein Gasdermin D Regulates Interleukin-1 Secretion from Living Macrophages. *Immunity*

Farache J, Zigmond E, Shakhar G & Jung S (2013) Contributions of dendritic cells and macrophages to intestinal homeostasis and immune defense. *Immunology & Cell Biology* **91:** 232–239

Feoktistova M, Geserick P, Kellert B, Dimitrova DP, Langlais C, Hupe M, Cain K, MacFarlane M, Häcker G & Leverkus M (2011) cIAPs Block Ripoptosome Formation, a RIP1/Caspase-8 Containing Intracellular Cell Death Complex Differentially Regulated by cFLIP Isoforms. *Mol. Cell* **43:** 449–463

Fernandes-Alnemri T, Yu J-W, Datta P, Wu J & Alnemri ES (2009) AIM2 activates the inflammasome and cell death in response to cytoplasmic DNA. *Nature* **458:** 509–513

Ferwerda B, Ferwerda G, Plantinga TS, Willment JA, van Spriel AB, Venselaar H, Elbers CC, Johnson MD, Cambi A, Huysamen C, Jacobs L, Jansen T, Verheijen K, Masthoff L, Morré SA, Vriend G, Williams DL, Perfect JR, Joosten LAB, Wijmenga C, et al (2009) Human Dectin-1 Deficiency and Mucocutaneous Fungal Infections. *http://dx.doi.org/10.1056/NEJMoa0901053* **361:** 1760–1767

Fink SL & Cookson BT (2005) Apoptosis, pyroptosis, and necrosis: mechanistic description of dead and dying eukaryotic cells. *Infect. Immun.* **73:** 1907–1916

Fitzgerald KA, McWhirter SM, Faia KL, Rowe DC, Latz E, Golenbock DT, Coyle AJ, Liao S-M & Maniatis T (2003) IKKε and TBK1 are essential components of the IRF3 signaling pathway. *Nature Immunology* **4:** 491–496

Forestier C-L, Machu C, Loussert C, Pescher P & Späth GF (2011) Imaging Host Cell-Leishmania Interaction Dynamics Implicates Parasite Motility, Lysosome Recruitment, and Host Cell Wounding in the Infection Process. *Cell Host & Microbe* **9:** 319–330

Franchi L, Amer A, Body-Malapel M, Kanneganti T-D, Özören N, Jagirdar R, Inohara N, Vandenabeele P, Bertin J, Coyle A, Grant EP & Núñez G (2006) Cytosolic flagellin requires Ipaf for activation of caspase-1 and interleukin 1β in salmonella-infected macrophages. *Nature Immunology* **7:** 576–582

Frasch SC, Henson PM, Nagaosa K, Fessler MB, Borregaard N & Bratton DL (2004) Phospholipid flip-flop and phospholipid scramblase 1 (PLSCR1) co-localize to uropod rafts in formylated Met-Leu-Phe-stimulated neutrophils. *J. Biol. Chem.* **279:** 17625–17633

Fuller GLJ, Williams JAE, Tomlinson MG, Eble JA, Hanna SL, Pöhlmann S, Suzuki-Inoue K, Ozaki Y, Watson SP & Pearce AC (2007) The C-type lectin receptors CLEC-2 and Dectin-1, but not DC-SIGN, signal via a novel YXXL-dependent signaling cascade. *J. Biol. Chem.* **282:** 12397–12409

Gaidt MM, Ebert TS, Chauhan D, Schmidt T, Schmid-Burgk JL, Rapino F, Robertson AAB, Cooper MA, Graf T & Hornung V (2016) Human Monocytes Engage an Alternative Inflammasome Pathway. *Immunity* **44:** 833–846

Gasser O & Schifferli JA (2004) Activated polymorphonuclear neutrophils disseminate anti-inflammatory microparticles by ectocytosis. *Blood* **104:** 2543–2548

Geijtenbeek TBH & Gringhuis SI (2009) Signalling through C-type lectin receptors: shaping immune responses. *Nature reviews. Immunology* **9:** 465–479

Geserick P, Hupe M, Moulin M, Wong WW-L, Feoktistova M, Kellert B, Gollnick H, Silke J & Leverkus M (2009) Cellular IAPs inhibit a cryptic CD95-induced cell death by limiting RIP1 kinase recruitment. *J Cell Biol* **187:** 1037–1054

Gewirtz AT, Navas TA, Lyons S, Godowski PJ & Madara JL (2001) Cutting Edge: Bacterial Flagellin Activates Basolaterally Expressed TLR5 to Induce Epithelial Proinflammatory Gene Expression. *J. Immunol.* **167:** 1882–1885

Gioannini TL & Weiss JP (2007) Regulation of interactions of Gram-negative bacterial endotoxins with mammalian cells. *Immunologic Research* **39:** 249–260

Girardin SE, Boneca IG, Carneiro LAM, Antignac A, Jéhanno M, Viala J, Tedin K, Taha M-K, Labigne A, Zäthringer U, Coyle AJ, DiStefano PS, Bertin J, Sansonetti PJ & Philpott DJ (2003a) Nod1 Detects a Unique Muropeptide from Gram-Negative Bacterial Peptidoglycan. *Science* **300:** 1584–1587

Girardin SE, Boneca IG, Viala J, Chamaillard M, Labigne A, Thomas G, Philpott DJ & Sansonetti PJ (2003b) Nod2 is a general sensor of peptidoglycan through muramyl dipeptide (MDP) detection. *J. Biol. Chem.* **278:** 8869–8872

Gong Y-N, Guy C, Olauson H, Becker JU, Yang M, Fitzgerald P, Linkermann A & Green DR (2017) ESCRT-III Acts Downstream of MLKL to Regulate Necroptotic Cell Death and Its Consequences. *Cell* **169:** 286–300.e16

Grassmé H, Jendrossek V, Bock J, Riehle A & Gulbins E (2002) Ceramide-Rich Membrane Rafts Mediate CD40 Clustering. *J. Immunol.* **168:** 298–307

Groß CJ, Mishra R, Schneider KS, Médard G, Wettmarshausen J, Dittlein DC, Shi H, Gorka O, Koenig P-A, Fromm S, Magnani G, Ćiković T, Hartjes L, Smollich J, Robertson AAB, Cooper MA, Schmidt-Supprian M, Schuster M, Schroder K, Broz P, et al (2016) K(+) Efflux-Independent NLRP3 Inflammasome Activation by Small Molecules Targeting Mitochondria. *Immunity* **45:** 761–773

Gross O, Yazdi AS, Thomas CJ, Masin M, Heinz LX, Guarda G, Quadroni M, Drexler SK & Tschopp J (2012) Inflammasome activators induce interleukin-1α secretion via distinct pathways with differential requirement for the protease function of caspase-1. *Immunity* **36:** 388–400

Guey B, Bodnar M, Manié SN, Tardivel A & Pétrilli V (2014) Caspase-1 autoproteolysis is differentially required for NLRP1b and NLRP3 inflammasome function. *Proc. Natl. Acad. Sci. U.S.A.* **111:** 17254–17259

Gulbins E (2003) Regulation of death receptor signaling and apoptosis by ceramide. *Pharmacological Research* **47:** 393–399

Hagar JA, Powell DA, Aachoui Y, Ernst RK & Miao EA (2013) Cytoplasmic LPS activates caspase-11: implications in TLR4-independent endotoxic shock. *Science* **341:** 1250–1253

Hayashi F, Smith KD, Ozinsky A, Hawn TR, Yi EC, Goodlett DR, Eng JK, Akira S, Underhill DM & Aderem A (2001) The innate immune response to bacterial flagellin is mediated by Toll-like receptor 5. *Nature* **410:** 1099–1103

Häcker H, Redecke V, Blagoev B, Kratchmarova I, Hsu L-C, Wang GG, Kamps MP, Raz E, Wagner H, Häcker G, Mann M & Karin M (2006) Specificity in Toll-like receptor signalling through distinct effector functions of TRAF3 and TRAF6. *Nature* **439:** 204–207

He S, Wang L, Miao L, Wang T, Du F, Zhao L & Wang X (2009) Receptor Interacting Protein Kinase-3 Determines Cellular Necrotic Response to TNF-α. *Cell* **137:** 1100–1111

He W-T, Wan H, Hu L, Chen P, Wang X, Huang Z, Yang Z-H, Zhong C-Q & Han J (2015) Gasdermin D is an executor of pyroptosis and required for interleukin-1β secretion. *Cell Res.* **25:** 1285–1298

He Y, Zeng MY, Yang D, Motro B & Núñez G (2016) NEK7 is an essential mediator of NLRP3 activation downstream of potassium efflux. *Nature* **530:** 354–357

Heilig R, Dick MS, Sborgi L, Meunier E, Hiller S & Broz P (2017) The Gasdermin-D pore acts as a conduit for IL-1β secretion in mice. *European Journal of Immunology*

Hemmi H, Takeuchi O, Sato S, Yamamoto M, Kaisho T, Sanjo H, Kawai T, Hoshino K, Takeda K & Akira S (2004) The Roles of Two IκB Kinase-related Kinases in Lipopolysaccharide and Double Stranded RNA Signaling and Viral Infection. *The Journal of experimental medicine* **199:** 1641–1650

Hess C, Sadallah S, Hefti A, Landmann R & Schifferli J-A (1999) Ectosomes Released by Human Neutrophils Are Specialized Functional Units. *J. Immunol.* **163:** 4564–4573

Hoebe K, Georgel P, Rutschmann S, Du X, Mudd S, Crozat K, Sovath S, Shamel L, Hartung T, Zähringer U & Beutler B (2005) CD36 is a sensor of diacylglycerides. *Nature* **433:** 523–527

Holopainen JM, Angelova MI & Kinnunen PKJ (2000) Vectorial Budding of Vesicles by Asymmetrical Enzymatic Formation of Ceramide in Giant Liposomes. *Biophysical Journal* **78:** 830–838

Honda K, Yanai H, Negishi H, Asagiri M, Sato M, Mizutani T, Shimada N, Ohba Y, Takaoka A, Yoshida N & Taniguchi T (2005) IRF-7 is the master regulator of type-I interferon-dependent immune responses. *Nature* **434:** 772–777

Horner SM, Liu HM, Park HS, Briley J & Gale M (2011) Mitochondrial-associated endoplasmic reticulum membranes (MAM) form innate immune synapses and are targeted by hepatitis C virus. *PNAS* **108:** 14590–14595

Hornung V & Latz E (2010) Intracellular DNA recognition. *Nature reviews. Immunology* **10:** 123–130

Hornung V, Ablasser A, Charrel-Dennis M, Bauernfeind F, Horvath G, Caffrey DR, Latz E & Fitzgerald KA (2009) AIM2 recognizes cytosolic dsDNA and forms a caspase-1-activating inflammasome with ASC. *Nature* **458:** 514–518

Hornung V, Bauernfeind F, Halle A, Samstad EO, Kono H, Rock KL, Fitzgerald KA & Latz E (2008) Silica crystals and aluminum salts activate the NALP3 inflammasome through phagosomal destabilization. *Nature Immunology* **9:** 847–856

Hornung V, Ellegast J, Kim S, Brzózka K, Jung A, Kato H, Poeck H, Akira S, Conzelmann K-K, Schlee M, Endres S & Hartmann G (2006) 5'-Triphosphate RNA Is the Ligand for RIG-I. *Science* **314:** 994–997

Huang Y-H, Liu X-Y, Du X-X, Jiang Z-F & Su X-D (2012) The structural basis for the sensing and binding of cyclic di-GMP by STING. *Nature Structural and Molecular Biology 2014 21:6* **19:** 728–730

Hwang YY & McKenzie ANJ (2013) Innate Lymphoid Cells in Immunity and Disease. In *Crossroads Between Innate and Adaptive Immunity IV* pp 9–26. New York, NY: Springer, New York, NY

Idone V, Tam C, Goss JW, Toomre D, Pypaert M & Andrews NW (2008) Repair of injured plasma membrane by rapid Ca2+-dependent endocytosis. *J Cell Biol* **180:** 905–914

Imtiyaz HZ, Rosenberg S, Zhang Y, Rahman ZSM, Hou Y-J, Manser T & Zhang J (2006) The Fas-associated death domain protein is required in apoptosis and TLR-induced proliferative responses in B cells. *J. Immunol.* **176:** 6852–6861

Irving AT, Mimuro H, Kufer TA, Lo C, Wheeler R, Turner LJ, Thomas BJ, Malosse C, Gantier MP, Casillas LN, Votta BJ, Bertin J, Boneca IG, Sasakawa C, Philpott DJ, Ferrero RL & Kaparakis-Liaskos M (2014) The Immune Receptor NOD1 and Kinase RIP2 Interact with Bacterial Peptidoglycan on Early Endosomes to Promote Autophagy and Inflammatory Signaling. *Cell Host & Microbe* **15:** 623–635

Ishikawa H & Barber GN (2008) STING is an endoplasmic reticulum adaptor that facilitates innate immune signalling. *Nature* **455:** 674–678

Jaeger BN, Donadieu J, Cognet C, Bernat C, Ordoñez-Rueda D, Barlogis V, Mahlaoui N, Fenis A, Narni-Mancinelli E, Beaupain B, Bellanné-Chantelot C, Bajénoff M, Malissen B, Malissen M, Vivier E & Ugolini S (2012) Neutrophil depletion impairs natural killer cell maturation, function, and homeostasis. *The Journal of experimental medicine* **209:** 565–580

Jaillon S, Galdiero MR, Del Prete D, Cassatella MA, Garlanda C & Mantovani A Neutrophils in innate and adaptive immunity. *Seminars in immunopathology* **35:** 377–394

Janeway CA (1989) Approaching the asymptote? Evolution and revolution in immunology. *Cold Spring Harb. Symp. Quant. Biol.* **54 Pt 1:** 1–13

Jimenez AJ, Maiuri P, Lafaurie-Janvore J, Divoux S, Piel M & Perez F (2014) ESCRT machinery is required for plasma membrane repair. *Science* **343:** 1247136–1247136

Jin T, Perry A, Jiang J, Smith P, Curry JA, Unterholzner L, Jiang Z, Horvath G, Rathinam VA, Johnstone RW, Hornung V, Latz E, Bowie AG, Fitzgerald KA & Xiao TS (2012) Structures of the HIN domain:DNA complexes reveal ligand binding and activation mechanisms of the AIM2 inflammasome and IFI16 receptor. *Immunity* **36:** 561–571

Jinek M, Chylinski K, Fonfara I, Hauer M, Doudna JA & Charpentier E (2012) A Programmable Dual-RNA–Guided DNA Endonuclease in Adaptive Bacterial Immunity. *Science* **337:** 816–821

John ALS & Abraham SN (2013) Innate Immunity and Its Regulation by Mast Cells. *J. Immunol.* **190:** 4458–4463

Johnstone RM (2006) Exosomes biological significance: A concise review. *Blood Cells, Molecules, and Diseases* **36:** 315–321

Jost PJ, Grabow S, Gray D, McKenzie MD, Nachbur U, Huang DCS, Bouillet P, Thomas HE, Borner C, Silke J, Strasser A & Kaufmann T (2009) XIAP discriminates between type I and type II FAS-induced apoptosis. *Nature* **460:** 1035–1039

Joung J, Konermann S, Gootenberg JS, Abudayyeh OO, Platt RJ, Brigham MD, Sanjana NE & Zhang F (2017) Genome-scale CRISPR-Cas9 knockout and transcriptional activation screening. *Nature Protocols* **12:** 828–863

Kagan JC, Su T, Horng T, Chow A, Akira S & Medzhitov R (2008) TRAM couples endocytosis of Toll-like receptor 4 to the induction of interferon-β. *Nature Immunology* **9:** 361–368

Kalra H, Drummen G & Mathivanan S (2016) Focus on Extracellular Vesicles: Introducing the Next Small Big Thing. *International Journal of Molecular Sciences 2016, Vol. 17, Page 170* **17:** 170

Kato H, Takeuchi O, Mikamo-Satoh E, Hirai R, Kawai T, Matsushita K, Hiiragi A, Dermody TS, Fujita T & Akira S (2008) Length-dependent recognition of double-stranded ribonucleic acids by retinoic acid–inducible gene-I and melanoma differentiation–associated gene 5. *The Journal of experimental medicine* **205:** 1601–1610

Katzmann DJ, Odorizzi G & Emr SD (2002) Receptor downregulation and multivesicular-body sorting. *Nature Reviews Molecular Cell Biology, Published online: 01 July 2003; | doi:10.1038/nrm1150* **3:** 893–905

Kawai T, Takahashi K, Sato S, Coban C, Kumar H, Kato H, Ishii KJ, Takeuchi O & Akira S (2005) IPS-1, an adaptor triggering RIG-I- and Mda5-mediated type I interferon induction. *Nature Immunology* **6:** 981–988

Kayagaki N, Stowe IB, Lee BL, O'Rourke K, Anderson K, Warming S, Cuellar T, Haley B, Roose-Girma M, Phung QT, Liu PS, Lill JR, Li H, Wu J, Kummerfeld S, Zhang J, Lee WP, Snipas SJ, Salvesen GS, Morris LX, et al (2015) Caspase-11 cleaves gasdermin D for non-canonical inflammasome signaling. *Nature*

Kayagaki N, Warming S, Lamkanfi M, Vande Walle L, Louie S, Dong J, Newton K, Qu Y, Liu J, Heldens S, Zhang J, Lee WP, Roose-Girma M & Dixit VM (2011) Non-canonical inflammasome activation targets caspase-11. *Nature* **479:** 117–121

Kayagaki N, Wong MT, Stowe IB, Ramani SR, Gonzalez LC, Akashi-Takamura S, Miyake K, Zhang J, Lee WP, Muszyński A, Forsberg LS, Carlson RW & Dixit VM (2013) Noncanonical inflammasome activation by intracellular LPS independent of TLR4. *Science* **341:** 1246–1249

Kofoed EM & Vance RE (2011) Innate immune recognition of bacterial ligands by NAIPs determines inflammasome specificity. *Nature* **477:** 592–595

Konno H, Konno K & Barber GN (2013) Cyclic dinucleotides trigger ULK1 (ATG1) phosphorylation of STING to prevent sustained innate immune signaling. *Cell* **155:** 688–698

Korsmeyer SJ, Wei MC, Saito M, Weiler S, Oh KJ & Schlesinger PH (2000) Pro-apoptotic cascade activates BID, which oligomerizes BAK or BAX into pores that result in the release of cytochrome c. *Cell Death & Differentiation* **7:** 1166–1173

Kortmann J, Brubaker SW & Monack DM (2015) Cutting Edge: Inflammasome Activation in Primary Human Macrophages Is Dependent on Flagellin. *J. Immunol.* **195:** 815–819

Kumar H, Kawai T & Akira S (2011) Pathogen Recognition by the Innate Immune System. *International Reviews of Immunology* **30:** 16–34

Kurt-Jones EA, Chan M, Zhou S, Wang J, Reed G, Bronson R, Arnold MM, Knipe DM & Finberg RW (2004) Herpes simplex virus 1 interaction with Toll-like receptor 2 contributes to lethal encephalitis. *PNAS* **101:** 1315–1320

Latz E, Xiao TS & Stutz A (2013) Activation and regulation of the inflammasomes. *Nature reviews. Immunology* **13:** 397–411

Le Cong, Ran FA, Cox D, Lin S, Barretto R, Habib N, Hsu PD, Wu X, Jiang W, Marraffini LA & Zhang F (2013) Multiplex Genome Engineering Using CRISPR/Cas Systems. *Science* **339:** 819–823

Li J, Zhou Y, Yang T, Wang N, Lian X & Yang L (2010) Gsdma3 is required for hair follicle differentiation in mice. *Biochemical and Biophysical Research Communications* **403:** 18–23

Lin S-C, Lo Y-C & Wu H (2010) Helical assembly in the MyD88–IRAK4–IRAK2 complex in TLR/IL-1R signalling. *Nature* **465:** 885–890

Liston A & Masters SL (2017) Homeostasis-altering molecular processes as mechanisms of inflammasome activation. *Nature reviews. Immunology* **17:** 208–214

Liu S, Chen J, Cai X, Wu J, Chen X, Wu Y-T, Sun L & Chen ZJ (2013) MAVS recruits multiple ubiquitin E3 ligases to activate antiviral signaling cascades. *eLife* **2:** 2217

Liu X, Zhang Z, Ruan J, Pan Y, Magupalli VG, Wu H & Lieberman J (2016) Inflammasome-activated gasdermin D causes pyroptosis by forming membrane pores. *Nature* **535:** 153–158

Loo Y-M & Gale M Jr. (2011) Immune Signaling by RIG-I-like Receptors. *Immunity* **34:** 680–692

Lunny DP, Weed E, Nolan PM, Marquardt A, Augustin M & Porter RM (2005) Mutations in Gasdermin 3 Cause Aberrant Differentiation of the Hair Follicle and Sebaceous Gland. *Journal of Investigative Dermatology* **124:** 615–621

Man SM, Zhu Q, Zhu L, Liu Z, Karki R, Malik A, Sharma D, Li L, Malireddi RKS, Gurung P, Neale G, Olsen SR, Carter RA, McGoldrick DJ, Wu G, Finkelstein D, Vogel P, Gilbertson RJ & Kanneganti T-D (2015) Critical Role for the DNA Sensor AIM2 in Stem Cell Proliferation and Cancer. *Cell* **162:** 45–58

Mantovani A, Cassatella MA, Costantini C & Jaillon S (2011) Neutrophils in the activation and regulation of innate and adaptive immunity. *Nature reviews. Immunology* **11:** 519–531

Mariathasan S, Newton K, Monack DM, Vucic D, French DM, Lee WP, Roose-Girma M, Erickson S & Dixit VM (2004) Differential activation of the inflammasome by caspase-1 adaptors ASC and Ipaf. *Nature* **430:** 213–218

Martinon F, Burns K & Tschopp J (2002) The inflammasome: a molecular platform triggering activation of inflammatory caspases and processing of proIL-beta. *Mol. Cell* **10:** 417–426

Mathivanan S, Ji H & Simpson RJ (2010) Exosomes: Extracellular organelles important in intercellular communication. *Journal of Proteomics* **73:** 1907–1920

McNeil PL, Vogel SS, Miyake K & Terasaki M (2000) Patching plasma membrane disruptions with cytoplasmic membrane. *Journal of Cell Science* **113:** 1891–1902

McWhirter SM, Fitzgerald KA, Rosains J, Rowe DC, Golenbock DT & Maniatis T (2004) IFN-regulatory factor 3-dependent gene expression is defective in Tbk1-deficient mouse embryonic fibroblasts. *PNAS* **101:** 233–238

Meng G, Zhang F, Fuss I, Kitani A & Strober W (2009) A Mutation in the Nlrp3 Gene Causing Inflammasome Hyperactivation Potentiates Th17 Cell-Dominant Immune Responses. *Immunity* **30:** 860–874

Meylan E, Curran J, Hofmann K, Moradpour D, Binder M, Bartenschlager R & Tschopp J (2005) Cardif is an adaptor protein in the RIG-I antiviral pathway and is targeted by hepatitis C virus. *Nature* **437:** 1167–1172

Miao EA, Alpuche-Aranda CM, Dors M, Clark AE, Bader MW, Miller SI & Aderem A (2006) Cytoplasmic flagellin activates caspase-1 and secretion of interleukin 1β via Ipaf. *Nature Immunology* **7:** 569–575

Miao EA, Mao DP, Yudkovsky N, Bonneau R, Lorang CG, Warren SE, Leaf IA & Aderem A (2010) Innate immune detection of the type III secretion apparatus through the NLRC4 inflammasome. *Proc. Natl. Acad. Sci. U.S.A.* **107:** 3076–3080

Micheau O, Lens S, Gaide O, Alevizopoulos K & Tschopp J (2001) NF-kappaB signals induce the expression of c-FLIP. *Mol. Cell. Biol.* **21:** 5299–5305

Miyake K & McNeil PL (1995) Vesicle accumulation and exocytosis at sites of plasma membrane disruption. *J Cell Biol* **131:** 1737–1745

Moffatt MF, Gut IG, Demenais F, Strachan DP, Bouzigon E, Heath S, Mutius von E, Farrall M, Lathrop M & Cookson WOCM (2010) A Large-Scale, Consortium-Based Genomewide Association Study of Asthma. *http://dx.doi.org/10.1056/NEJMoa0906312* **363:** 1211–1221

Moffatt MF, Kabesch M, Liang L, Dixon AL, Strachan D, Heath S, Depner M, Berg von A, Bufe A, Rietschel E, Heinzmann A, Simma B, Frischer T, Willis-Owen SAG, Wong KCC, Illig T, Vogelberg C, Weiland SK, Mutius von E, Abecasis GR, et al (2007) Genetic variants regulating ORMDL3 expression contribute to the risk of childhood asthma. *Nature* **448:** 470–473

Mojica FJM, Díez-Villaseñor CS, García-Martínez J & Soria E Intervening Sequences of Regularly Spaced Prokaryotic Repeats Derive from Foreign Genetic Elements. *J Mol Evol* **60:** 174–182

Moltke von J, Ayres JS, Kofoed EM, Chavarría-Smith J & Vance RE (2013) Recognition of bacteria by inflammasomes. *Annual Review of Immunology* **31:** 73–106

Monteleone M, Stow JL & Schroder K (2015) Mechanisms of unconventional secretion of IL-1 family cytokines. *Cytokine* **74:** 213–218

Morgan BP & Campbell AK (1985) The recovery of human polymorphonuclear leucocytes from sublytic complement attack is mediated by changes in intracellular free calcium. *Biochemical Journal* **231:** 205–208

Morita E & Sundquist WI (2004) RETROVIRUS BUDDING. *http://dx.doi.org/10.1146/annurev.cellbio.20.010403.102350* **20:** 395–425

Morita E, Sandrin V, Chung HY, Morham SG, Gygi SP, Rodesch CK & Sundquist WI (2007) Human ESCRT and ALIX proteins interact with proteins of the midbody and function in cytokinesis. *The EMBO journal* **26:** 4215–4227

Moulin M, Anderton H, Voss AK, Thomas T, Wong WWL, Bankovacki A, Feltham R, Chau D, Cook WD, Silke J & Vaux DL (2012) IAPs limit activation of RIP kinases by TNF receptor 1 during development. *The EMBO journal* **31:** 1679–1691

Muñoz-Planillo R, Kuffa P, Martínez-Colón G, Smith BL, Rajendiran TM & Núñez G (2013) K+ Efflux Is the Common Trigger of NLRP3 Inflammasome Activation by Bacterial Toxins and Particulate Matter. *Immunity* **38:** 1142–1153

Muruve DA, Pétrilli V, Zaiss AK, White LR, Clark SA, Ross PJ, Parks RJ & Tschopp J (2008) The inflammasome recognizes cytosolic microbial and host DNA and triggers an innate immune response. *Nature* **452:** 103–107

Nabhan JF, Hu R, Oh RS, Cohen SN & Lu Q (2012) Formation and release of arrestin domain-containing protein 1-mediated microvesicles (ARMMs) at plasma membrane by recruitment of TSG101 protein. *Proc. Natl. Acad. Sci. U.S.A.* **109:** 4146–4151

Nakamura N, Lill JR, Phung Q, Jiang Z, Bakalarski C, de Mazière A, Klumperman J, Schlatter M, Delamarre L & Mellman I (2014) Endosomes are specialized platforms for bacterial sensing and NOD2 signalling. *Nature* **509:** 240–244

Newton K & Dixit VM (2012) Signaling in Innate Immunity and Inflammation. *Cold Spring Harbor perspectives in biology* **4:** a006049–a006049

O'Neill KL, Huang K, Zhang J, Chen Y & Luo X (2016) Inactivation of prosurvival Bcl-2 proteins activates Bax/Bak through the outer mitochondrial membrane. *Genes Dev.* **30:** 973–988

Oberst A, Pop C, Tremblay AG, Blais V, Denault J-B, Salvesen GS & Green DR (2010) Inducible dimerization and inducible cleavage reveal a requirement for both processes in caspase-8 activation. *Journal of Biological Chemistry* **285:** 16632–16642

Ouyang S, Song X, Wang Y, Ru H, Shaw N, Jiang Y, Niu F, Zhu Y, Qiu W, Parvatiyar K, Li Y, Zhang R, Cheng G & Liu Z-J (2012) Structural Analysis of the STING Adaptor Protein Reveals a Hydrophobic Dimer Interface and Mode of Cyclic di-GMP Binding. *Immunity* **36:** 1073–1086

Ozinsky A, Underhill DM, Fontenot JD, Hajjar AM, Smith KD, Wilson CB, Schroeder L & Aderem A (2000) The repertoire for pattern recognition of pathogens by the innate immune system is defined by cooperation between Toll-like receptors. *PNAS* **97:** 13766–13771

O'Donnell MA, Perez-Jimenez E, Oberst A, Ng A, Massoumi R, Xavier R, Green DR & Ting AT (2011) Caspase 8 inhibits programmed necrosis by processing CYLD. *Nature Cell Biology, Published online: 15 July 2002; | doi:10.1038/ncb822* **13:** 1437–1442

Palm NW & Medzhitov R (2009) Pattern recognition receptors and control of adaptive immunity. *Immunological Reviews* **227:** 221–233

Park J-H, Kim Y-G, McDonald C, Kanneganti T-D, Hasegawa M, Body-Malapel M, Inohara N & Núñez G (2007) RICK/RIP2 Mediates Innate Immune Responses Induced through Nod1 and Nod2 but Not TLRs. *J. Immunol.* **178:** 2380–2386

Parnas O, Jovanovic M, Eisenhaure TM, Herbst RH, Dixit A, Ye CJ, Przybylski D, Platt RJ, Tirosh I, Sanjana NE, Shalem O, Satija R, Raychowdhury R, Mertins P, Carr SA, Zhang F, Hacohen N & Regev A (2015) A Genome-wide CRISPR Screen in Primary Immune Cells to Dissect Regulatory Networks. *Cell* **162:** 675–686

Piao W, Ru LW, Piepenbrink KH, Sundberg EJ, Vogel SN & Toshchakov VY (2013) Recruitment of TLR adapter TRIF to TLR4 signaling complex is mediated by the second helical region of TRIF TIR domain. *PNAS* **110:** 19036–19041

Pichlmair A, Schulz O, Tan CP, Näslund TI, Liljeström P, Weber F & Sousa CRE (2006) RIG-I-Mediated Antiviral Responses to Single-Stranded RNA Bearing 5'-Phosphates. *Science* **314:** 997–1001

Pichlmair A, Schulz O, Tan CP, Rehwinkel J, Kato H, Takeuchi O, Akira S, Way M, Schiavo G & Reis e Sousa C (2009) Activation of MDA5 requires higher-order RNA structures generated during virus infection. *Journal of Virology* **83:** 10761–10769

Platt RJ, Chen S, Zhou Y, Yim MJ, Swiech L, Kempton HR, Dahlman JE, Parnas O, Eisenhaure TM, Jovanovic M, Graham DB, Jhunjhunwala S, Heidenreich M, Xavier RJ,

Langer R, Anderson DG, Hacohen N, Regev A, Feng G, Sharp PA, et al (2014) CRISPR-Cas9 Knockin Mice for Genome Editing and Cancer Modeling. *Cell* **159:** 440–455

Poltorak A, He X, Smirnova I, Liu M-Y, Van Huffel C, Du X, Birdwell D, Alejos E, Silva M, Galanos C, Freudenberg M, Ricciardi-Castagnoli P, Layton B & Beutler B (1998) Defective LPS Signaling in C3H/HeJ and C57BL/10ScCr Mice: Mutations in Tlr4 Gene. *Science* **282:** 2085–2088

Ponomareva L, Liu H, Duan X, Dickerson E, Shen H, Panchanathan R & Choubey D (2013) AIM2, an IFN-inducible cytosolic DNA sensor, in the development of benign prostate hyperplasia and prostate cancer. *Mol. Cancer Res.* **11:** 1193–1202

Pop C, Fitzgerald P, Green DR & Salvesen GS (2007) Role of proteolysis in caspase-8 activation and stabilization. *Biochemistry* **46:** 4398–4407

Pop C, Oberst A, Drag M, Van Raam BJ, Riedl SJ, Green DR & Salvesen GS (2011) FLIPL induces caspase 8 activity in the absence of interdomain caspase 8 cleavage and alters substrate specificity. *Biochemical Journal* **433:** 447–457

Pourcel C, Salvignol G & Vergnaud G (2005) CRISPR elements in Yersinia pestis acquire new repeats by preferential uptake of bacteriophage DNA, and provide additional tools for evolutionary studies. *Microbiology (Reading, Engl.)* **151:** 653–663

Qiao Q, Yang C, Zheng C, Fontán L, David L, Yu X, Bracken C, Rosen M, Melnick A, Egelman EH & Wu H (2013) Structural architecture of the CARMA1/Bcl10/MALT1 signalosome: nucleation-induced filamentous assembly. *Mol. Cell* **51:** 766–779

Quarato G, Guy CS, Grace CR, Llambi F, Nourse A, Rodriguez DA, Wakefield R, Frase S, Moldoveanu T & Green DR (2016) Sequential Engagement of Distinct MLKL Phosphatidylinositol-Binding Sites Executes Necroptosis. *Mol. Cell* **61:** 589–601

Raab M, Gentili M, de Belly H, Thiam HR, Vargas P, Jimenez AJ, Lautenschlaeger F, Voituriez R, Lennon-Duménil AM, Manel N & Piel M (2016) ESCRT III repairs nuclear envelope ruptures during cell migration to limit DNA damage and cell death. *Science* **352:** 359–362

Reddy A, Caler EV & Andrews NW (2001) Plasma Membrane Repair Is Mediated by Ca2+-Regulated Exocytosis of Lysosomes. *Cell* **106:** 157–169

Ricci J-E, Muñoz-Pinedo C, Fitzgerald P, Bailly-Maitre B, Perkins GA, Yadava N, Scheffler IE, Ellisman MH & Green DR (2004) Disruption of mitochondrial function during apoptosis is mediated by caspase cleavage of the p75 subunit of complex I of the electron transport chain. *Cell* **117:** 773–786

Roberts TL, Idris A, Dunn JA, Kelly GM, Burnton CM, Hodgson S, Hardy LL, Garceau V, Sweet MJ, Ross IL, Hume DA & Stacey KJ (2009) HIN-200 Proteins Regulate Caspase Activation in Response to Foreign Cytoplasmic DNA. *Science* **323:** 1057–1060

Rogers C, Fernandes-Alnemri T, Mayes L, Alnemri D, Cingolani G & Alnemri ES (2017) Cleavage of DFNA5 by caspase-3 during apoptosis mediates progression to secondary necrotic/pyroptotic cell death. *Nat Commun* **8:** 14128

Roy D, Liston DR, Idone VJ, Di A, Nelson DJ, Pujol C, Bliska JB, Chakrabarti S & Andrews NW (2004) A Process for Controlling Intracellular Bacterial Infections Induced by Membrane Injury. *Science* **304:** 1515–1518

Runkel F, Marquardt A, Stoeger C, Kochmann E, Simon D, Kohnke B, Korthaus D, Wattler F, Fuchs H, Hrabé de Angelis M, Stumm G, Nehls M, Wattler S, Franz T & Augustin M (2004) The dominant alopecia phenotypes Bareskin, Rex-denuded, and Reduced Coat 2 are caused by mutations in gasdermin 3. *Genomics* **84:** 824–835

Rühl S & Broz P (2015) Caspase-11 activates a canonical NLRP3 inflammasome by promoting K +efflux. *European Journal of Immunology* **45:** 2927–2936

Sagulenko V, Thygesen SJ, Sester DP, Idris A, Cridland JA, Vajjhala PR, Roberts TL, Schroder K, Vince JE, Hill JM, Silke J & Stacey KJ (2013) AIM2 and NLRP3 inflammasomes activate both apoptotic and pyroptotic death pathways via ASC. *Cell Death & Differentiation* **20:** 1149–1160

Saito T, Owen DM, Jiang F, Marcotrigiano J & Gale M Jr. (2008) Innate immunity induced by composition-dependent RIG-I recognition of hepatitis C virus RNA. *Nature* **454:** 523–527

Saitoh T, Fujita N, Hayashi T, Takahara K, Satoh T, Lee H, Matsunaga K, Kageyama S, Omori H, Noda T, Yamamoto N, Kawai T, Ishii K, Takeuchi O, Yoshimori T & Akira S (2009) Atg9a controls dsDNA-driven dynamic translocation of STING and the innate immune response. *Proc. Natl. Acad. Sci. U.S.A.* **106:** 20842–20846

Sakahira H, Enari M & Nagata S (1998) Cleavage of CAD inhibitor in CAD activation and DNA degradation during apoptosis. *Nature* **391:** 96–99

Saleh M (2011) The machinery of Nod-like receptors: refining the paths to immunity and cell death. *Immunological Reviews* **243:** 235–246

Salvesen GS & Riedl SJ (2008) Caspase mechanisms. *Adv. Exp. Med. Biol.* **615:** 13–23

Sander JD & Joung JK (2014) CRISPR-Cas systems for editing, regulating and targeting genomes. *Nat. Biotechnol.* **32:** 347–355

Sanjana NE, Shalem O & Zhang F (2014) Improved vectors and genome-wide libraries for CRISPR screening. *Nature Methods* **11:** 783–784

Sauer J-D, Witte CE, Zemansky J, Hanson B, Lauer P & Portnoy DA (2010) Listeria monocytogenes triggers AIM2-mediated pyroptosis upon infrequent bacteriolysis in the macrophage cytosol. *Cell Host & Microbe* **7:** 412–419

Sborgi L, Rühl S, Mulvihill E, Pipercevic J, Heilig R, Stahlberg H, Farady CJ, Müller DJ, Broz P & Hiller S (2016) GSDMD membrane pore formation constitutes the mechanism of pyroptotic cell death. *The EMBO journal* **35:** 1766–1778

Scheffer LL, Chandra Sreetama Sen, Sharma N, Medikayala S, Brown KJ, Defour A & Jaiswal JK (2014) Mechanism of Ca2+-triggered ESCRT assembly and regulation of cell membrane repair. *Nat Commun* **5:** 5646

Schissel SL, Jiang X-C, Tweedie-Hardman J, Jeong T-S, Camejo EH, Najib J, Rapp JH, Williams KJ & Tabas I (1998) Secretory Sphingomyelinase, a Product of the Acid Sphingomyelinase Gene, Can Hydrolyze Atherogenic Lipoproteins at Neutral pH IMPLICATIONS FOR ATHEROSCLEROTIC LESION DEVELOPMENT. *J. Biol. Chem.* **273:** 2738–2746

Schmid-Burgk JL, Chauhan D, Schmidt T, Ebert TS, Reinhardt J, Endl E & Hornung V (2015a) A genome-wide CRISPR screen identifies NEK7 as an essential component of NLRP3 inflammasome activation. *Journal of Biological Chemistry***:** jbc.C115.700492

Schmid-Burgk JL, Gaidt MM, Schmidt T, Ebert TS, Bartok E & Hornung V (2015b) Caspase-4 mediates non-canonical activation of the NLRP3 inflammasome in human myeloid cells. *European Journal of Immunology* **45:** 2911–2917

Schumann RR, Leong, Flaggs GW, Gray PW, Wright SD, Mathison JC, Tobias PS & Ulevitch RJ (1990) Structure and function of lipopolysaccharide binding protein. *Science* **249:** 1429–1431

Schwander M, Sczaniecka A, Grillet N, Bailey JS, Avenarius M, Najmabadi H, Steffy BM, Federe GC, Lagler EA, Banan R, Hice R, Grabowski-Boase L, Keithley EM, Ryan AF, Housley GD, Wiltshire T, Smith RJH, Tarantino LM & Müller U (2007) A Forward Genetics Screen in Mice Identifies Recessive Deafness Traits and Reveals That Pejvakin Is Essential for Outer Hair Cell Function. *J. Neurosci.* **27:** 2163–2175

Seth RB, Sun L, Ea C-K & Chen ZJ (2005) Identification and Characterization of MAVS, a Mitochondrial Antiviral Signaling Protein that Activates NF-κB and IRF3. *Cell* **122:** 669–682

Shalem O, Sanjana NE, Hartenian E, Shi X, Scott DA, Mikkelsen TS, Heckl D, Ebert BL, Root DE, Doench JG & Zhang F (2014) Genome-scale CRISPR-Cas9 knockout screening in human cells. *Science* **343:** 84–87

Shang G, Zhu D, Li N, Zhang J, Zhu C, Lu D, Liu C, Yu Q, Zhao Y, Xu S & Gu L (2012) Crystal structures of STING protein reveal basis for recognition of cyclic di-GMP. *Nature Structural and Molecular Biology 2014 21:6* **19:** 725–727

Shi H, Wang Y, Li X, Zhan X, Tang M, Fina M, Su L, Pratt D, Bu CH, Hildebrand S, Lyon S, Scott L, Quan J, Sun Q, Russell J, Arnett S, Jurek P, Chen D, Kravchenko VV, Mathison JC, et al (2016) NLRP3 activation and mitosis are mutually exclusive events coordinated by NEK7, a new inflammasome component. *Nature Immunology* **17:** 250–258

Shi J, Zhao Y, Wang K, Shi X, Wang Y, Huang H, Zhuang Y, Cai T, Wang F & Shao F (2015a) Cleavage of GSDMD by inflammatory caspases determines pyroptotic cell death. *Nature*

Shi J, Zhao Y, Wang Y, Gao W, Ding J, Li P, Hu L & Shao F (2014) Inflammatory caspases are innate immune receptors for intracellular LPS. *Nature*

Shi P, Tang A, Xian L, Hou S, Zou D, Lv Y, Huang Z, Wang Q, Song A, Lin Z & Gao X (2015b) Loss of conserved Gsdma3 self-regulation causes autophagy and cell death. *Biochemical Journal* **468:** 325–336

Shibata T, Takemura N, Motoi Y, International YG2012 PRAT4A-dependent expression of cell surface TLR5 on neutrophils, classical monocytes and dendritic cells. *academic.oup.com*

Shimada K, Crother TR, Karlin J, Dagvadorj J, Chiba N, Chen S, Ramanujan VK, Wolf AJ, Vergnes L, Ojcius DM, Rentsendorj A, Vargas M, Guerrero C, Wang Y, Fitzgerald KA, Underhill DM, Town T & Arditi M (2012) Oxidized Mitochondrial DNA Activates the NLRP3 Inflammasome during Apoptosis. *Immunity* **36:** 401–414

Shu C, Yi G, Watts T, Kao CC & Li P (2012) Structure of STING bound to cyclic di-GMP reveals the mechanism of cyclic dinucleotide recognition by the immune system. *Nature Structural and Molecular Biology 2014 21:6* **19:** 722–724

Simons M & Raposo G (2009) Exosomes – vesicular carriers for intercellular communication. *Current Opinion in Cell Biology* **21:** 575–581

Smith KD, Andersen-Nissen E, Hayashi F, Strobe K, Bergman MA, Barrett SLR, Cookson BT & Aderem A (2003) Toll-like receptor 5 recognizes a conserved site on flagellin required for protofilament formation and bacterial motility. *Nature Immunology* **4:** 1247–1253

Sun L, Wu J, Du F, Chen X & Chen ZJ (2013) Cyclic GMP-AMP Synthase Is a Cytosolic DNA Sensor That Activates the Type I Interferon Pathway. *Science* **339:** 786–791

Sun W, Li Y, Chen L, Chen H, You F, Zhou X, Zhou Y, Zhai Z, Chen D & Jiang Z (2009) ERIS, an endoplasmic reticulum IFN stimulator, activates innate immune signaling through dimerization. *PNAS* **106:** 8653–8658

Suzuki J, Umeda M, Sims PJ & Nagata S (2010) Calcium-dependent phospholipid scrambling by TMEM16F. *Nature* **468:** 834–838

Szomolanyi-Tsuda E, Liang X, Welsh RM, Kurt-Jones EA & Finberg RW (2006) Role for TLR2 in NK cell-mediated control of murine cytomegalovirus in vivo. *Journal of Virology* **80:** 4286–4291

Tam C, Idone V, Devlin C, Fernandes MC, Flannery A, He X, Schuchman E, Tabas I & Andrews NW (2010) Exocytosis of acid sphingomyelinase by wounded cells promotes endocytosis and plasma membrane repair. *J Cell Biol* **189:** 1027–1038

Tanaka S, Tamura M, Aoki A, Fujii T, Komiyama H, Sagai T & Shiroishi T (2007) A new Gsdma3 mutation affecting anagen phase of first hair cycle. *Biochemical and Biophysical Research Communications* **359:** 902–907

Tassi I, Cella M, Castro I, Gilfillan S, Khan WN & Colonna M (2009) Requirement of phospholipase C-γ2 (PLCγ2) for Dectin-1-induced antigen presentation and induction of TH1/TH17 polarization. *European Journal of Immunology* **39:** 1369–1378

Tenev T, Bianchi K, Darding M, Broemer M, Langlais C, Wallberg F, Zachariou A, Lopez J, MacFarlane M, Cain K & Meier P (2011) The Ripoptosome, a Signaling Platform that Assembles in Response to Genotoxic Stress and Loss of IAPs. *Mol. Cell* **43:** 432–448

Tenthorey JL, Kofoed EM, Daugherty MD, Malik HS & Vance RE (2014) Molecular Basis for Specific Recognition of Bacterial Ligands by NAIP/NLRC4 Inflammasomes. *Mol. Cell* **54:** 17–29

Théry C, Ostrowski M & Segura E (2009) Membrane vesicles as conveyors of immune responses. *Nature reviews. Immunology* **9:** 581–593

Togo T, Krasieva TB & Steinhardt RA (2000) A decrease in membrane tension precedes successful cell-membrane repair. *Molecular biology of the cell* **11:** 4339–4346

Trajkovic K, Hsu C, Chiantia S, Rajendran L, Wenzel D, Wieland F, Schwille P, Brügger B & Simons M (2008) Ceramide Triggers Budding of Exosome Vesicles into Multivesicular Endosomes. *Science* **319:** 1244–1247

Travassos LH, Carneiro LAM, Ramjeet M, Hussey S, Kim Y-G, Magalhães JG, Yuan L, Soares F, Chea E, Le Bourhis L, Boneca IG, Allaoui A, Jones NL, Núñez G, Girardin SE & Philpott DJ (2010) Nod1 and Nod2 direct autophagy by recruiting ATG16L1 to the plasma membrane at the site of bacterial entry. *Nature Immunology* **11:** 55–62

Triantafilou M, Morath S, Mackie A, Hartung T & Triantafilou K (2004) Lateral diffusion of Toll-like receptors reveals that they are transiently confined within lipid rafts on the plasma membrane. *Journal of Cell Science* **117:** 4007–4014

Ulrichts P & Tavernier J (2008) MAPPIT analysis of early Toll-like receptor signalling events. *Immunology Letters* **116:** 141–148

Unterholzner L, Keating SE, Baran M, Horan KA, Jensen SB, Sharma S, Sirois CM, Jin T, Latz E, Xiao TS, Fitzgerald KA, Paludan SR & Bowie AG (2010) IFI16 is an innate immune sensor for intracellular DNA. *Nature Immunology* **11:** 997–1004

Upton JW, Kaiser WJ & Mocarski ES (2010) Virus Inhibition of RIP3-Dependent Necrosis. *Cell Host & Microbe* **7:** 302–313

Upton JW, Kaiser WJ & Mocarski ES (2012) DAI/ZBP1/DLM-1 complexes with RIP3 to mediate virus-induced programmed necrosis that is targeted by murine cytomegalovirus vIRA. *Cell Host & Microbe* **11:** 290–297

Uzri D & Gehrke L (2009) Nucleotide sequences and modifications that determine RIG-I/RNA binding and signaling activities. *Journal of Virology* **83:** 4174–4184

van BLITTERSWIJK WJ, van der LUIT AH, VELDMAN RJ, VERHEIJ M & BORST J (2003) Ceramide: second messenger or modulator of membrane structure and dynamics? *Biochemical Journal* **369:** 199–211

van Laer L, Huizing EH, Verstreken M, van Zuijlen D, Wauters JG, Bossuyt PJ, Van de Heyning P, McGuirt WT, Smith RJH, Willems PJ, Legan PK, Richardson GP & Van Camp G (1998) Nonsyndromic hearing impairment is associated with a mutation in DFNA5. *Nature Genetics 1998 20:2* **20:** 194–197

Walev I, Bhakdi SC, Hofmann F, Djonder N, Valeva A, Aktories K & Bhakdi S (2001) Delivery of proteins into living cells by reversible membrane permeabilization with streptolysin-O. *PNAS* **98:** 3185–3190

Wallach D, Kang T-B, Dillon CP & Green DR (2016) Programmed necrosis in inflammation: Toward identification of the effector molecules. *Science* **352:** aaf2154–aaf2154

Wang H, Sun L, Su L, Rizo J, Liu L, Wang L-F, Wang F-S & Wang X (2014) Mixed Lineage Kinase Domain-like Protein MLKL Causes Necrotic Membrane Disruption upon Phosphorylation by RIP3. *Mol. Cell* **54:** 133–146

Wang L, Du F & Wang X (2008) TNF-α Induces Two Distinct Caspase-8 Activation Pathways. *Cell* **133:** 693–703

Wang Y, Gao W, Shi X, Ding J, Liu W, He H, Wang K & Shao F (2017) Chemotherapy drugs induce pyroptosis through caspase-3 cleavage of a gasdermin. *Nature* **547:** 99–103

Weng D, Marty-Roix R, Ganesan S, Proulx MK, Vladimer GI, Kaiser WJ, Mocarski ES, Pouliot K, Chan FK-M, Kelliher MA, Harris PA, Bertin J, Gough PJ, Shayakhmetov DM, Goguen JD, Fitzgerald KA, Silverman N & Lien E (2014) Caspase-8 and RIP kinases regulate bacteria-induced innate immune responses and cell death. *Proc. Natl. Acad. Sci. U.S.A.***:** 201403477

Wilson JE, Petrucelli AS, Chen L, Koblansky AA, Truax AD, Oyama Y, Rogers AB, Brickey WJ, Wang Y, Schneider M, Mühlbauer M, Chou W-C, Barker BR, Jobin C, Allbritton NL, Ramsden DA, Davis BK & Ting JPY (2015) Inflammasome-independent role of AIM2 in suppressing colon tumorigenesis via DNA-PK and Akt. *Nature medicine* **21:** 906–913

Wolf AJ, Reyes CN, Liang W, Becker C, Shimada K, Wheeler ML, Cho HC, Popescu NI, Coggeshall KM, Arditi M & Underhill DM (2016) Hexokinase Is an Innate Immune Receptor for the Detection of Bacterial Peptidoglycan. *Cell* **166:** 624–636

Wu C, Orozco C, Boyer J, Leglise M, Goodale J, Batalov S, Hodge CL, Haase J, Janes J, Huss JW & Su AI (2009a) BioGPS: an extensible and customizable portal for querying and organizing gene annotation resources. *Genome Biology 2009 10:11* **10:** R130

Wu H, Romieu I, Sienra Monge JJ, Li H, Del Rio Navarro BE & London SJ (2009b) Genetic variation in ORM1-like 3 (ORMDL3) and gasdermin-like (GSDML) and childhood asthma. *Allergy* **64:** 629–635

Wu J, Sun L, Chen X, Du F, Shi H, Chen C & Chen ZJ (2013) Cyclic GMP-AMP Is an Endogenous Second Messenger in Innate Immune Signaling by Cytosolic DNA. *Science* **339:** 826–830

Xu L-G, Wang Y-Y, Han K-J, Li L-Y, Zhai Z & Shu H-B (2005) VISA Is an Adapter Protein Required for Virus-Triggered IFN-β Signaling. *Mol. Cell* **19:** 727–740

Yamamoto M, Sato S, Hemmi H, Hoshino K, Kaisho T, Sanjo H, Takeuchi O, Sugiyama M, Okabe M, Takeda K & Akira S (2003a) Role of Adaptor TRIF in the MyD88-Independent Toll-Like Receptor Signaling Pathway. *Science* **301:** 640–643

Yamamoto M, Sato S, Hemmi H, Uematsu S, Hoshino K, Kaisho T, Takeuchi O, Takeda K & Akira S (2003b) TRAM is specifically involved in the Toll-like receptor 4–mediated MyD88-independent signaling pathway. *Nature Immunology* **4:** 1144–1150

Yin Q, Tian Y, Kabaleeswaran V, Jiang X, Tu D, Eck MJ, Chen ZJ & Wu H (2012) Cyclic di-GMP Sensing via the Innate Immune Signaling Protein STING. *Mol. Cell* **46:** 735–745

Yoneyama M, Kikuchi M, Matsumoto K, Imaizumi T, Miyagishi M, Taira K, Foy E, Loo Y-M, Gale M, Akira S, Yonehara S, Kato A & Fujita T (2005) Shared and Unique Functions of the DExD/H-Box Helicases RIG-I, MDA5, and LGP2 in Antiviral Innate Immunity. *J. Immunol.* **175:** 2851–2858

Yoneyama M, Kikuchi M, Natsukawa T, Shinobu N, Imaizumi T, Miyagishi M, Taira K, Akira S & Fujita T (2004) The RNA helicase RIG-I has an essential function in double-stranded RNA-induced innate antiviral responses. *Nature Immunology* **5:** 730–737

Yu J, Kang MJ, Kim BJ, Kwon JW, Song YH, Choi WA, Shin YJ & Hong SJ (2011) Polymorphisms in GSDMA and GSDMB are associated with asthma susceptibility, atopy and BHR. *Pediatric Pulmonology* **46:** 701–708

Yu X, Acehan D, Ménétret J-F, Booth CR, Ludtke SJ, Riedl SJ, Shi Y, Wang X & Akey CW (2005) A Structure of the Human Apoptosome at 12.8 Å Resolution Provides Insights into This Cell Death Platform. *Structure* **13:** 1725–1735

Yuan S, Yu X, Topf M, Ludtke SJ, Wang X & Akey CW (2010) Structure of an Apoptosome-Procaspase-9 CARD Complex. *Structure* **18:** 571–583

Zanoni I, Tan Y, Di Gioia M, Broggi A, Ruan J, Shi J, Donado CA, Shao F, Wu H, Springstead JR & Kagan JC (2016) An endogenous caspase-11 ligand elicits interleukin-1 release from living dendritic cells. *Science* **352:** 1232–1236

Zanoni I, Tan Y, Di Gioia M, Springstead JR & Kagan JC (2017) By Capturing Inflammatory Lipids Released from Dying Cells, the Receptor CD14 Induces Inflammasome-Dependent Phagocyte Hyperactivation. *Immunity* **47:** 697–709.e3

Zha X, Pierini LM, Leopold PL, Skiba PJ, Tabas I & Maxfield FR (1998) Sphingomyelinase Treatment Induces ATP-independent Endocytosis. *J Cell Biol* **140:** 39–47

Zhang D-W, Shao J, Lin J, Zhang N, Lu B-J, Lin S-C, Dong M-Q & Han J (2009) RIP3, an energy metabolism regulator that switches TNF-induced cell death from apoptosis to necrosis. *Science* **325:** 332–336

Zhang Z, Bin Yuan, Bao M, Lu N, Kim T & Liu Y-J (2011) The helicase DDX41 senses intracellular DNA mediated by the adaptor STING in dendritic cells. *Nature Immunology* **12:** 959–965

Zhao Y, Yang J, Shi J, Gong Y-N, Lu Q, Xu H, Liu L & Shao F (2011) The NLRC4 inflammasome receptors for bacterial flagellin and type III secretion apparatus. *Nature* **477:** 596–600

Zhong B, Yang Y, Li S, Wang Y-Y, Li Y, Diao F, Lei C, He X, Zhang L, Tien P & Shu H-B (2008) The Adaptor Protein MITA Links Virus-Sensing Receptors to IRF3 Transcription Factor Activation. *Immunity* **29:** 538–550

Zhou Y, Jiang X, Gu P, Chen W, Zeng X & Gao X (2012) Gsdma3 Mutation Causes Bulge Stem Cell Depletion and Alopecia Mediated by Skin Inflammation. *The American Journal of Pathology* **180:** 763–774

Zigmond E & Jung S (2013) Intestinal macrophages: well educated exceptions from the rule. *Trends in Immunology* **34:** 162–168

Zou H, Henzel WJ, Liu X, Lutschg A & Wang X (1997) Apaf-1, a Human Protein Homologous to C. elegans CED-4, Participates in Cytochrome c–Dependent Activation of Caspase-3. *Cell* **90:** 405–413

Zwaal RFA & Schroit AJ (1997) Pathophysiologic Implications of Membrane Phospholipid Asymmetry in Blood Cells. *Blood* **89:** 1121–1132

7 Thank you…

… to Petr for being a great boss. That statement per se could be enough but I would like to point out why I think you were an amazing boss. I always had the feeling we were aiming for the same goal and I am extremely grateful for all the support, both personally and scientifically I got from you. Science is more often than not disappointing but I never felt discouraged by you and this saved me from so much additional frustration.

… to Jean Pieters. I received my basic scientific education in your lab, from which I am profiting still today. You were always very helpful with all my applications, gave a lot of career-related input and are a great mentor. Thank you for taking time to read my thesis and serve on my committee.

… to Daniel Pinschewer for similar career-related support and input during my committee meetings.

…to Sebastian Hiller for serving on my defense committee and for the great collaboration we could set up during my PhD

… to Timm Maier for chairing my defense

… to the past and present members of the Broz lab. The amazing group is really what helped me to come to the lab. I always appreciated the motivating atmosphere, great discussion, funny lunchbreaks, shared suffering and moderate drinking sessions during and after apéros.

… to all the administrative assistants (especially Michaela Hanisch and Maja Güntensperger-Heckel), making sure things run as smoothly as they do.

… to all the members of the scientific platforms: Janine, Wolf, Alexia and Kai

…members of the wash and media kitchen: Verena, Fatima and Elisabete

…my parents, Harald and Evi, for constantly supporting me in every way possible throughout my life and education.

... to my wife Samantha for being the most patient, sensitive, understanding and loving person I know. Thank you for sharing my life with me and supporting my professional ambitions by taking the next big step with me.